# NOTE TO USERS

This reproduction is the best copy available.

# HYDRODYNAMICS OF TURBULENT BED CONTACTOR WITH NON-NEWTONIAN LIQUIDS

by

Hadil Abukhalifeh

B.Sc. in Chemical Engineering
Kuwait University, Kuwait, 1986

A thesis

presented to Ryerson University

in partial fulfillment of the

requirements for the degree of

Master of Applied Science

in the Program of

Chemical Engineering

Toronto, Ontario, Canada, 2004

©Hadil Abukhalifeh 2004

UMI Number: EC52951

INFORMATION TO USERS

The quality of this reproduction is dependent upon the quality of the copy submitted. Broken or indistinct print, colored or poor quality illustrations and photographs, print bleed-through, substandard margins, and improper alignment can adversely affect reproduction.

In the unlikely event that the author did not send a complete manuscript and there are missing pages, these will be noted. Also, if unauthorized copyright material had to be removed, a note will indicate the deletion.

# BORROWER'S PAGE

Ryerson University requires the signature of all persons using or photocopying this thesis. Please sign below, and give address and date.

| NAME | ADDRESS | DATE |
|------|---------|------|
|      |         |      |
|      |         |      |
|      |         |      |
|      |         |      |
|      |         |      |
|      |         |      |
|      |         |      |

# ABSTRACT

# Hydrodynamics of Turbulent Bed Contactor
# With Non-Newtonian Liquids

Hadil Abukhalifeh, 2004
Master of Applied Science
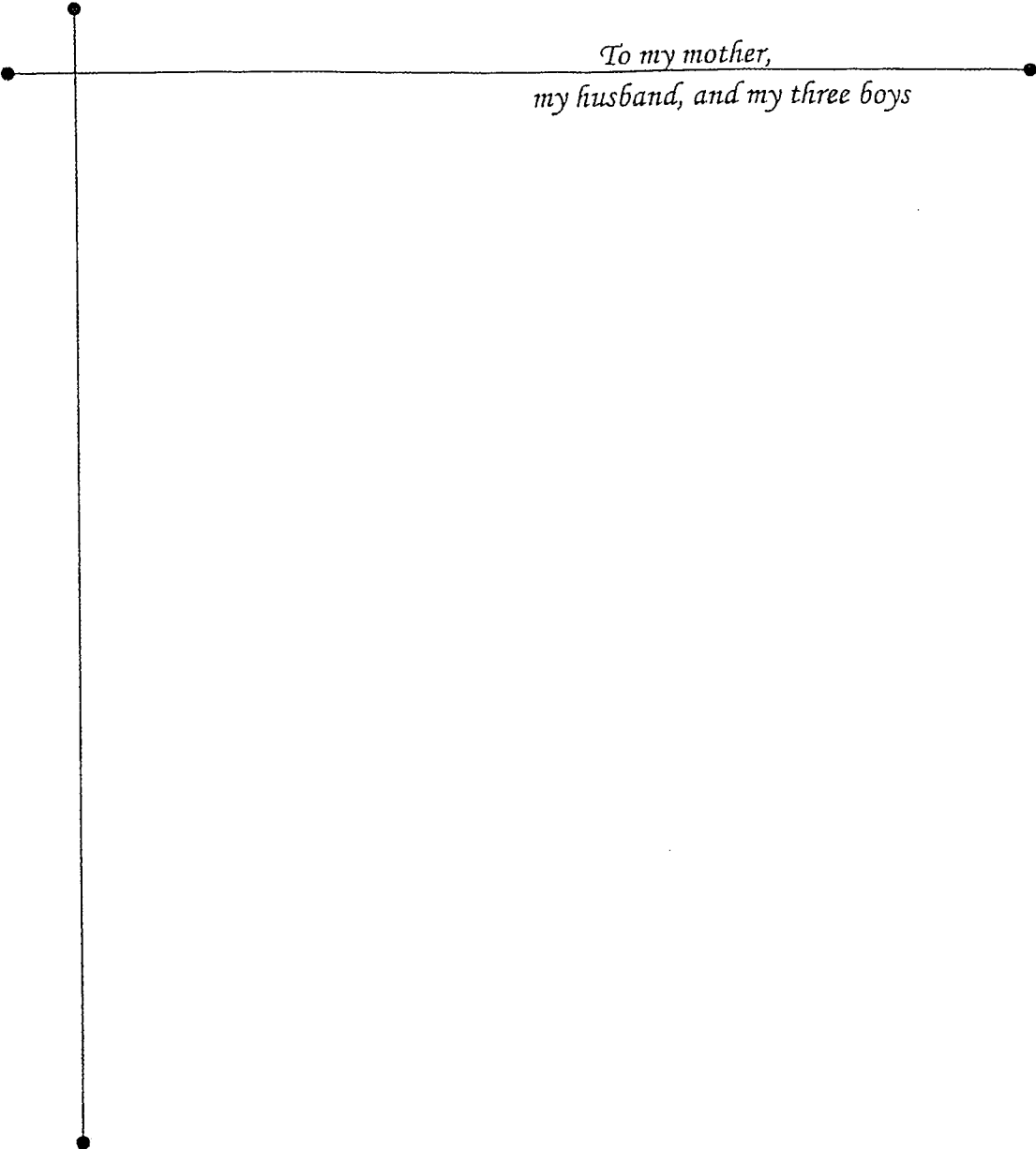In the Program of
Chemical Engineering
Ryerson University

Little information is available in literature in terms of the hydrodynamic characteristics in a turbulent bed contractor (TBC) with viscous liquids. In this study, the hydrodynamic characteristics in three–phase turbulent bed contactor with counter current flow of air and non-Newtonian liquid was studied and compared with that of Newtonian liquid under consistent conditions. Aqueous solutions of carboxy methyl cellulose (CMC) with apparent viscosities ranged between 5 to 25 cP were used as non-Newtonian liquid. The hydrodynamic parameters investigated were: bed pressure drop, minimum fluidization velocity, liquid holdup, bed expansion, and gas holdup. The effect of rheological properties of the CMC aqueous solutions and operating parameters on hydrodynamic characteristics of the TBC were examined. Results showed that increasing CMC concentration increased the net pressure drop across the bed and the liquid holdup, while the gas holdup and bed expansion decreased. At that quoted apparent viscosity range, aqueous solutions of CMC behaved as Newtonian viscous liquids in the TBC.

# ACKNOWLEDGEMENTS

*To my mother,*
*my husband, and my three boys*

vi

# Table of Contents

# LIST OF TABLES

# LIST OF FIGURES

## APPENDIX A

xx

xxii

# NOMENCLATURE

| Symbol | | Units |
|---|---|---|
| **English** | | |
| | | |
| $Ar$ | Archimedes number | Dimensionless |
| $D$ | Column inside diameter | m |
| $d_P$ | Packing diameter | mm |
| | | m (in Equations) |
| $\dfrac{dv}{dx}$ | Rate of deformation | $s^{-1}$ |
| $f$ | Open area fraction | Dimensionless |
| $Fr_L$ | Froude number, in liquid $(G_L / \rho_L)^2 / g d_P$ | Dimensionless |
| $g$ | Acceleration due to gravity | $m/s^2$ |
| $G_L$ | Liquid mass flow rate per unit area | $kg/m^2.s$ |
| $H$ | Expanded bed height | m |
| $H_S$ | Static bed height | m |
| $H_S / D$ | Relative static bed height | Dimensionless |
| $H / H_S$ | Relative expanded bed height | Dimensionless |
| $k$ | Fluid consistency factor | $Pa.s^n$ |
| $L$ | Liquid volumetric flow rate | gpm |
| $n$ | Fluid behavior index | Dimensionless |
| $\Delta P$ | Net pressure drop | kPa |
| $Re_L$ | Reynolds number in liquid, $d_P G_L / \mu_L$ | Dimensionless |
| $S$ | Cross sectional area of column | $m^2$ |
| $U_{mf}$ | Minimum fluidization velocity | m/s |

| | | |
|---|---|---|
| $U_g$ | Superficial gas velocity | m/s |
| $U_L$ | Liquid velocity | m/s |
| $W$ | Weight of the packing | kg.m/s$^2$ |

**Greek**

| | | |
|---|---|---|
| $\varepsilon_0$ | Static bed voidage | m$^3$/m$^3$ |
| $\varepsilon$ | Bed voidage | m$^3$/m$^3$ |
| $\varepsilon_{L,St}$ | Liquid holdup based on static bed volume | m$^3$/m$^3$ |
| $\varepsilon_L$ | Liquid holdup based on expanded bed volume | m$^3$/m$^3$ |
| $\varepsilon_g$ | Gas holdup based on expanded bed volume | m$^3$/m$^3$ |
| $\varepsilon_{g,St}$ | Gas holdup based on static bed volume | m$^3$/m$^3$ |
| $\varepsilon_S$ | Solid holdup based on expanded bed volume | m$^3$/m$^3$ |
| $\varepsilon_{S,St}$ | Solid holdup based on static bed volume | m$^3$/m$^3$ |
| $\rho_S$ | Packing density | kg/m$^3$ |
| $\rho_L$ | Liquid density | kg/m$^3$ |
| $\rho_g$ | Gas density | kg/m$^3$ |
| $\tau$ | Shear stress | N/m$^2$ |
| $\gamma$ | Shear rate | $s^{-1}$ |
| $\gamma_{eff}$ | Effective shear rate | $s^{-1}$ |
| $\mu_L$ | Liquid viscosity | Pa.s |
| $\mu_{L,eff}$ | Effective or apparent liquid viscosity | Pa.s |
| $\mu_g$ | Gas viscosity | Pa.s |
| $\sigma$ | Surface tension | N/m |

**Abbreviations**

| | |
|---|---|
| CMC | Carboxy methyl cellulose |
| TBC | Turbulent bed contactor |

# CHAPTER 1

# INTRODUCTION

## 1.1 Fluidization Phenomena

The term "fluidization" was invented to describe a certain mode of contacting granular particles with fluids (gas or liquid). The particles are contained in a column with porous bottom. As the fluid is passed upward through the porous bottom into the bed, there is a certain rate of flow at which the particles are just suspended. In this condition the particles are disengaged somewhat from each other and moved around. In its mobility the suspended bed resembles a liquid of high viscosity with a characteristic hydrostatic head. These properties, reminiscent as they are of the properties of liquids, make it appears that the particles bed has been "rendered fluid". Hence the operation of achieving this is termed "fluidization".

Several researchers have studied fluidization characteristics over the last decades (Othmer (1956); Zenz and Othmer (1960); Kunii and Levenspiel (1991); Leva (1959); Epstien (1981); and Fan (1989)).

Based on the state of particles motion, three operational regimes in a bed of particles with a fluid (gas, liquid, or both) flow were described by Fan (1989).

1. Fixed bed regime: when the drag force on the particles from fluid flow is less than the weight of the particles and therefore, the particles remain motionless.

2. Expanded bed regime: with an increase in gas/liquid velocity the drag force counterbalances the weight of the particles, the bed is in the state of minimum fluidization, which marks the minimum fluidization velocity, and operation is in the expanded bed regime.

3. Transport regime: when the drag force is greater than the terminal velocity of the particles in gas/liquid medium and therefore the particles are transported from the bed.

The pressure drop across the bed increases sharply through the fixed bed regime with increasing superficial gas velocity. When the pressure drop begins leveling off, the bed is in the expanded bed regime. Fluidization can be with two phases of liquid-solid or gas-solid, and

with three phases of gas-liquid-solid. The advantages of fixed bed systems over fluidization bed systems are low macro mixing yielding small axial dispersion of phases; high controllability over product selectivity for complex reactions; low solids attrition and consumption, hence permitting precious metal catalysts to be used for the reaction. The major advantages of fluidization systems over fixed bed systems are high macro mixing, yielding large axial dispersion of phases; ability in achieving significant temperature uniformity without the aid of external means; ease in heat supply and removal, hence temperature controllability; ease in catalyst replacement and hence high controllability of catalyst activity and minimum flow maldistribution (Fan, 1989).

## 1.2 Three Phase Fluidization

Gas-liquid-solid fluidization became a subject for fundamental research only about three decades ago. Gas-liquid-solid fluidization systems are fields where solid are in non-stationary state. These fluidization systems encompass both the expanded bed and transport regimes. It can be classified mainly into four modes of operation (Fan, 1989), these modes are shown in Figure 1-1: co-current three phases fluidization with liquid as the continuous phase (mode I-a); co-current three phases fluidization with gas as the continuous phase (mode I-b); counter-current three phase fluidization with liquid as the continuous phase and the liquid density exceeds the solids density (mode II-a); counter-current three phase fluidization with gas as the continuous phase and the liquid density usually significantly exceeds the solid density (mode II-b). The vigorous movement of wetted particles gives rise to excellent gas – liquid contacting. The state of gas–liquid–solid fluidization is strongly dependent on the geometry of the bed, methods of gas-liquid injection and the presence of a retaining grid or internals. Gas-Liquid-Solid fluidized beds have emerged in recent years as one of the most promising devices for three-phase operation as evidenced in its wide use for chemical, petrochemical, electrochemical and biochemical processing. Most notably, three-phase fluidization beds have been fully developed and demonstrated in processing technology; as three–phase reactors, they have been employed for the hydrogenation and hydro-desulfurization of residual oil, coal liquefaction, turbulent contacting absorption for flue gas desulfurization, and the biooxidation process for waste water treatment. Early reviews of gas–liquid–solid fluidization applications were made by Ostergaard (1977), Fan (1989) and Epstein (1981).

2

| Mode | I-a | I-b | II-a | II-b |
|---|---|---|---|---|
| Schematic Diagram of Gas-Liquid-Solid Fluidization | | | | |
| Continuous Phase | Liquid | Gas | Liquid | Gas |
| Flow Direction | Coccurent Up-flow | | Countercurrent flow | |
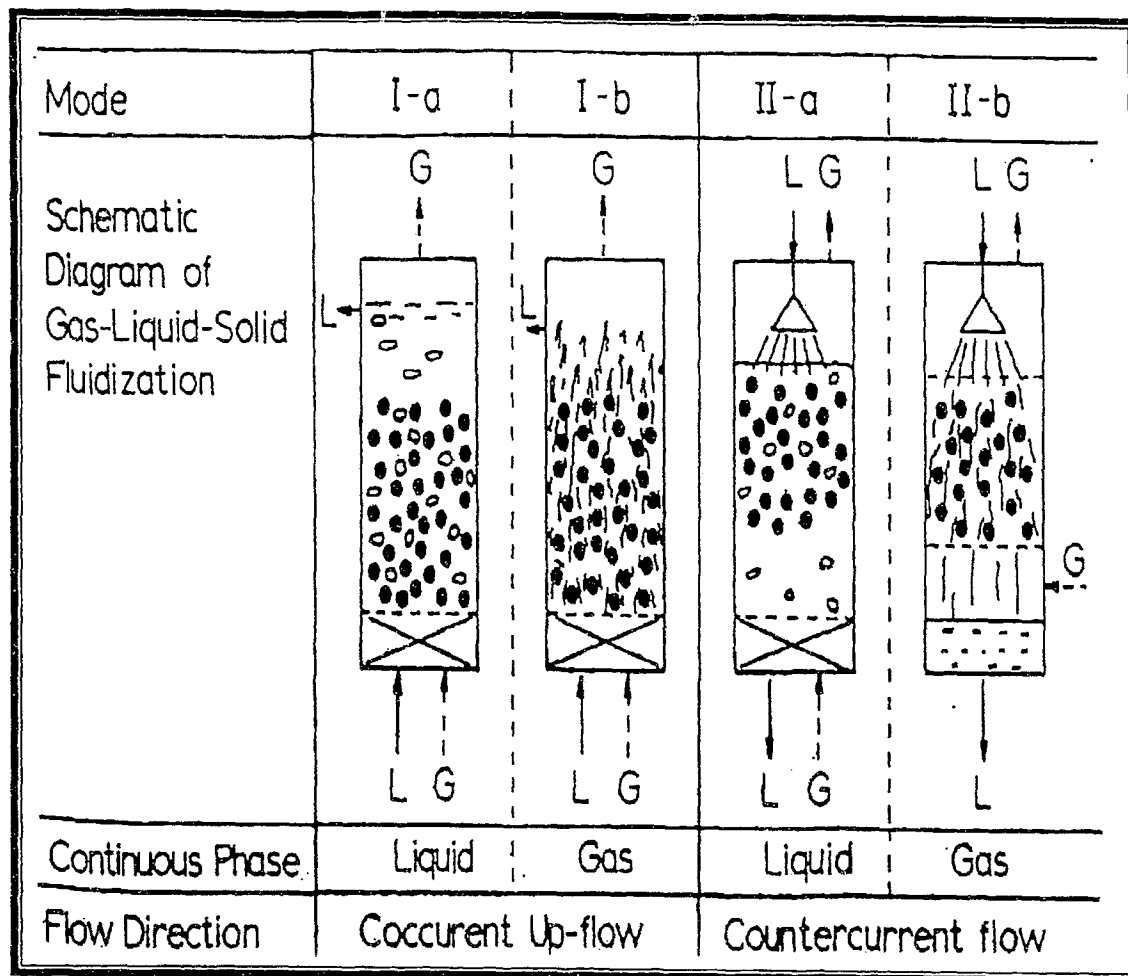
Figure 1-1 Three-phase fluidization modes of operation, Fan (1989).

3

## 1.3 Turbulent Bed Contactor

A turbulent bed contactor (TBC) is a countercurrent three phase fluidized bed with gas usually serving as the continuous phase and liquid as the dispersed phase. Inert particles are used to enhance the contact between the flowing fluid phases. Gas continuous fluidized beds have been used as contactors for such industrial applications as scrubbing and absorption. The gas and liquid flow rates in the TBC are much higher than those possible in conventional countercurrent packed beds, since the bed can easily expand to reduce the hydrodynamic resistance so the bed doesn't flood even at high flow rates of the gas and the liquid. TBC's are of high mass and heat transfer rates while capital costs are much lower than those of packed towers for a given throughput (Muroyama and Fan, 1985). TBC's have been effective in removing particulate material in gas or liquid streams without the plugging tendency of the fixed bed (Douglas, 1964). A TBC has been used for physical, chemical, and biochemical processing. In physical processing, it is used for air-cooling, humidification or dehumidification, particulate removal, and lactose granulation. In chemical processing, it has tremendous potential for flue gas desulfurization, absorption, scrubbing, desorption and distillation. In biochemical processing, it is used for alcohol fermentation. Disadvantages of TBC's include higher operating costs due to increased gas velocities, vibrational problems and erosion of the fluidized packing (Vunjak–Novakovic et al., 1987a). TBC's are also susceptible to gas by–passing or channeling and back mixing in the liquid phase with the attendant loss in the driving force advantage of countercurrent flow. It has a strong slugging tendency, which can result in prohibitive vibration effects. The hydrodynamic behavior of TBC's is a complex subject which includes three areas, i.e., the general bed behavior, the mechanics of bubbles and bubble wakes, and flow models. The description of general bed behavior includes observation about pressure drop, minimum fluidization velocity, phase holdups, flow regimes, solids wettability, and bed rheology. Most of the data reported have been obtained over a narrow range of operation variables or related to some specific gas – liquid contacting process, hence, not always consistent and comparable.

Differences existed in material and density of particles, particle size, column to particle diameter, and the open area of supporting grid.

4

## 1.4 NON-NEWTONIAN FLUIDS

Fluids may be classified according to the effects produced under the action of a shear stress. They are classified as Newtonian if there is a linear relation between the magnitude of the applied shear stress and the resulting rate of deformation, that is, $\tau \propto dv/dx$. In non-Newtonian fluids, there is a nonlinear relationship between the magnitude of the applied shear stress and the rate of deformation. When the shear rate is varied, the shear stress doesn't vary in the same proportion or even in the same direction. The viscosity of such fluids will therefore change as the shear rate is varied. The viscosity of Newtonian fluids such as air and water is independent of the shear rate, while non-Newtonian fluids exhibit viscosity characteristics that are a function of shear rate. Non-Newtonian effects can play a dramatic role in modelling already complex problems such as multi-phase separation due to the changing shear the fluid experiences as it progresses through the system.

Non-Newtonian fluids may be grouped into three general classes: time-independent, time-dependent, and viscoelastic fluids. Time-independent fluids may be further subdivided into three types: shear thinning or pseudoplastic, viscoplastic, and shear thickening or dilatant fluids.

Pseudoplastic is the type of fluid, which will display a decreasing viscosity with an increasing shear rate as shown in Figure 1-2. The most common fluids are paints, emulsions, and dispersions of many types. It is sometimes called "shear thinning".

Several fluidized beds operate with non-Newtonian liquids in food, polymer processing and biotechnology. Many biomedia exhibit low surface tensions and high viscosities with strongly non-Newtonian flow behavior.

Non-Newtonian behavior can be simply expressed through an equation and the coefficients of a model can be used to infer performance of a fluid under conditions of use. Non-Newtonian flow behaviors described by a power law model of Ostwald-de Waele as

$$\tau = k\gamma^n \qquad \text{Where } 0<n<1 \qquad (1\text{-}1)$$

The empirical relationship describes the shear stress $\tau$ as a function of the shear rate $\gamma$, the consistency index $k$, and the flow behavior index $n$.

The lower the value of $n$, the greater the degree of viscous non-Newtonian flow behavior or pseudoplasticity. The values of $n$ and $k$ are determined over a wide range of shear rates.

5

In Newtonian liquids, the relation between shear stress and shear rate is linear and the viscosity is evaluated independently of shear rate:

$$\tau = \mu \dot{\gamma} \tag{1-2}$$

However, the linear relation between shear stress and shear rate is not valid for pseudoplastic liquids, and the flow curve is usually expressed by the power law model.

By analogy with Newtonian liquids, the effective viscosity for the power law liquid is defined as follows:

$$\mu_{eff} = k \dot{\gamma}_{eff}^{\,n-1} \tag{1-3}$$

From the flow curve measured by a Rheometer, the corresponding average shear rate $\dot{\gamma}$ to $\mu$ can be estimated.

To estimate the effective viscosity in the fluidized bed, the effective shear rate, which originates from the relative velocity between gas and liquids, in the column has to be known. Also, the fluid consistency index $k$, and the flow behavior index $n$ must be determined. Combining these values, the effective viscosity can be obtained using equation (1-3).

Non-Newtonian media are frequently encountered in many fields. For instance, the solutions of high molecular weight synthetic polymers and foams employed in enhanced oil recovery operations are all non-Newtonian in character (Wu et al., 1992). Likewise, the micro-emulsions encountered in the production of crude also exhibit non-Newtonian fluid behavior. Other examples include the filtration of polymer melts and sewage sludges using sand pack filters, catalytic polymerization reactions, leaching of uranium from waste process streams, food processing (Shilton and Niranjan, 1993) fermentation and other bioprocessing applications (Baker et al. 1981).

6

## 1.5 Carboxy Methyl Cellulose (CMC)

CMC is cellulose ether, produced by reacting alkali cellulose with sodium monochloroacetate under rigidly controlled conditions. Figure 1-3 shows the structure of CMC (with degree of substitution of 1.0). It is a long chain polymer, as the molecular weight increases, the viscosity of CMC solutions increases rapidly. Solutions of all CMC types are shear thinning and the rheological behavior is usually characterized by the Ostwald-deWaele (or power law) model. The rheological properties of CMC are strongly related to the molecular weight and concentration. CMC is available in low, medium, high viscosity form. They have rheological properties similar to "real" industrial media like fermentation broths and liquid suspensions of small particles. CMC is often used to thicken, suspend, stabilize, gel or modify the flow characteristics of aqueous solutions or suspensions. Small amount of CMC dissolved in water greatly modify its properties. The most obvious immediate change is an increase in viscosity. These properties and functions make it suitable for use in a broad range of applications in the food, pharmaceutical, cosmetics, paper, and other industries.

The physical properties of the CMC solutions differ only slightly from those of water. In general, effective viscosities range between 1 and 3000 mPa.s at 20°C, for CMC solutions of (0-8wt %) concentrations. For the quoted range of effective viscosities, density varies from 998.23 to 1004 $kg/m^3$ and the surface tension is between 0.065 and 0.079 N/m (Schumpe et al. (1989)). Few researchers have studied the rheological behavior of the different kinds of carboxy methyl cellulose aqueous solutions such as Gomez-Diaz and Navaza (2002), Cheng and Shao-yen (1995). These studies concluded that these solutions have non- Newtonian pseudoplastic behavior practically in all cases, and have high shear stability over long periods.

7
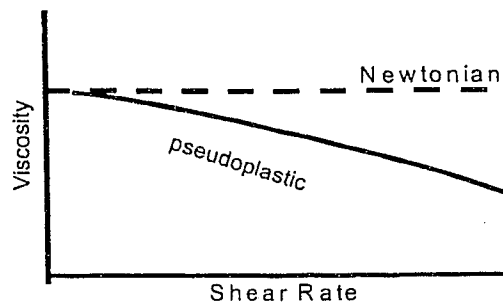
Figure 1-2 Effect of shear rate on viscosity for pseudoplastic liquids.
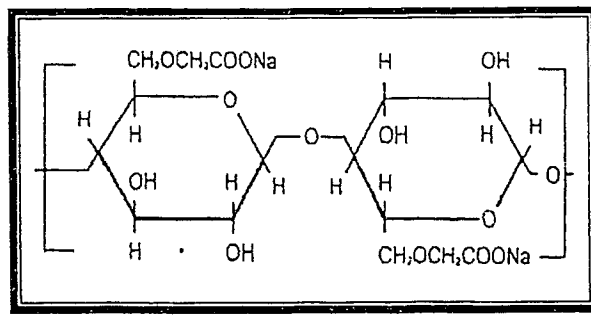


Figure 1-3 CMC structure (Hercules).

8

## 1.6 Research Objective

The hydrodynamic characteristics in three-phase turbulent bed contactor (TBC) with counter current flow of gas and liquid has been studied. However, few works have been published deal with effect of viscosity of Newtonian liquids on hydrodynamic parameters in a turbulent bed contactor. No work has been reported on hydrodynamic bed characteristics of turbulent bed contactor under countercurrent flow of gas and liquid with non-Newtonian liquids. Therefore, this study was conducted to investigate the effect of rheological properties of non-Newtonian liquids (CMC aqueous solutions) on bed hydrodynamic parameters under different operating variables. These parameters are the net pressure drop, minimum fluidization velocity, liquid holdup, bed expansion, and gas holdup. In addition, the effect of gas and liquid flow rate, static bed height, and particle properties were examined at various rheological parameters.

9

# CHAPTER 2

# LITERATURE REVIEW

This Chapter summarizes the literature relevant to this study, which concerns the hydrodynamics of the turbulent bed contactor with Newtonian and Non-Newtonian liquids.

## 2.1 Introduction

Countercurrent three-phase fluidization with gas as the continuous phase was first described by Keilback (1959). He demonstrated this mode for industrial purposes and gave the contactor the name "floating bed scrubber". It has been given a variety of names. Douglas (1964) refers this type of fluidization as a "turbulent bed contactor" (TBC), Tichy and Douglas (1972) as a "mobile bed contactor", O'Neill et al. (1972) as a "fluidized packing contactor". The English literature refers it as a "turbulent contact absorber" (TCA). The process has been widely used as an alternative to the conventional packed bed in absorption, distillation, cooling and humidification, and pollution control. Numerous studies of the hydrodynamics of the TBC dating back to sixties. Many empirical correlations have been published on the hydrodynamics of the TBC. Much of the literature on TBC's prior to 1989 has been summarized by Fan (1989).

## 2.2 Hydrodynamics of Turbulent Bed Contactor (TBC)

Our focus would be on those aspects that are relevant to our objectives.

### 2.2.1 Types of Operation

Two types of TBC operation were identified by O'Neill et al. (1972). In type I operation (fluidization without incipient flooding), low density particles less than 300 $Kg/m^3$ are used and the onset of fluidization occurs at a gas velocity lower than the flooding point for the equivalent countercurrent packed bed. In type II operation (fluidization due to incipient flooding), particles with a density greater than 300 $Kg/m^3$ are used and the onset of fluidization occurs at flooding point (incipient flooding). The flooding point here refers to the state in which the entire voidage of the packed bed are filled with liquid, which corresponds to the upper bound of operation of a conventional packed bed. For beads density greater than, 1300 $Kg/m^3$ fluidization is impossible.

The type of operation depends largely on particle density and to a lesser extent on particles diameter, and liquid flow rate. Vunjak-Novakovic et al. (1987a) using air-water systems

10

reported that for a given particle size, the required particle density for demarcation of operations decreases with increasing liquid flow rate, and it decreases with decreasing particle size for a given liquid flow rate. O'Neill et al. (1972) had stressed the advantages of operating in the incipient flooding regime because it results in conditions of higher interfacial contact of gas and liquid unless the pressure loss is too high to be acceptable for the particular application. In that case type I with a much lower pressure loss may be used. Some discrepancies in the earlier work have been eliminated by the knowledge of the two types of operation.

## 2.2.2 Bed Pressure Drop

The pressure drop through the bed, the most important parameter in TBC operation, determines the energy consumption required during operation and characterizes the hydrodynamic behavior of the system.

A common feature of the studies is that they equate the pressure drop in TBC to the sum of the weights per unit area of packing and liquid holdup, independent of mode of operation, or

$$\Delta P = (\rho_S \varepsilon_S + \rho_L \varepsilon_L) g H \tag{2-1}$$

$$\Delta P = (\rho_S \varepsilon_{S,St} + \rho_L \varepsilon_{L,St}) g H_S \tag{2-2}$$

The pressure drop due to the weight of the dry packing is constant, but that due to liquid hold up is a function of operating conditions and the geometry of the system (supporting grid open area, column diameter, and bed internals).

Although there is agreement on the form of equation (2-1) and (2-2), there are discrepancies in the effect reported of some variables of these studies. For example, Rama et al. (1983) claimed that the pressure drop in the fully fluidized state is almost independent of gas velocity. Tichy and Douglas (1972) found the pressure drop to be independent of packing size. On the other hand, Barile and Meyer (1971) reported that pressure drop increases with decreasing packing size. Thus, Barile and Mayer's results consistently show an effect of packing size. Kito et al. (1976e) and Wozniak (1977) reported that pressure drop is affected by packing height through its effect on liquid holdup. Guerriere et al. (1995) reported that pressure drop increases consistently with increasing liquid flow rate, and to increase with increasing gas velocity at low bed

11

heights and to decrease slightly with increasing gas velocity at high bed heights and high liquid flow rates. At mid-range bed heights and liquid flow rates, pressure drop approached being independent of gas velocity. For small grid open areas the pressure drop sharply increases with gas velocity (Blyakher et al., 1967, and Balabekov et al. 1969b). Soundarajan and Krishnaiah (1998) reported that pressure drop across each stage in a multi-stage TBC increased with increasing in gas and liquid velocities, particle density and static bed height, and with decrease in free open area of the supporting grid.

Many investigators, Barile and Mayer (1971), O'Neill et al. (1972), Tichy and Douglas (1972), Uysal (1978), Vunjak-Novakovic et al. (1980, 1987a, b) have used forms of equations (2-1) and (2-2) in their pressure drop correlations. Other correlations are purely empirical in nature.

Many empirical correlations for the pressure drop of the TBC are found in the literature, and are summarized by Fan (1989).

### 2.2.3 Minimum Fluidization Velocity

Several definitions can be found in the literature for the minimum fluidization velocity. Kito et al. (1976d) defined the minimum fluidization velocity as the gas velocity at which the rapid increase in pressure drop through fixed bed region starts to level off and reaches constant value. Chen and Douglas (1968) defined the minimum fluidization velocity at which the bed expansion begins. The conventional method of determining minimum fluidization velocity is from pressure drop data by finding the value of the superficial gas velocity at which the fixed bed and fluidized bed curves intersect. Another common method is the expanded bed height method, which involves the extrapolation of expanded bed height versus the superficial gas velocity curve to the point where the expanded bed height equals the static bed height. The latter method is limited by the difficulty of discerning the top of the expanded bed height of a TBC, especially in the slugging regime. The geometry of the experimental system, especially the open area of the supporting grid, as well as the operating conditions has significant effect on minimum fluidization velocity.

Tichy and Douglas (1972), Kito et al. (1976e) and Rama et al. (1983) reported that transition from fixed to fluidized bed behavior progresses very gradually. The transition range increases with an increase in static bed height and decreases with an increase in liquid flow rate.

12

Vunjak-Novakovic et al. (1987) also observed the transition range. He referred to as partial fluidization. It was reported by Chen and Douglas (1968), Kito et al. (1976), Vunjak-Novakovic et al. (1987a), that the minimum fluidization velocity decreases with increasing liquid flow rate and with increasing packing diameter. Kito et al. (1976d) reported that the minimum fluidization velocity increases with increasing packing density, and it is independent of static bed height and independent of grid open area which was in contrast with Gel'perin et al. (1968b) who reported that minimum fluidization velocity is a function of the open area of the grid. Guerriere et al. (1995) found that minimum fluidization velocity is independent of static bed height, and dependency on particle diameter was not consistent. Many correlations for estimating minimum fluidization velocity are purely empirical. Different models were applied to estimate minimum fluidization velocity, which may yield different correlation equations.

### 2.2.4 Liquid Holdup

The liquid holdup is a complex function of process variables such as the gas and liquid velocities, the properties of the packings, the characteristics of the supporting grid, and the physical properties of the liquid. It is a balance of viscous, gravity, and surface tension forces.

It is the amount of liquid retained per unit cross sectional area of the bed. The liquid hold up in a TBC consists of the operational or dynamic hold up and static holdup. The static liquid holdup is that clings to the column wall and other stationary surfaces. It is not supported by the gas stream and therefore doesn't contribute significantly to the pressure drop. There are several methods of liquid holdup measurement described in the literature: the transient tracer response method, the shut-off method, and the pressure drop method. Ercan et al. (1989) recommended that the pressure drop method using pressure transducers is accurate and easy.

Chen and Douglas (1968) found that liquid holdup is independent of gas flow rate, but increase with increasing liquid flow rate and with decreasing packing size. Kito et al. (1976e, 1978) and Kuroda and Tabei (1981) studied the effect of open area of supporting grid on the liquid holdup. Vunjak–Novakovic and Vukovic (1980) developed liquid holdup correlations for the two types of fluidization. Guerriere et al. (1995) modified pressure drop method of liquid holdup determination by incorporating the fluidization index. However, liquid holdup results showed significant departure from the literature. Soundarajan and Krishnaiah (1998)

13

analyzed the correlations reported in the literature and concluded that the liquid holdup increases with increase in liquid velocity, and with decrease in free open area of the supporting grid, static bed height and diameter of the particle. O'Neill et al. (1972) claimed that liquid holdup increases with increasing gas velocity.

Bruce et al. (2004) found that liquid holdup is almost independent of gas velocity, increased with increasing in liquid flow rate, decreased with increasing in particle diameter, static bed height and free open area of the distributor plate for type I operation.

Many correlations proposed by researchers based on ranges of applicability and validity.

## 2.2.5 Bed Expansion

Bed expansion is an important design parameter. Some of the measurement techniques that are used in literature to obtain the data are: visual observation of the expansion and analysis of photographs taken with a high-speed camera. Chen and Douglas (1968) reported that the bed height increases linearly with increasing gas velocity and also increases with increasing liquid velocity. Two regions of bed expansion have been reported by Gel'prin et al. (1968b) and Balabekov et al. (1969b). Tichy and Douglas (1972) reported that the reduced bed height $H/H_S$ is independent of both the static bed height and the packing density, while the open area of the distributing grid affects the bed expansion. Vunjak-Novakovic et al. (1987b) developed correlations for type I and type II operations. Soundarajan and Krishnaiah (1998) claimed that bed expansion for each stage in a multi-stage TBC increased with increase in liquid and gas velocities and with decrease in free open area of the supporting grid.

Theory is very limited concerning bed expansion so the data are correlated in terms of empirical correlations (Muroyama and Fan (1985)). These correlations do not give reliable predictions because they are limited to specific experimental conditions and show considerable range of disagreement in the values predicted. The importance of the various operating variable varies considerably from one correlation to another. The measurement of expanded bed height in a TBC is limited by the significant tendency toward slugging. Except at minimum fluidization conditions, a certain degree of oscillation is always present. The most common measurement method used in the literature is simply observing maximum and minimum heights over a period of time and estimating an average.

14

## 2.2.6 Gas Holdup

It is the amount of gas retained per unit cross sectional area of the bed. Limited information is available in literature regarding gas holdup in TBC's. Balabekov et al. (1969b) showed that gas holdup increased with increasing gas velocity, but independent of liquid velocity at a constant gas velocity. He proposed an equation to determine the gas holdup when expanded bed height and liquid holdup are known. Gel'perin et al. (1968b) conducted the earliest studies of gas holdup using heavy particles with grids having small open areas. Kito et al. (1978) reported that the gas holdup is nearly independent of packing density, liquid viscosity and static bed height. In addition the gas holdup increases with increasing gas velocity, but it is unaffected by the liquid velocity and the opening area of the supporting grid. Vunjack–Novakovic et al. (1987b) proposed empirical correlations for gas holdup for partially and fully fluidized beds. Soundarajan and Krishnaiah (1999) reported that gas holdup in a single TBC stage increases with increase in gas velocity and is almost independent of particle density, free open area, static bed height, and liquid velocity for the type I and type II operations. Several correlations for gas holdup in a TBC are given in Fan (1989). The correlation by Kito et al. (1978) covers a wide range of physical properties of particles and operating conditions.

15

## 2.3 Turbulent Bed Contactor with Viscous Media

A large body of knowledge on three-phase fluidization with non-Newtonian liquids exits in the literature, the majority of which deals with liquid continuous systems with cocurrent flow configuration. Cocurrent systems with non-Newtonian liquid phase have been studied extensively and have been used in abroad range of applications. A substantial amount of information and excellent reviews is available in the published literature (Patwari et al. (1986), Dharwadkar and Sawart (1987), Kawase et al. (2001)).

The performance of turbulent bed contactor under the condition of Newtonian liquid stagnant flow was studied by Kito et al. (1976). The dependence of gas holdup, mass transfer coefficient and the interfacial area on process variables was investigated. The process variables were gas flow rates, the free opening area of the supporting grid, the diameter and density of packing, the liquid properties and static packing heights. A sieve plate and perforated plate with free opening areas of 31.5% and 1.27% were used. Spheres used had diameters of 1.1 cm, 2.65 cm and 2.87 cm, and densities of 1 g/cm$^3$ and 0.5 g/cm$^3$. The static packing height was varied from 5 cm to 20 cm. Liquids used were water, 25 wt% glycerol solution, 45 wt% glycerol solution, 65 wt% glycerol solution, 80 wt% glycerol solution, methanol, and ethanol. Liquid viscosity varied from 1.00 cP to 60 cP. All liquids have Newtonian behavior. Surface tension forces of the liquids were varied from 22 dyne/cm to 70 dyne/cm. In the fully fluidized mobile bed, the free opening of the supporting grid, the density and diameter of the packings, the diameter of the bed, and the viscosity of the liquid affected very little if any on the gas holdup. The interfacial area increased with increasing gas velocity. Empirical correlations were determined for gas holdup and interfacial areas.

Kito et al. (1978) examined the dependence of liquid and gas holdup on physical properties of liquid such as viscosity and surface tension. Effect of other variables such as liquid and gas velocities, the diameter of particles, the characteristics of the supporting grid, and static bed height on liquid and gas holdup were studied. The system investigated was a turbulent bed contactor. Sieve plates were used as the supporting grid with 71%, 70.5% and 84% free opening area. The diameter of fluidized spheres was 0.97 cm, 1.16 cm, and 2.85 cm. The static

16

bed height of packing was varied from 10 cm to 30 cm. Liquids used were water, 25 wt% glycerol solution, 65 wt% glycerol solution, and ethanol. All were with Newtonian character. Liquids viscosities were varied from 1.00 cP to 14.45 cP. The liquid surface tension was varied from 22.5 dyne/cm to 72.8 dyne/cm. The gas holdup was found to be unaffected by the liquid viscosity, the free opening of the supporting grid, the static bed height and the packing diameter. The liquid viscosity and the surface tension forces of the liquid affected the liquid holdup. Correlations were presented for the gas and liquid holdups in terms of independent process variables.

Kuroda and Tabei (1981) investigated empirically the effect of the physical properties of the liquid on the minimum fluidizing velocity and the apparent coefficient of friction in a turbulent bed contactor on the basis of the equation of motion for one dimensional, two-phase flow in a gas-liquid system. The turbulent bed contactor was of 10 cm internal diameter. The particles used ranged in diameter from 1 cm to 2.85 cm and in density from 0.17 g/cm$^3$ to 0.76 g/cm$^3$. Metal screens and porous plate as the supporting grid with 71.2%, 70.5%, 84%, and 4% free opening area were used. Liquids of water, 25 wt% glycerol solution, 65 wt% glycerol solution and ethanol were used. All liquids were with Newtonian behavior. Their viscosities ranged from 1.00 cP to14.45 cP. The apparent coefficient of friction was found to decrease as the gas velocity increased or as the liquid velocity and liquid viscosity decreased. The minimum fluidizing gas velocity decreased while the velocity and viscosity of the liquid increased. Correlations were derived theoretically to express the minimum fluidizing gas velocity in terms of the apparent coefficient of friction and another, which gave the relation between the apparent coefficient of friction and the liquid holdup.

Tabei and Kuroda (1998) studied the effect of gas and liquid velocities, packing density, static bed height, column diameter and liquid viscosity on axial mixing in a mobile bed. Axial dispersion coefficient was evaluated by a pulse response method experimentally. The liquid used was 25 wt % glycerol, 65 wt % glycerol, and water. All solutions were Newtonian. The axial dispersion coefficient of liquid flow increased with increasing the liquid viscosity, and the column diameter. It decreased with increasing static bed height.

17

The literature above shows that limited number of studies is available in literature on topic of this research.

# CHAPTER 3

# EXPERIMENTAL WORK

The turbulent bed contactor (TBC) and experimental setup used in the present study was designed and built at Ryerson by Guerriere et al. (1995). It was modified by the author to accommodate the research objectives. A data acquisition system was integrated with the experimental setup to monitor, record, and manipulate the experimental parameters.

A schematic of the experimental setup is given in Figure 3-1.

This chapter is consisted of two main sections: Experimental System and Experimental Methodology.

## 3.1 Experimental System

### 3.1.1 TBC Column

The TBC column was made of clear acrylic to facilitate visual observation with inner diameter of 29 cm and a height of 1.3 m. An open section had been made in the side of the acrylic column to allow for the addition and removal of different beads to the fluidized bed.

A supporting grid was placed at the bottom of the bed to support the solid beads. A mist eliminator made of plastic mesh was located at the top of the column to minimize liquid droplets entrained in the air within the TBC. The bottom of the liquid distributor was located 92 cm from the supporting grid. The lower column, the region below the supporting grid to the air entrance, was constructed of PVC. This 90 cm long region was used to straighten the airflow, by means of small sections of plastic straws, and as an exit for the downward flowing liquid. A picture of the TBC is shown in Figure 3-2. The fluidized beads were hollow polypropylene spheres. Beads densities and diameters were chosen so that fluidization was under type I and type II operations. Table 3-1 shows dimensions of the columns, the properties of the beads, and the grid specifications. The humidification tower has a diameter of 0.46 m and height of 1.2 m was packed with saddle packing to a height of 65 cm. The water distributor was located 50cm from the bottom of the tower. A valve controlled water entering and the flow of liquid could be monitored using inline rotameter. The air entering the bottom of the tower, exiting from the top.

19
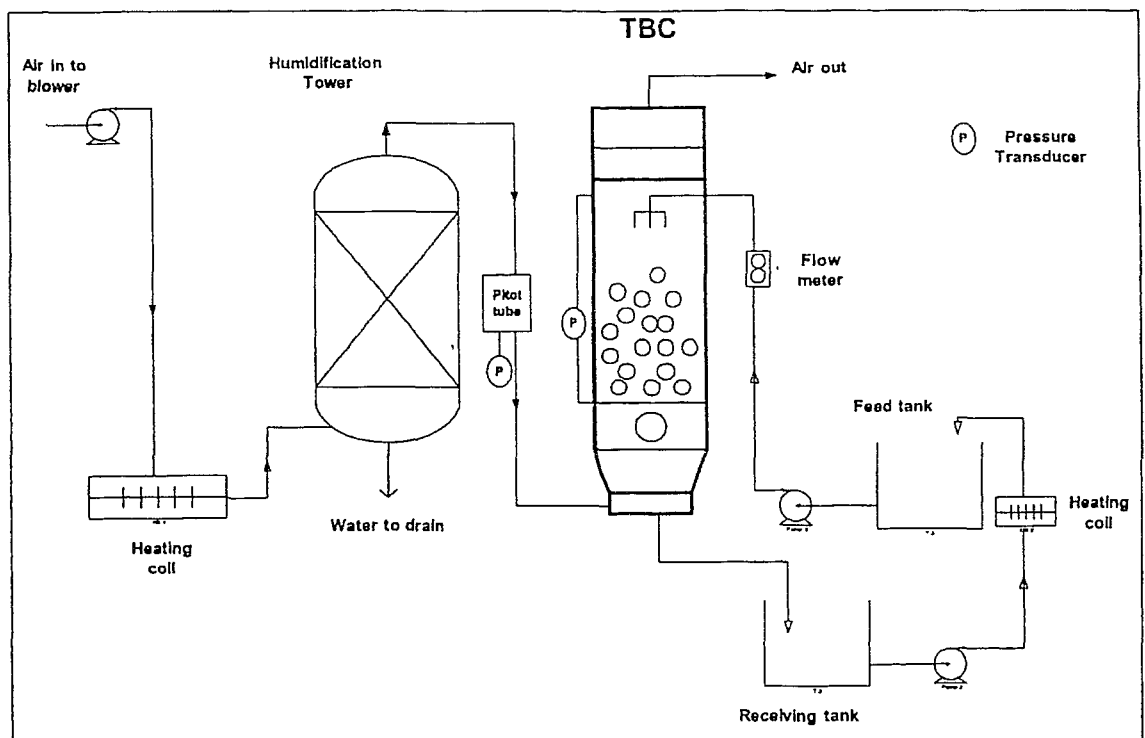
Figure 3-1 Experimental Set up

20
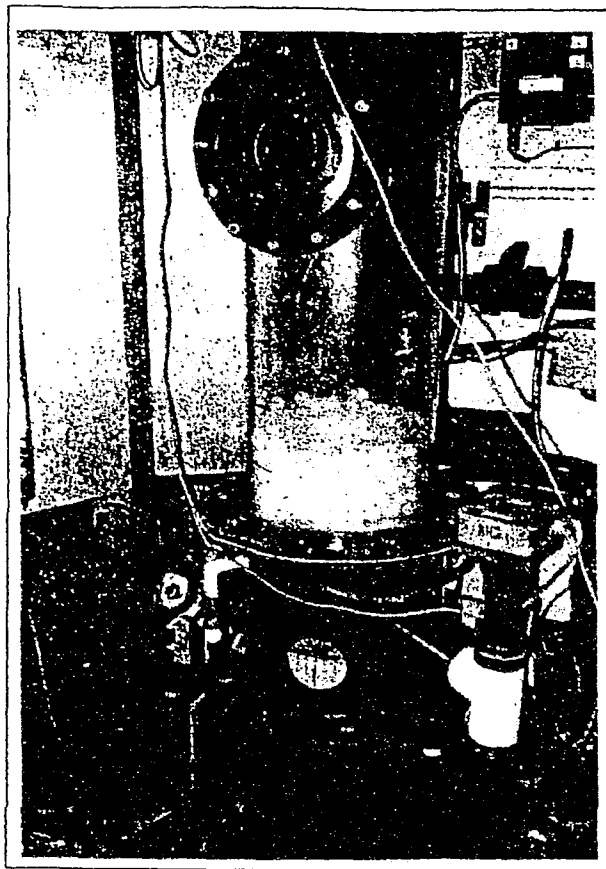
Figure 3-2 TBC Column

21

| Column Dimensions | | |
| --- | --- | --- |
| | | |
| | Diameter (mm) | Length (m) |
| TBC | 290 | 1.3 |
| Humidification Tower | 460 | 1.2 |
| | | |
| Grid | | |
| | | |
| Wire Diameter (mm) | 0.64 | |
| Wire Spacing (mm) | 1.34 x 1.92 | |
| Open area | 35% | |
| | | |
| | | |
| Beads Properties | | |
| | Diameter (mm) | Density (kg/m$^3$) |
| Beads 1 | 20 | 315 |
| Beads 2 | 26 | 380 |
| Beads 3 | 38 | 177 |

Table 3-1 Experimental Specifications

22

### 3.1.2 Bed Pressure Drop

Bed pressure drop was measured between a level just below the grid and one at the top of the acrylic section. At each level four pressure taps were equally spaced radially around the column. The taps were connected to sides of the differential pressure transducer (MKS Baretron model 220B) to measure time-averaged values of pressure drop. Frequent calibration checks against a manometer proved good instrument stability. This system measured the total pressure drop in the column between the two levels of pressure taps. The net pressure drop across the bed was obtained from the total pressure drop by subtracting the pressure drop in the empty column. The empty column pressure drop was due to friction of the internals of the column (wall, the grid, and liquid distributor). It was measured by running the column empty. Pressure drop in the empty column is shown in Figure 3-3.



$$P_{empty} = 0.0063U^2 + 0.0009U$$
$$R^2 = 0.9999$$
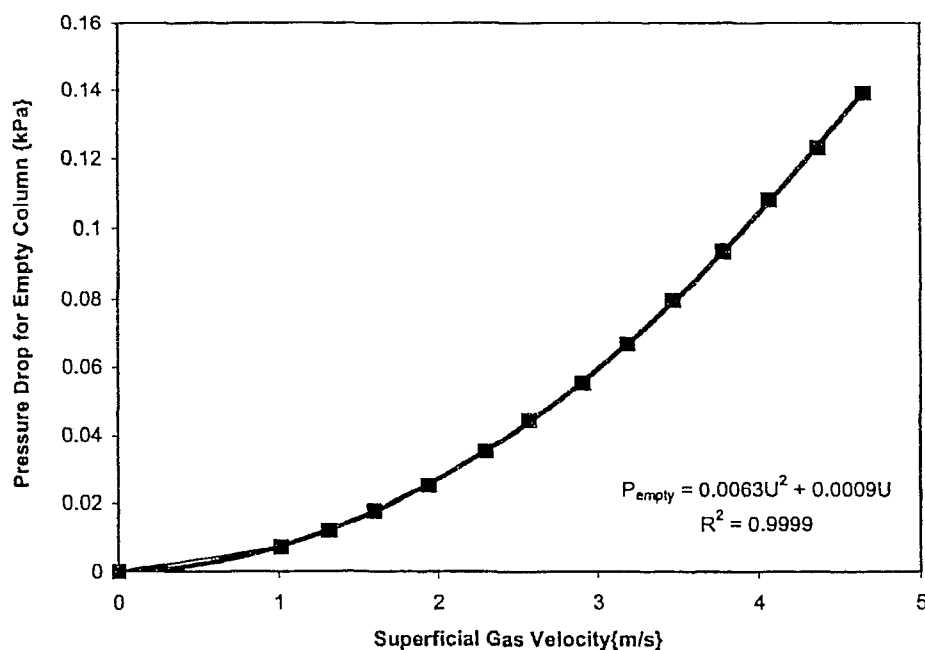
Figure 3-3 Pressure Drop in Empty Column

23

### 3.1.3 Gas Flow

Air was used as the gas phase for the three-phase fluidization system. An 11 kW centrifugal blower was used to supply the air to the system. The blower was located in the room beside the fluidized bed. The air was saturated to within 93% relative humidity in the saturation column using hot water. The velocity of the gas flow was determined using a pitot tube placed in the center of a straight piece of PVC piping The pitot pressure difference was measured with an MKS Baretron model 220B differential pressure transducers. Gas entered the bottom of the TBC column at an angle of 45° below the horizontal, expanded through a cone and then entered the straightener. The straightener consisted of a nest of 6 mm thin-walled plastic tubes 25 mm long filling most of the column cross-section except for a layer of 13mm tubes adjacent to the column wall. The larger tubes at the wall reduced the tendency for low velocities near the wall. After leaving the mist eliminator the air was exhausted through a horizontal duct to the outside. Air temperatures were measured with thermistors (YSI model 105). Air humidity was measured with two polymer probes, one at the exit from the top of the column and one in the feed line to the bottom.

Gas velocity calibration was achieved by conducting traverses across the empty column with a second pitot tube. The average velocity across the column cross-section (the superficial gas velocity) to each stationary pitot reading was determined. The calibration curve for the velocity inside the column is shown in Figures 3-4. The superficial velocity of the airflow in the fluidized bed could then be calculated from the determined calibration relationship:

$$U^2 = 18.527 * P \tag{3-1}$$

where $U$ is the superficial air velocity in m/s, and $P$ is the differential reading of the pitot tube in torr.

$$U = (18.5274 \cdot P_{pitot})^{1/2}$$
$$R^2 = 0.9944$$
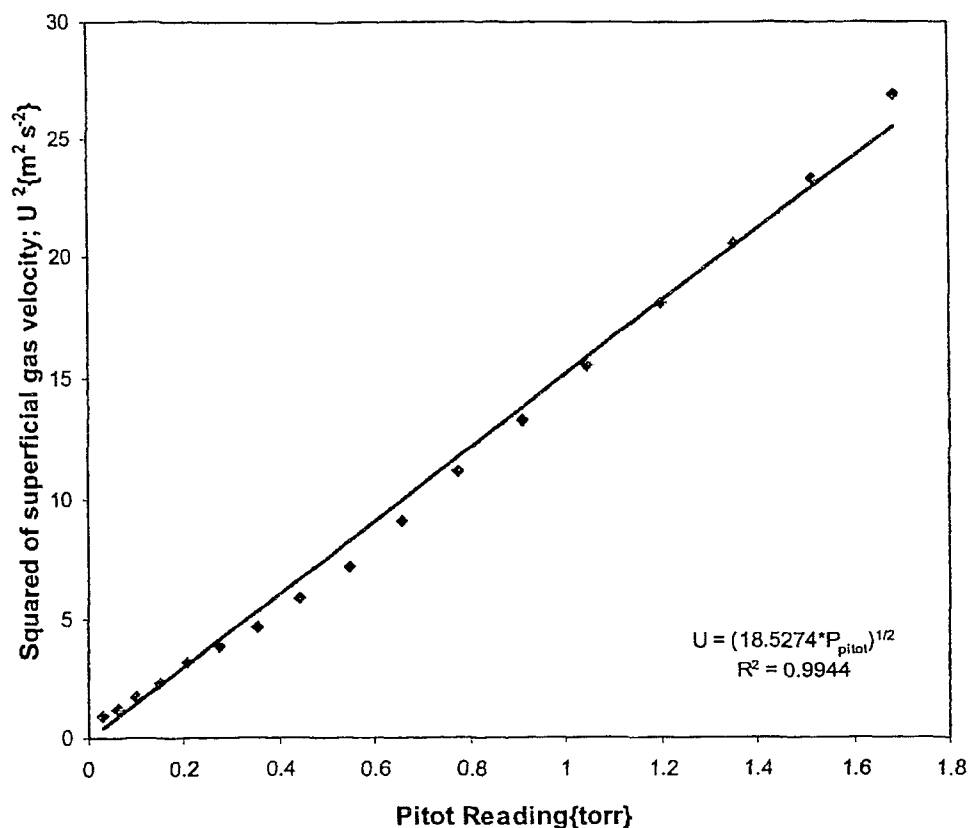
Figure 3-4 Velocity Calibration Curve for the Column

### 3.1.4 Liquid Flow

The liquid feed was held in two tanks, approximately 95 cm diameter and 90 cm height, and fed to the top of the column by a 3500 rpm, 374 HP pump (WEG Industries, Model B56C129). The flow rate to the column was controlled by a valve and monitored using rotameter. The liquid distributor was constructed of CPVC piping. The main pipe having an I.D. of 19 mm branched symmetrically into four nozzles, each of 13 mm I.D. The centers of the nozzles defined the four corners of a square of side length 8.8 cm. The liquid distributor was centered within the column. The liquid that exited the lower column was carried by gravity to recycle tanks located one floor below the column. The liquid could then be returned to the feed tanks by means of a recycle pump. Liquid temperatures were measured with

25

thermistors (YSI model 105). The viscosity of the liquid was measured in a constant-temperature bath by Brookfield viscometer. The spindle-speed combination for the viscosity type of the solution was chosen, and the dial reading was recorded and converted to viscosity.

### 3.1.5 Data Acquisition

The data acquisition system consisted of a Daytronic System10 DataPac connected to a PC. The DataPac relayed digital output on different channels, which were controlled and calibrated using the Daytronic System10 software. The DataPac was configured to supply information on 20 channels. Pressure, temperature and other parameters measurements can be captured by the DataPac with the use of a simple Basic program (see Appendix C). All instrumentation was connected through a data logger to a PC. Each instrument transmitted an electrical signal to the data logger. The data logger scanned each channel 20 times consecutively transmitted the data to a PC which would calculate averages for each channel. The basic program collected the averaged values of the parameters and stored them in batches. Each batch contained 20 averages of the values provided by the data logger. The number of batches collected would be decided by the operator. A batch of 20 data sets was chosen based on 400 individual readings from the data logger. These measurements were taken at defined intervals and saved to the computer's hard drive.

Most calculations were done via EXCEL spreadsheets into which raw data could be imported for processing.

### 3.1.6 Experimental Errors and Sensitivity

Table 3-2 shows the instrument's range and sensitivity used in this study; and an estimate of the uncertainties in the measurement of particular quantities.

| Instrument | Range | Sensitivity |
|---|---|---|
| YSI Thermistors | 0-100 °C | ± 0.01 °C |
| Baretron Pressure Transducer | 0-10 torr | ± 0.0001 torr |
| Moisture Probes | 0-100% RH | ± 2% RH |
| Rotameter | 1-18 gpm | ± 0.1 gpm |
| Balance | 0-1000 g | ± 0.00001 g |
| Brookfield Viscometer | 0-100 cP | ± 1 cP |
| | | |
| Quantity | Uncertainty/Error | |
| Gas and liquid temperature | ± 0.1 °C | |
| Pressure drop | ± 1% | |
| Gas velocity | ± 1% | |
| Liquid flow rate | ± 2% | |
| Expanded bed height | ± 3% | |
| Viscosity Reading | ± 1% | |

Table 3-2 Instrument Ranges and Sensitivity and

Measurements Uncertainties.

## 3.2 Experimental Methodology

Before pursuing the research objective, three preliminary studies were conducted, consisting of: two-phase fluidization experiments using air and beads only; three-phase fluidization experiments using air-water-beads, where water is the Newtonian liquid; and measurements to verify the rheological behavior of aqueous solutions of carboxy methyl cellulose. The first preliminary study verified the reliability of the system and its limitations; the second preliminary study provided the author with data for comparison. The third one provided the author with rheological parameters, which are needed for the study.

### 3.2.1 Preliminary Studies

### 3.2.1.1 Air/Beads Operation

In this section dry beads were fluidized by air flowing upward in the column. Experiments were conducted to measure net pressure drop across the bed for 20 mm and 38mm diameter beads, and four relative static bed heights of 0.25, 0.5, 0.75, and 1.00. Each increment in bed

27

height was achieved by adding a known weight of beads. Thus the theoretical pressure drop or the buoyant weight of the bed contents per unit area was known with high certainty. For each bead and bed height combination, gas velocity was varied in increments, allowing sufficient time to reach steady state after each adjustment. Gas velocity ranged from about 0.1 m/s, which was well below minimum fluidization conditions to about 6 m/s. Thus pressure drop data were recorded through both the fixed bed and fluidized regions. Each data point consisted of 400 scans of column pressure drop and pitot tube reading, over an interval of one minute. Data was stored in the form of 20 averages of 20 scans each. The 20 averages per data point were time stamped allowing a check for steady state conditions. All TBC runs were conducted with air at 20°C and relative humidity of 93%.

### 3.2.1.2 Air/Water/Beads Operation

In this operation, the beads were fluidized under the action of air flowing upward through the column and water flowing downward. Experiments were conducted for the same beads sizes and relative static bed heights as indicated in section 3.2.1.1. For each bead/bed height combination, four liquid flow rates ($L$) were used. All combinations were run at $L$ values of 2, 4, 8, and 14 gpm. For each combination of $d_p, H_s / D$, and $L$ gas velocity ($U_g$) was increased in small increments from the possible setting allowed by the system to the highest. For each data point, 400 scans of each parameter were taken over a one-minute interval, including the following parameters: column pressure drop, pitot tube reading, and gas and liquid temperatures. A one-minute pause to reach steady state was taken after each adjustment in $U_g$.

An example table of the output obtained is shown in Table B-6 in Appendix B.

### 3.2.1.3 Rheology of CMC Solutions

Carboxy methyl cellulose was supplied by Hercules; (7L, degree of substitution 0.65 – 0.9, low viscosity type, purified grade, molecular weight about 90,000). It has a high solubility in water and good resistance to viscosity degradation. It was desired to verify the rheological behavior of aqueous solutions of carboxy methyl cellulose sodium using shear stress / shear rate data at different concentrations.

The solution was prepared by mass using a balance. The concentration of the solutions made up in tap water was 0.2%, 0.4%, 0.8%, and 1% wt CMC .The required amount of powder was added slowly, over a period of minutes into the vortex of an agitator in the beaker.

28

AR 2000 Rheometer (TA instruments) was used to determine the shear stress or apparent viscosity over a shear rate range of 10 to 1200 $s^{-1}$, at a temperature of 20 °C. The results obtained are tabulated in Tables B.1 to B.5 for different concentrations and shown in Appendix B.

The sample flow curve for 1wt% CMC solution is shown in Figure 3-5. The flow curves for other concentrations are shown in Appendix A, as Figures A-1 to A-4. These curves show that the apparent viscosity decreases when the shear rate increases, which means the solutions exhibit shear-thinning behavior corresponds to a non-Newtonian and pseudoplastic fluid. Increasing the concentration of the polymer caused a notable increase in the apparent viscosity as illustrated in Figure 3-6.

The experimental flow curve data were fit with Oswald–de Waele model and the rheological parameters $n$ and $k$ were determined. Table 3-3 shows the rheological parameters and physical properties obtained for CMC aqueous solutions used in this study. It is clear that with increasing CMC concentration, the flow behavior index $n$ decreases and the flow consistency index $k$ increases.

| Liquid | $n(-)$ | $k(Pa.s^n)$ | $\rho(kg/m^3)$ | $\sigma(N/m)$ |
|---|---|---|---|---|
| Water | 1 | – | 998.23 | 0.0728 |
| 0.2 wt% CMC | 0.984 | 0.0041 | 999 | 0.0728 |
| 0.4 wt% CMC | 0.976 | 0.0062 | 999.88 | 0.0728 |
| 0.8 wt% CMC | 0.957 | 0.0144 | 1001 | 0.073 |
| 1.0 wt% CMC | 0.899 | 0.0266 | 1002 | 0.0733 |

Table 3-3 Rheological parameters for CMC solutions
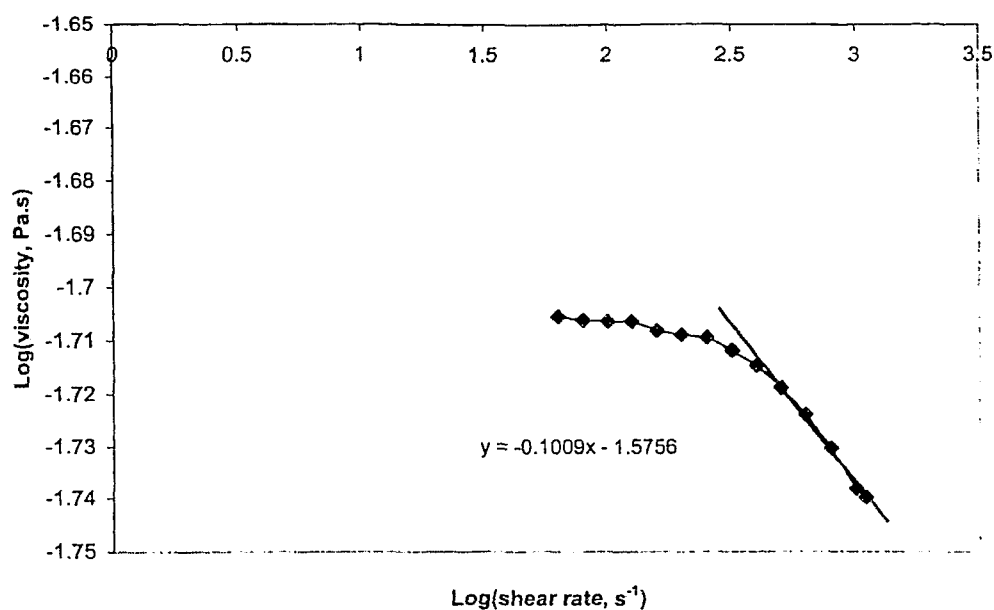
Figure 3-5 Flow curve for 1 wt%CMC aqueous solution at 20° C
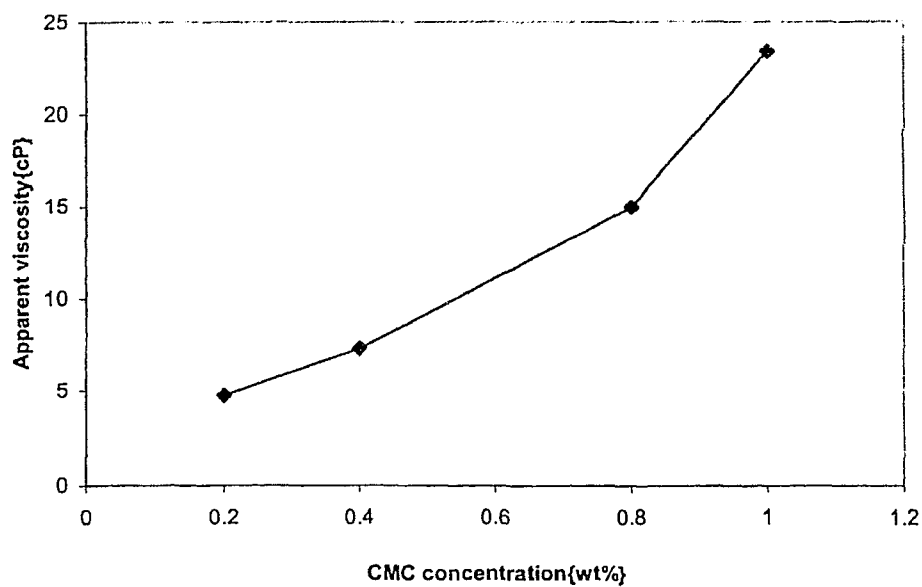


Figure 3-6  Effect of CMC concentration on apparent viscosity
at shear rate=10 s$^{-1}$

30

### 3.2.2 Experiments with Aqueous CMC Solutions

In these experiments, the beads were fluidized under the action of air flowing upward through the column and aqueous solutions of CMC flowing downward. Experiments were conducted for the same beads sizes and relative static bed heights as indicated in section 3.2.1.1 under four aqueous CMC concentrations of 0.2, 0.4, 0.8, and 1.00 wt% CMC. For each CMC solution's concentration/ bead/bed height combination, four liquid flow rates ($L$) were used. All combinations were run at $L$ values of 2, 4, 8, and 14 gpm. For each combination of $d_P, H_S / D$, wt% CMC, and $L$ gas velocity ($U_g$) was increased in small increments from the possible setting allowed by the system to the highest. For each data point, 400 scans of each parameter were taken over a one-minute interval, including the following parameters: column pressure drop, pitot tube reading, and gas and liquid temperatures. A one-minute pause to reach steady state was taken after each adjustment in $U_g$. A sample of the calculated results can be found in Table B-7 in Appendix B.

### 3.2.3. Experimental Design

In order to carry out a thorough study of the system, an experimental design was setup as shown in Table 3-4. This set up is repeated for beads sizes 20 mm and 38 mm, and for some sets of conditions for 26 mm.

31

| Static bed height | Superficial gas velocity | Water | | 0.2wt%CMC | | 0.4wt%CMC | | 0.8wt%CMC | | 1wt%CMC | |
|---|---|---|---|---|---|---|---|---|---|---|---|
| $H_s/D = 0.25$ | $U_g = 0.3-4 m/s$ | $L = 2gpm$ | $\Delta P, U_{mf}, H$ | $L = 2gpm$ | $\Delta P, U_{mf}, H$ | $L = 2gpm$ | $\Delta P, U_{mf}, H$ | $L = 2gpm$ | $\Delta P, U_{mf}, H$ | $L = 2gpm$ | $\Delta P, U_{mf}, H$ |
| | . | $L = 4gpm$ | . | $L = 4gpm$ | . | $L = 4gpm$ | . | $L = 4gpm$ | . | $L = 4gpm$ | . |
| | . | $L = 8gpm$ | . | $L = 8gpm$ | . | $L = 8gpm$ | . | $L = 8gpm$ | . | $L = 8gpm$ | . |
| | . | $L = 14gpm$ | . | $L = 14gpm$ | . | $L = 14gpm$ | . | $L = 14gpm$ | . | $L = 14gpm$ | . |
| $H_s/D = 0.5$ | $U_g = 0.3-4 m/s$ | $L = 2gpm$ | $\Delta P, U_{mf}, H$ | $L = 2gpm$ | $\Delta P, U_{mf}, H$ | $L = 2gpm$ | $\Delta P, U_{mf}, H$ | $L = 2gpm$ | $\Delta P, U_{mf}, H$ | $L = 2gpm$ | $\Delta P, U_{mf}, H$ |
| | . | $L = 4gpm$ | . | $L = 4gpm$ | . | $L = 4gpm$ | . | $L = 4gpm$ | . | $L = 4gpm$ | . |
| | . | $L = 8gpm$ | . | $L = 8gpm$ | . | $L = 8gpm$ | . | $L = 8gpm$ | . | $L = 8gpm$ | . |
| | . | $L = 14gpm$ | . | $L = 14gpm$ | . | $L = 14gpm$ | . | $L = 14gpm$ | . | $L = 14gpm$ | . |
| $H_s/D = 0.75$ | $U_g = 0.3-4 m/s$ | $L = 2gpm$ | $\Delta P, U_{mf}, H$ | $L = 2gpm$ | $\Delta P, U_{mf}, H$ | $L = 2gpm$ | $\Delta P, U_{mf}, H$ | $L = 2gpm$ | $\Delta P, U_{mf}, H$ | $L = 2gpm$ | $\Delta P, U_{mf}, H$ |
| | . | $L = 4gpm$ | . | $L = 4gpm$ | . | $L = 4gpm$ | . | $L = 4gpm$ | . | $L = 4gpm$ | . |
| | . | $L = 8gpm$ | . | $L = 8gpm$ | . | $L = 8gpm$ | . | $L = 8gpm$ | . | $L = 8gpm$ | . |
| | . | $L = 14gpm$ | . | $L = 14gpm$ | . | $L = 14gpm$ | . | $L = 14gpm$ | . | $L = 14gpm$ | . |
| $H_s/D = 1.00$ | $U_g = 0.3-4 m/s$ | $L = 2gpm$ | $\Delta P, U_{mf}, H$ | $L = 2gpm$ | $\Delta P, U_{mf}, H$ | $L = 2gpm$ | $\Delta P, U_{mf}, H$ | $L = 2gpm$ | $\Delta P, U_{mf}, H$ | $L = 2gpm$ | $\Delta P, U_{mf}, H$ |
| | . | $L = 4gpm$ | . | $L = 4gpm$ | . | $L = 4gpm$ | . | $L = 4gpm$ | . | $L = 4gpm$ | . |
| | . | $L = 8gpm$ | . | $L = 8gpm$ | . | $L = 8gpm$ | . | $L = 8gpm$ | . | $L = 8gpm$ | . |
| | . | $L = 14gpm$ | . | $L = 14gpm$ | . | $L = 14gpm$ | . | $L = 14gpm$ | . | $L = 14gpm$ | . |

Table 3-4 Experimental Design

32

# CHAPTER 4

# RESULTS AND DISCUSSION

The chapter is divided into five sections. Each section discusses one of the hydrodynamic parameters of the TBC. The five sections are: bed pressure drop, minimum fluidization velocity, liquid holdup, bed expansion, and gas holdup.

Please note that the determined figures presented in this chapter are not inclusive of all the experimental results of this research work. The reader is referred also to numerous results that are placed in Appendix A which are part and parcel of this work. This was done to facilitate the presentation and discussion of the work done and to maintain a reasonable consistency and focus of the discussion process.

## 4.1 Bed Pressure Drop

The total pressure drop across the bed is the sum of the net pressure drop due to the bed contents, and the pressure losses encountered at the column wall, the supporting grids and other bed internals. Several researchers (Blyakher et al. (1967); Gel'perin et al. (1968b); and levsh et al. (1968b)) have observed that pressure losses due to the supporting grid are strongly affected by grid geometry. Wall effects may also be significant for units having small column diameter to particle diameter ratios. Tichy and Douglas (1972) observed that when the ratio of column to particle diameter was as low as 11, the pressure loss due to wall effect was significant. Wall effect is very small and can be neglected for large diameter columns.

Several net pressure drop correlations for a TBC are listed by Fan (1989) and include dependency on the weight of solids holdup and the liquid present in the bed (Aksel and Yakovenko (1969), Kito et al. (1976e), Gel'perin et al. (1968b), Wozniak (1977), O'Neill et al. (1972)). The general form is:

$$\Delta P = (1 - \varepsilon_o)(\rho_S - \rho_g)H_S g + \Delta P_L \qquad (4\text{-}1)$$

The first term on the right side of equation (4-1) simply represents the buoyant weight of the beads per unit area of the column, and is equal to $W/S$. Most correlations omit the density of the gas ($\rho_g$) since it is negligible in comparison to the density of the solid ($\rho_S$). The second term on the right side, $\Delta P_L$, is the pressure drop due to the liquid. In all cases it is taken as the

33

weight of liquid holdup per unit area, and is equal to the product of liquid holdup, density of the liquid ($\rho_L$), $g$, and static bed height ($H_S$).

Equation (4-1) can be written in this form:

$$\Delta P = (\rho_S - \rho_g)(1 - \varepsilon_O)gH_S + \rho_L\varepsilon_{L,St}gH_S \qquad (4\text{-}2)$$

The limiting case for zero liquid flow rates is:

$$\Delta P = (\rho_S - \rho_g)(1 - \varepsilon_O)gH_S \qquad (4\text{-}3)$$

Equation (4-3) gives the pressure drop for two-phase operation.

In the initial experiments, the dry beads were fluidized by air to assess the reliability of the experimental system. Pressure drop results for all bed heights and both bead sizes are shown in Figures 4-1 and 4-2. Also shown is the relationship with theoretical value given by equation (4-3) and designated as W/S.

These curves illustrate the classical behavior of two-phase counter current operation. As superficial gas velocity was increased from the lowest value, the fixed bed remained unchanged under the influence of static fractional forces. At the first instance of bed expansion, the pressure drop decreased slightly due to the corresponding decrease in interstitial velocity, and then rose again with increasing gas velocity. The results for both beads show that the present experimental pressure drop values deviate from those predicted by equation (4-3) by ± 0 to 4%. The negative discrepancy between experimental net pressure drop values and the theoretical values can be due to the formation of preferential bubble paths which reduces gas flow in other parts of the bed and results in a lower net pressure drop (Boherill and Bloore (1963)). However, the positive discrepancy can be explained by the kinetic energy losses due to independent particle motion and wall effects (Morse (1949), Bhat et al. (1963)). The maximum gas velocity for each of the pressure drop curves reported in all sections was limited by the power out put of the blower.

Sample of net pressure drop curves for water and aqueous CMC solutions are shown in Figures 4-3a and Figure 4-3b for 20 mm and 38 mm beads for a set of conditions. These figures indicate the existence of three hydrodynamic states within the range of gas velocities studied.

34
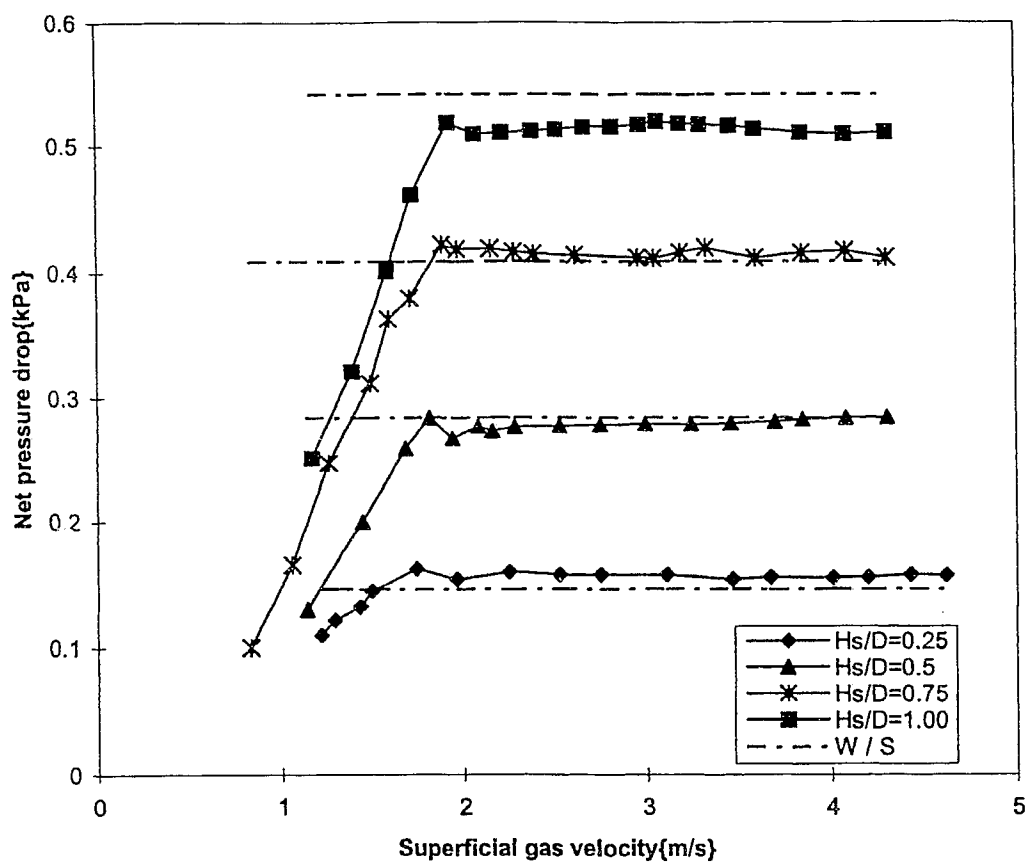
Figure 4-1 Net pressuredrop vs superficial gas velocity for air/beads at
dp=20mm

35
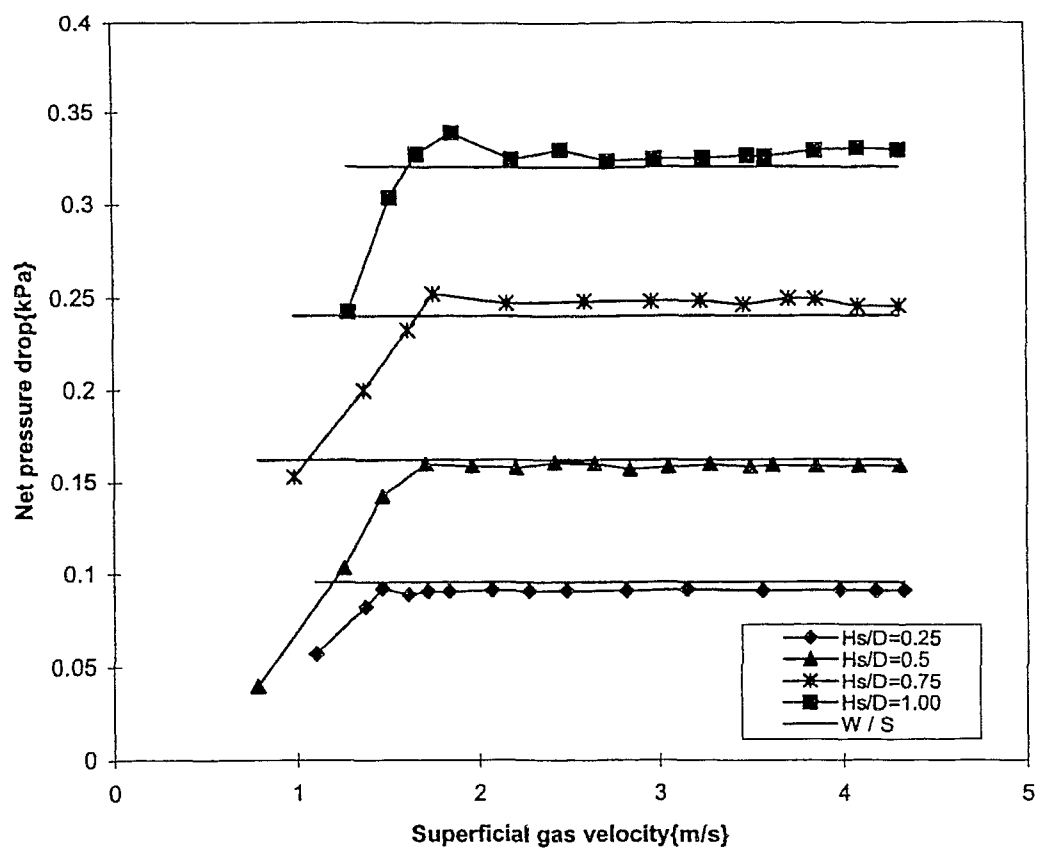
Figure 4-2  Net pressure drop vs superficial gas velocity for air/beads at
dp=38mm

36

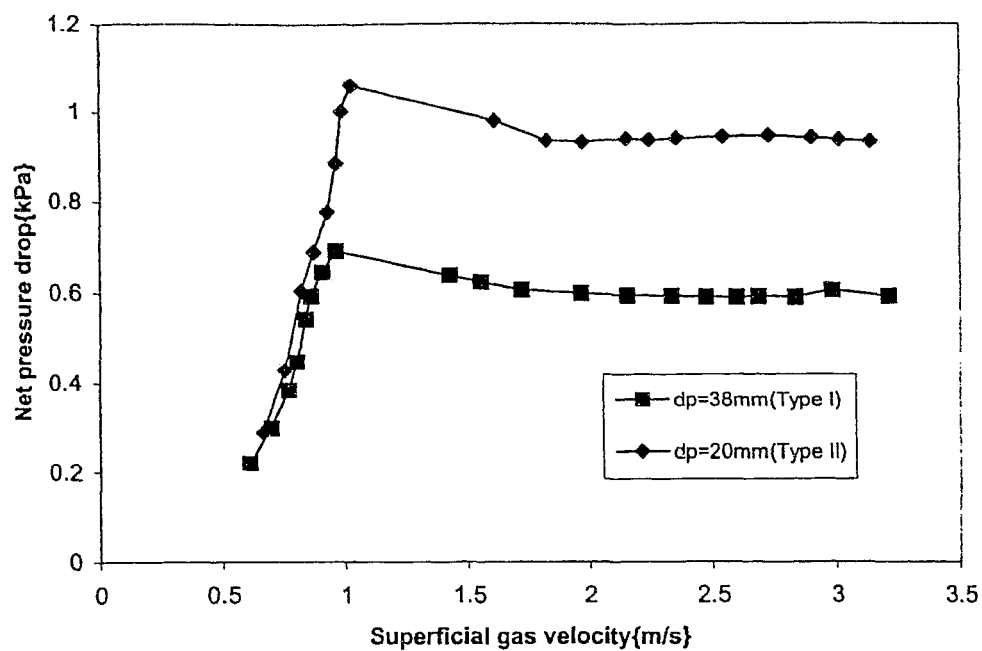Figure 4-3a  Net pressure drop vs superficial gas velocity for
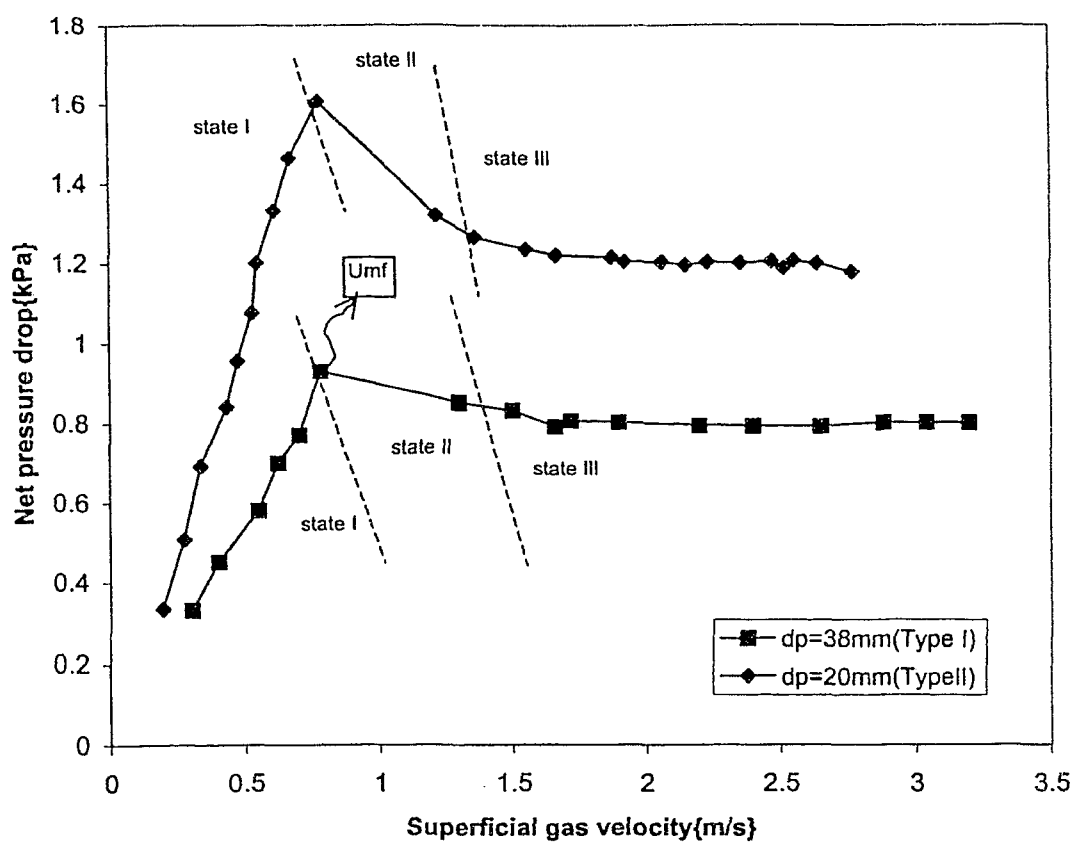air/water/beads  at Hs/D=0.5, L=4gpm

37

Figure 4-3b  Net pressure drop vs superficial gas velocity for
air/CMC/beads at Hs/D=0.5, L=8gpm, 0.8 wt %CMC

38

In the first state (stationary packing) the spheres are in close mutual contact and the bed volume remains unchanged with some variations of the velocity. The liquid flows down the center of the packing in film form while gas passes predominantly along the column walls. A liquid layer on the bottom grid below the beads accumulated as the gas velocity increases (see Figure 4-4a and 4-4b). This state exists in a narrow range of flow velocities. A peak in the net pressure drop occurs at the upper limit of the compact bed. This upper limit being the start of fluidization. The existence of a pressure peak is due to increase of the amount of liquid in the bed and above the grid before the instant when the compact bed loses its stability, and to the interaction of the spheres with each other and with the walls of the column. The magnitude of the pressure peak varies with the liquid flow rate, the static bed height, and the properties of the beads. Type I and type II operations follow the same behavior as shown in these figures.

The second state (initial fluidization) begins immediately beyond the stability limit of the compact bed and is characterized by bursting in the center as shown in Figure 4-4c. In this state, fluidization takes place in a certain proportion of the packing without intense motion of the spheres. A fast increase of the gas velocity in this regime is noticed due to flowing down of the liquid layer and the proportional increase of the number of moving spheres in the bed, which leads to increase of the cross section open passage of gas.

The third state (fully fluidization) is characterized by increasing motion of the phases and instability of the interface (see Figures 4-4d and 4-4e). The existence of three regions on the curve relating bed pressure drop to gas velocity were recognized by Levsh et al. (1968b) and Balabekov et al. (1969a,b; 1971) for air-water systems.

The net pressure drop across the bed reaches almost constant value with increasing gas velocity. These figures shows that fluidization of the bed begins, at a pressure difference somewhat greater than the resistance of the fluidization bed. Since the fully fluidization state is the optimal regime for mass and heat transfer processes, our discussion would be limited to this regime.

The pressure drop for fully fluidization state is independent of gas velocity as shown in the sample curves in Figure 4-5. Other figures for other conditions, which illustrate these findings, can be found in Appendix A., as Figures A-5 to A-12. The general trend of net pressure drop dependency on liquid flow rate is an increasing tendency with increasing (L) as shown in

Figure 4-6. The same trend observed for all other bed combinations as shown in Appendix A, as Figures A-13 to A-21. The rate of increase is almost steady for all liquid flow rates at all static bed heights for both beads diameters, except some deviations are observed at high static bed heights range and high CMC concentrations.

The variation of net pressure drop with static bed height is illustrated in Figure 4-7 for a set of conditions and for the other sets of conditions in Figures A-22 to A-27, in Appendix A. In general terms, $\Delta P$ increases with increasing static bed height. This is consistently true for all liquid flow rates, CMC concentrations and beads diameters. The influence of increasing static bed height on net pressure drop is more dramatic at high CMC concentrations.

Since no studies reported in the literature for non-Newtonian conditions in TBC's, the experimental results of the present study are compared with estimated values obtained using correlations reported in the literature for Newtonian conditions, with modifications added to the correlations by substituting the liquid viscosity with effective liquid viscosity. The estimation of the effective viscosity of non-Newtonian liquid in fluidized beds is difficult. This is basically because of the difficulty in defining the shear rates. A common approach in evaluating the shear rate involves assuming that an average shear rate exists in the column and proportional to superficial gas and liquid velocities (Shi et al, 1990). The range of the shear rates in the fluidized bed can be estimated by:

$$\gamma_{eff} = 2U_g / \varepsilon d_p \tag{4-4}$$

and

$$\gamma_{eff} = 2(U_g + U_L) / \varepsilon d_p \tag{4-5}$$

for two and three phase systems (Miura and Kawase, 1998). It should be noted, however, that the shear rates in the fluidized bed are not uniform and the above equations are only estimations. In the present work, the above equation (4-5) will be used to calculate the shear rates and these values will be substituted in equation (1-3) to calculate the effective viscosities.

For example, Kito et al. (1976e) fluidized 19.5 mm and 28.5 mm polypropylene beads of 540 kg/m$^3$ and 290 kg/m$^3$ density in a column of 100 mm with Newtonian liquids. The Kito correlation for $\Delta P$ has the general form of equation (2-1) and is given below:

$$\Delta P = (\rho_S \varepsilon_S + \rho_L \varepsilon_L)gH = (\rho_S(1-\varepsilon_o) + \rho_L \varepsilon_{L,St})gH_S \qquad \text{where}$$

40

$$\varepsilon_{L,St} = 12.8(H_S/d_P)^{-0.4}(fd/D)^{-0.58}(gd_P^{\;3}\rho_S^{\;2}/\mu_{L,eff}^{\;2})^{0.09}(U_L/\sqrt{gd_P})^{1.66}$$

$$\times (d_P U_L \rho_L/\mu_{L,eff})^{-0.34}(d_P U_L^{\;2}\rho_L/\sigma)^{-0.34} \qquad (4\text{-}6)$$

Vunjak-Novakovic et al. (1987a,b) used 20mm and 38mm polypropylene beads of density 413 kg/m and 190 kg/m.

The Vunjak-Novakovic correlation has the general form of equation (2-1) and is given below:

$$\Delta P = (\rho_S \varepsilon_S + \rho_L \varepsilon_L)gH = (\rho_S(1-\varepsilon_O) + \rho_L \varepsilon_{L,St})gH_S \qquad \text{where}$$

Type (I):

$$\varepsilon_{L,St} = 6.4848\,\text{Re}_L^{-0.1387}\,Fr_L^{0.4287}(H_S/D)^{-0.5672} + 0.02 \qquad (4\text{-}7)$$

Type (II):

$$\varepsilon_{L,St} = 7.326\,\text{Re}_L^{-0.0591}\,Fr_L^{0.4354}(H_S/D)^{-0.4328}(\rho_S/\rho_L)^{.0904} + 0.02 \qquad (4\text{-}8)$$

The conditions of the present study were substituted into equations (4-6) and (4-7) and (4-8) to obtain estimated values of net pressure drop. Estimated values can be found in Table B-8 in Appendix B. The predicted values are plotted in Figures 4-8 and 4-9 and compared with present experimental results, for two sets of conditions. The correlation by Kito et al. (1976e) over predicts the net pressure drop for the fully fluidized state while the correlation by Vunjak-Novakovic (1987a, b) under predicts the net pressure drop. The actual curve lies somewhere between the two correlations depicted in Figures 4-8 and 4-9.

Effect of CMC Concentration:

Expressions of liquid viscosity in the following analyses have been expressed in terms of weight percent of CMC in solutions, since the viscosity of the CMC solutions is not constant at various shear rates (shear thinning liquids).

Sample curves for the effect of increasing the concentration of CMC aqueous solutions on the net pressure drop across the bed is shown in Figure 4-10 and 4-11 for sets of conditions. Graphs for the remaining combinations of parameters are shown in Appendix A, as Figures A-28 to A-35. These curves show that net pressure drop has the same water trends; with increase in pressure drop as the CMC concentration increases at all liquid flow rates, static bed heights, and beads diameters. For low CMC concentrations (0.2 wt % CMC and 0.4 wt% CMC solutions), the increase in net pressure drop values than water is very small, while the increase

41

becomes more significant as the concentration of CMC increases. The net pressure drop increases markedly at 1wt%CMC for all cases. A plausible explanation is given by the shear-thinning phenomenon, which exist in pseudoplastic liquids. At high superficial gas velocities the shear rates in the system are higher and therefore the viscosity is lowered almost to water viscosity. This leads to no significant deviation from water for net pressure drop at low range of CMC concentrations. For higher concentrations, which means higher viscosities and higher pseudoplasticity, as the superficial gas velocities increase the shear rates in the system are higher and as a shear-thinning liquid, it is expected that the apparent viscosity of the solution decreases markedly for higher concentrations. But it is observed that the net pressure drop across the column increases as the CMC concentration increases. A possible explanation is that the overall effect of rheological properties on pressure drop depends on the competition between the effects of viscosity and shear thinning anomaly. The viscosity causes the increase in pressure drop. On the other hand, the increase in the non-Newtonian anomaly or shear thinning reduces the effective viscosity of CMC aqueous solution and reduces the pressure drop. According to the results obtained, the influence of the rheological properties is insignificant, while the viscosity is the predominant factor and the CMC solutions exhibit a behavior similar to viscous Newtonian liquids.

These higher effective viscosity values alter the balance by creating an additional force arising from increasing the surface friction, which correspondingly, increases the liquid retained in the bed. Another force arising from viscous dissipation, resulting from holding the bed structure together by liquid bridging. This means that additional "bed weight "is seen by the flowing gas. This effect is more obvious at higher static bed heights and higher CMC concentrations where the particles are anchoring to the wall, resulting an additional down wards acting force. For complete fluidization to occur, the induced drag has to counteract the buoyant particle weight plus any additional "bed weight ", hence, resulting in a higher net pressure drop.

Since it was very difficult to obtain hallow particles with same density and different sizes or vice versa, the effect of both the parameters is represented in terms of Archimedes number, $Ar$, where

42

$$Ar = gd_P^3 \rho_g (\rho_s - \rho_g)/\mu_g^2 \qquad\qquad (4\text{-}9)$$

The larger Archimedes number is either due to increase in density or diameter of the particle. The net pressure drop decreases with increase in Archimedes number as shown in Figure 4-12 for a set of conditions. Similar trend is observed for all bed conditions. As the particle diameter or density increases, the surface area per unit volume of the bed and voidage of the bed decreases, and hence, less liquid flows on the surface of the particles and less liquid retained in the bed which means less net pressure drop. In contrary, as the density increases the expansion of the bed decreases which increase the gas interstitial velocity. As a result the friction force increases and hence more liquid retained in the bed. It seems that increasing the diameter has more impact than increasing the density. This indicates that the density of the particles have insignificant effect on the net pressure drop of the bed.

Figure 4-4a Stationary state
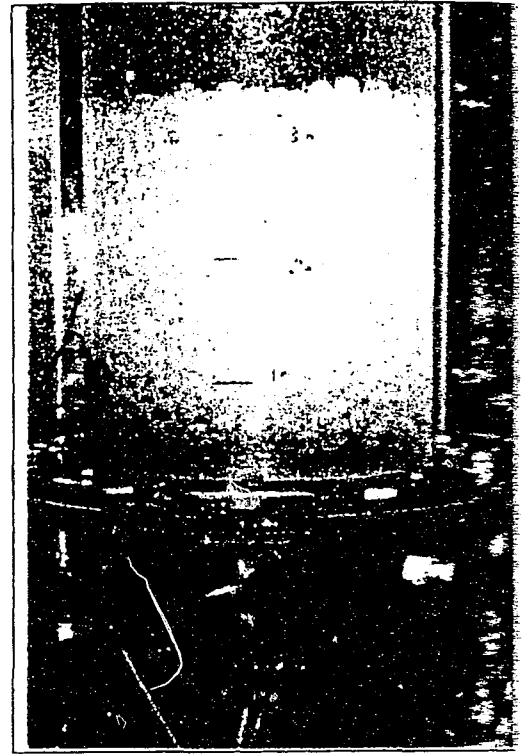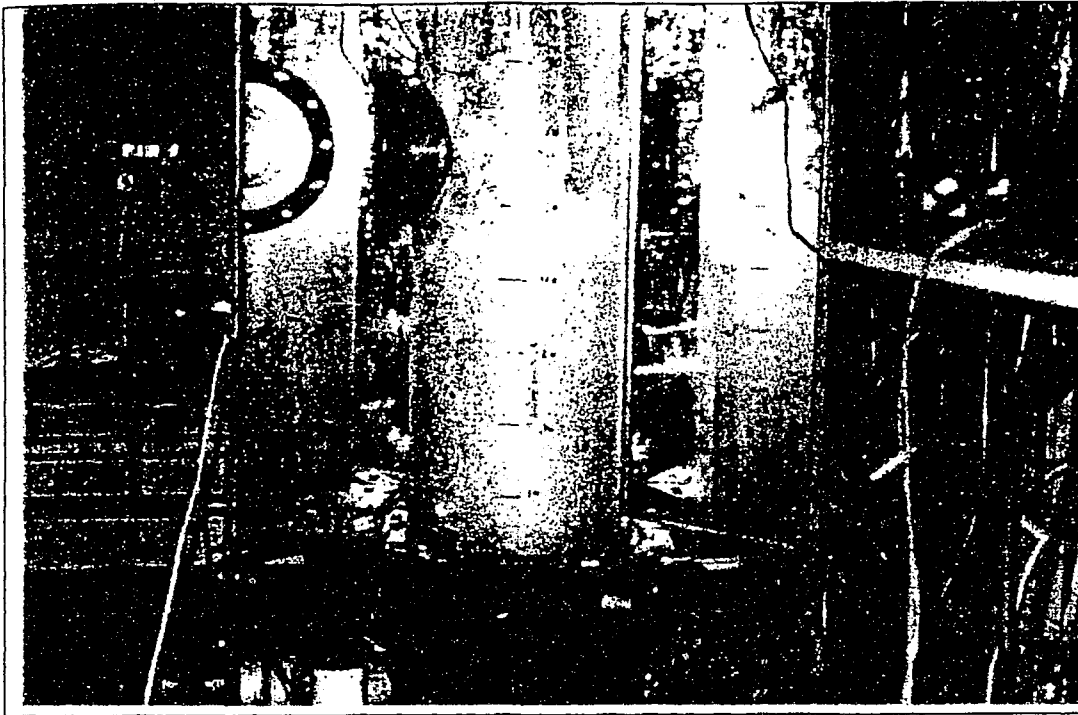


Figure 4-4b Stationary state
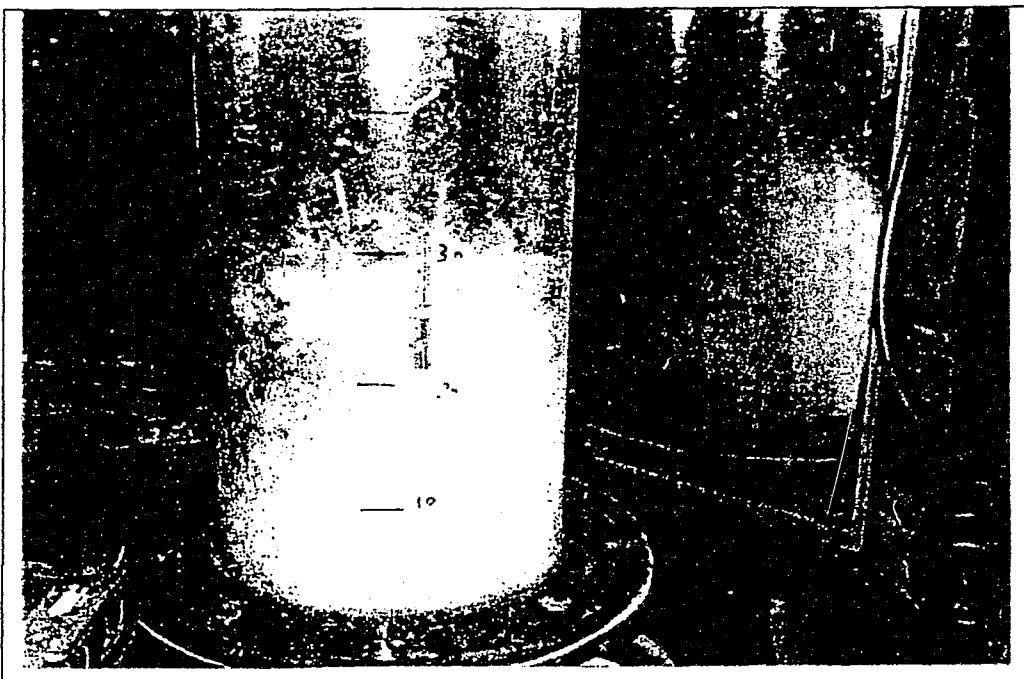
44

Figure 4-4c Initial fluidization



Figure 4-4d Fully fluidization state
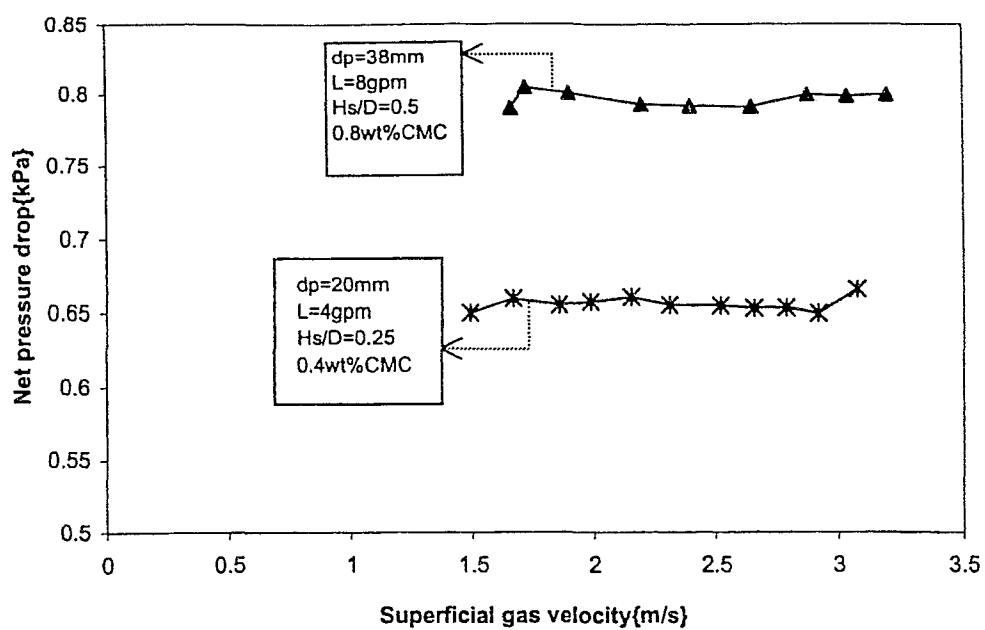
45

Figure 4-4e Fully fluidization state

46

Figure 4-5  Effect of superficial gas velocity on net pressure drop
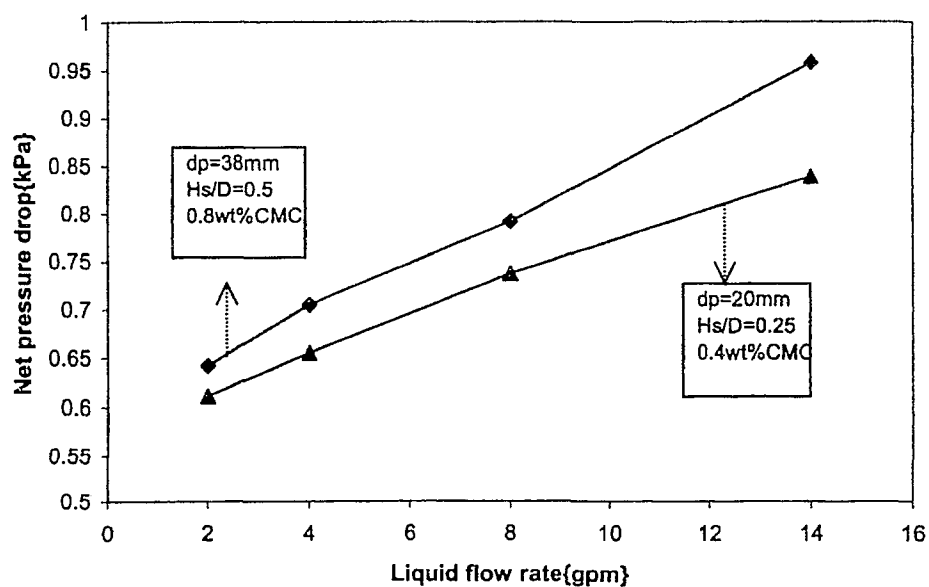


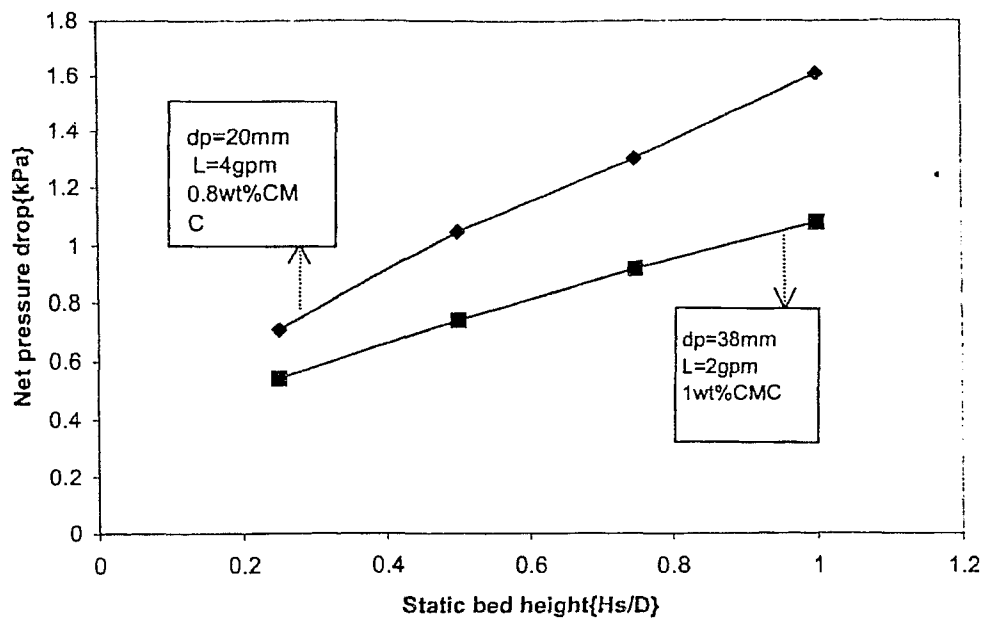Figure 4-6  Effect of liquid flow rate on net pressure drop

47

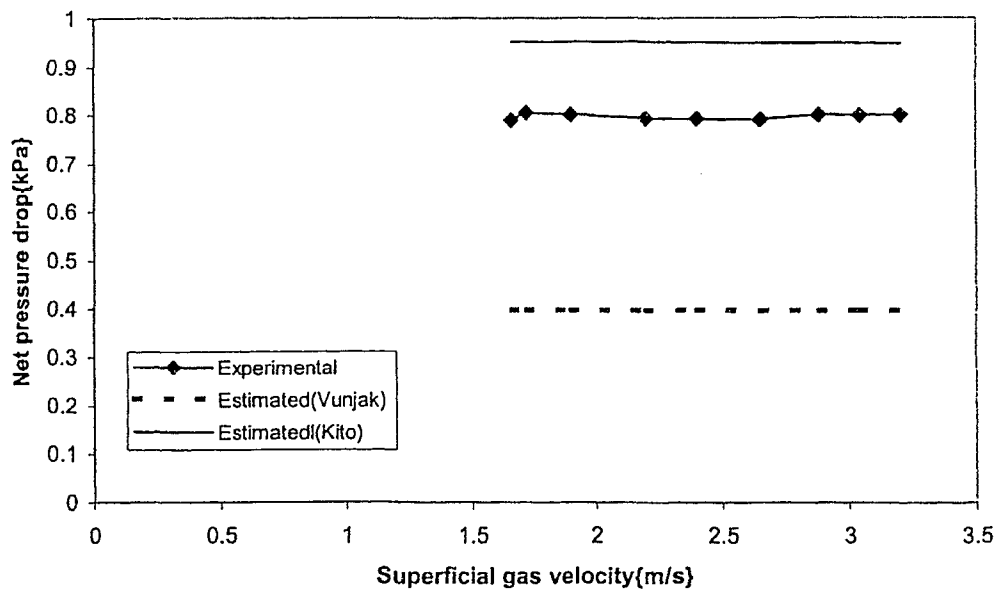Figure 4-7  Effect of static bed height on net pressure drop



Figure 4-8   Experimental and estimated values for net pressure drop at
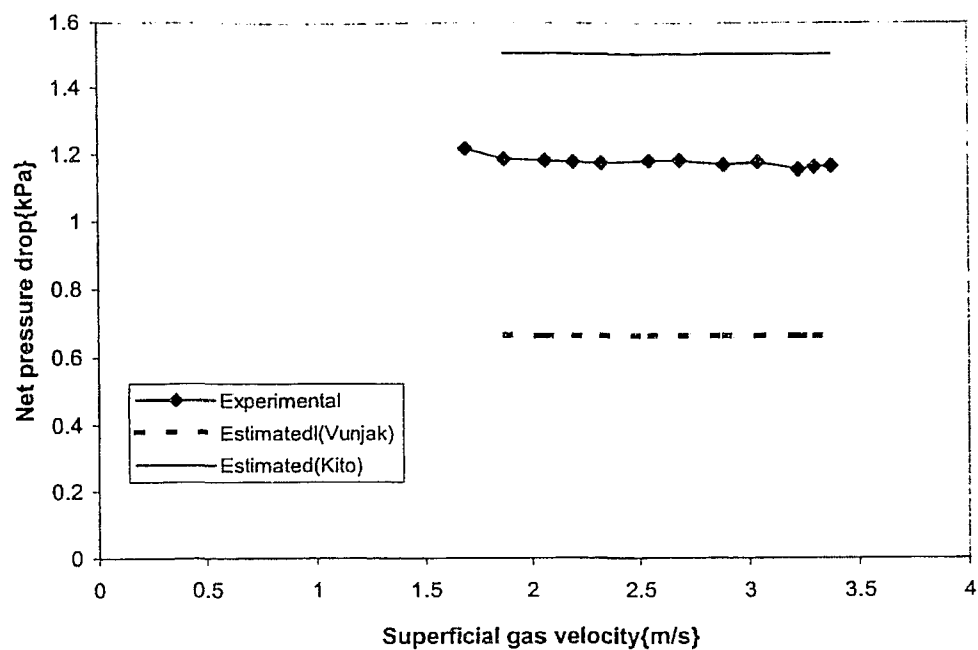Hs/D=0.5, dp=38mm, L=8gpm, 0.8wt%CMC

48

Figure 4- Experimental and estimated net pressure drop for
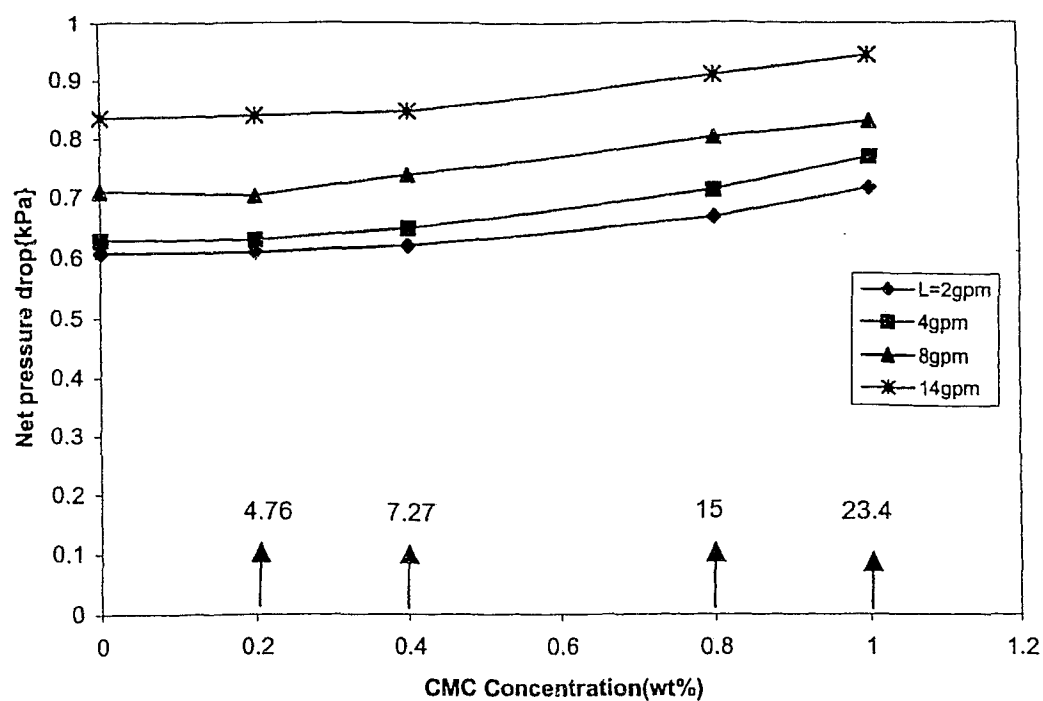$U_g$=0.75, dp=20mm, L=4gpm, 0.4wt%CMC

49

Figure 4-10  Effect of CMC concentration on net pressure drop at
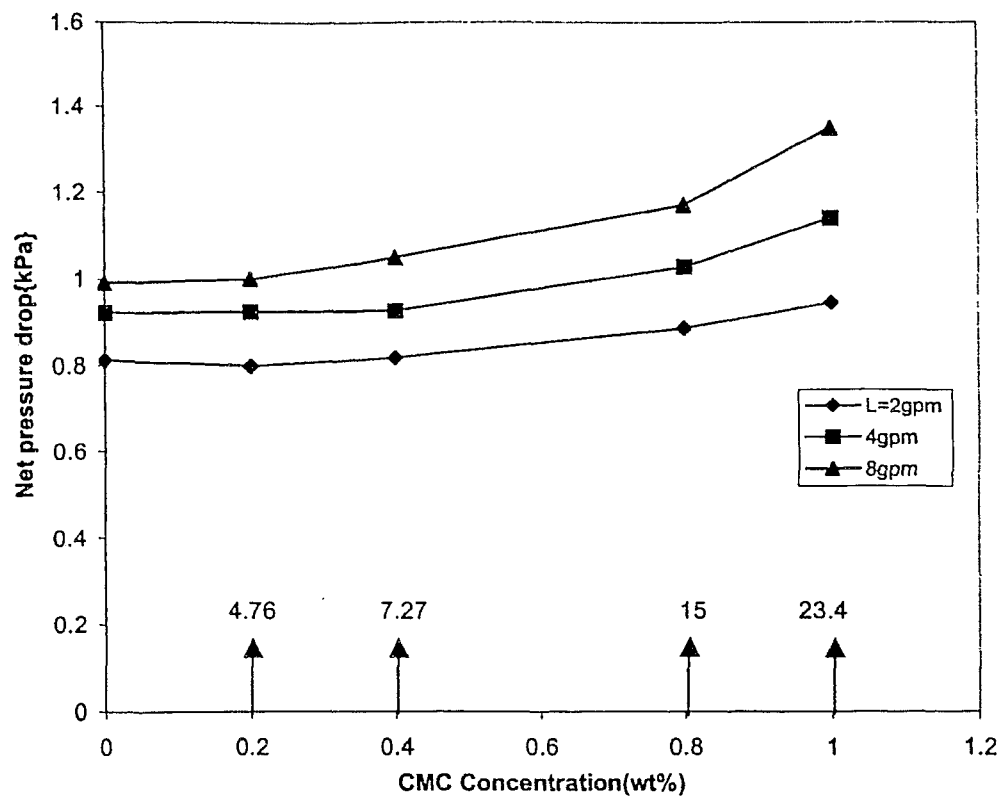Hs/D=0.25, dp=20mm,($\uparrow$ viscosity,cP at 10 s$^{-1}$)

50

Figure 4-11 Effect of CMC concentration on net pressure drop at
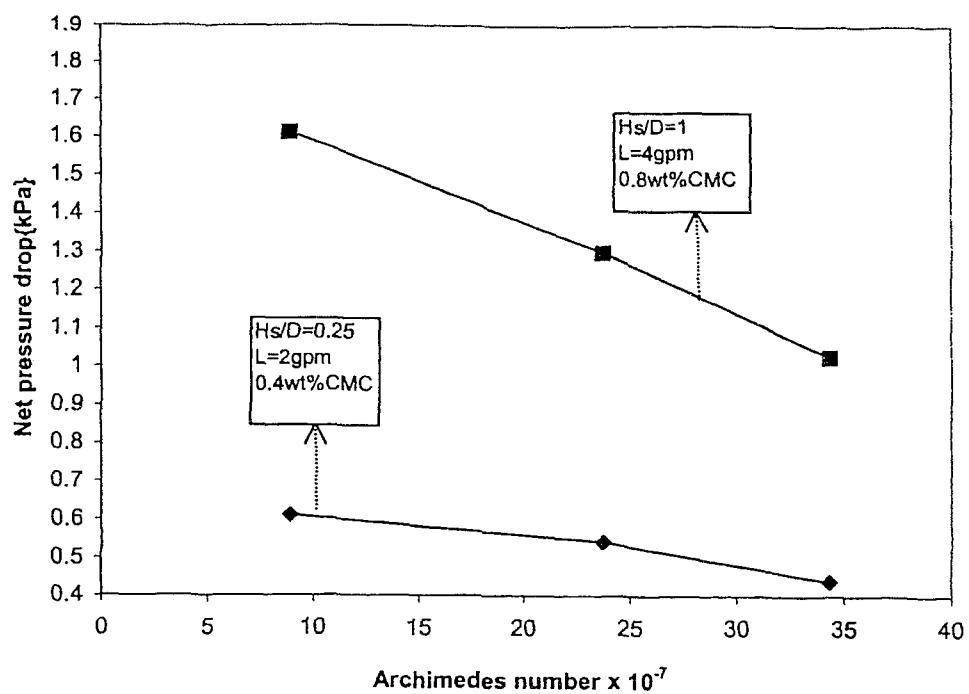Hs/D=0.5, dp=20mm,( ↑ viscosity,cP at 10 s$^{-1}$)

51

Figure 4-12 Effect of Archimedes number on net pressure drop

52

## 4.2 Minimum Fluidization Velocity

The minimum fluidization velocity, $U_{mf}$, in this study is the velocity at the upper limit of the stationary packing state at which fluidization starts with the break down of the packed bed structure (see Figure 4-3b). Experimental values of $U_{mf}$ for each combination of wt % CMC, $d_P$, $H_S / D$, and $L$ are shown in Table 4-1 and 4-2. Values for all bed heights and all CMC concentrations are grouped for each value of L for ease of comparison. Results of Table 4-1 and Table 4-2 suggest $U_{mf}$ dependency on $H_S / D$ and $L$ for both type I and type II. The variation of $U_{mf}$ with liquid flow rate is shown in sample curves of Figures 4-13 and 4-14 for sets of conditions. The rest of other figures are in Appendix A, Figures A-36 to A-46. As seen, the general trend of $U_{mf}$ dependency on liquid flow rate is a decreasing tendency with increasing $L$. Similar trend is observed for all other bed conditions. The rate of decrease becoming less significant for the mid-range liquid flow rate and up ($L>$4gpm) for both beads. Another observation is the dramatic decrease in $U_{mf}$ when the liquid phase is added to the gas-solid fluidized bed.

$U_{mf}$ data obtained at various static bed heights are plotted in sample Figure 4-15. Other figures for other conditions are in Appendix A, as Figures A-47 to A-53. The basic feature of these results is that $U_{mf}$ increases with increasing static bed height for all liquid flow rates, CMC concentrations and both beads diameters.

Where experimental conditions were reasonably consistent, $U_{mf}$ were estimated using literature correlations with viscosity modification as explained in section 4.1. The calculated results are compared to the experimental values for a set of conditions. The correlations used are as follows:

Tichy and Douglas (1972):

$$U_{mf} = \frac{1}{\rho_g}(0.36355 + 57.9d_P - 1.848G_L^{0.6}d_P^{0.5}) \tag{4-10}$$

Balabekov et al. (1971):

$$d_P U_{mf} \rho_g / \mu_g = 142(f\rho_S / \rho_L)^{0.33}(.005/d_P)^{-2.2} \times$$
$$\exp\left[-7.3 \times 10^{-6}(\rho_S / \rho_L)^{-0.33}(.005/d_P)^{1.14}(2d_P G_L / 3\mu_L(1-\varepsilon_n)\right] \tag{4-11}$$

The correlations encompass both type I and type II operation. This comparison is shown graphically in Figure 4-16 and Figure 4-17. The Tichy and Douglas (1972) correlation under predicts $U_{mf}$ values for $d_p$ =20 mm and over predicts $U_{mf}$ values for $d_p$ =38 mm. There is a significant inconsistency between predictions of Balabekov et al. (1971) correlation and experimental data. The values of the Balabekov correlation were independent of the liquid flow rate.

Effect of Archimedes number, $Ar$, on minimum fluidization velocity doesn't follow any consistent trend for both beads, hence, no conclusion can be made.

Effect of CMC Concentration

Determination of the minimum fluidization velocities for CMC solutions has revealed a number of features presented in Figures 4-18 and Figure 4-19. Figures for remaining combinations are shown in Appendix A, as Figures A-54 to A-61.

The minimum fluidization velocity $U_{mf}$ decreases at lower CMC concentrations. However, this effect is reversed for the higher CMC concentrations. The decrease in $U_{mf}$ is most likely due to the viscous CMC solution, where more liquid fills up the bed voidage and covering the surface of the packing, which increase the interstitial gas velocity, therefore, the induced drag counteract the "bed weight " earlier. So minimum fluidization begins to occur earlier. As the CMC concentration increases, higher thickness of the liquid film results, which increases the gas interstitial gas velocity and therefore the surface friction. But at the same time interparticle forces starts to be more significant at higher concentrations, which stabilizes the higher interstitial gas velocity. This tended to reduce the drag. Therefore, higher superficial gas velocity in the cohesive bed is required to give the appropriate drag.

This reverse effect at which $U_{mf}$ increases with increasing CMC concentrations can be detected by expanding the range of CMC concentration (higher than 1 wt% CMC). Investigating wider ranges shows the general trend that is followed by $U_{mf}$ with increasing CMC concentrations.

54

| Hs/D | L(gpm) | water | 0.2wt%CMC | 0.4wt%CMC | 0.8wt%CMC | 1wt%CMC |
|------|--------|-------|-----------|-----------|-----------|---------|
| 0.25 | 2 | 0.91 | 0.88 | 0.852 | 0.878 | 0.901 |
| 0.5 | " | 1.052 | 0.962 | 0.885 | 1.026 | 1.24 |
| 0.75 | " | 1.1 | 0.997 | 0.892 | 0.982 | 1.239 |
| 1 | " | 1.195 | 1 | 0.93 | 1.09 | 1.25 |
| | | | | | | |
| 0.25 | 4 | 0.9 | 0.851 | 0.719 | 0.785 | 0.872 |
| 0.5 | " | 0.964 | 0.9 | 0.735 | 0.964 | 1.06 |
| 0.75 | " | 0.987 | 0.967 | 0.81 | 0.969 | 1.1 |
| 1 | " | 1.028 | 0.99 | 0.912 | 0.984 | 1.2 |
| | | | | | | |
| 0.25 | 8 | 0.777 | 0.689 | 0.614 | 0.671 | 0.727 |
| 0.5 | " | 0.855 | 0.837 | 0.696 | 0.782 | 0.818 |
| 0.75 | " | 0.874 | 0.832 | 0.72 | 0.805 | 0.899 |
| 1 | " | 0.966 | 0.877 | 0.764 | — | — |
| | | | | | | |
| 0.25 | 14 | 0.72 | 0.6 | 0.585 | 0.62 | 0.699 |
| 0.5 | " | 0.792 | 0.72 | 0.62 | 0.75 | — |
| 0.75 | " | 0.852 | — | — | — | — |
| 1 | " | 0.9 | — | — | — | — |
| | | | | | | |

Table 4-1 Minimum fluidization velocities ($U_{mf}$) for $d_P$=38 mm

| Hs/D | L(gpm) | water | 0.2%wt CMC | 0.4%wt CMC | 0.8wt% CMC | 1wt% CMC |
|------|--------|-------|------------|------------|------------|----------|
| 0.25 | 2 | 0.976 | 0.834 | 0.787 | 0.899 | 0.921 |
| 0.5 | " | 1.061 | 1.009 | 0.96 | 0.989 | 1.1 |
| 0.75 | " | 1.36 | 1.054 | 1 | 1.25 | 1.3 |
| 1 | " | 1.39 | 1.247 | 1.2 | 1.388 | 1.42 |
| | | | | | | |
| 0.25 | 4 | 0.912 | 0.801 | 0.767 | 0.792 | 0.88 |
| 0.5 | " | 1.024 | 0.947 | 0.93 | 0.95 | 1 |
| 0.75 | " | 1.21 | 1.01 | 0.991 | 1.19 | 1.285 |
| 1 | " | 1.33 | 1.108 | 1.085 | 1.36 | 1.399 |
| | | | | | | |
| 0.25 | 8 | 0.745 | 0.641 | 0.601 | 0.66 | 0.739 |
| 0.5 | " | 0.835 | 0.821 | 0.79 | 0.85 | 0.92 |
| 0.75 | " | 1.09 | 0.97 | 0.82 | 0.985 | - |
| 1 | " | 1.1 | 1.07 | 0.92 | - | - |
| | | | | | | |
| 0.25 | 14 | 0.638 | 0.536 | 0.431 | 0.564 | 0.664 |
| 0.5 | " | 0.723 | - | - | - | - |
| 0.75 | " | 0.933 | - | - | - | - |
| 1 | " | 0.99 | - | - | - | - |
| | | | | | | |

Table 4-2 Minimum fluidization velocities ($U_{mf}$) for $d_p$ =20 mm

56
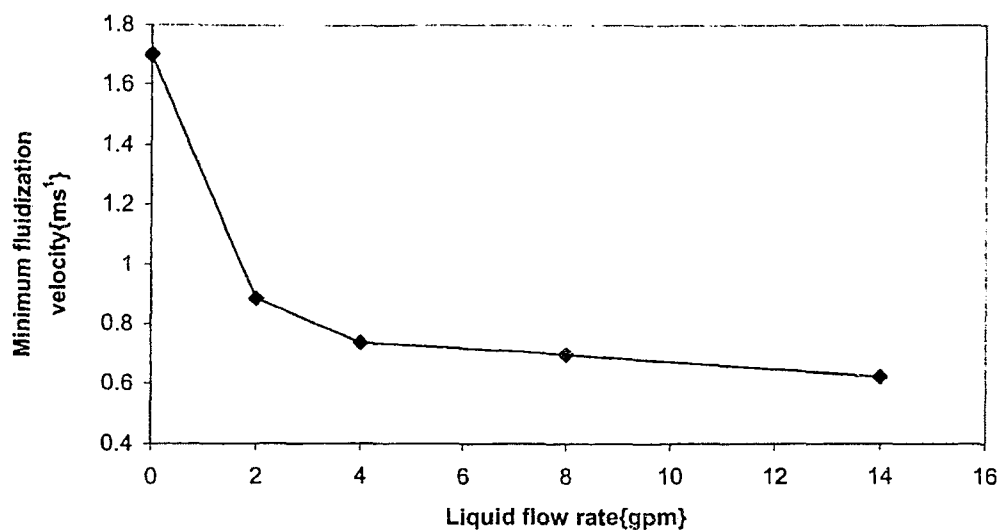
Figure 4-13    Effect of liquid flow rate on minimum fluidization velocity  at
Hs/D=0.5, dp=38mm, 0.4wt%CMC
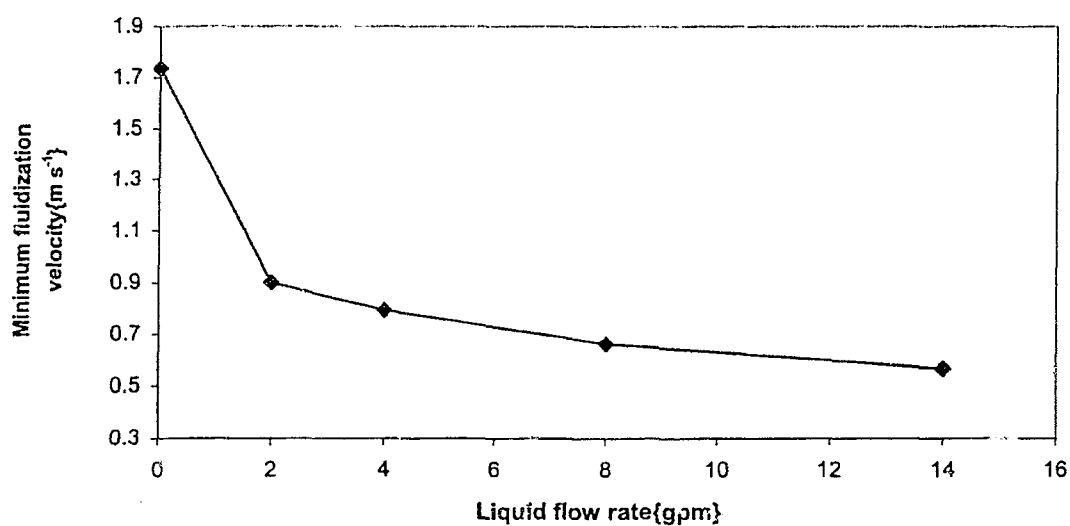


Figure 4-14   Effect of liquid flow rate on minimum fluidization velocity
at Hs/D=0.25, dp=20mm, 0.8wt%CMC

57
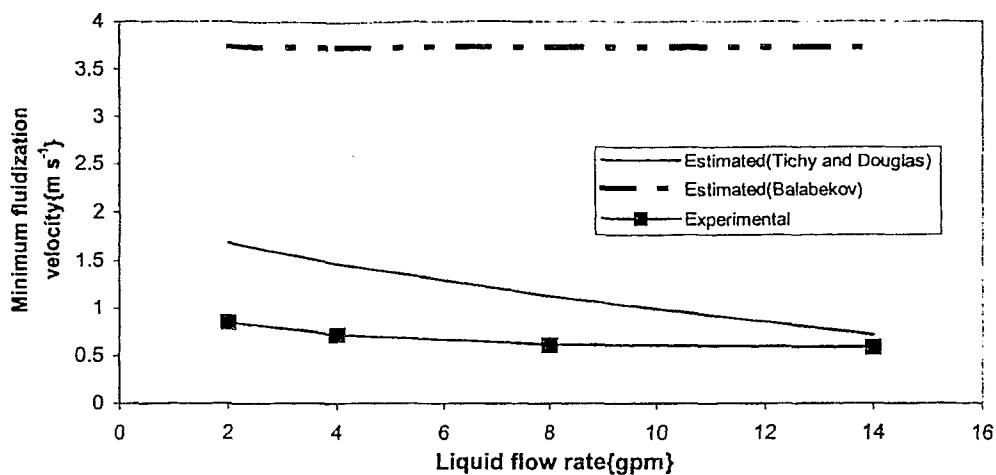
Figure 4-17  Estimated and experimental at Hs/D=0.25,  0.4%CMC,
dp=38mm
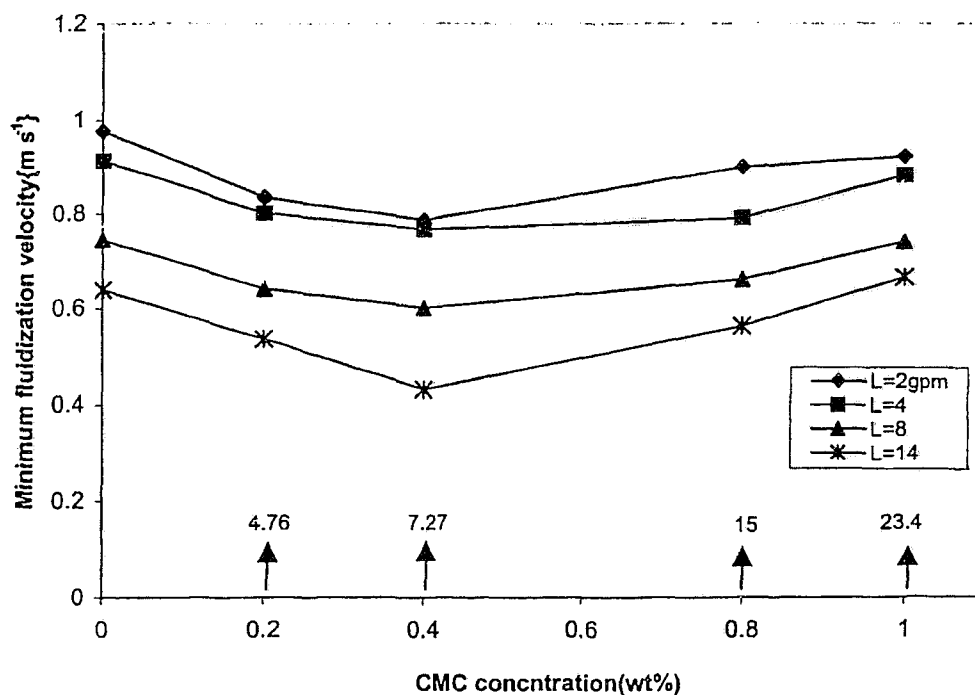


Figure 4-18   Effect of CMC concentration on minimum fluidization
velocity at Hs/D=0.25, dp=20mm,( $\blacktriangle$  viscosity, cP at 10 s$^{-1}$)

59
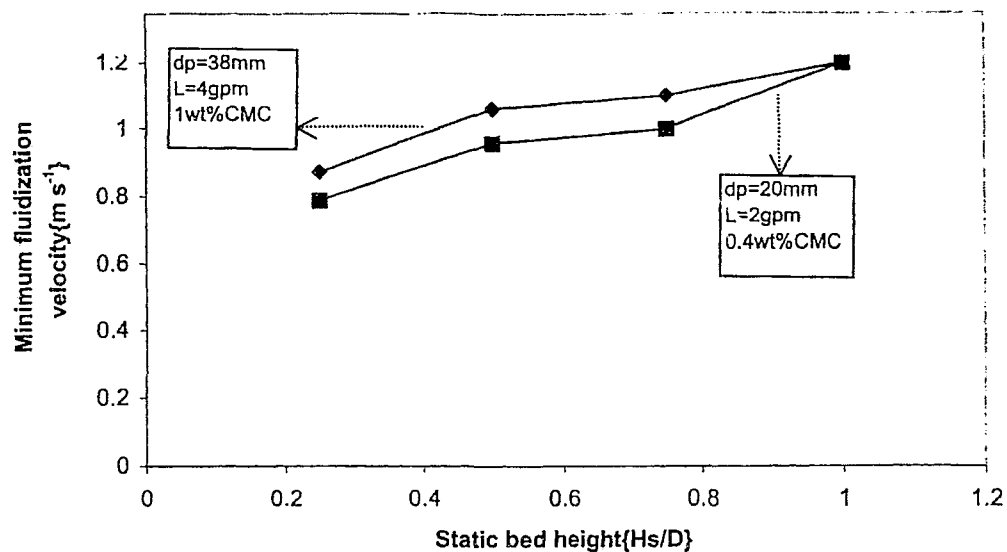
Figure 4-15 Effect of static bed height on minimum fluidization velocity
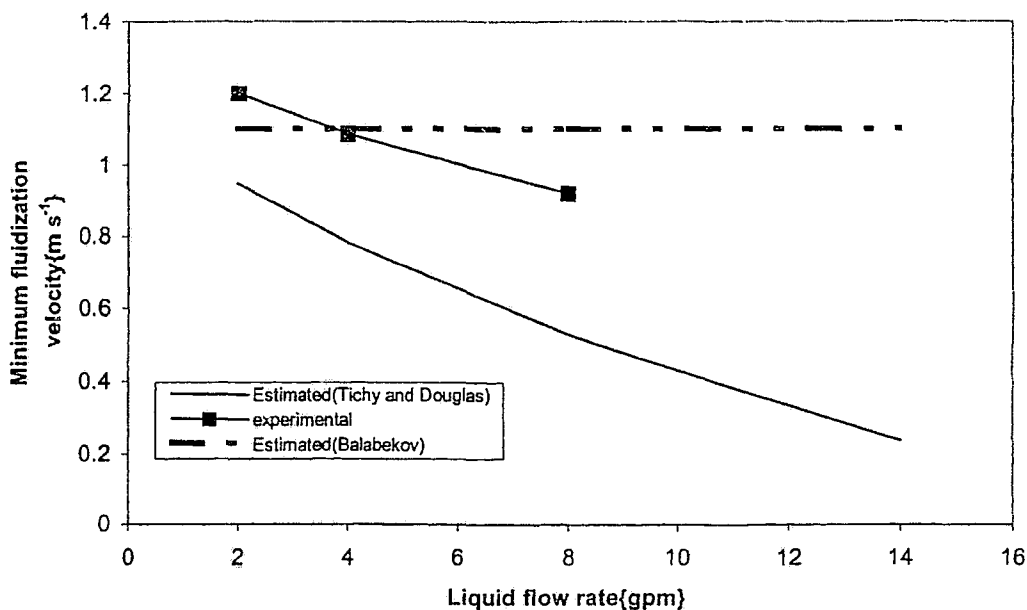


Figure 4-16 Experimental and estimated values for minimum
fluidization velocity at Hs/D=1.00, dp=20mm, 0.4%wtCMC

58
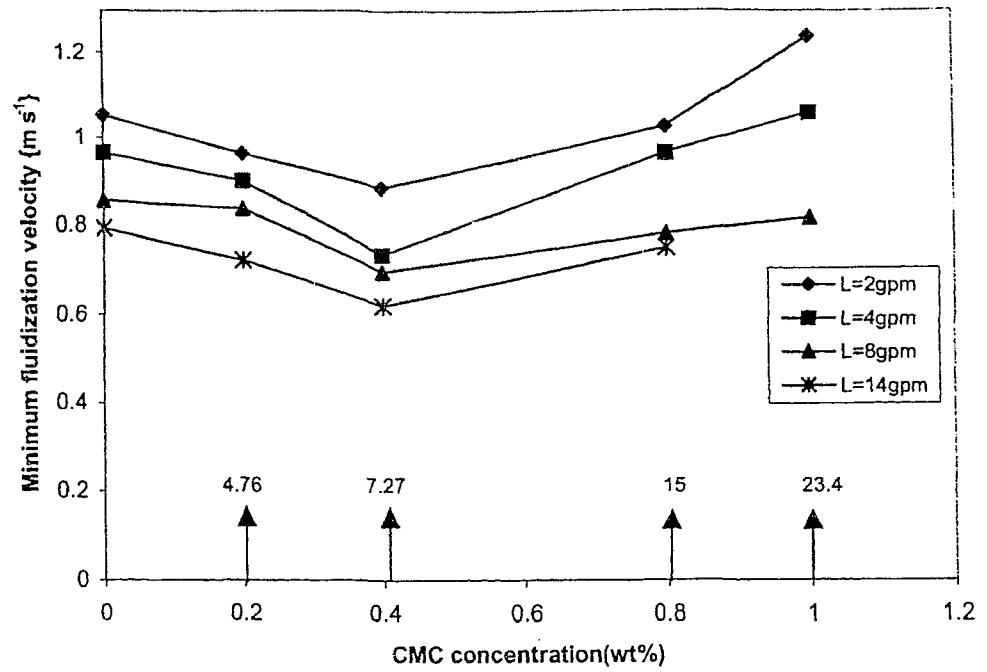
Figure 4-19　Effect of CMC concentration on minimum fluidization velocity at Hs/D=0.5, dp=38μm,(　viscosity ,cP at 10 s$^{-1}$)

60

## 4.3 Liquid Hold Up

Liquid hold up may be expressed alternatively as $\varepsilon_L$ or $\varepsilon_{L,St}$, depending on whether the volume of liquid is normalized to the static or expanded bed volume. The amount of liquid per cross-sectional area of the bed relates more directly to $\varepsilon_{L,St}$, as $H_S$ is a system constant while $H$ is in addition a function of gas velocity and liquid flow rate. The conventional pressure drop method determining liquid hold up is to measure the net pressure drop across the bed and subtract the buoyant weight of the solids per unit cross sectional area of the column. The difference is the weight of the operational liquid held in the bed per unit area. Expressing operational liquid hold up based on static bed volumes as $\varepsilon_{L,St}$, the pressure drop due to the presence of liquid as $\Delta P_L$, and the buoyant weight as W/S, then:

$$\Delta P - W / S = \Delta P_L = \rho_L \varepsilon_{L,St} g H_S \qquad (4\text{-}12)$$

$$\varepsilon_{L,St} = \frac{\Delta P - W / S}{\rho_L g H_S} \qquad (4\text{-}13)$$

Where $W$, the weight of the particles, was measured directly before placing the particles in the column. Equation (4-13) was used to determine the experimental $\varepsilon_{L,St}$ for all runs.

The effect of gas velocity on liquid holdup is shown in example curves of Figure 4-20. The remaining sets of conditions are in Appendix A, as Figures A-62 to A-69. These results show that the liquid hold up is independent of gas velocity in the fully fluidized regime for all liquid flow rates, CMC concentrations, both beads, and static bed heights. Since the liquid flow rate is constant, the bed expands with increasing superficial gas velocity in order to maintain a constant interstitial gas velocity, hence, constant liquid holdup.

The variation of the liquid holdup ($\varepsilon_{L,St}$) with liquid flow rate is illustrated in Figure 4-21 for sets of conditions, and for the other sets in Figures A-70 to A-77, in Appendix A. In general, the liquid holdup increased with increasing liquid flow rate following the same trend observed for Newtonian liquid (Abukhalifeh et al. (2003)). This is consistently true for all CMC concentrations, static bed heights, and both beads. The liquid holdup ($\varepsilon_{L,St}$) increases steadily

61

with liquid flow rate for both beads, but the rate of increase becomes more moderate at high static bed heights.

The dependency of $\varepsilon_{L,St}$ on static bed height is shown in example curve of Figure 4-22 for sets of conditions, while others are found in Appendix A, as Figures A-78 to A-82. An inverse relationship can be seen where $\varepsilon_{L,St}$ decreases with increasing static bed height at all CMC concentrations, $L$, and both beads. This inverse relationship can be seen by inspection of equation (4-13). The liquid holdup decreases markedly between $Hs/D = 0.25$ and $Hs/D = 0.5$ for all CMC concentrations. Then, the influence of static bed height becomes rather moderate for higher static bed heights range. Values of $\varepsilon_{L,St}$ for representative conditions are compared with estimated values obtained from the correlations of Kito et al. (1976e)) and Vunjak-Novikovac et al. (1987a) written in section 4.1, with modification suggested for effective liquid viscosity. As shown in Figures 4-23 and 4-24, the correlation by Kito et al. (1976e) over predicts the liquid holdup, while the correlation by Vunjak-Novikovac et al. (1987a) under predicts the liquid holdup. The experimental curve lies between the two correlations depicted. The effect of Archimedes number is illustrated in Figure 4-25. The liquid holdup decreases with increasing in Archimedes number for all bed conditions. The effect of packing density on liquid holdup is marginal in contrast to the effect of packing diameter.

Effect of CMC Concentration:

The comparison of liquid hold up in terms of static bed volume for different CMC concentrations for given sets of conditions is shown in Figure 4-26 and 4-27, other cases are in Appendix A, as Figures A-83 to A-90. From these figures, it is evident that the liquid hold up in the column is increasing with an increase in CMC concentration for all $L$, $Hs/D$, and both beads diameters. For low CMC concentrations, the liquid hold up increase is insignificant compared with water. At higher CMC concentrations, the rate of increase of $\varepsilon_{L,St}$ becomes more significant. The dramatic increase in $\varepsilon_{L,St}$ is clear at high CMC concentration (1wt% CMC) for all cases.

As discussed in section 4.1, increasing the CMC concentration increases effective viscosity of the CMC solution. The influence of non-Newtonian flow characteristics is insignificant

62

compared to viscosity effect. As a result, viscosity of the CMC solution is still higher than water viscosity after shear effects, hence, interstitial gas velocity increased. The increase in interstitial gas velocity may exert a drag on the liquid flowing down the bed, impeding the liquid flow, which increases the amount of liquid retained in the bed. Another possible explanation is that in dilute solutions at law shear rates ($\tau \to 0$, $\gamma \to 0$), and at high shear rates ($\tau \to \infty$, $\gamma \to \infty$), the solutions display Newtonian behavior. In addition, for dilute solutions, the total decrease in apparent viscosity is not large and the minimal value of apparent viscosity at $\gamma \to \infty$ is frequently high. As a result, the resultant apparent viscosity is relatively higher than water viscosity, which raises the liquid holdup in the bed.
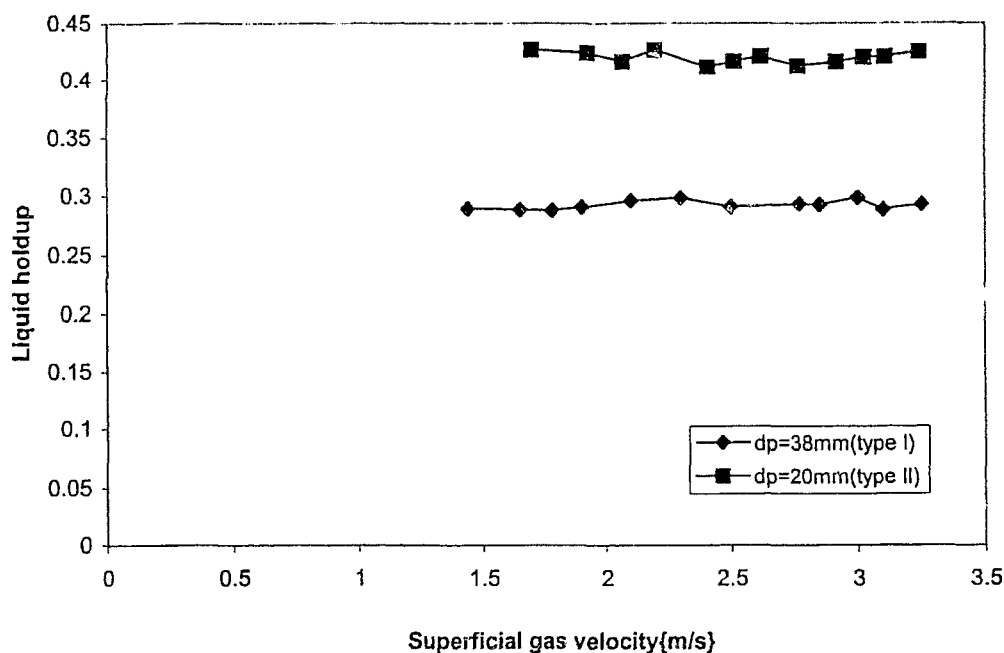


Figure 4-20  Effect of superficial gas velovity on liquid holdup at
Hs/D=0.75, L=4gpm
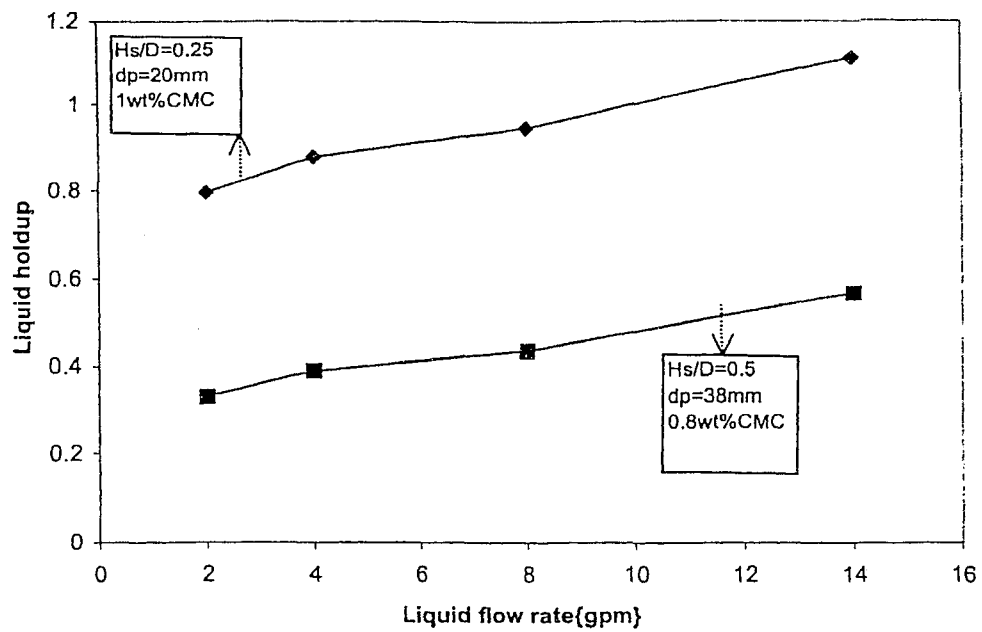
Figure 4-21  Effect of liquid flow rate on liquid holdup

64
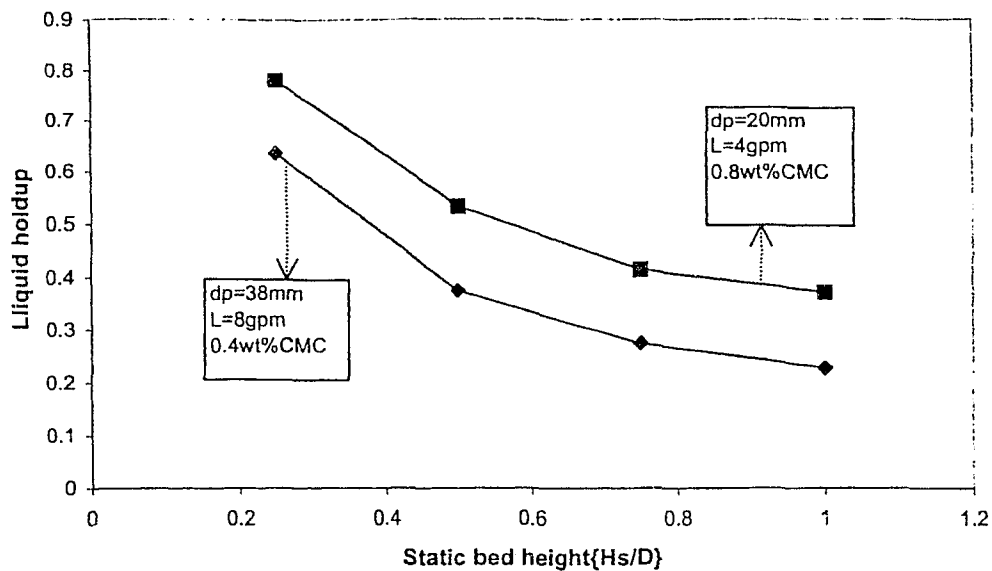
Figure 4-22  Effect of static bed height on liquid holdup
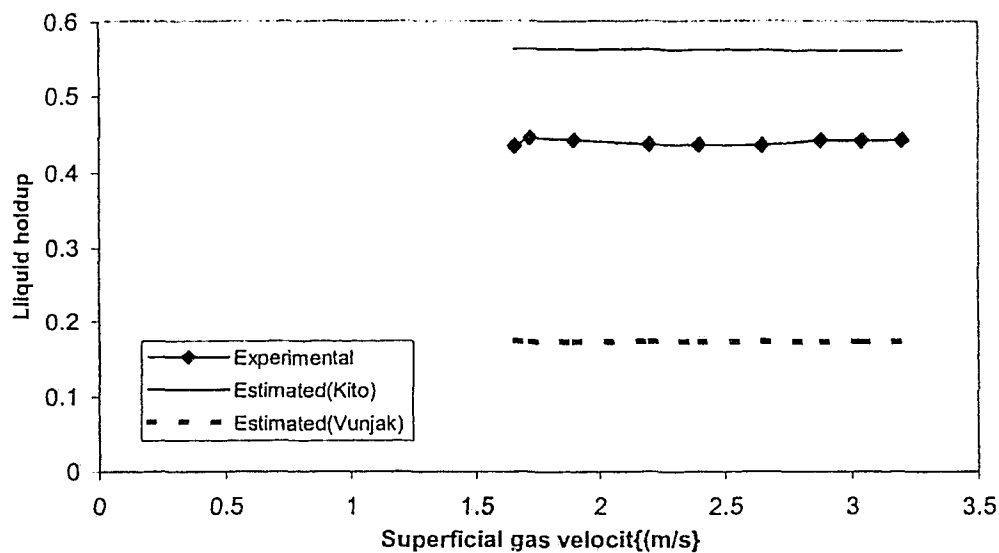


Figure 4-23  Estimated and experimental liquid holdup at Hs/D=0.5,
dp=38mm, L=8gpm, 0.8%CMC

65
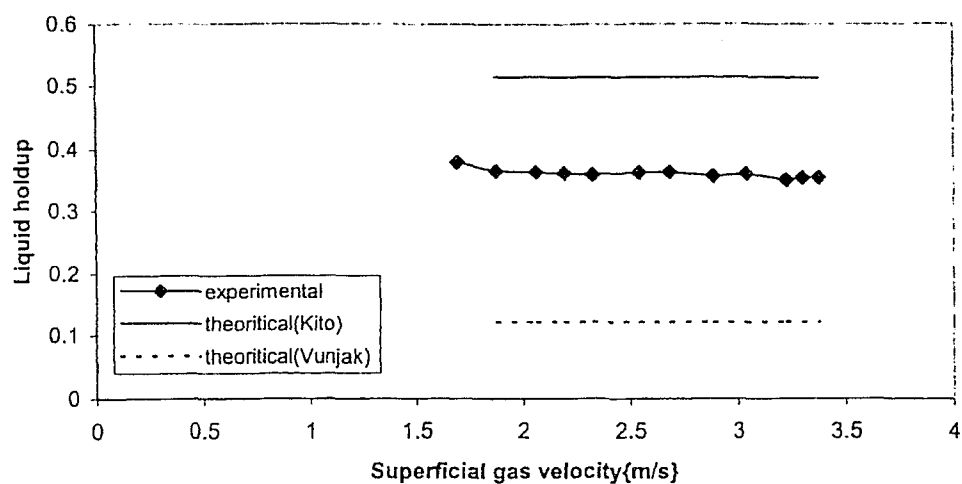
Figure 4-24 Experimental and theoretical liquid holdup at Hs/D=0.75, dp=20mm, L=4gpm, 0.4%CMC
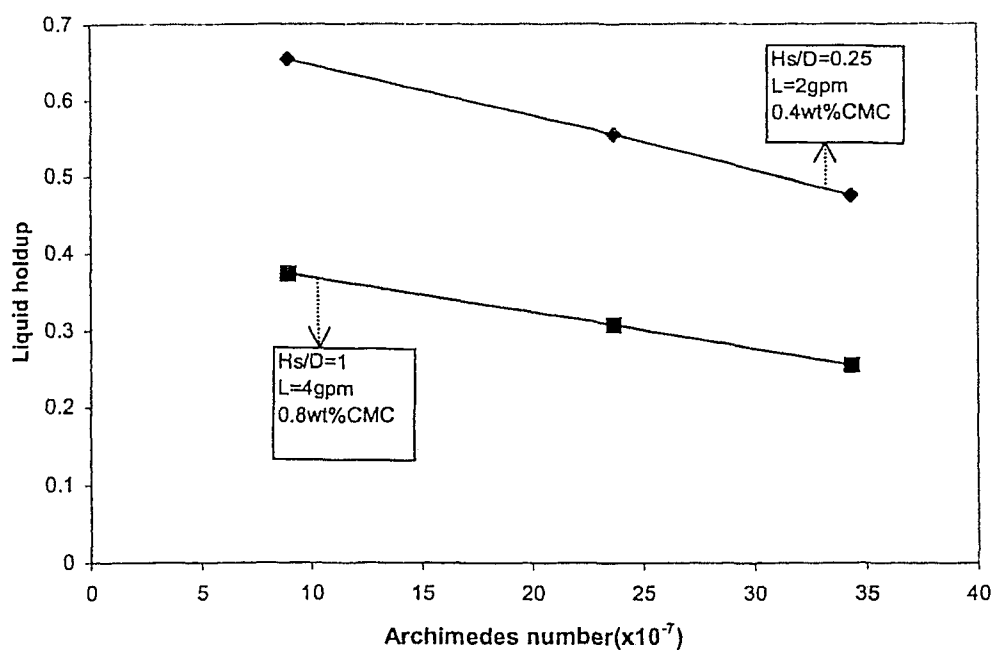


Figure 4-25 Effect of Archimedes number on liquid holdup

66
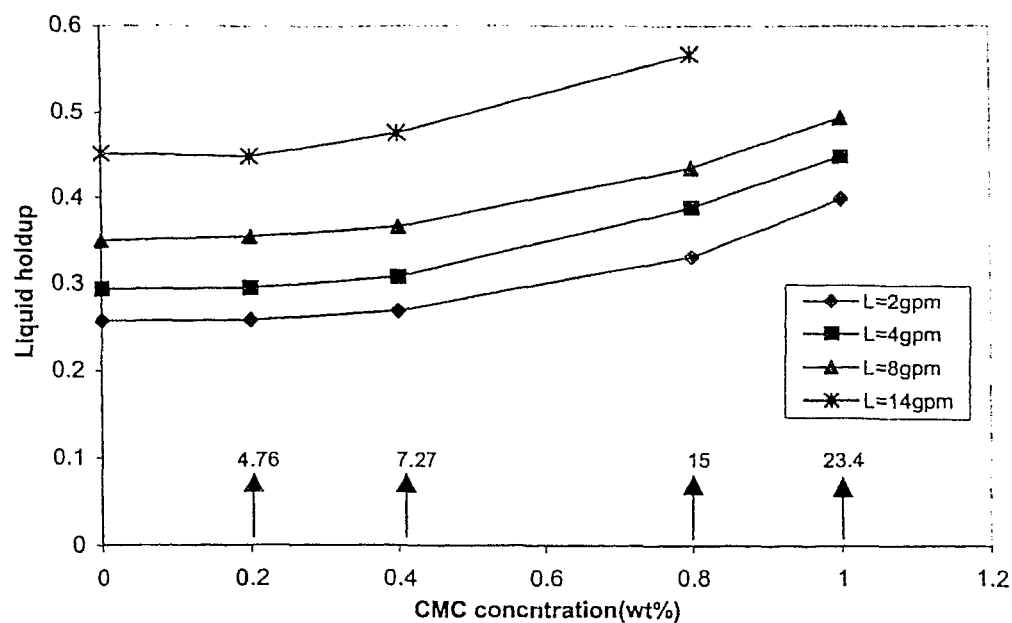
Figure 4-26  Effect of CMC concentration on liquid holdup at Hs/D=0.5, dp=38mm, ( $\uparrow$ viscosity,cP, at $10\ s^{-1}$ )
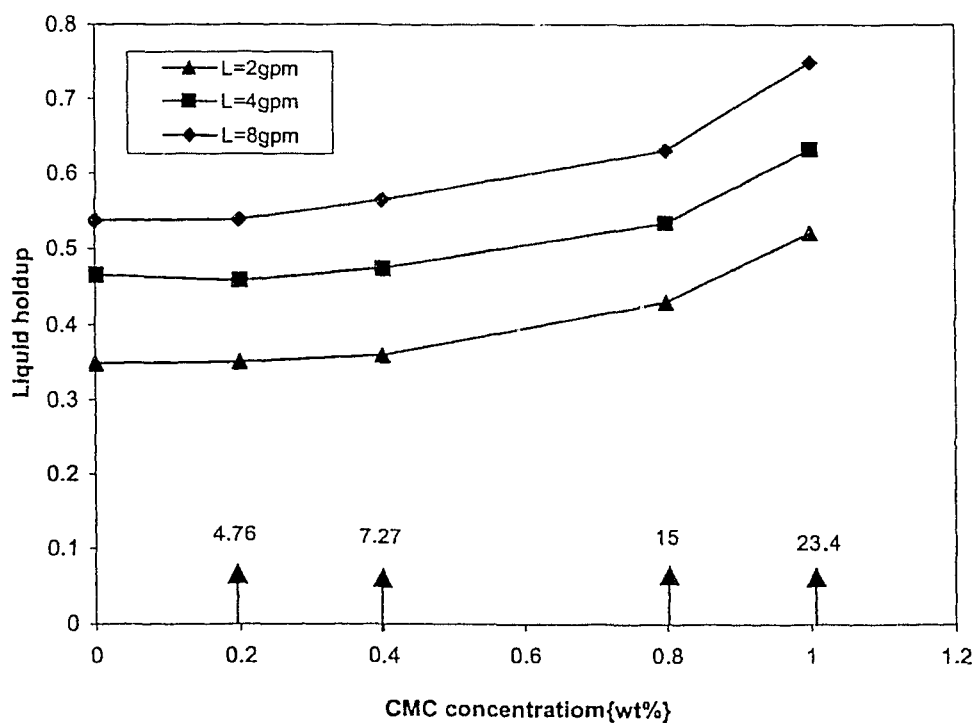


Figure 4-27  Effect of CMC concentration on liquid holdup at Hs/D=0.5, dp=20mm,( $\uparrow$ viscosity, cP, at $10\ s^{-1}$ )

67

## 4.4 Bed Expansion

As the gas velocity was increased beyond the minimum fluidization velocity, the gas drag caused the beads to burst in the center created a flow of beads upward. The beads moved up ward in the center and down ward at the wall.

With higher gas velocities flat slugs were generated lifting the entire bed to higher heights from which beads rained back down through the slug. Further increase in gas velocities caused the beads to reach their highest point of travel.

For 38 mm particles, at high static bed heights and at low gas velocities during fluidization it was observed that the particles started lining up at the wall. Once a single particle layer was set on the grid around the wall, subsequent stacking of the remaining particles as one layer over the other took place within a minute. This was seen to form and break off on its own, or as the gas velocity increased. This could be attributed to the greater force of adhesion of the particles to the wall. This force of adhesion, which arises as a result of the interfacial tension and the liquid bridge formed between the particles and the wall.

The measurement method used for bed height expansion in this study is simply observing maximum and minimum heights over a period of time and estimating an average. The effect of gas velocity on relative expanded bed height is illustrated in the example curves of Figures 4-28 and 4-29. Other combinations are shown in Appendix A, as Figures A-91 to A-98. Relative expanded bed height increases with increasing superficial gas velocity. Similar trend is observed for all other combinations.

The experimental results in these figures show that there are two regions on the bed expansion curve: region I and region II. Relative expanded bed height increases linearly and steadily with gas velocity in region I. At a critical gas velocity of about 2.5 m/s, region II starts at which the rate of increase becomes more dramatic. At high liquid flow rates no critical gas velocities are observed and the rate of increase of $H/H_s$ with gas velocity remains constant.

The existence of two regions on the curve relating bed expansion to gas velocity was reported by Balabekov et al. (1969a, 1971), Gel'perin et al. (1968b), and Vunjak-Novakovic et al. (1987b) for air-water systems. The variations of expansion of bed with superficial gas velocity are consistent in trend with Newtonian liquid (Abukhalifeh et al. (2003)).

68

The example curve in Figure 4-30 shows the variation of $H/H_S$ with liquid flow rate. The general trend is increasing tendency with increasing $L$ as shown in Figures A-99 to A-107, in Appendix A. The increase in relative expanded bed height with increasing $L$ is rather moderate in the high range of liquid flow rates, while that effect becomes stronger at low liquid flow rates range for both beads. Some exceptions can be seen which can be due to lack of high certainty in measuring bed expansion.

Relative expanded bed height data obtained at various static bed heights are plotted in sample Figures 4-31 and 4-32. Other cases are in Appendix A, as Figures A-116 to A-121. The basic feature of these results is that $H/H_S$ decreases with increasing static bed height for all liquid flow rates, CMC concentrations, and beads diameters. A significant decrease in $H/H_S$ occurs at low static bed height range, but at mid to high static bed height range ($H_S/D$ =0.5, 0.75, 1) a less significant decrease resulted for all cases.

The variation of relative bed expansion with Archimedes number, $Ar$, is shown in the example curves in Figure 4-33. At $H_S/D$ =0.25 and $H_S/D$ =0.5, the inverse relationship can be seen. In contrary, at $H_S/D$ =0.75 and $H_S/D$ =1, the direct proportion is clear. Similar trends for all bed conditions at each static bed height are observed. A general explanation for this decrease in relative expanded bed height at low static bed height range is that the particle diameter increase results a decrease in the surface area per unit volume with less liquid flows. Therefore, a lower interstitial gas velocity and a decrease in bed height. For high static bed height range, the increase in particle density would increase the interstitial gas velocity; as a result bed height increases. It is apparent that a competition between two parameters involved: diameter and density of the packing, and which one dominated the effect rather than the other depend on the static bed height.

Estimated values for bed expansion were calculated using the equations (4-14) and (4-15) proposed by Vunjak-Novakovic et al. (1987b), and equation (4-16) proposed by O'Neill et al. (1972) for Newtonian liquid.

Type I:

$$H/H_S = (1-\varepsilon_O + 2.48\times 10^{-3}(H_S/D)^{-0.567}d_p{}^{-0.568}G_L{}^{0.719} + 0.02)$$
$$/(1-0.628U_g{}^{0.237})$$

(4-14)

69

Type II:

$$H/H_S = (1 - \varepsilon_O + 4.43 \times 10^{-3} (H_S / D)^{-0.437} d_P^{-0.494} G_L^{0.812} (\rho_S / \rho_L)^{0.09} + 0.02)$$
$$/(1 - 0.628 U_g^{0.237})$$ (4-15)

$$H/H_S = \frac{1 - \varepsilon_O}{1 - \varepsilon}$$ (4-16)

Where

$$\varepsilon = \left\{ K[(27 + 4K)/108]^{1/2} + K/2 \right\}^{1/3} - \left\{ K[(27 + 4K)/108]^{1/2} - K/2 \right\}^{1/3}$$ (4-17)

$$K = \left[ \frac{U_g^{1/2} + U_L^{1/2} (\rho_L / \rho_g)^{1/4}}{0.775 (g d_P \rho_L / 6 \rho_g)^{1/4}} \right]^4$$ (4-18)

A comparison between experimental values and correlations values is shown graphically in Figures 4-34 and 4-35. For $d_P$=20 mm, values predicted with O'Neill correlation agreed very well with experimental results at low gas velocities. However, for $d_P$=38 mm, values predicted with Vunjak-Novakovic correlation have good agreement with experimental results at high gas velocities.


Effect of CMC Concentration

The effect of increasing viscosity of liquid phase in the TBC has a retarding effect on bed expansion. Graphs for all combinations of $H/H_S$ versus CMC concentrations are found in Appendix A, Figures A-108 to A-115. Example curves in Figures 4-36 and 4-37 show that increasing the concentration of CMC solution decreases the relative bed expansion.

As discussed in section 4.1, at higher CMC concentrations, higher viscosities obtained. The bed becomes denser, which decreases the bed voidage, hence the interstitial gas velocity increases. However, interparticle forces increased, these forces stabilizes the effect of interstitial gas velocity. The net act is to attain lower values of expansion. The higher the interparticle forces, the lower the likelihood for the energy imparted by the flowing gas is to break the network of interparticle bonds. The most dramatic decrease in $H/H_S$ with increasing CMC concentrations is at the highest range of CMC concentrations.
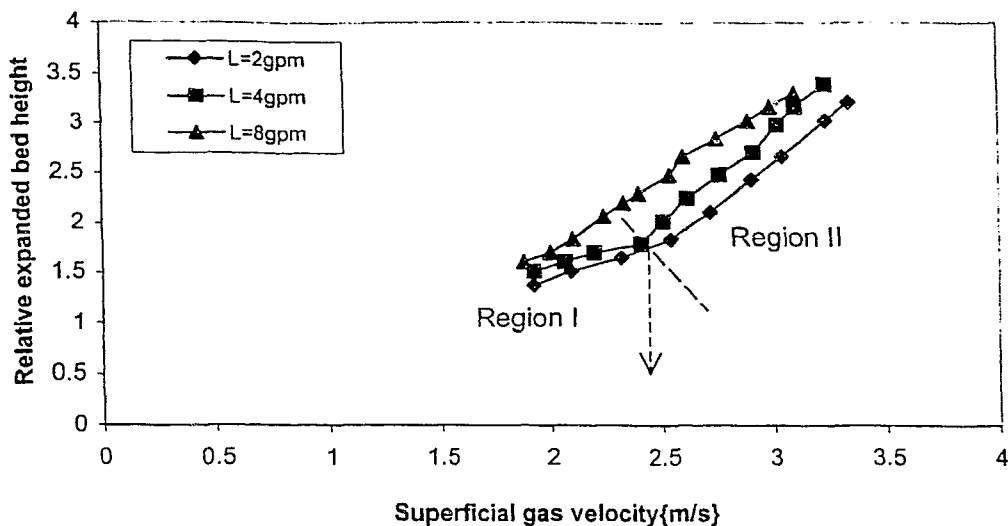
Figure 4-28  Effect of superficial gas velocity on expanded bed height at
Hs/D=0.75, dp=20mm, 0.8%CMC
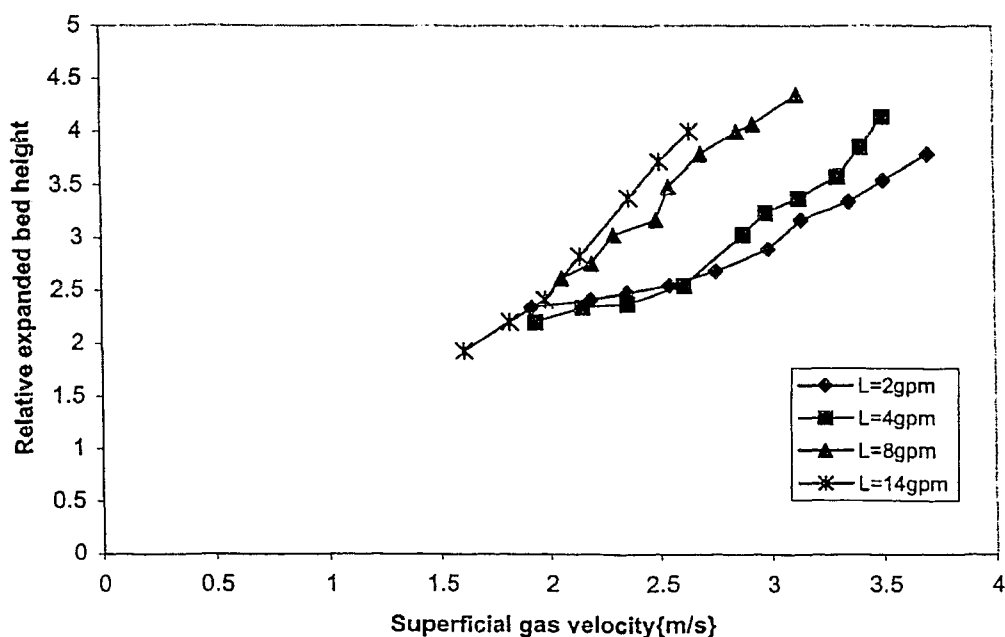


Figure 4-29  Effect of superficial gas velocity on expanded bed height
at Hs/D=0.5, dp=38mm, 0.4%CMC

71
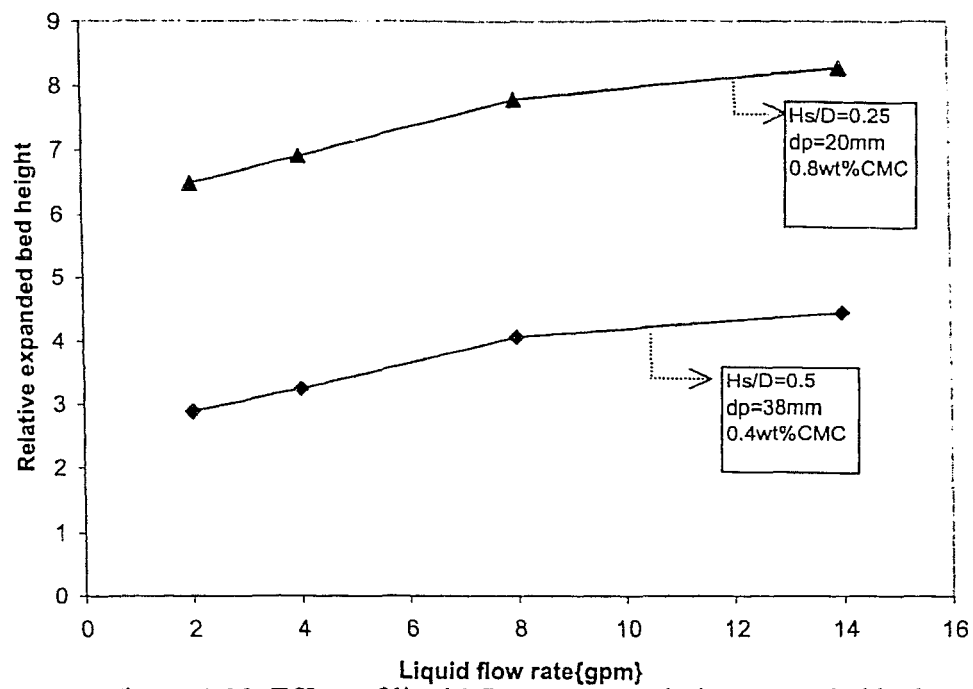
Figure 4-30  Effect of liquid flow rate on relative expanded bed height(H/Hs)

72
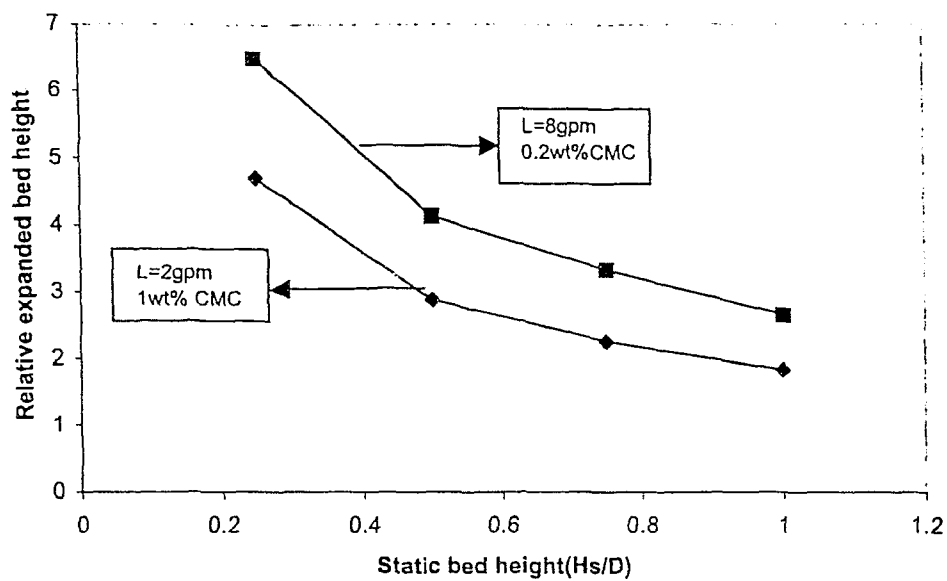
Figure 4-31 Effect of static bed height on relative expanded bed
height at dp=38mm
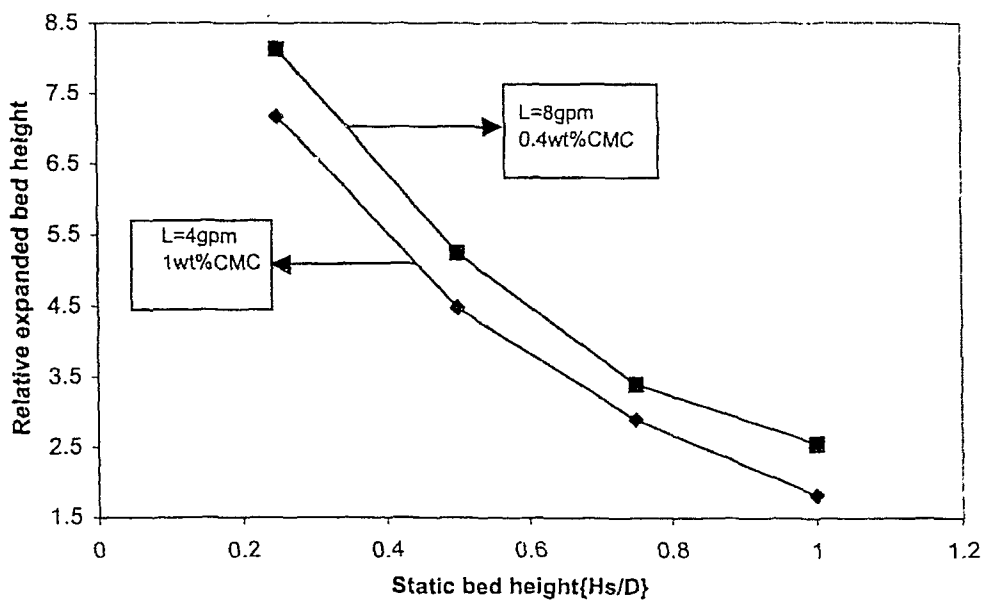


Figure 4-32 Effect of static bed height on relative expanded bed
height at dp=20mm
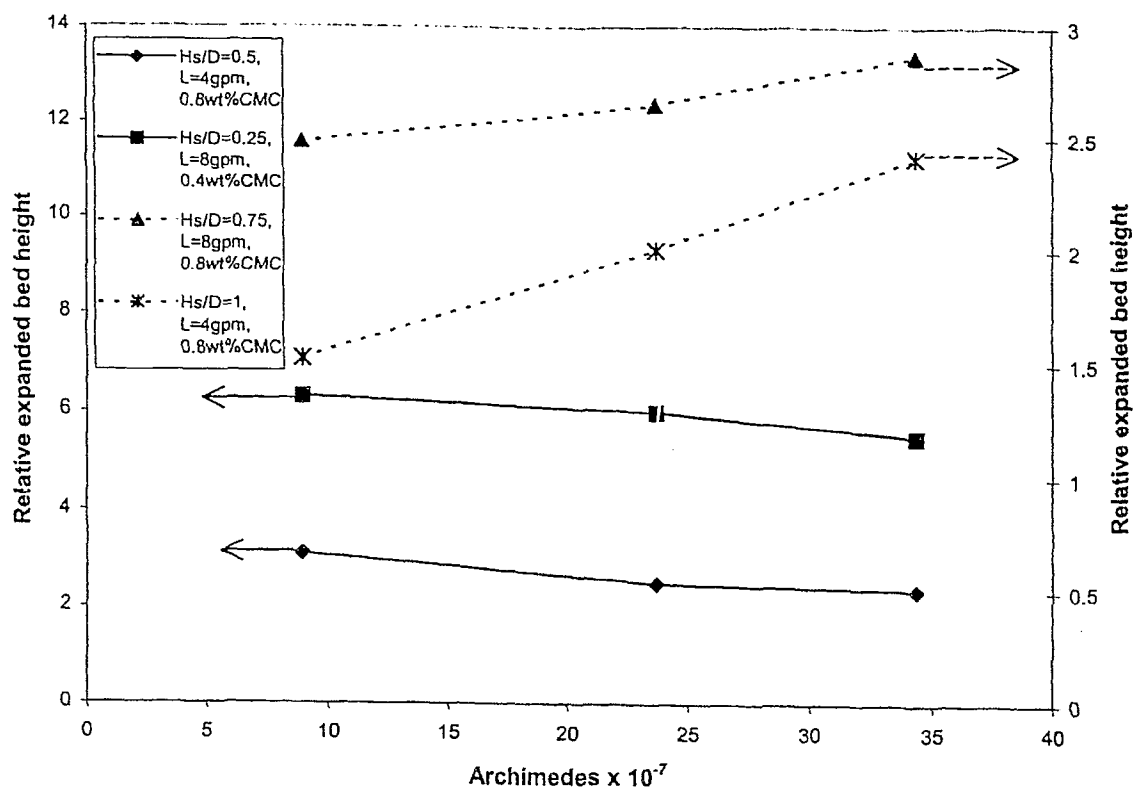
Figure 4-33  Effect of Archimedes number on relative bed expansion {H/Hs}

74
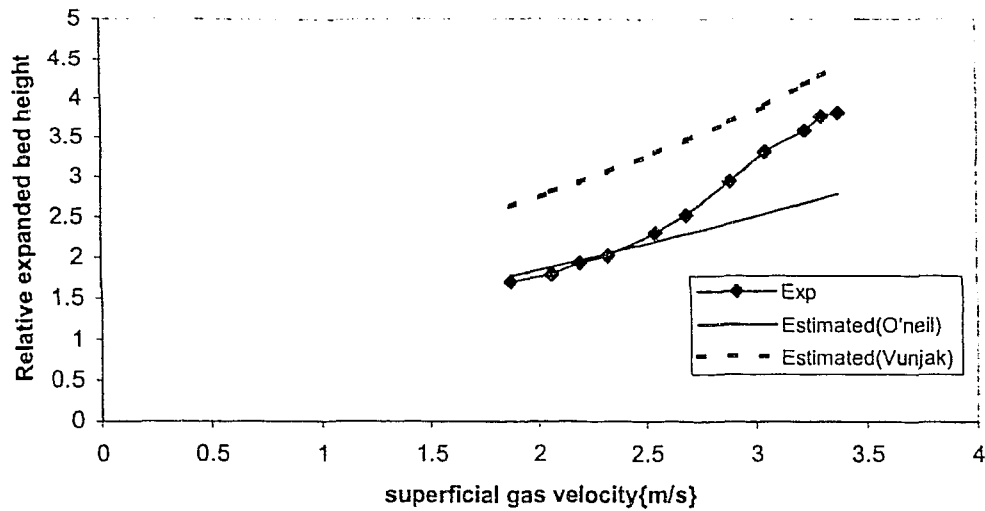
Figure 4-34  Experimental and estimated relative expanded bed height at
Hs/D=0.75, dp=20mm, L=4gpm, 0.4%CMC
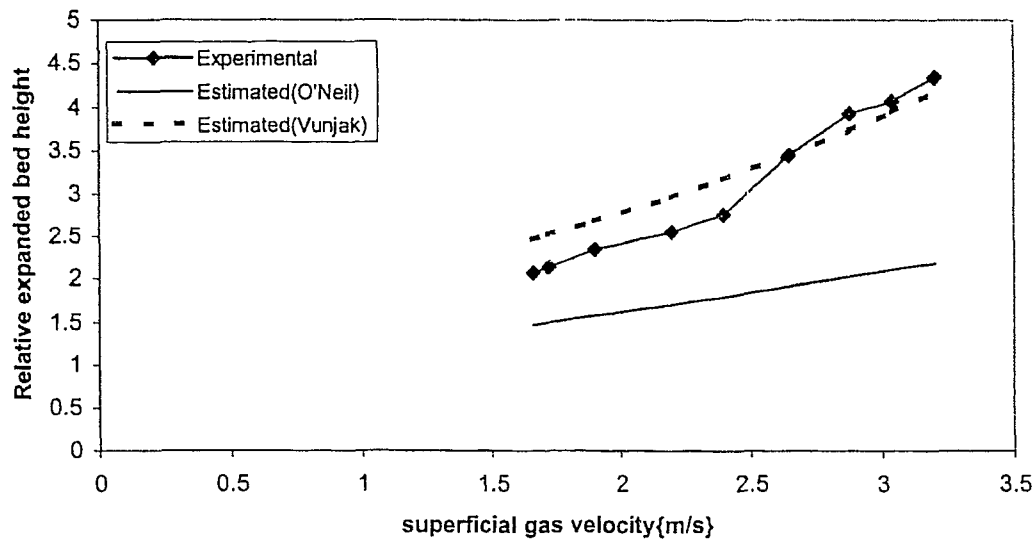


Figure 4-35  Estimated and experimental relative expanded bed height
at Hs/D=0.5, dp=38mm, L=8gpm, 0.8%CMC

75
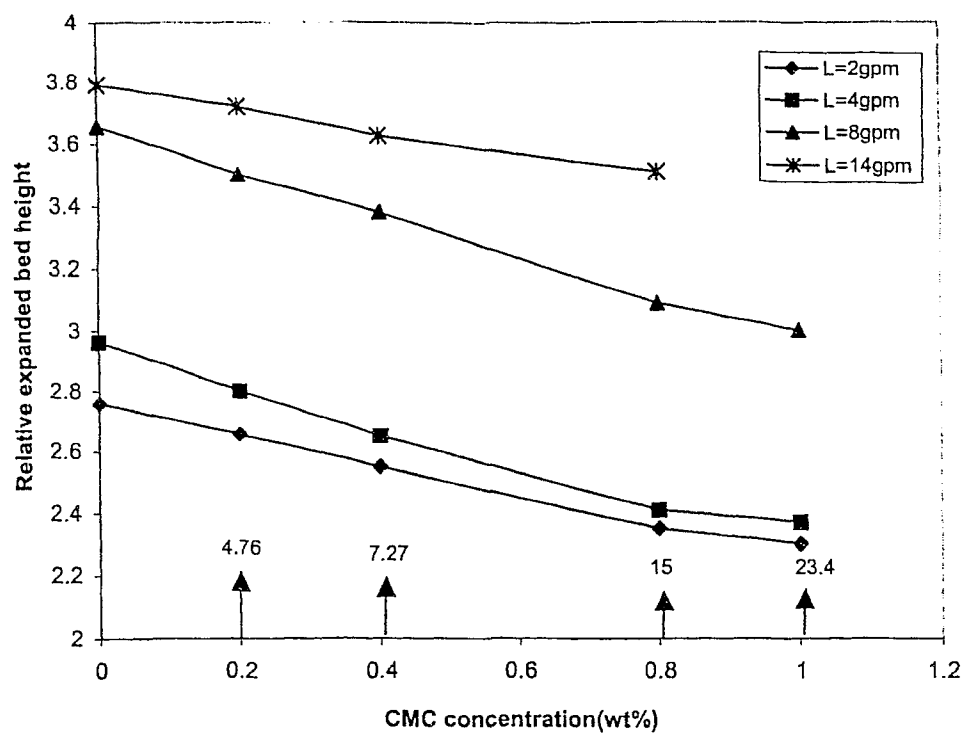
Figure 4-36  Effect of CMC concentration on relative bed expansion at
Hs/D=0.5, dp=38mm,( ↑ viscosity,cP, at 10 s$^{-1}$)

76
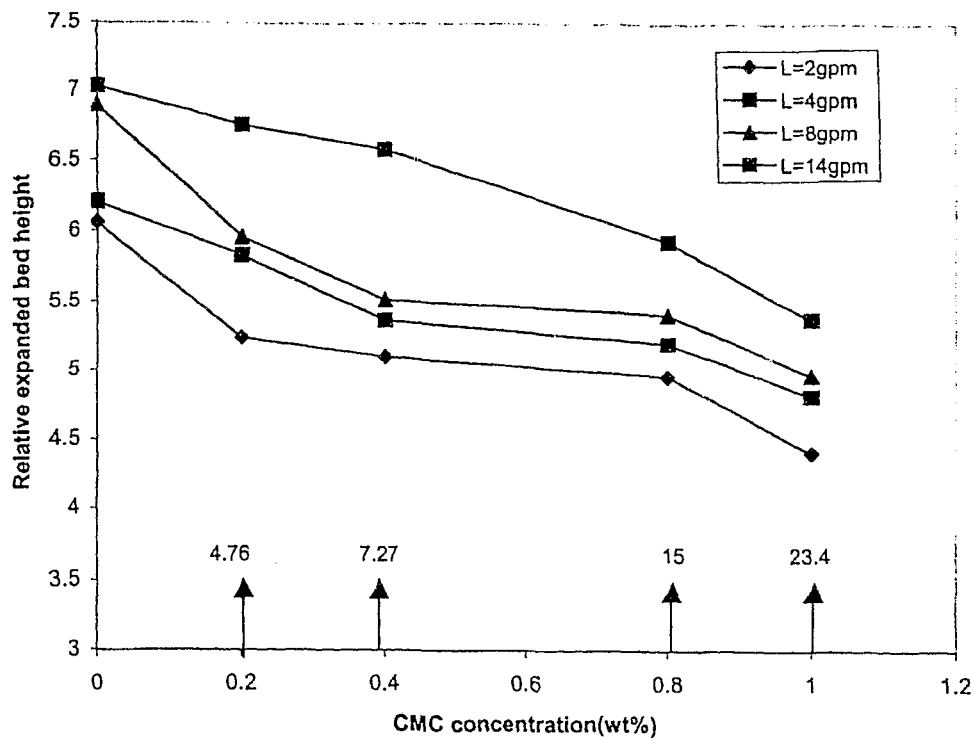
Figure 4-37 Effect of CMC concentration on relative expanded bed height at dp=20mm, Hs/D=0.25,(▲ viscosity,cP, at 10 s⁻¹)

77

## 4.5 Gas Hold Up

The relation between fractional hold up of liquid ($\varepsilon_L$), gas ($\varepsilon_g$) and solid ($\varepsilon_S$) phases,

$$\varepsilon_L + \varepsilon_g + \varepsilon_S = 1 \tag{4-19}$$

$$\varepsilon_{L,St} + \varepsilon_{g,St} + \varepsilon_{S,St} = H/H_S \tag{4-20}$$

may be written with reference to either the expanded or static bed volume. The gas phase hold up is the most difficult to measure experimentally. Consequently gas hold up has normally been obtained by difference, using the volume balance equations. It can be determined indirectly from liquid hold up and bed expansion. Sample curves in Figure 4-38 give determined values of $\varepsilon_G$ plotted against $U_g$, for sets of conditions. Other figures with different combinations of bed conditions are in Appendix A, as Figures A-145 to A-152. This example curves illustrate the gas hold up dependency on gas velocity. The gas hold up increases linearly with increasing gas velocity. Similar trend is observed for other conditions for both beads.

The variation of gas holdup ($\varepsilon_g$) with liquid flow rate is illustrated in the sample curves in Figure 4-39 and for other combinations in Appendix A, as Figures A-130 to A-138. In general terms, the gas holdup varies slightly with increasing liquid flow rate. It doesn't follow a consistent trend for all cases.

The effect of static bed height on gas holdup is shown in the sample curves in Figure 4-40 for sets of conditions and in Appendix A, a Figures A-139 to A-144 for the rest of sets. The basic feature is the decrease in gas holdup with increasing static bed height. However, the variation in gas holdup is not significant for $d_P = 38$ mm for all combinations. But for $d_P = 20$ mm, the gas holdup ($\varepsilon_g$) decreases markedly for all combinations.

Estimated values for gas holdup were calculated using equation (4-21) proposed by Vunjak-Novikovac et al. (1987b) and equation (4-22) proposed by Kito et al. (1976e) for gas holdup with Newtonian liquids:

$$\varepsilon_g = 0.628 U_g^{0.237} \tag{4-21}$$

$$\varepsilon_g = 0.19 (d_P U_g^2 \rho_L / \sigma)^{0.11} (U_g / \sqrt{g d_P})^{0.22} \tag{4-22}$$

78

A comparison between experimental values and correlations values is shown in Figures 4-41 and 4-42. Good agreement between experimental and predicted data by Kito correlation at high gas velocities for both beads, while Vunjak-Novakovic correlation over predicts the gas holdup.

Effect of CMC Concentration

As seen in Figure 4-43 and Figures A-122 to A-129 in Appendix A, the general trend of gas holdup dependency on CMC concentrations is a decreasing tendency with increasing CMC concentration for all bed conditions.

This could be due to the increase in surface friction, since the effective viscosity of the CMC solutions is still higher than water viscosity after shear effects. As a result of increasing surface friction, the liquid holdup increases. So more liquid is retained in the bed, therefore, less gas holdup. The viscosity effect on gas holdup becomes stronger at the high range of CMC concentration (1wt% CMC) or all cases.

The effect of Archimedes number on gas holdup is seen in example curves in Figure 4-44. The same trend observed with the relative expanded bed height is seen with the gas holdup. For low to mid range of static bed height, the gas holdup decreases with increasing Archimedes number, while for mid to high range static bed height, an increase in gas holdup results with increasing Archimedes number.

79
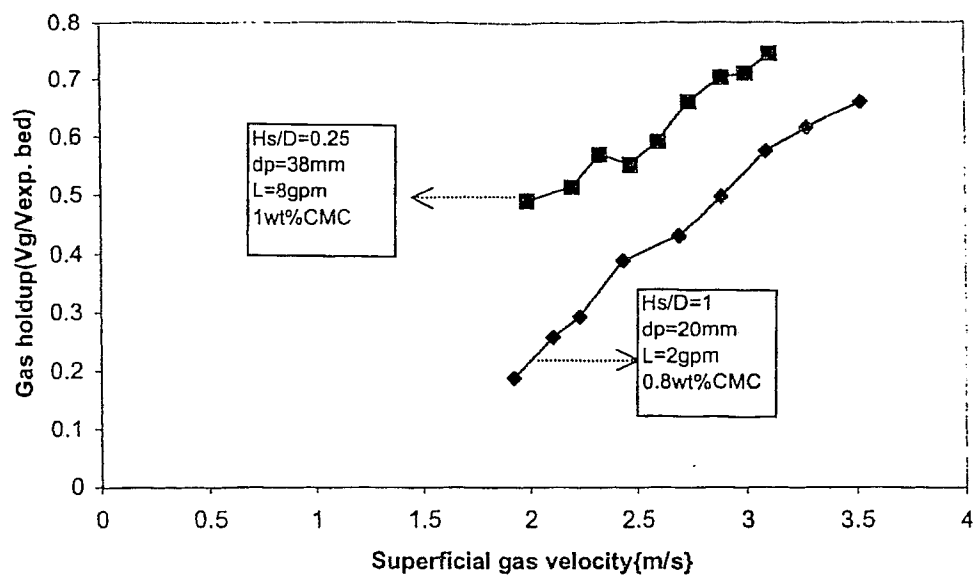
Figure 4-38 Effect of superficial gas velocity on gas holdup
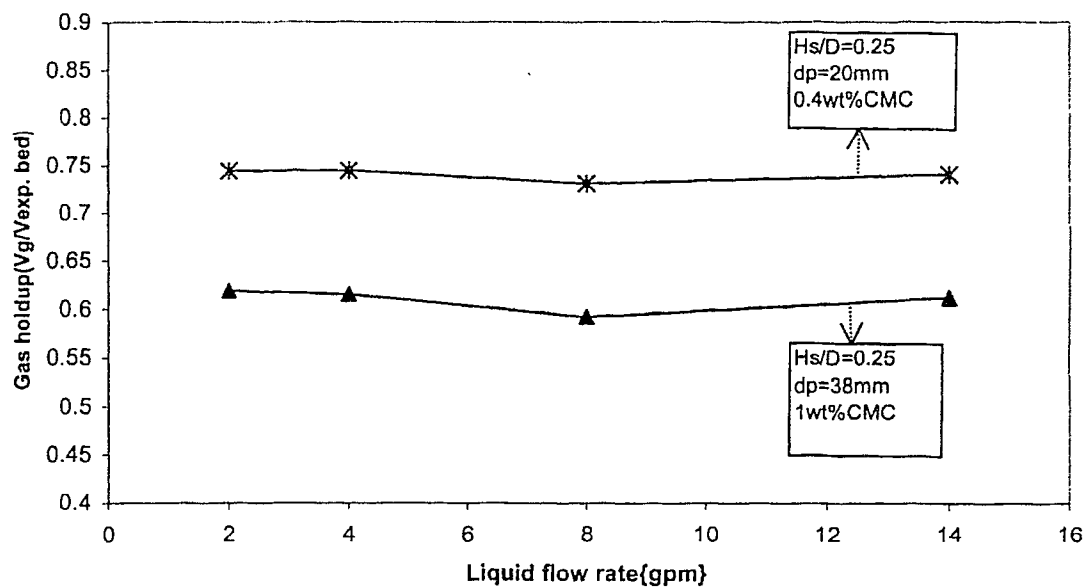


Figure 4-39 Effect of liquid flow rate on gas holdup

80
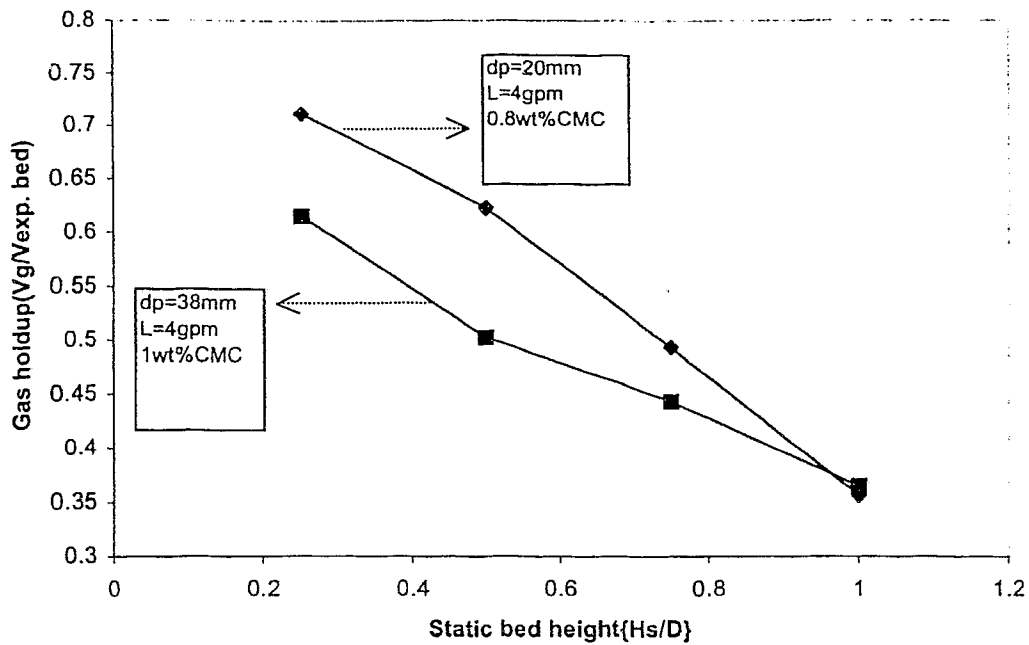
Figure 4-40  Effect of static bed height on gas holdup
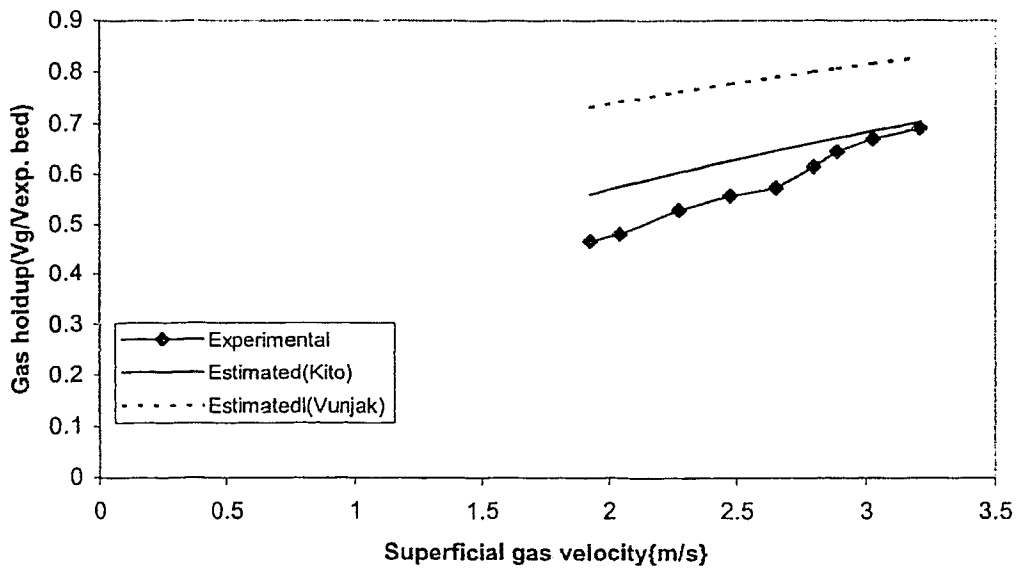


Figure 4-41  Experimental and estimated gas holdup at Hs/D=0.5,
dp=38mm, L=4gpm, 0.8%CMC

81
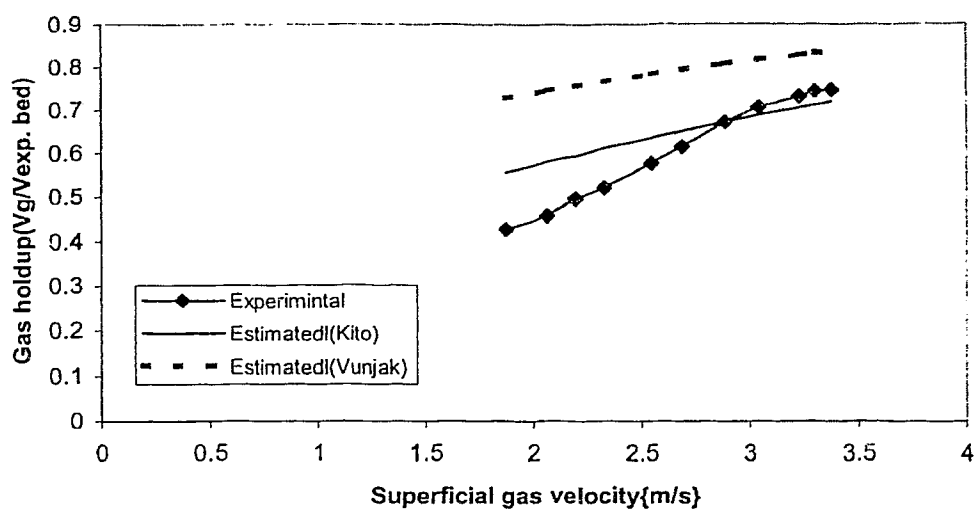
Figure 4-42 Experimental and estimated gas holdup at dp=20mm,
Hs/D=0.75, L=4gpm, 0.4%CMC
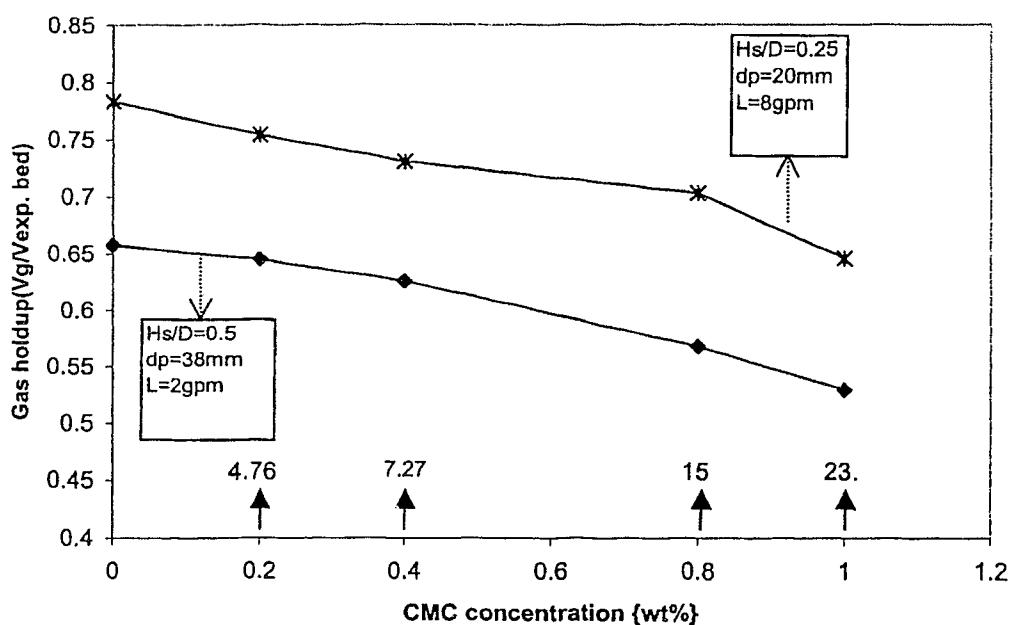


Figure 4-43 Effect of CMC concentration on gas holdup
( ↑ viscosity,cP, at 10 s$^{-1}$ )

82
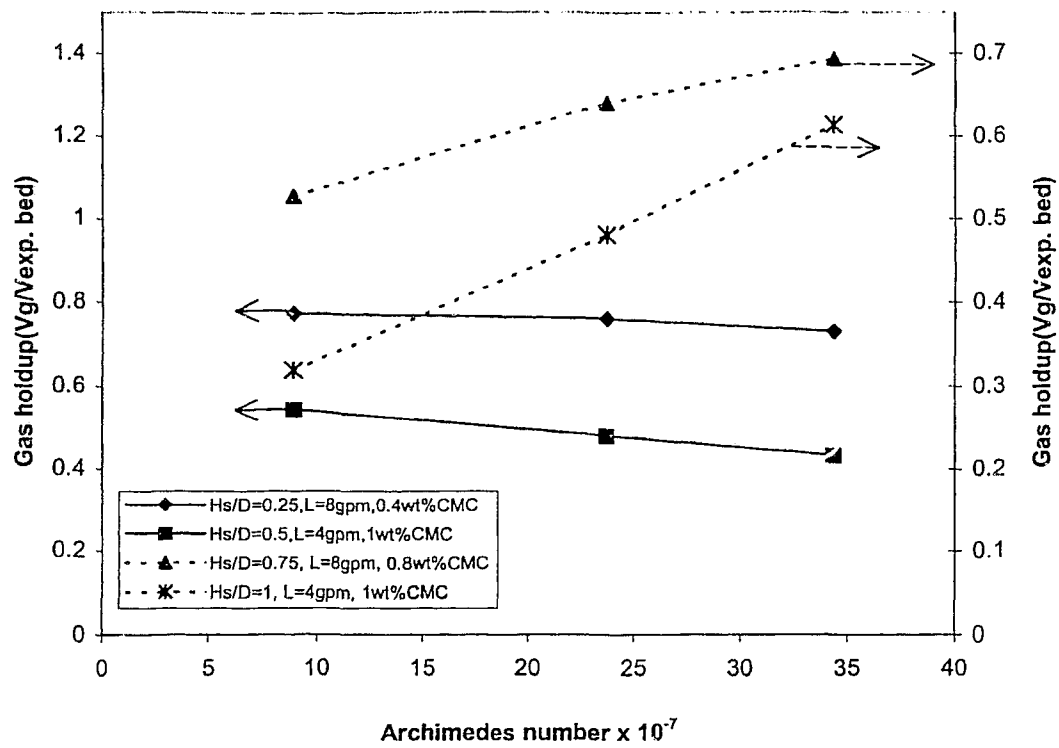
Figure 4-44  Effect of Archimedes number on gas holdup

83

# CHAPTER 5

# CONCLUSIONS

The following are the summary of conclusions for pioneer work on hydrodynamic characteristics of a three-phase turbulent bed contactor (TBC) with counter current flow of gas and liquid using aqueous solutions of CMC as non-Newtonian liquid:

1. Net pressure drop, liquid holdup, expanded bed height, minimum fluidization velocity and gas holdup were measured for two bead sizes, four static bed heights, four liquid flow rates, and four CMC concentrations.

2. Net pressure drop was found to increase consistently with increasing apparent viscosity of aqueous solution of CMC. A very small increase was observed at low CMC concentrations (0.2 wt % and 0.4 wt %), while the impact becomes stronger at higher CMC concentrations (0.8 wt %, 1 wt %).

3. Net pressure drop with aqueous solutions of CMC was independent of superficial gas velocity. It was found to increase consistently with increasing liquid flow rate and static bed height.

4. Liquid holdup as determined from the pressure drop method, was found to increase consistently with increasing apparent viscosity of aqueous solutions of CMC. The increase becomes more significant as the CMC concentration increased.

5. Liquid holdup dependency on gas velocity was similar to that of the net pressure drop, and it decreased with increasing static bed height. Liquid hold up increases consistently with increasing liquid flow rate for all CMC aqueous solutions.

6. Minimum fluidization velocity was found to decrease as the apparent viscosity increases for low concentrations (0.2 wt %, 0.4 wt %). However, it increased as the apparent viscosity increased at higher CMC concentrations (0.8 wt %, 1 wt %). Expanding the range of apparent viscosities to be investigated can show the general trend followed by $U_{mf}$ with increasing CMC concentrations.

7. Generally, minimum fluidization velocity was found to decrease with increasing liquid flow rate.

8. Minimum fluidization velocity was found to increase with increasing the static bed height. The increase was more significant with bed of 20 mm diameter packing.

9. Expanded bed height was found to increase approximately linearly with increasing gas velocity over most of the range, with a more rapid increase at critical gas velocity of about 2.5 m/s. It increased with increasing liquid flow rate and decrease with increasing static bed height.

10. Increasing the apparent viscosity of the aqueous CMC solutions had a retardation effect on expanded bed height. It was found to decrease with increasing CMC concentration.

11. Gas holdup was found to increase linearly with increasing superficial gas velocity. Dependency of the gas holdup on static bed height varied with type of the operation. For type I, gas hold up was found to be approximately independent of static bed height, while for type II it decreased with increasing static bed height.

12. Gas hold up was found to decrease with increasing the apparent viscosity of CMC solutions. The degree of decreasing was more significant as the CMC concentration increased.

13. Gas holdup was found to be unaffected by increasing liquid flow rate generally, with some deviations in some cases.

14. The variation of net pressure drop, liquid hold up, minimum fluidization velocity with liquid flow rate were each consistent in trend with Newtonian liquids in the literature, as were the variations, of expansion of bed with superficial gas velocity and static bed height.

15. The estimated net pressure drop, liquid hold up, Umf, H/Hs and gas hold up using correlations in the literature showed disagreement between experimental results and estimated values. This suggests that shear rates estimation, variable system geometry, packing specifications, and operating parameters may have contributed significantly to the inconsistencies.

16. The effect of Archimedes number on net pressure drop and liquid holdup follow the same trend. It decreases with increasing Archimedes number.

17. Archimedes number effect on relative expanded bed height was to decrease H/Hs with increasing $Ar$ for low static bed height range, and the effect was reversed for high static bed height range.

18. The influence of Archimedes number on gas holdup followed the same behavior of relative bed expansion.

19. It was expected that as the pseudoplasticity of the CMC solutions increases, the shear effects on effective viscosity caused by the gas and liquid phases become more significant, which should be translated to further decrease in effective viscosity. But the results showed that the fluidized bed behaves qualitatively similar to beds of Newtonian liquids with viscosities higher than water.

20. It is postulated, therefore, that non-Newtonian liquids, over that quoted range of rheological parameters ($n$, $k$) and apparent viscosities, exhibit a behavior similar to that of Newtonian viscous liquids in TBC's.

# CHAPTER 6

# RECOMMENDATIONS FOR FUTURE WORK

The following recommendations are offered for future work.

1. Extend the present study of the hydrodynamic behavior of the TBC to liquids that have higher viscosity values (higher pseudoplasticity).

2. Study the effect of non-Newtonian liquids on hydrodynamic behavior of the TBC with higher free open area of the supporting grid.

3. Further study can be conducted on the effect of particle diameter and particle density individually on bed behavior with non-Newtonian liquids.

4. Develop a new model which describe the character of three phase fluidization at turbulent bed contactor (TBC) under gas-liquid counter current conditions.

# CHAPTER 9

## REFERENCES

Abukhalifeh, H., M. Fayed, R. Dhib, "Hydrodynamics of Turbulent Bed Contactor with Viscous Liquids," presented to the 53$^{rd}$ Canadian Chemical Engineering Conference, Hamilton, (October, 2003).

Aksel'rod, L. A., and M. M. Yakovenko, "Certain Hydrodynamic Aspects of Mass Transfer Equipment with Mobile Spherical Packing," Theort. Found. Chem. Eng., 3, 124 (1969).

Baker, C. G. J., Margaritis, A. Bergougnou, "Fluidization Principles and Applications to Biotechnology", Advances in biotechnology, 1, 635-641 (1981).

Balabekov, O. S., E.Ya. Tarat, P.G. Romankov, M.F.Mikhalev, "Hydrodynamic Characteristics of Columns with Wetted Fluidized Spherical Packings," J. App. Chem. U.S.S.R., 42, 2128 (1969b).

Balabekov, O. S., P.G. Romankov, E.Ya. Tarat, M.F. Mikhalev, "Operating Conditions of Columns with Wetted Moving Spherical Packings," J. App. Chem. U.S.S.R., 42, 1454 (1969a).

Balabekov, O. S., P.G. Romankov, E.Ya. Tarat, M.F. Mikhalev, "Hydrodynamic Design Calculations for Equipment with Wetted Fluidized Spherical Packing," J. App. Chem. U.S.S.R., 44, 1061-1068 (1971).

Barile, R. G., and D.W. Meyer, "Turbulent Bed Cooling Tower," Chem. Eng. Prog. Symp. Ser., No.119, 67, 134 (1971).

Bhat, G. N., K. Guconic-Murphy, and W. Weingaertner, Brit. Chem. Eng., 8, 813 (1963).

Blyakher, I.G., L.Y. Zhivaikini, and N.A. Yuroskaya, "Investigation of Hydrodynamics and Mass Transfer in Equipment with Mobile Packing," Int. Chem. Eng., 7, 485 (1967).

Boherill, J. S. M., and P.D. Bloore, Can. J. Chem. Eng., 41, 111 (1963).

Bruce, A. E. R., P.S.T Sai, K. Krishnaiah, "Liquid Holdup in Turbulent Bed Contactor," Chem. Eng. J., 99(3), 203, (2004).

Chen, B. H., and W. J. M. Douglas, "Liquid Holdup and Minimum Fluidization Velocity in a Turbulent Contactor," Can. J. Chem. Eng., 46, 245 (1968).

Cheng, L., K. Shao-yen, "Effects of Temperature and Concentration on the Steady Shear Properties of Aqueous Solutions of CMC," International Communication in Heat and Mass

Transfer, 22(2), 157 (1995).

Dharwadkar S. V., S. B Sawart, "Gas Hold up in Highly Viscous Pseudoplastic Non Newtonian Solutions in Three Phase Sparged Reactors," Can. J. Chem. Eng., 65, 406-411 (1987).

Douglas, W.J.M., "Heat and Mass Transfer in a Turbulent Bed Contactor," Chem. Eng. Prog., 60, No.7, 66(1964).

Epstein N., "Three Phase Fluidization: Some Knowledge Gaps," Can. J. Chem. Eng, 59, 649-657, (1981).

Ercan, C., A. R. P. Van Heiningen, W. J. M. Douglas, "Hydrodynamics and Mass Transfer in Mobile Bed Contacting," L.K Duraiswami, A.S. Muzumdar (Eds.), Transport in Fluidized Particle Systems, Elsevier, Amsterdam, 171, (1989).

Fan, L. S., "Gas- Liquid- Solid Fluidization Engineering," Butterworths, London, MA, USA, (1989).

Gel'perin, N. I., V.Z Grishko, V.I. Savchenko, V.M. Shchedro, "Investigation of the Operation of Absorption Apparatus with a Refluxed Ball Packing Type of Pseudoliquified Layer," (UDC 621 .57. 046, 55, 096, 5.001, 5) Translated, No.1 (22, 1966).

Gel'Perin, N. I., V. I. Savchenko, and V.Z. Grishko, "Some Hydrodynamic Laws of Absorption Apparatus Packed with Fluidized Spheres," Theor. Found. Chem. Eng., 2, 65 (1968 b).

Gomez-Diaz, D., and J. M. Navaza, "Rheological Characterization of Aqueous Solutions of CMC," Journal of Environmental, Agricultural and Food Chemistry, 1(1), (2002).

Guerriere, R. A., M. E. Fayed, A. J. Matchett, "Mass Transfer in a Turbulent Bed Contactor," Trans. IchemE., 73, Part A, 246-251 (1995).

Kawase, Y., T. Takahashi, H. Miura, "Effect of Pseudoplastic Behavior of Liquid in Cocurrent Three Phase Fluidized Beds on Bed Expansion," Chem. Eng. Sc., 56, 6047-6053 (2001).

Kielback, A.W., "The Development of Floating-Bed Scrubbers," Chem. Eng. Prog. Symp. Ser., 57, No.35, 51(1959).

Kito, M., Y. Kayama, T. Sakai, S. Sugiyama, "Minimum Fluidization Velocity in a Mobile Bed," Kagaku Kogaku Ronbunshu, 2, 21 (1976d).

Kito, M., M.Shimada, T. Sakai, S. Sugiyama, C. Wen, "Performance of Turbulent Bed Contactor: Gas holdup and Interfacial Area under Liquid Stagnant Flow," Fluidization Technology, D.L. Keairns, Ed., I, 411, Hemisphere (1976).

Kito, M., T. Monma, Y. Kayama, T. Sagai, S. Sugiyama, "Pressure Drop and Bed Expansion in a Mobile Bed," Kagaku Kogaku Ronbunsha, 2, 476 (1976e).

Kito, M., K. Tabei, K. Murata, "Gas and Liquid Holdups in Mobile Beds under the Counter-current Flow of Air and Liquid," Ind. Eng. Chem. Process Des. Dev., 17, 4, 568 (1978).

Kunii, D., and O. Levenspiel, "Fluidization Engineering," Butterworth-Heinemann, (1991).

Kuroda, M., and K. Tabei, "Theoretical Discussion of the Minimum Fluidizing Velocity in a Mobile Bed," Int. Chem. Eng., 21(2), 219 (1981).

Leva, M., "Fluidization," McGraw-Hill, New York, (1959).

Levsh, I. P., M. I. Niyasov, N.I. Krainev, F.F. Ganikhanova, "Mass Transfer in Absorbers with Fluidized Packed Beds," Int. Chem. Eng., 8, 379 (1968b).

Miura, H., Y. Kawase, "Minimum Liquid Fluidization Velocity in Two- and Three Phase Fluidized Beds with Non-Newtonian Fluids," Powder Technology, 97, 124-128 (1998).

Morse, R. D., Ind. Eng. Chem., 41, 1117 (1949).

Muroyama, K., L.S. Fan, "Fundamentals of Gas – Liquid- Solid Fluidization," AIChE Journal, 31, 1 (1985).

O'Neill, B.K., D.J. Nicklin, N.J Morgan, L.S. Leung, "The Hydrodynamics of Gas –Liquid Contacting Towers with Fluidized Packing," Can. J. Chem. Eng., 50, 9 (1972).

Ostergaard, K., "Fluid Mechanics of Three Phase Fluidization," Can. Chem. Eng. Conf., Calgary, Alberta (1977).

Othmer, D. F., "Fluidization," Van Nostrand Reinhold, New York, (1956).

Patwari, A. N., K. Nguyen-Tien, A. Schumpe, W. D. Deckwer, "Three Phase Fluidized Beds With Viscous Liquids: Hydrodynamics and Mass Transfer," Chem. Eng. Comm., 40, 49-65 (1986).

Rama, O. P., D.Rao, V. Subba Rao, "Hydrodynamics of a Mobile Bed Contactor with Low Density Packing Particles of Different Shapes," Can. J. Chem. Eng., 61, 863 (1983).

Schumpe, A., W. D. Deckwer, K. D. P. Nigam, "Gas Liquid Mass Transfer in Three Phase Fluidized Beds with Viscous Pseudoplastic Liquids," Can. J. Chem. Eng., 67, 873-877

90

(1989).

Shi, L.K., J. P. Riba, H. Angelino, "Estimation of Effective Shear Rate for Aerated Non-Newtonian Liquids in Air Lift Bioreactors," Chem. Eng. Comm., 89, 25-35(1990).

Shilton, N. C., and K. Niranjan, "Fluidization and Its Application to Food Processing," Food Structure, 12, 199-215 (1993).

Soundarajan, K., and K. Krishnaiah, "Pressure Drop and Phase Holdups in Multistage Turbulent Bed Contactor with Down Comers," Indian J. Chem. Tech., 5, 179(1998).

Soundarajan, K., and K. Kvishnaiah, "Hydrodynamics of Single – Stage Turbulent Bed Contactor with Down Comer," Indian J. Tech., 6, 152 (1999).

Tabei, K., and M. Kuroda, "Axial Mixing Relationship of Liquid Flow and Packings in Mobile Bed," Kagaku Kogaku Ronbunshu, 24(3), 520 (1998).

Tichy, J., and W.J.M. Douglas, "Bed Expansion in a Mobile Bed Contactor," Can. J. Chem. Eng., 50, 702 (1972).

Uysal, B. Z., "Hydrodynamic and Particulate Recovery Studies in Mobile Bed Contacting," Ph. D. Thesis, McGill Univ., (1978).

Vunjak-Novakovic, G. V., D. V. Vukovic, H. Lihman, "Hydrodynamics of Turbulent Bed Contactors 2, Pressure Drop, Bed Expansion, and Minimum Fluidization Velocity," Ind. Chem. Res., 26, 967 (1987b).

Vunjak-Novakovic, G.V., and D.V. Vukovic, "Hydrodynamics and Mass Transfer Performance of Turbulent Bed Contact Absorbers," Fluidization, G. R. Grace and G.M. Matsen, Eds., 253, Plenum press, New York (1980).

Vunjak-Novakovic, G.V., D.V Vukovic, H. Lihman, "Hydrodynamics of Turbulent Bed Contactors 1, Operating Regimes and Liquid Holdup," Ind. Eng. Chem. Res., 26, 958 (1987a).

Wozniak, M., "Pressure Drop and Effective Interfacial Area in a Column with a Mobile Bed," Int. Chem. Eng., 17, 553 (1977).

Wu, Y. S., K. Pruess, and P. A. Witherspoon, "Flow and Displacement of Bingham Non-Newtonian Fluids in Porous Media," Reservoir Engineering, 7, 369-376 (1992).

Zenz, F. A., D. F. Othmer, "Fluidization and Fluid-Particle Systems," Van Nostrand Reinhold, New York, (1960).

# APPENDIX A

# ADDITIONAL THESIS RESULTS' FIGURES
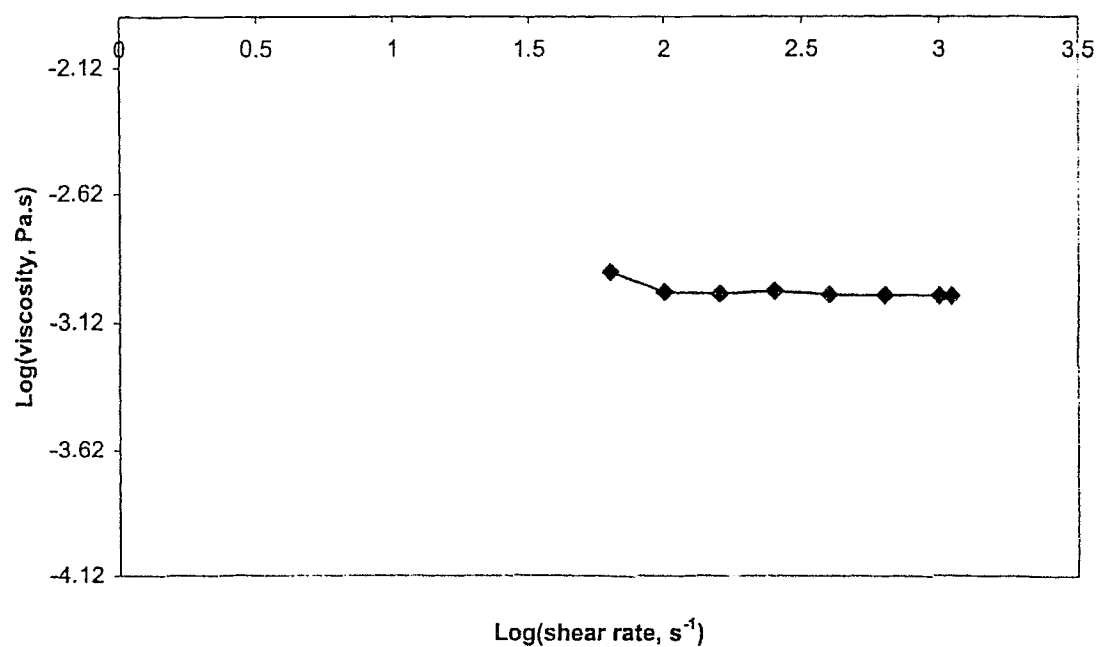


Figure A-1 Flow curve for water at 20° C

92
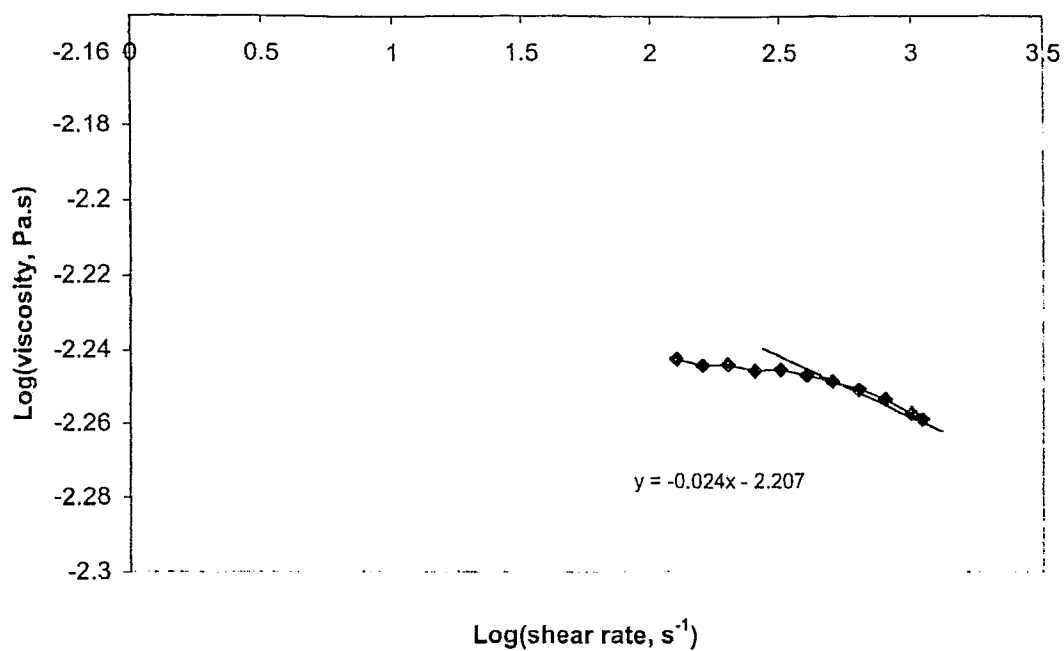
Figure A-2 Flow curve for 0.4 wt%CMC aqueous solution at 20°
C
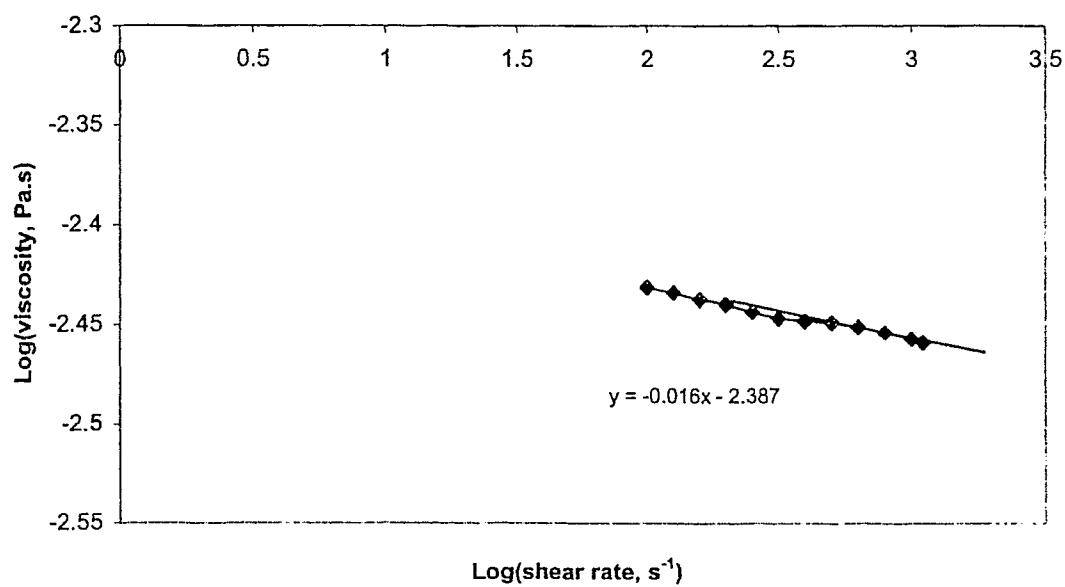


Figure A-3 Flow curve for 0.2 wt%CMC aqueous solution at 20° C

93
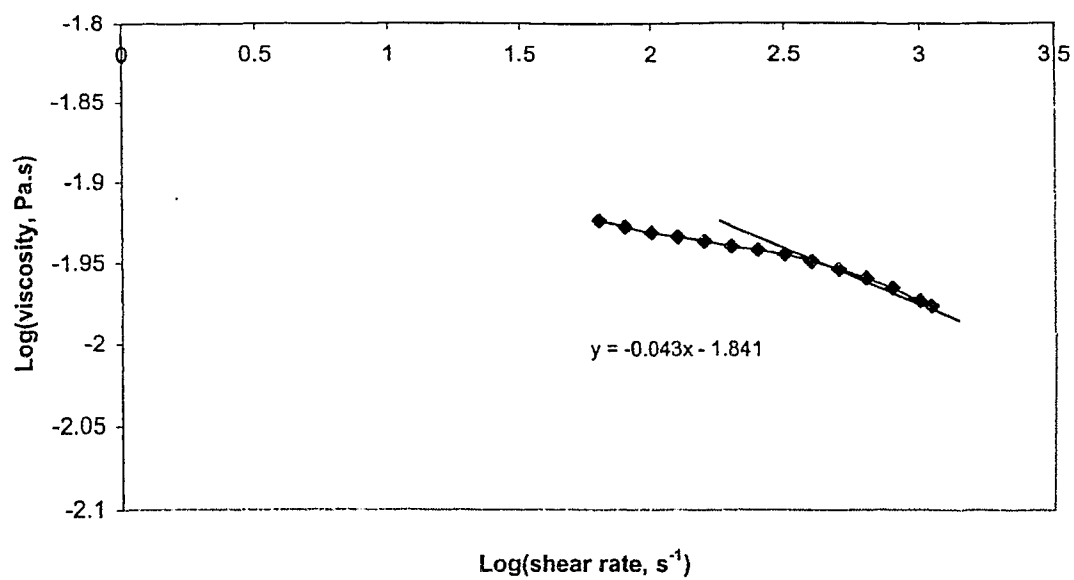
Figure A-4 Flow curve for 0.8 wt%CMC aqueous solution at 20° C

94
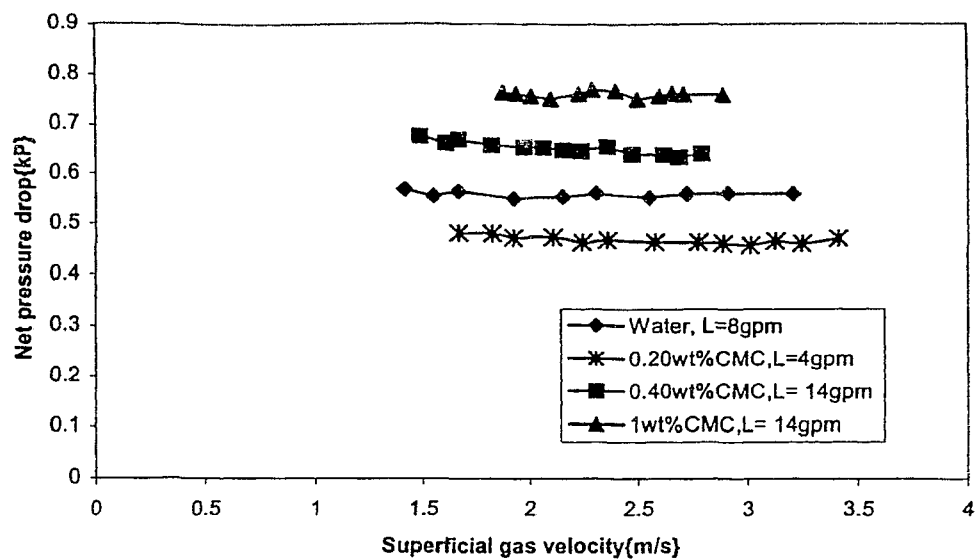
Figure A-5  Effect of superficial gas velocity on net pressure drop at
dp=38mm, Hs/D=0.25
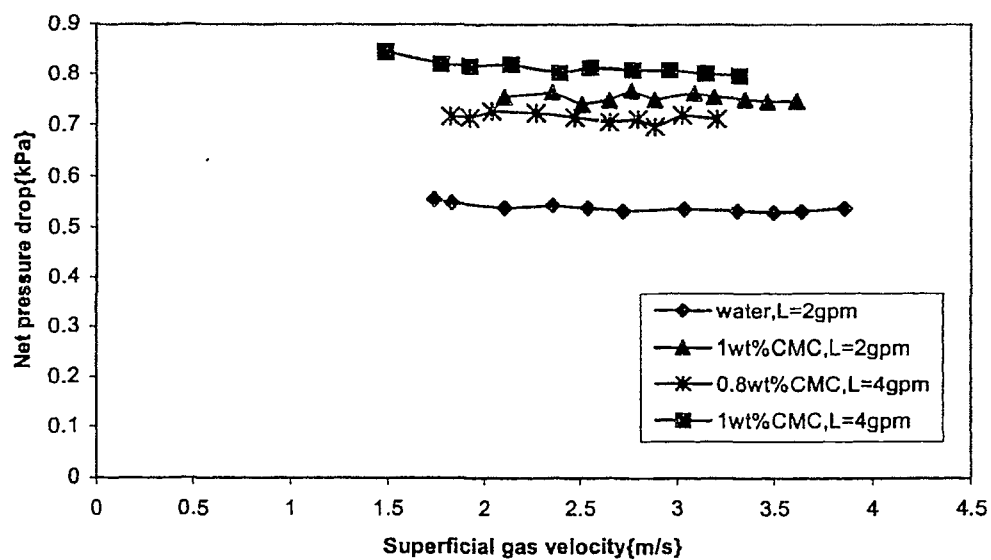


Figure A-6  Effect of superficial gas velocity on net pressure dop
at Hs/D=0.5, dp=38mm

95
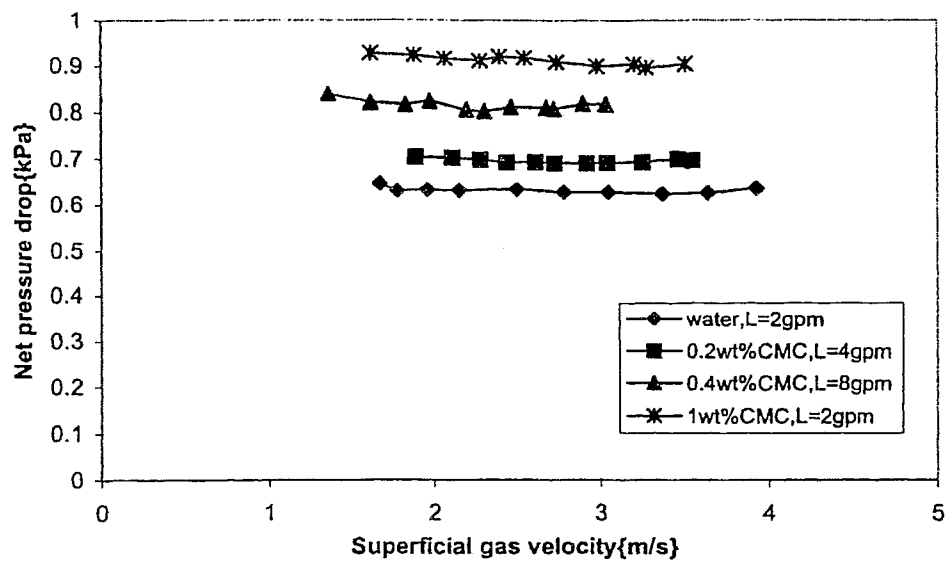
Figure A-7 Effect of superficial gas velocity on net pressure drop at
Hs/D=0.75, dp=38mm
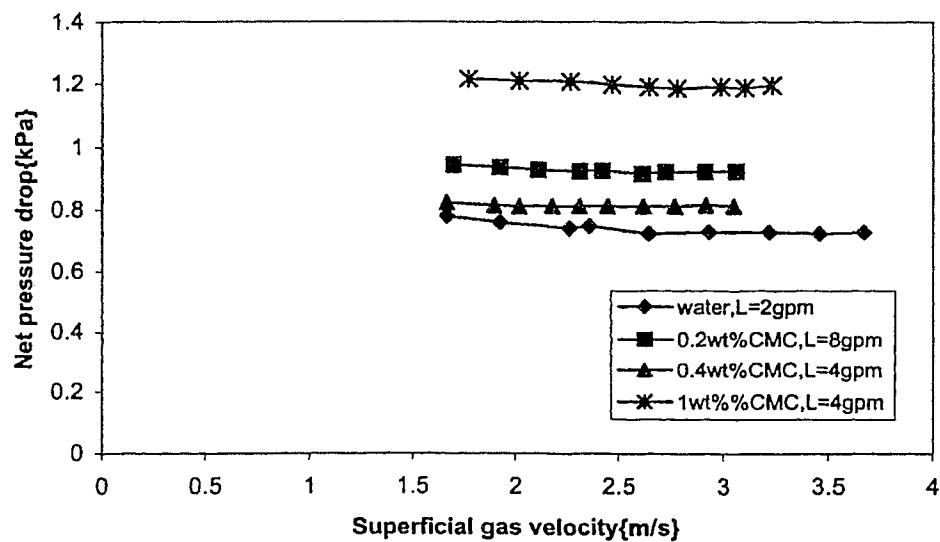


Figure A-8 Effect of superficial gas velocity on net pressure drop
at Hs/D=1, dp=38mm

96
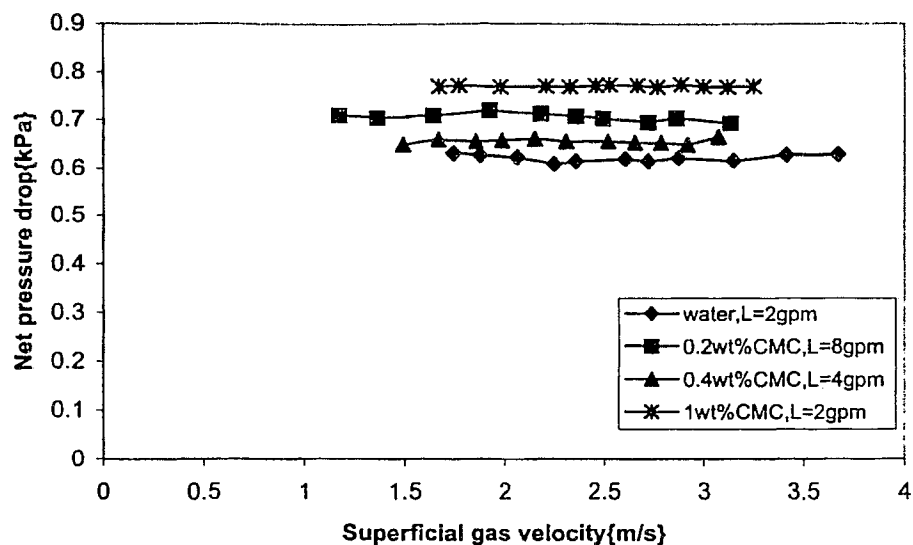
Figure A-9 Effect of superficial gas velocity on net pressure drop at sets of conditions at dp=20mm,Hs/D=0.25
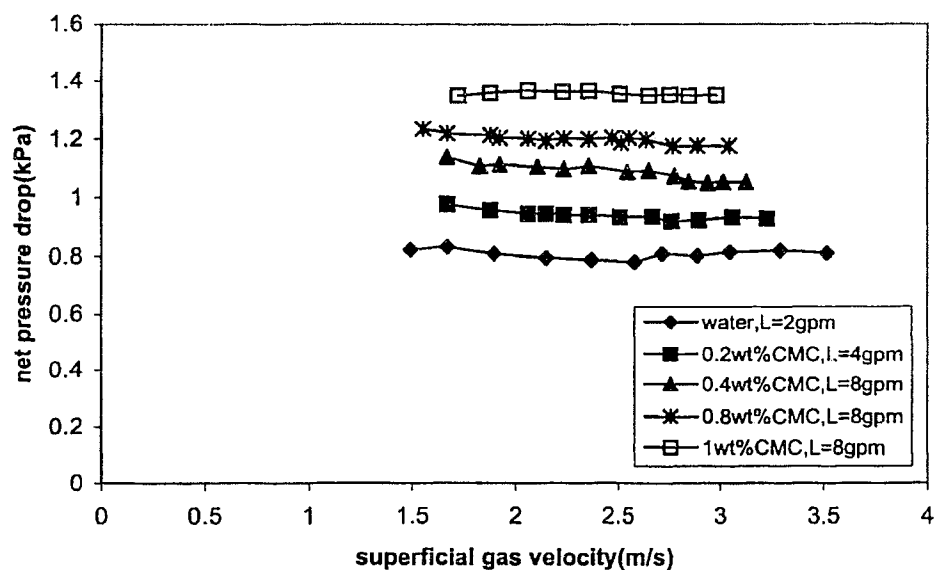


Figure A-10 Effect of superficial gas velocity on net pressure drop at Hs/D=0.5,dp=20mm

97
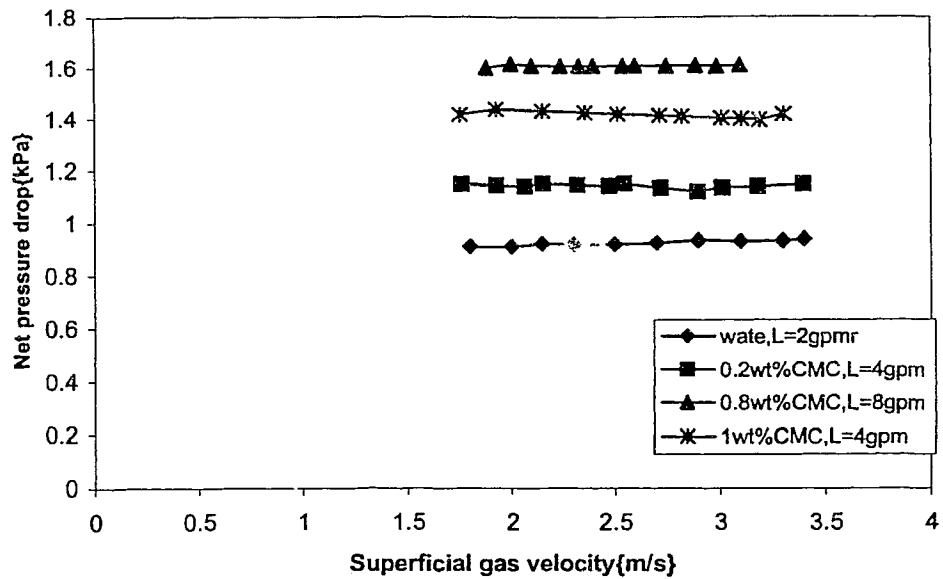
Figure A-11 Effect of superficial gas velocity on net pressure drop at Hs/D=0.75, dp=20mm
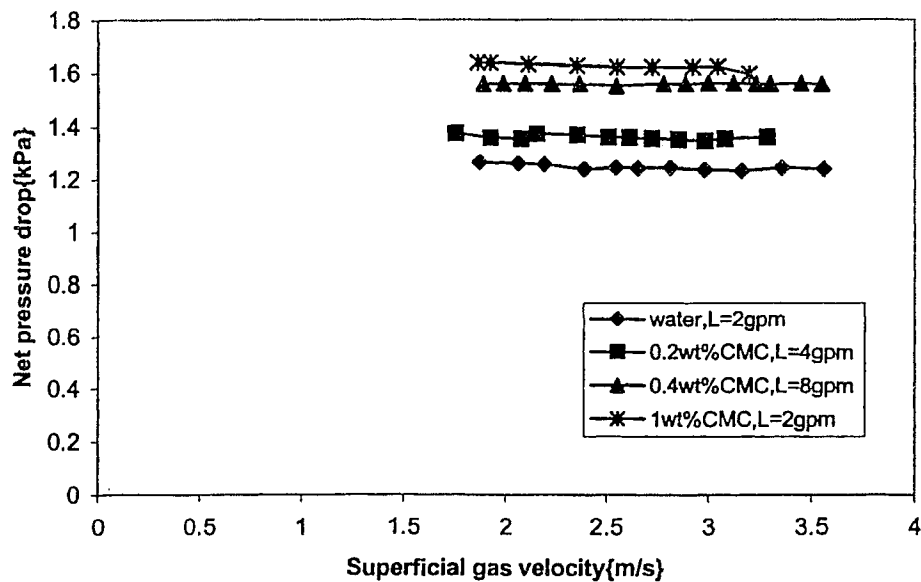


Figure A-12 Effect of superficial gas velocity on net pressure drop at Hs/D=1, dp=20mm

98
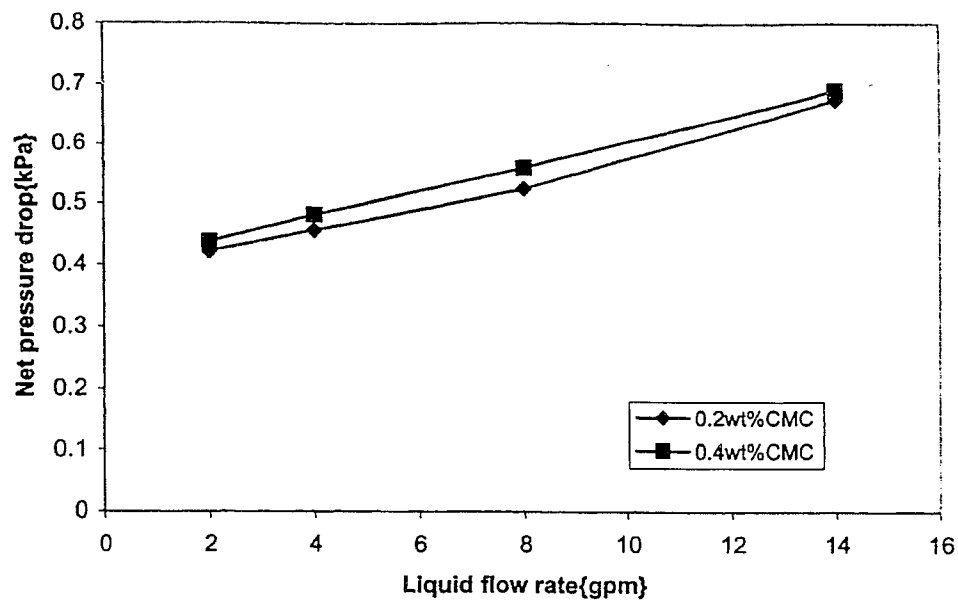
Figure A-13  Effect of liquid flow rate on net pressure drop
at dp=38mm Hs/D=0.25
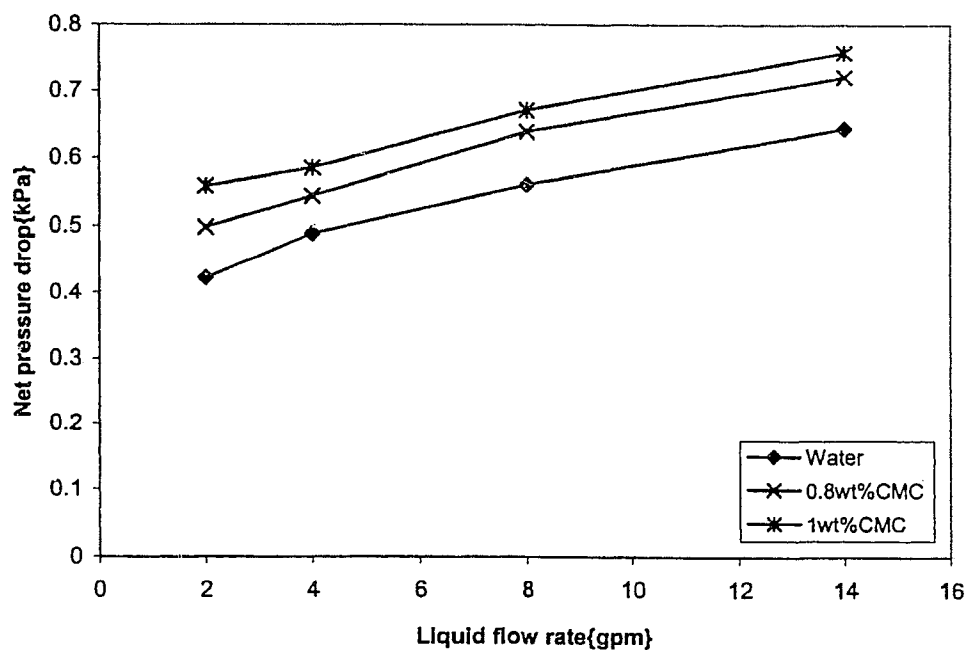


Figure A-14  Effect of liquid flow rate on net pressure drop
at Hs/D=0.25, dp=38mm

99
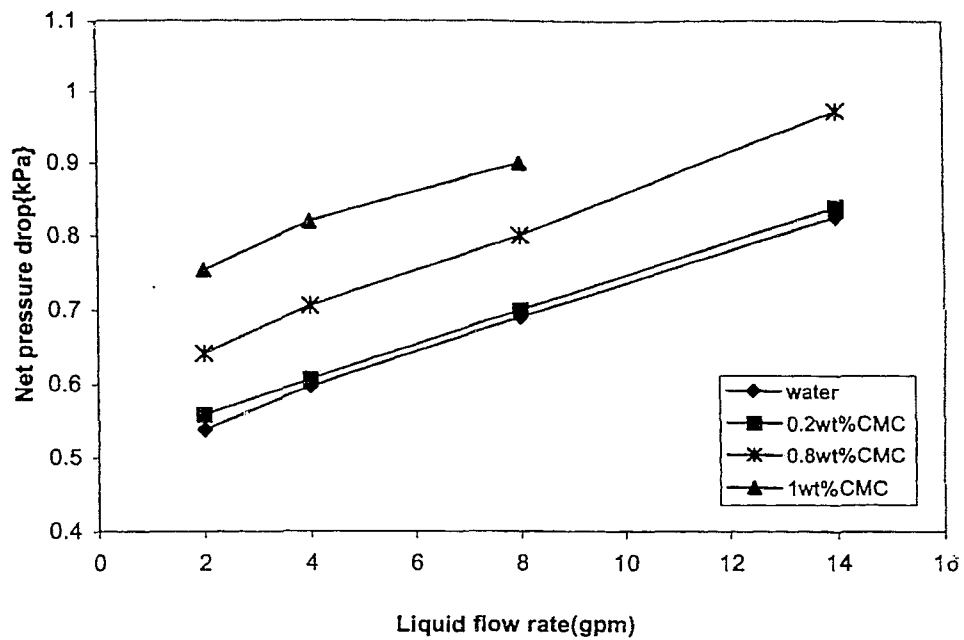
Figure A-15 Effect of liquid flow rate on net pressure drop at
Hs/D=0.5, dp=38mm
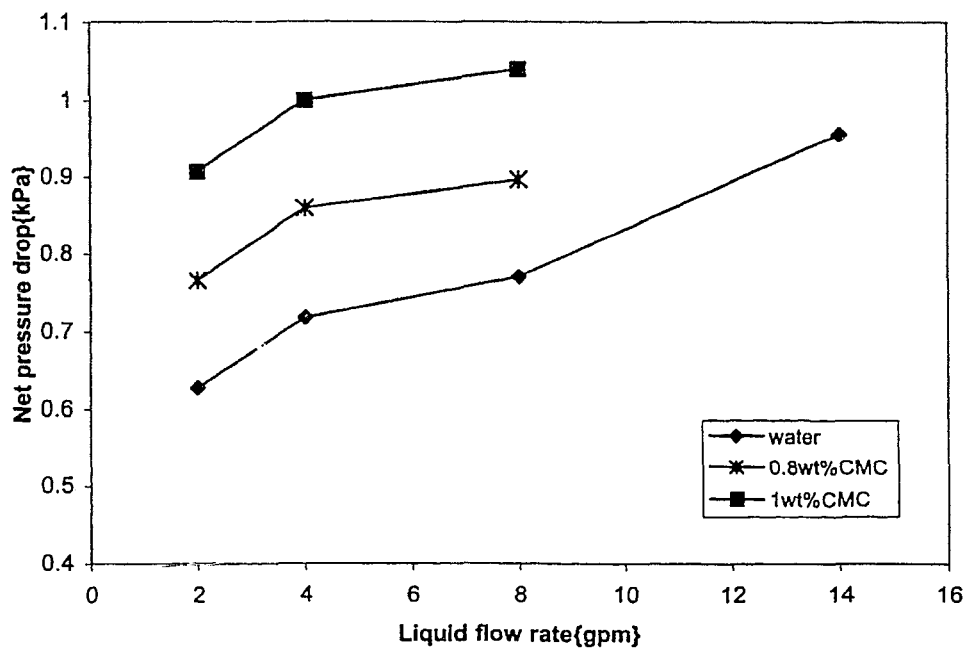


Figure A-16  Effect of liquid flow rate on net pressure drop at
Hs/D=0.75, dp=38mm

**100**
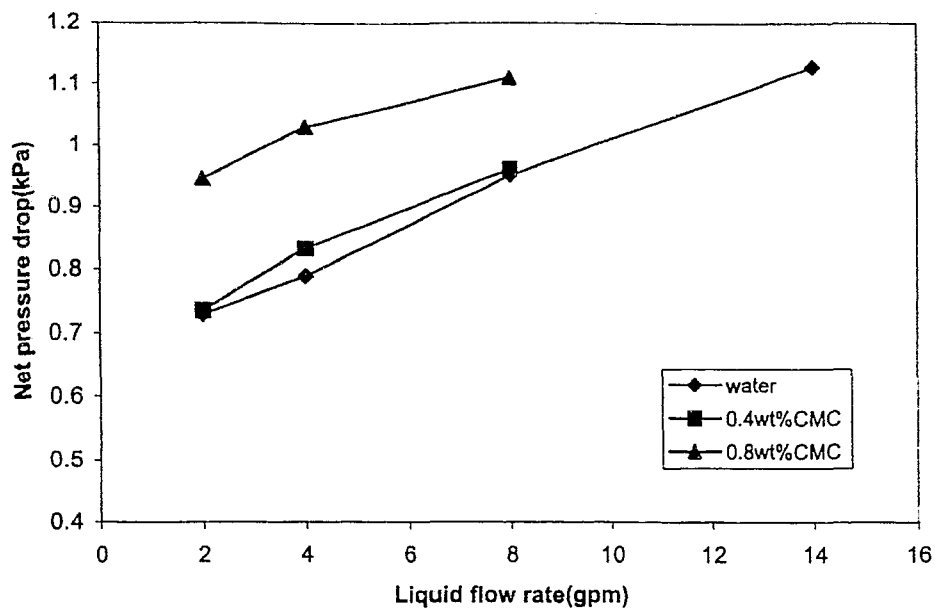
Figure A-17  Effect of liquid flow rate on net pressure drop at
Hs/D=1 , dp=38mm
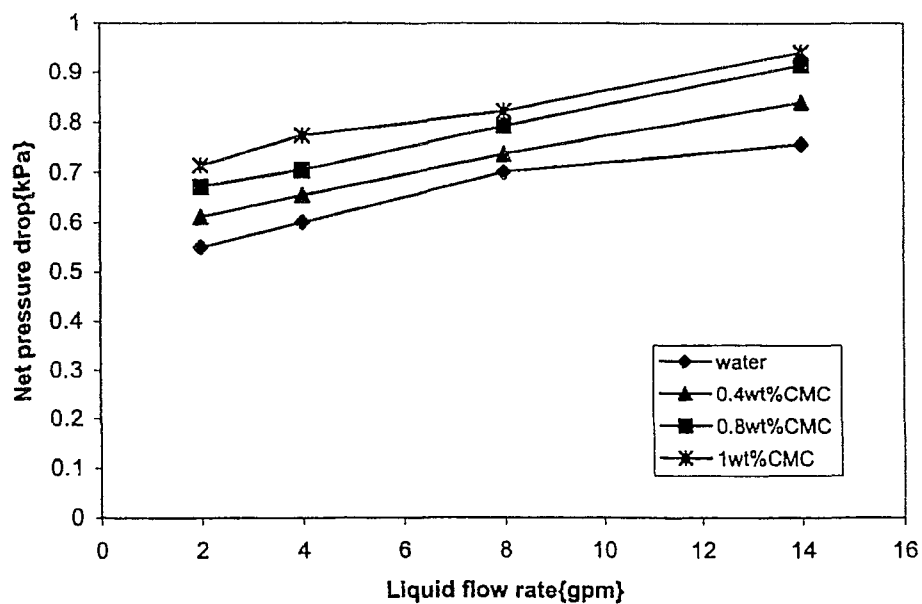


Figure A-18  Effect of liquid flow rate on net pressure drop at
dp=20mm,Hs/D=0.25

101
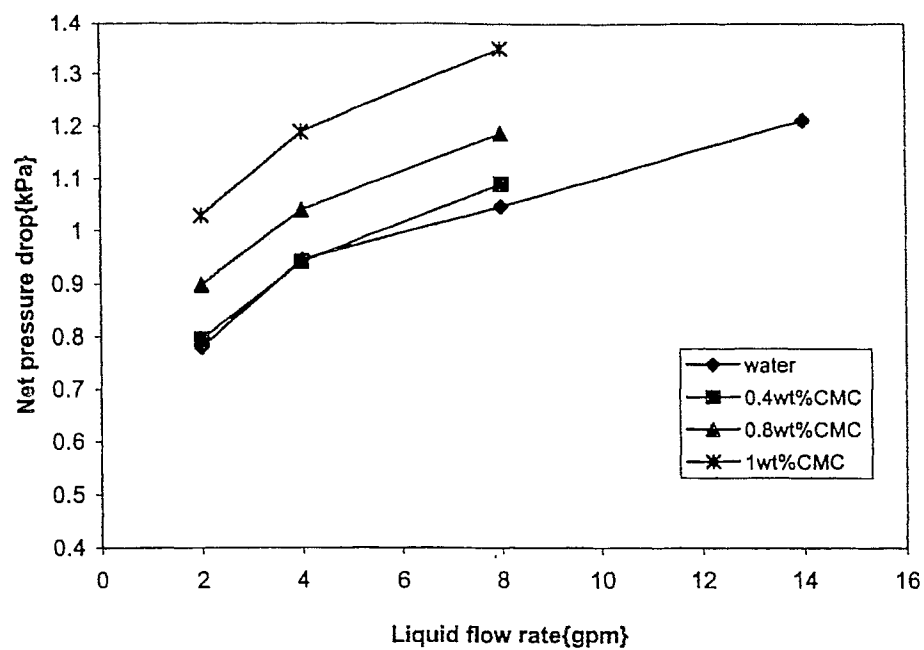
Figure A-19  Effect of liquid flow rate on net pressure drop at
Hs/D=0.5,dp=20mm
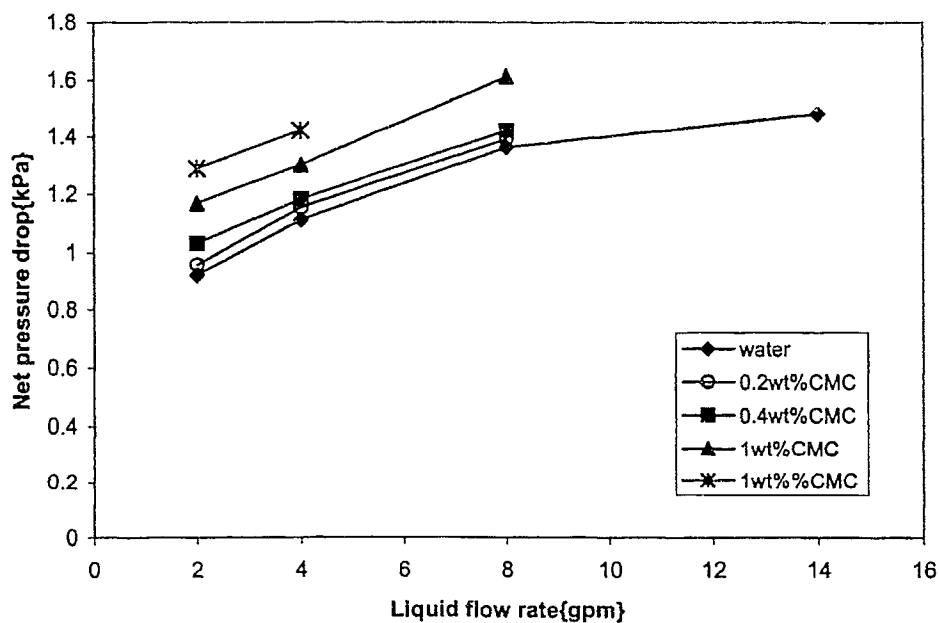


Figure A-20  Effect of liquid flow rate on net pressure drop
atHs/D=0.75,dp=20mm

102
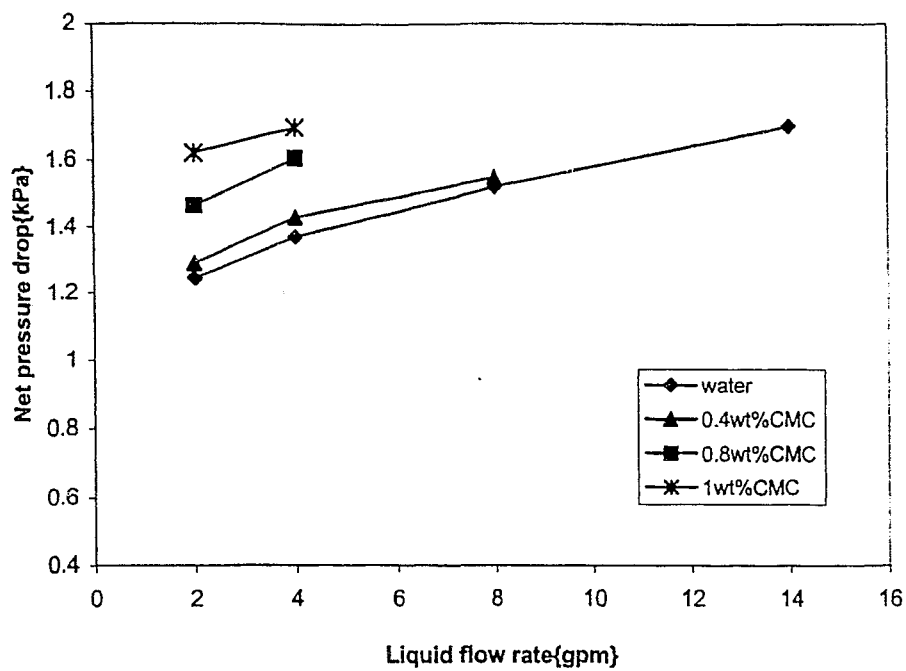
Figure A-21  Effect of liquid flow rate on net pressure drop at
Hs/D=1, d$_p$=20mm
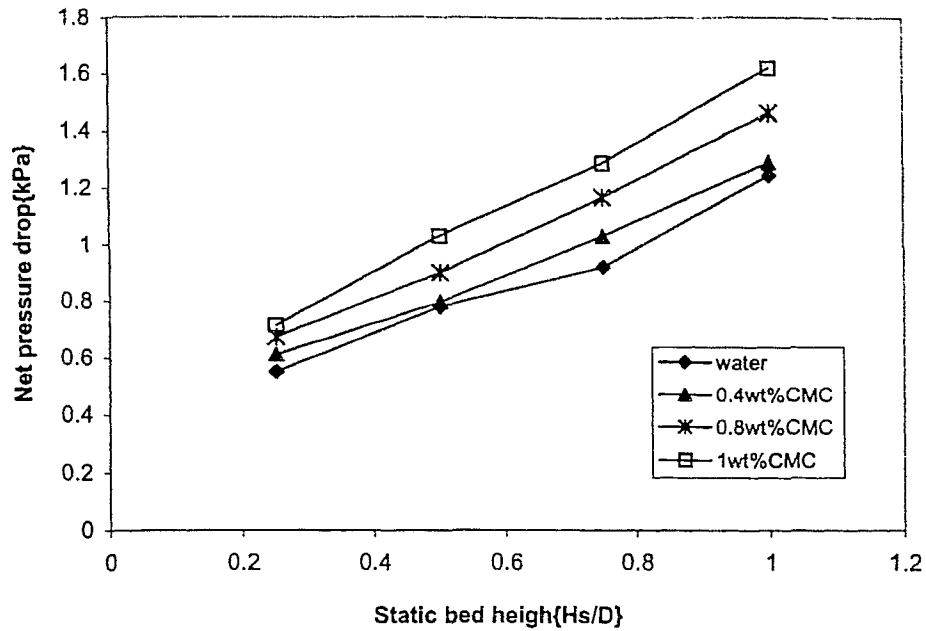
Figure A-22  Effect of static bed height on net pressure drop
at dp=20mm, L=2gpm
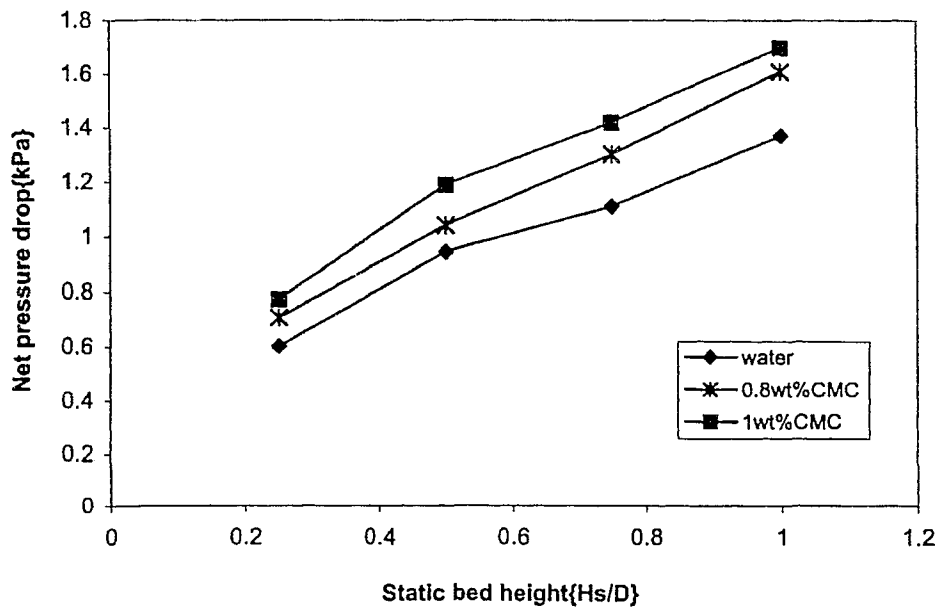


Figure A-23  ffect of static bed height on net pressure drop at
dp=20mm,Ug=2.5m/s,L=4gpm

104
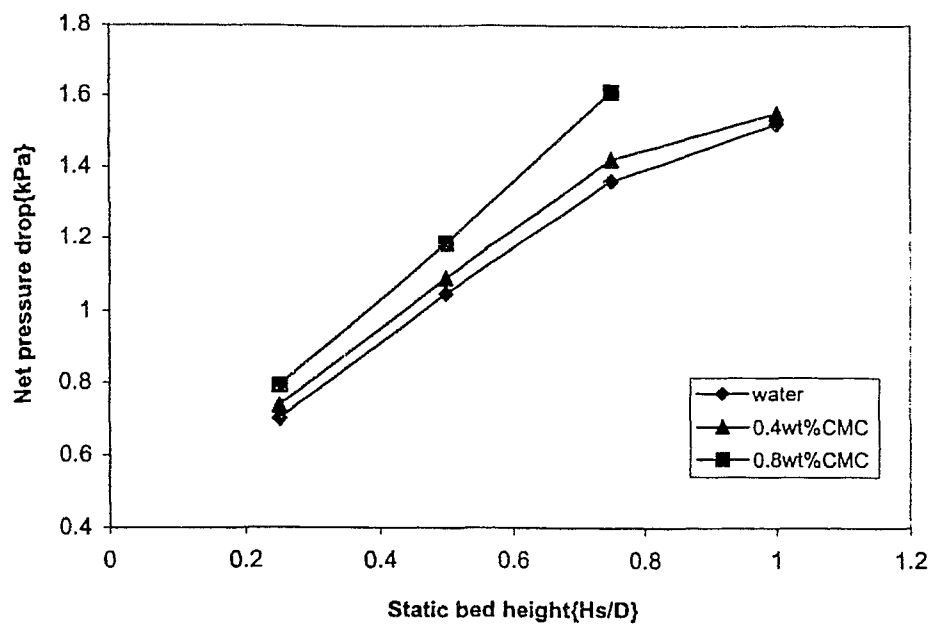
Figure A-24  Effect of static bed height on net pressure drop at
dp=20mm, L=8gpm
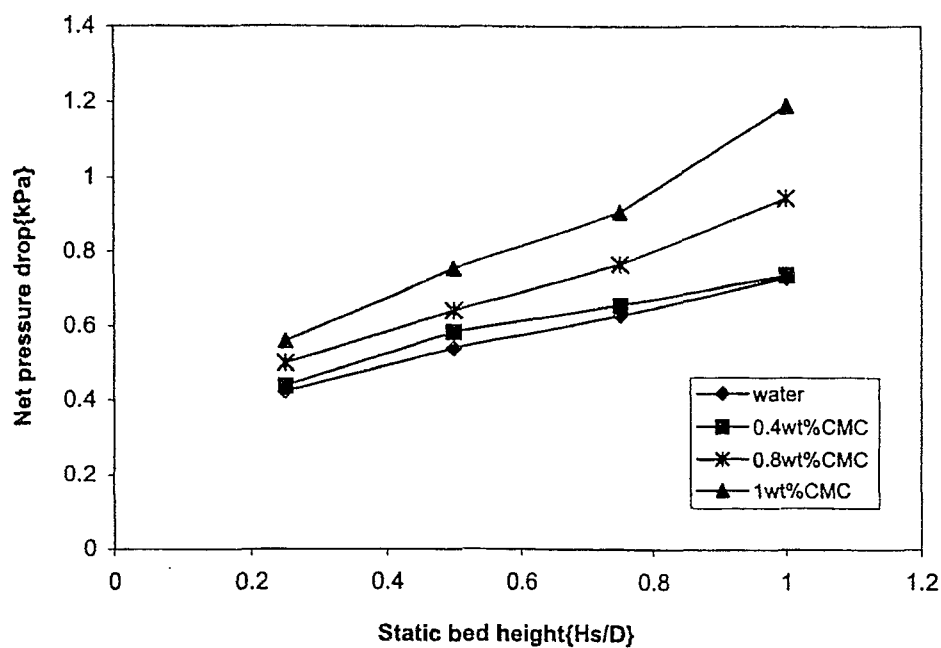


Figure A-25  Effect of static bed height on net pressure drop
at dp=38mm, L=2gpm

105
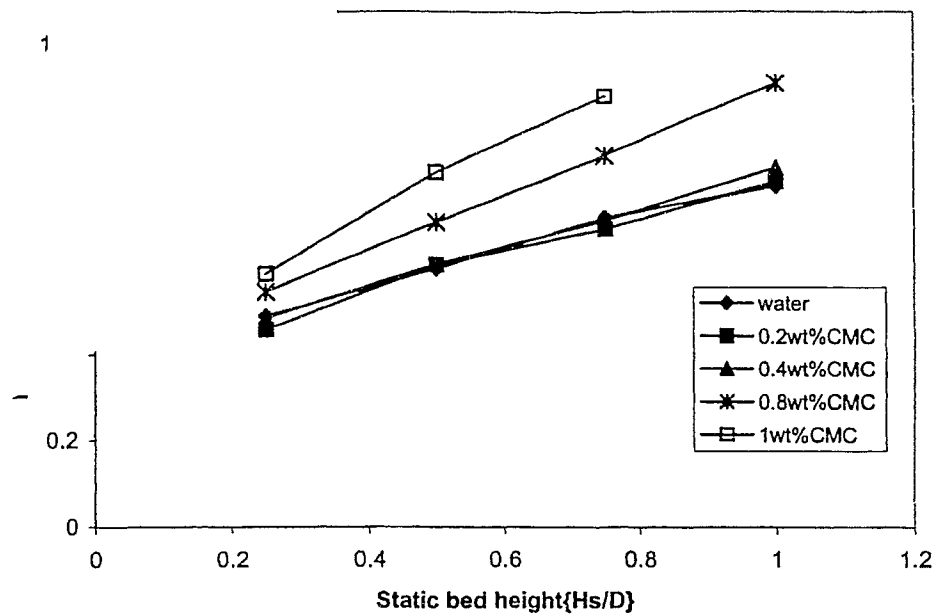
Figure A-26  Effect of static bed height on net pressure drop
at dp=38mm, L=4gpm
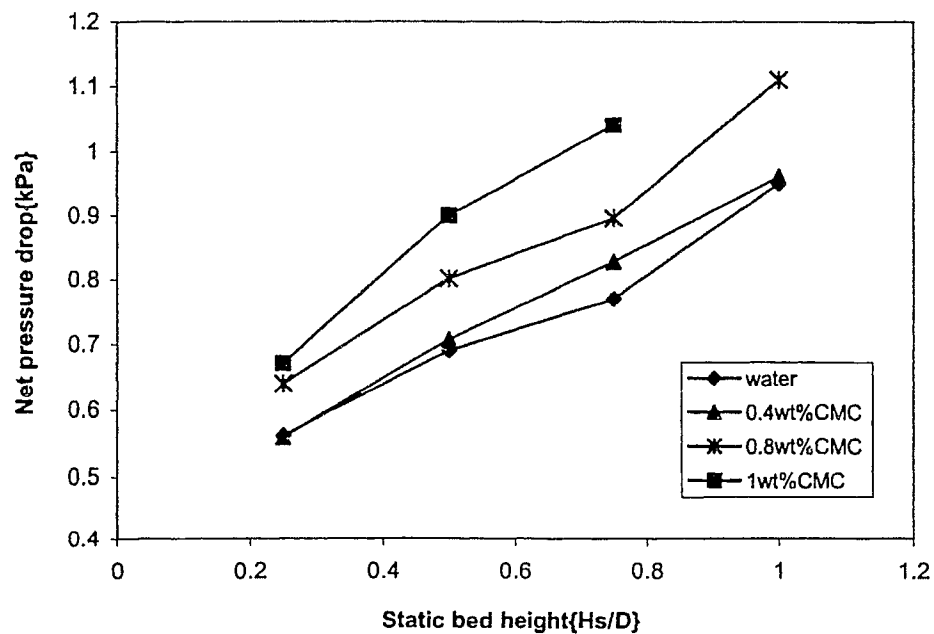


Figure A-27  Effect of static bed height on net pressure drop
at L=8gpm,dp=38mm

106
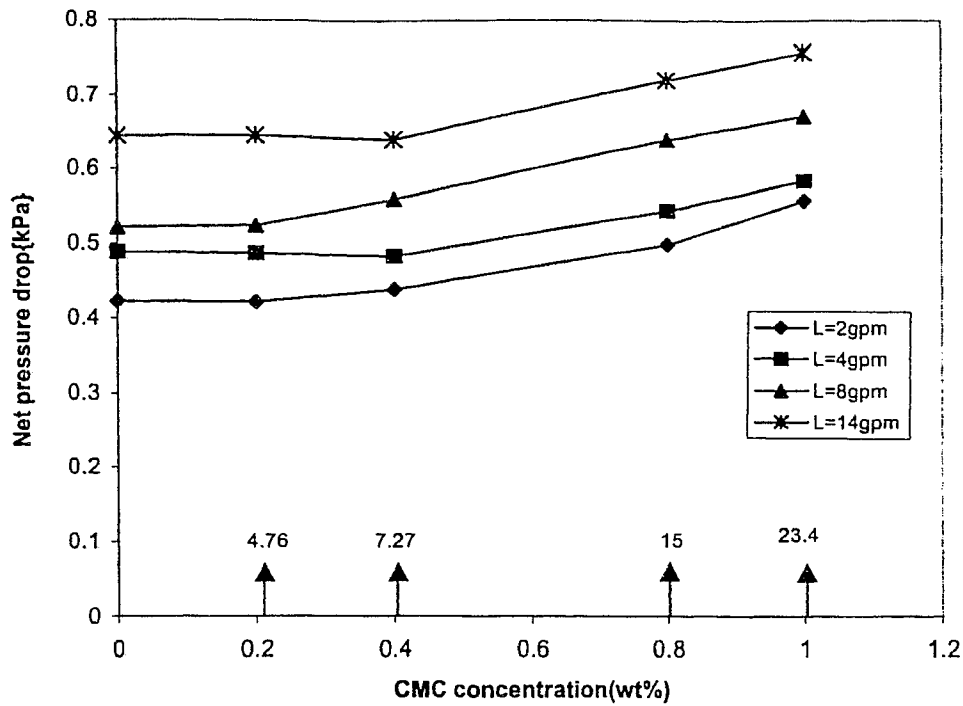
Figure A-28  Effect of CMC concentration on net pressure drop
at Hs/D=0.25, dp=38mm,  ( ▲ viscosity,cP,10 s$^{-1}$)
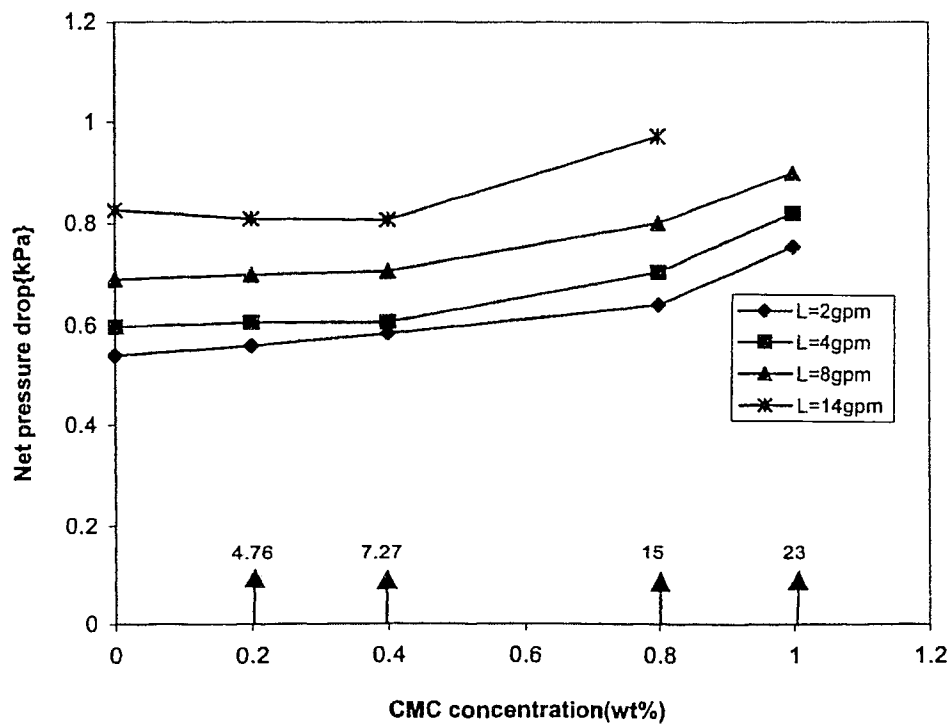


Figure A-29  Effect of CMC concentration on net pressure drop
at Hs/D=0.5 ,dp=38mm, ( ▲ viscosity,cP,at 10 s$^{-1}$)

107
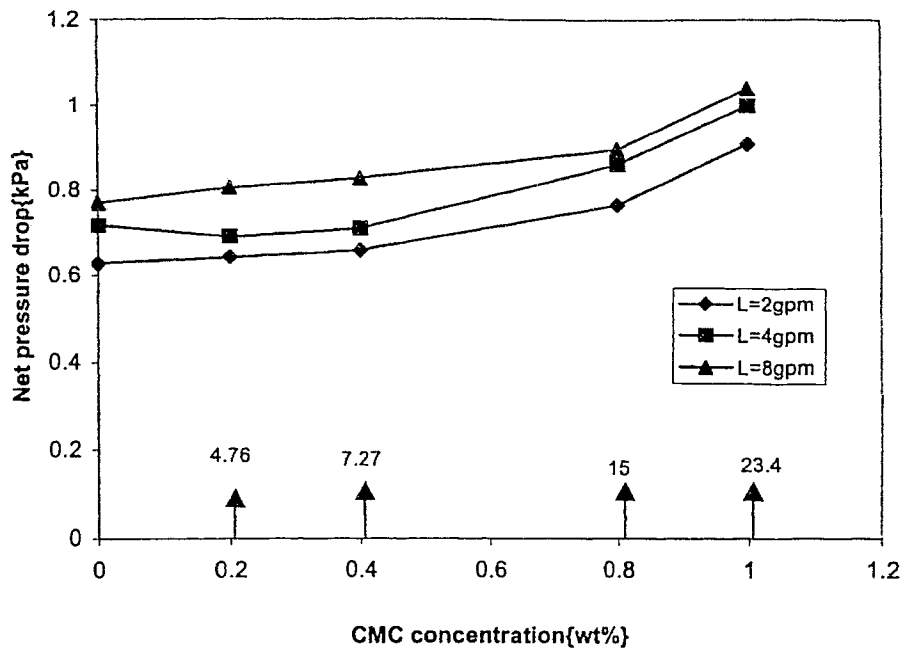
Figure A-30  Effect of CMC concentration on net pressure drop
at Hs/D=0.75,dp=38mm, (▲ viscosity,cP,at 10 s$^{-1}$)
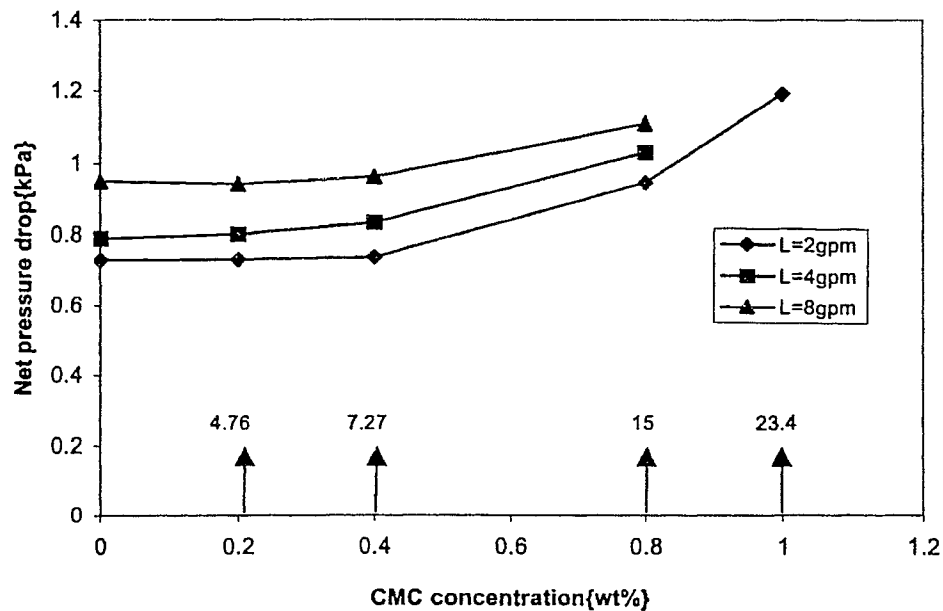


Figure A-31  Effect of CMC concentration on net pressure drop
at Hs/D=1,dp=38mm,(▲ viscosity,cP,at 10 s$^{-1}$)

108
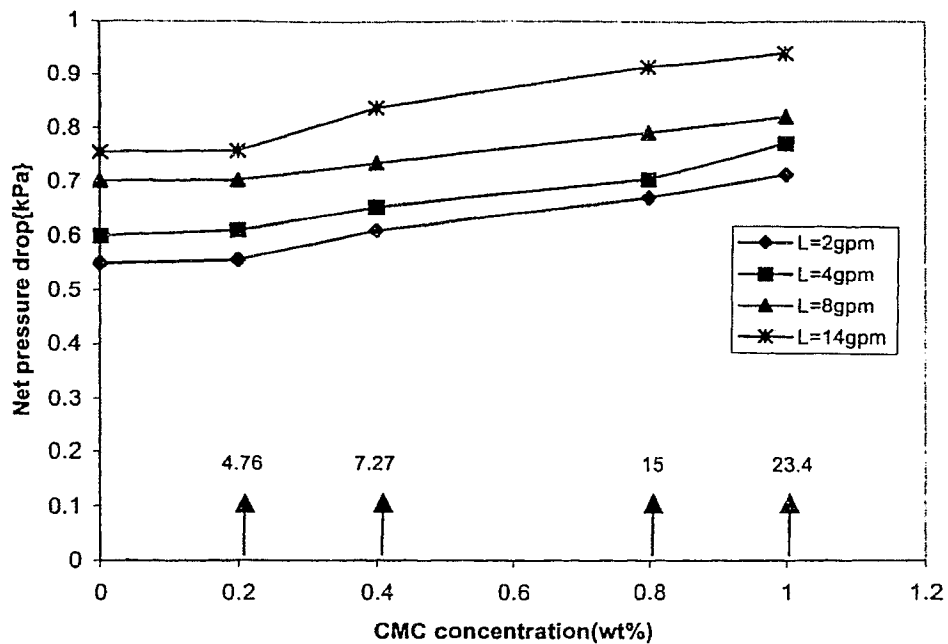
Figure A-32 Effect of CMC concentration on net pressure drop at dp=20mm,Hs/D=0.25,($\uparrow$ viscosity,cP, at 10 s$^{-1}$ )
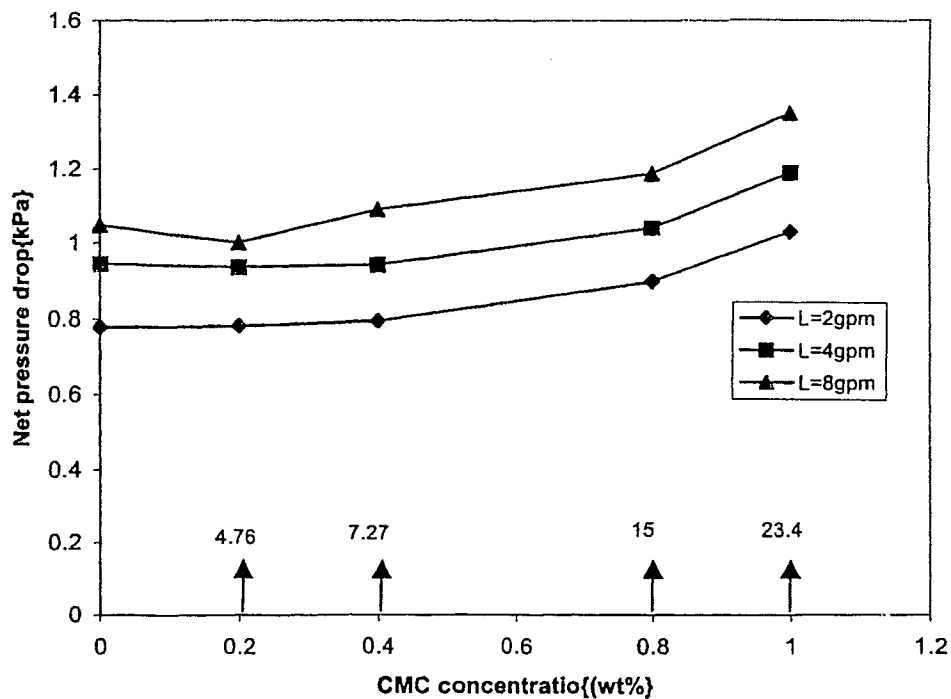


Figure A-33 Effect of CMC concentration on net pressure drop at Hs/D=0.5,dp=20mm,($\uparrow$ viscosity,cP,at 10 s$^{-1}$)

109

## Figure A-34

Net pressure drop{kPa}

1.8
1.6
1.4
1.2
1
0.8
0.6
0.4
0.2
0

L=2gpm
L=4gpm
L=8gpm

4.76    7.27    15    23.4

0    0.2    0.4    0.6    0.8    1    1.2

CMC concentration{wt%}
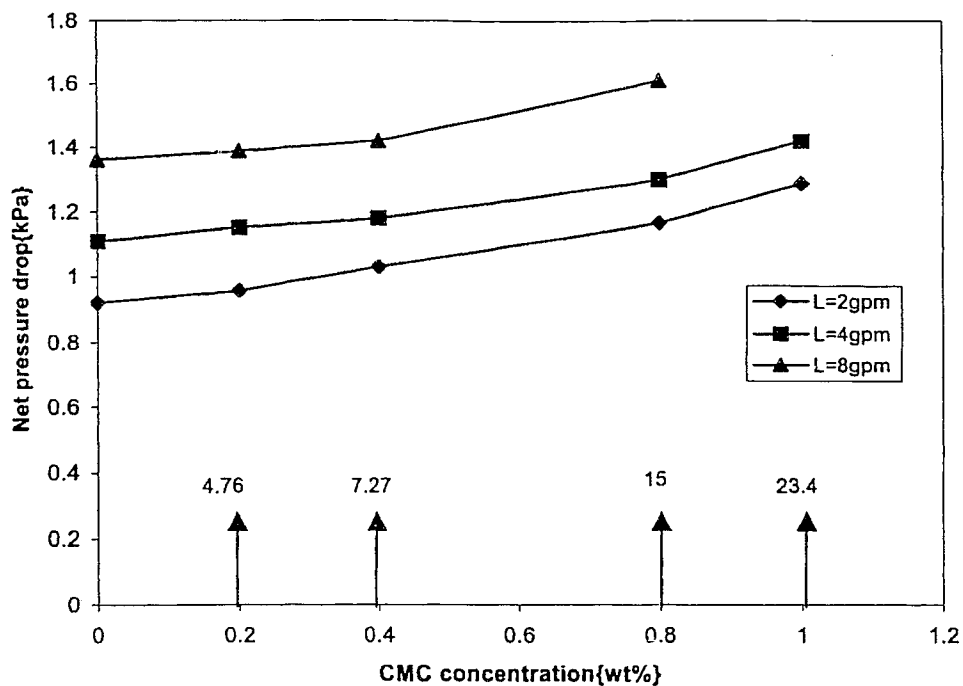
Figure A-34 Effect of CMC concentration on net pressure drop at Hs/D=0.75,dp=20mm,( ↑viscosity,cP,at 10 s$^{-1}$)

## Figure A-35

Net pressure drop{kPa}

1.8
1.6
1.4
1.2
1
0.8
0.6
0.4
0.2
0

L=2gpm
L=4gpm
L=8gpm

4.76    7.27    15    23.4

0    0.2    0.4    0.6    0.8    1    1.2

CMC concentration{wt%}
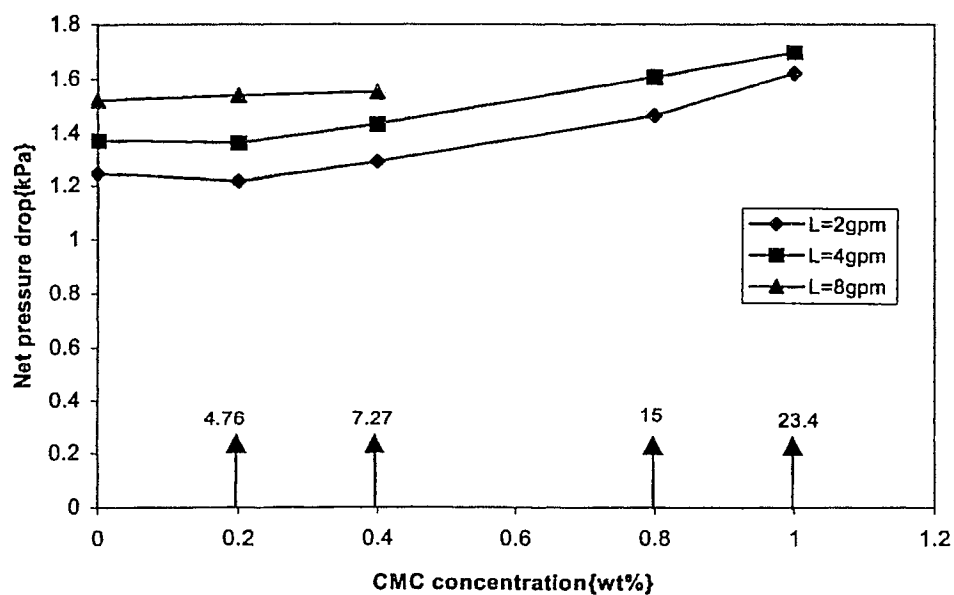
Figure A-35 Effect of CMC concentration on net pressure drop at Hs/D=1,dp=20mm,( ↑viscosity,cP,at 10 s$^{-1}$)

110
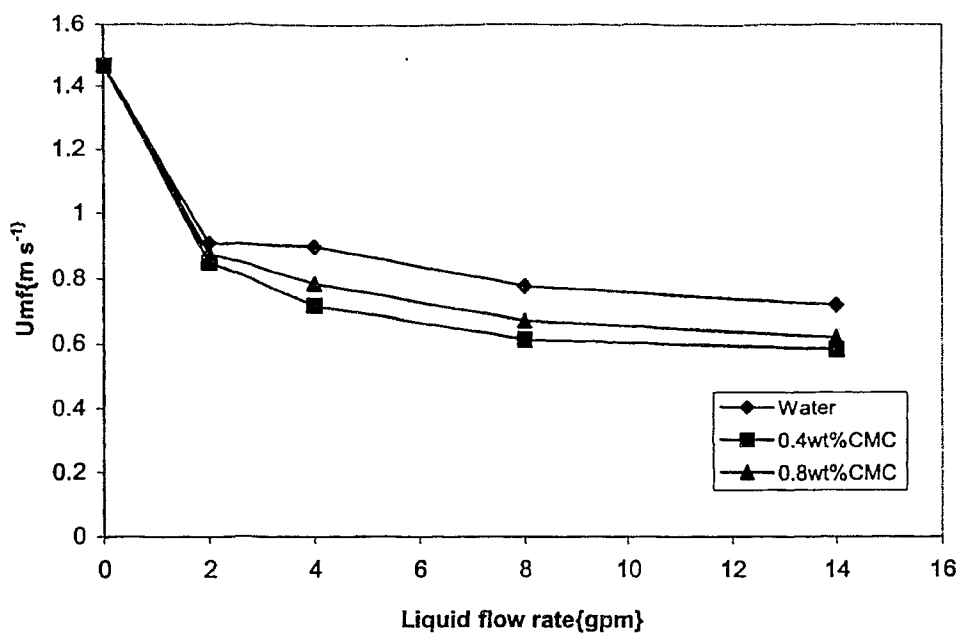
Figure 36 Effect of liquid flow rate on minimum fluidization velocity
at Hs/D=0.25 ,dp=38mm
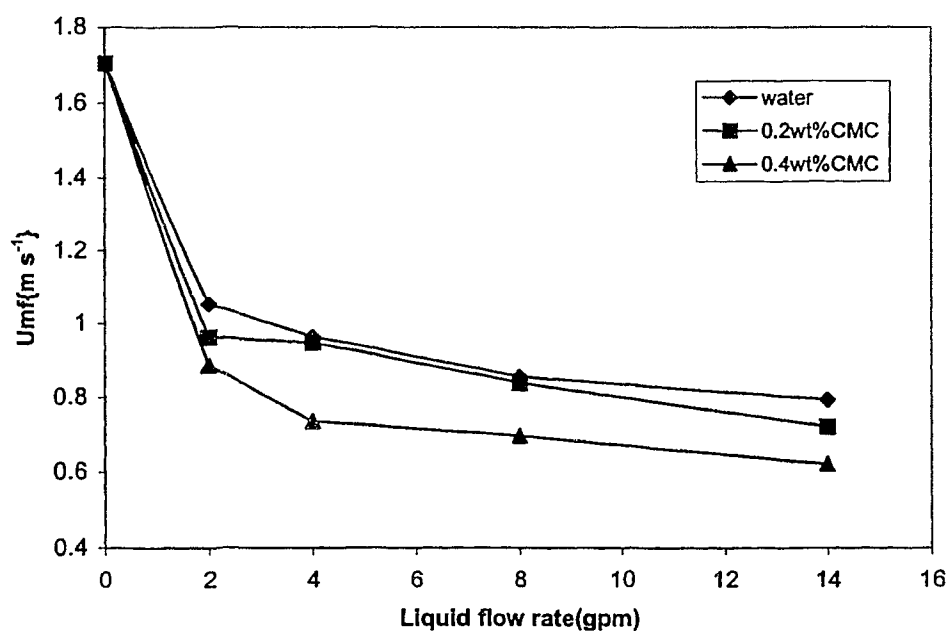


Figure A-37 Effect of liquid flow rate on minimum fluidization velocity
at Hs/D=0.5, dp=38mm

111
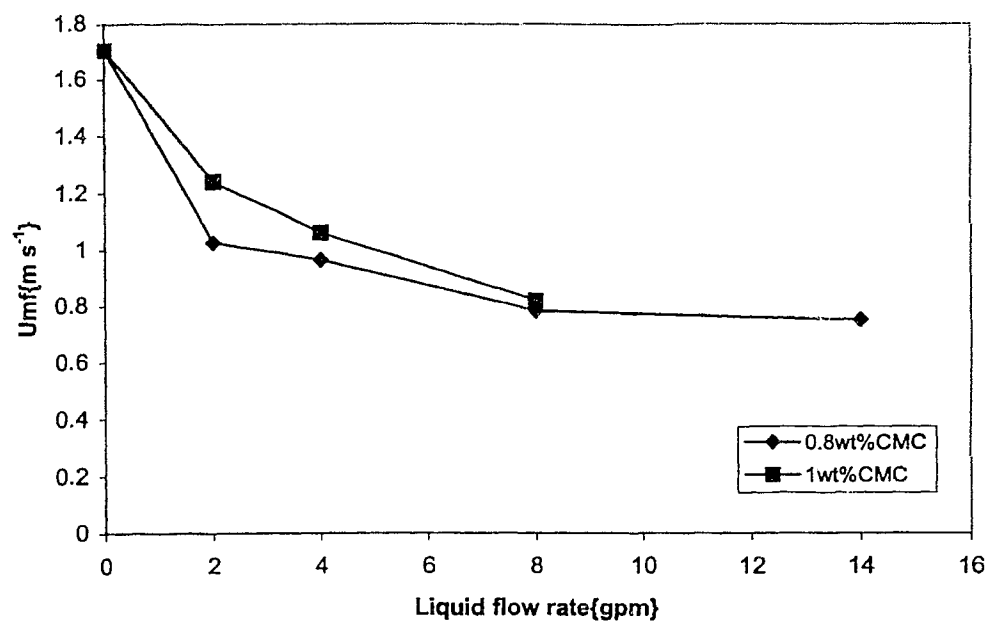
Figure A-38 Effect of liquid flow rate on minimum fluidization velocity
at Hs/D=0.5, dp=38mm
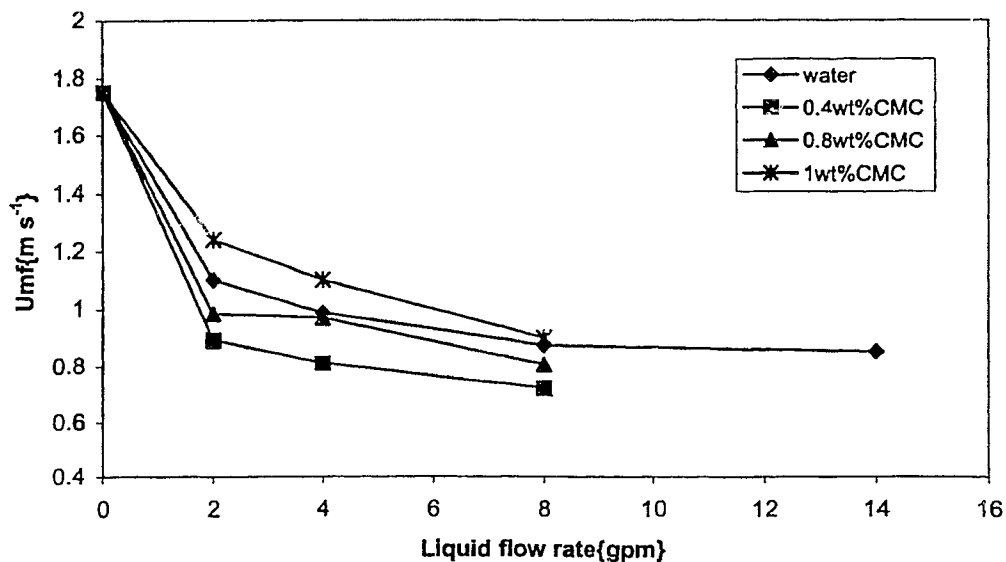


Figure A-39 Effect of liquid flow rate on minimum fluidization velocity
at Hs/D=0.75,dp=38mm,

112
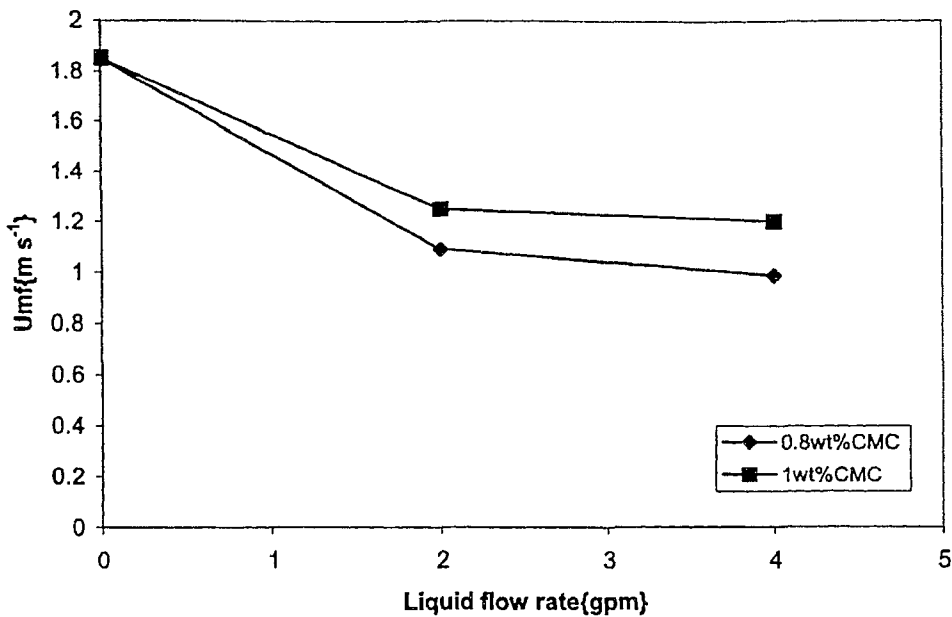
Figure A-40  Effect of liquid flow rate on minimumfluidization velocity
at HsD=1,dp=38mm
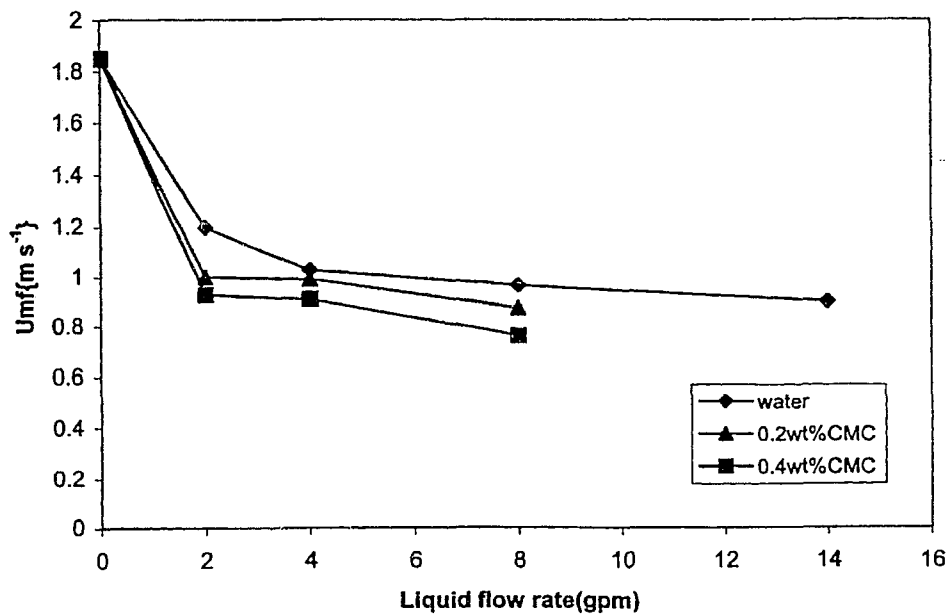


Figure A-41  Effect of liquid flow rate on minimumfluidization velocity at
Hs/D=1,dp=38mm

113
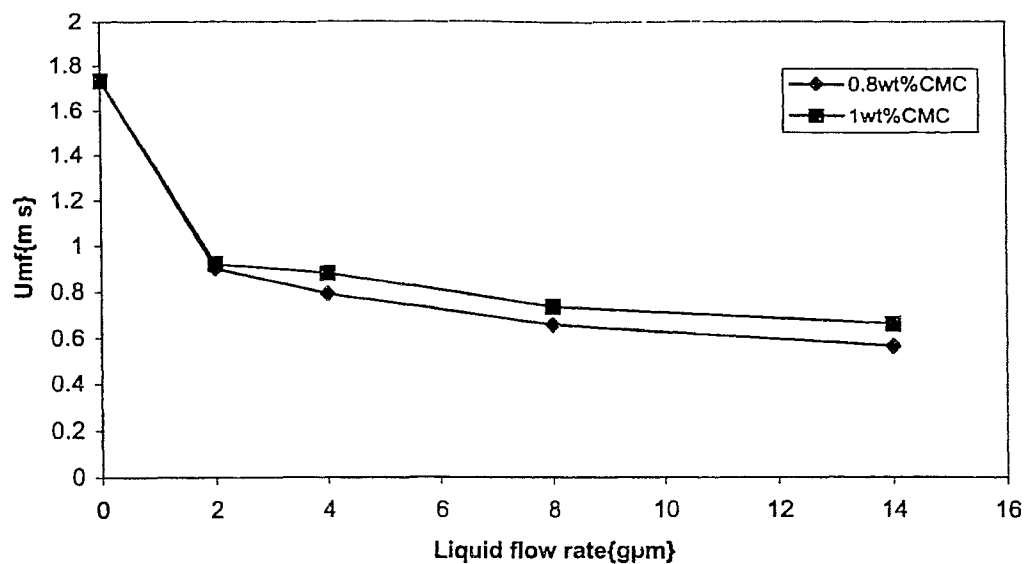
Figure A-42  Effect of liquid flow rate on minimum fluidization velocity
at dp=20mm,Hs/D=0.25
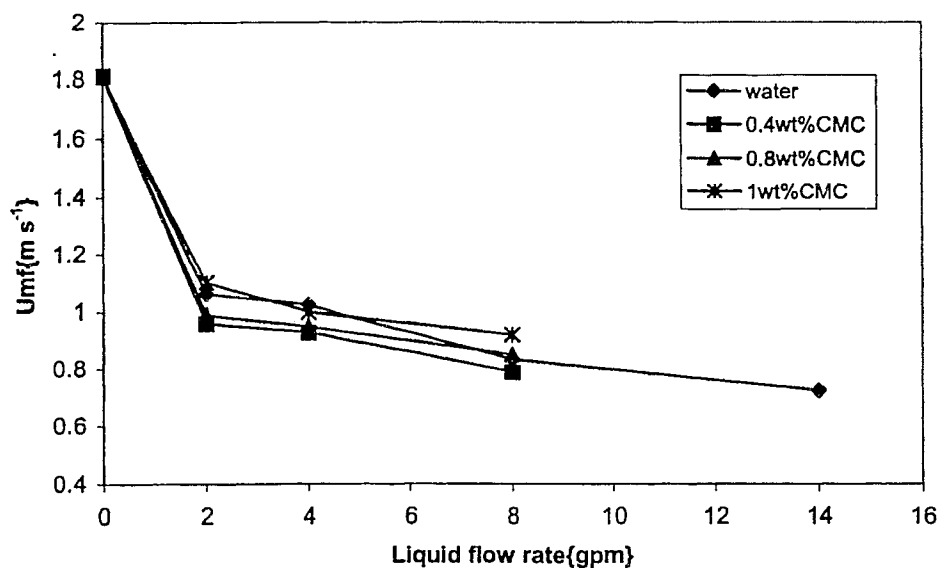


Figure A-43  Effect of liquid flow rate on minimum fluidization velocity
at Hs/D=0.5,dp=20mm

114
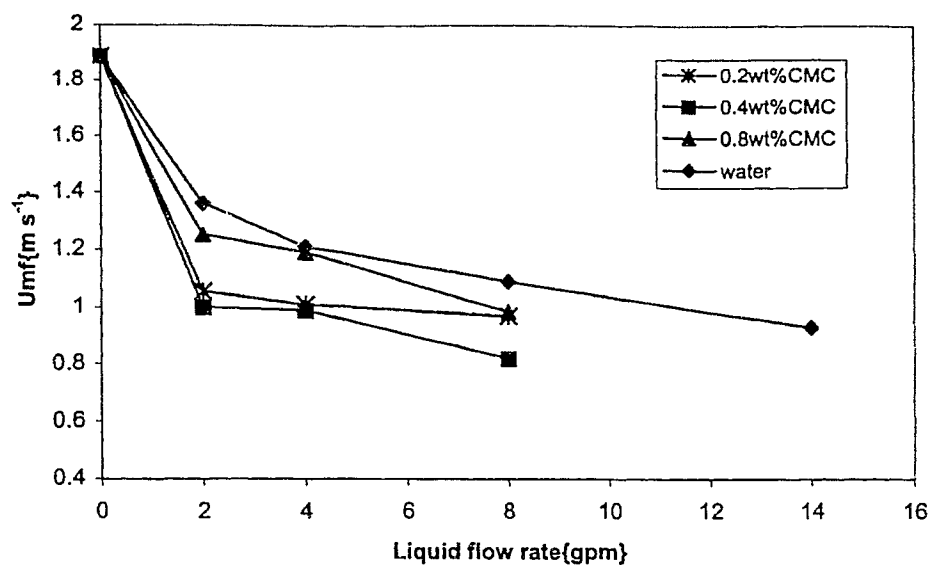
Figure A-44  Effect of liquid flow rate on minimum fluidization velocity at
Hs/D=0.75,dp=20mm
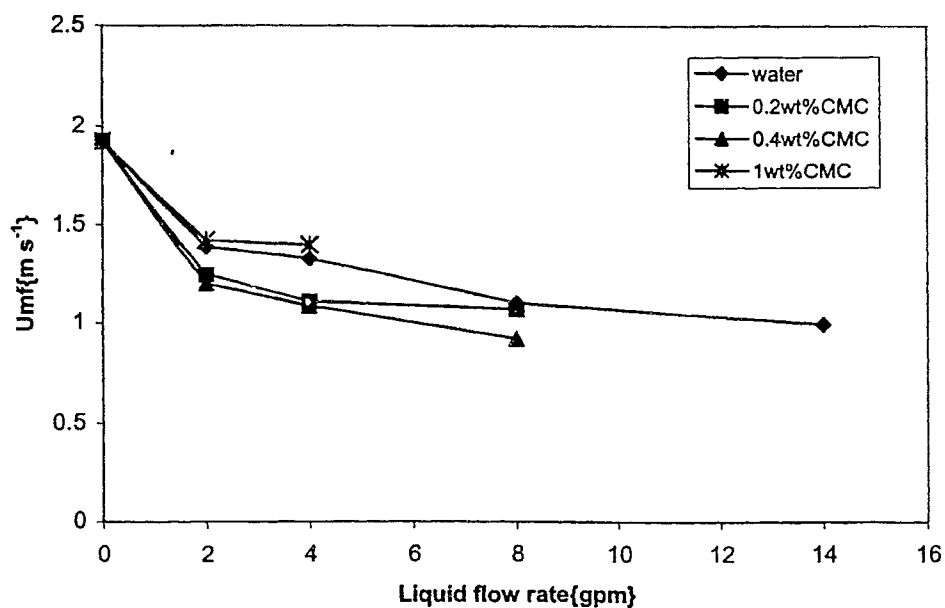


Figure A-45  Effect of liquid flow rate on minimum fluidization velocity
at Hs/D=1,dp=20mm

115
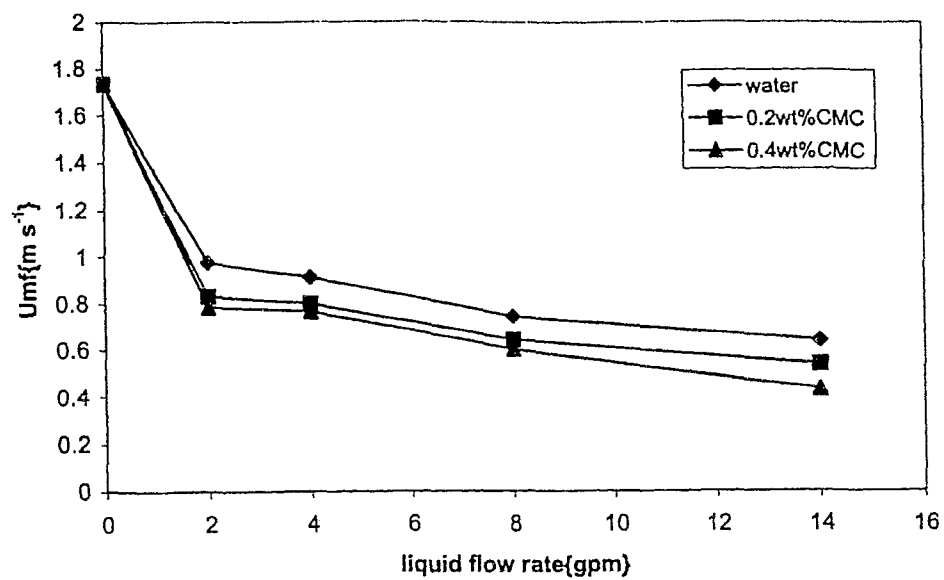
Figure A-46  Effect of liquid flow rate on minimum fluidization velocity
at dp=20mm,Hs/D=0.25

116
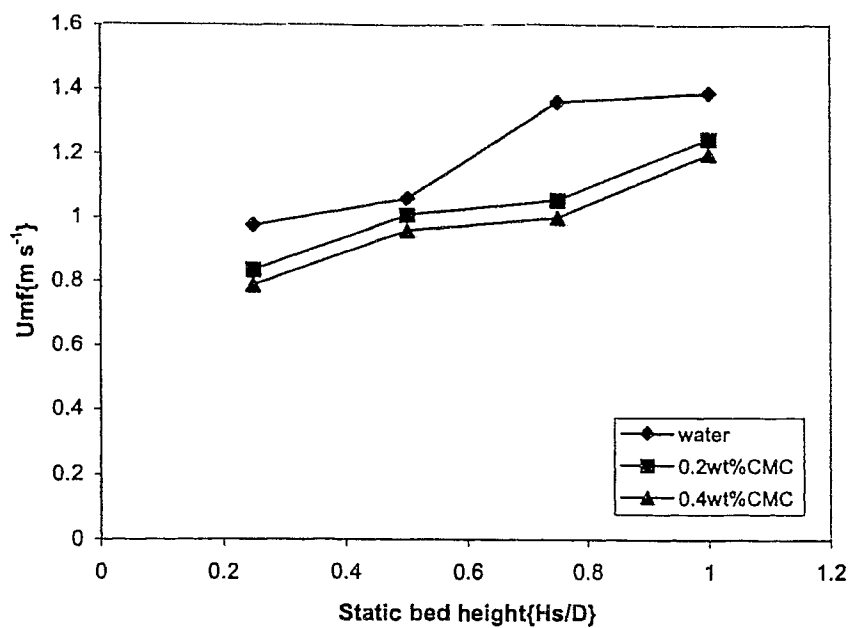
Figure A-47 Effect of static bed height on minimum fluidization
velocity at dp=20,L=2gpm
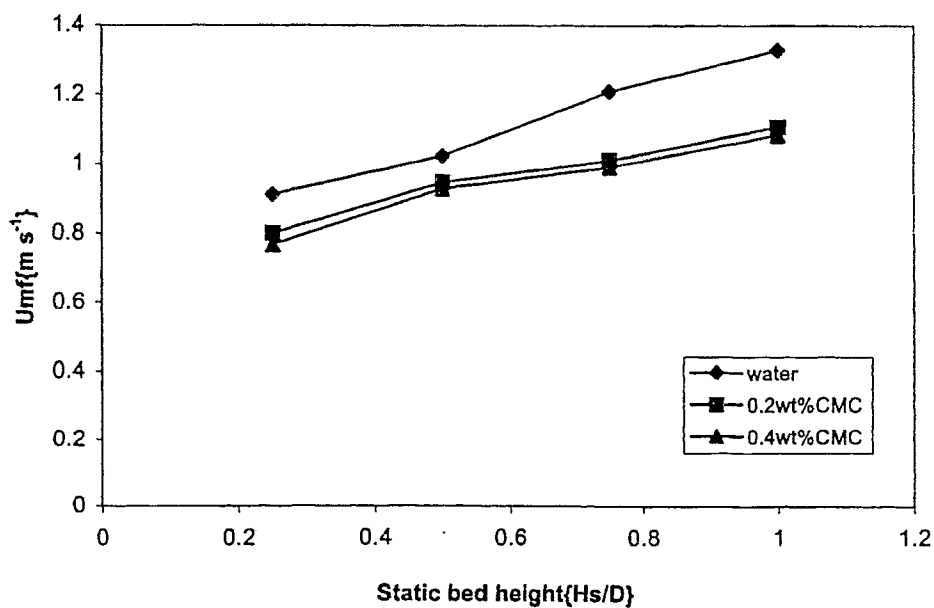


Figure A-48 Effect of static bed height on minimum
fluidization velocity at dp=20mm,L=4gpm

117
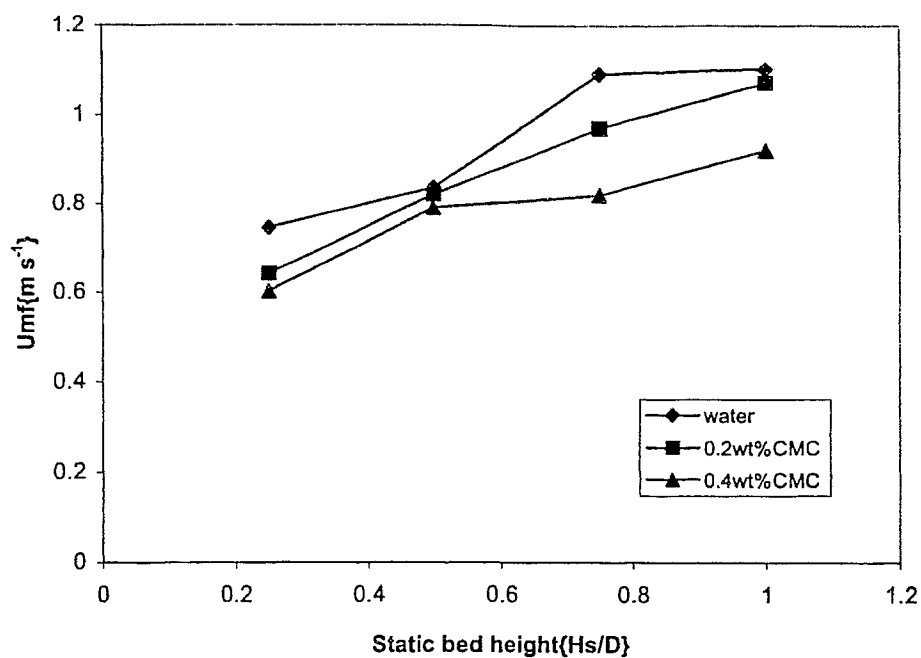
Figure A-49 Effect of static bed height on minimum fluidization
velocity at dp=20mm,L=8gpm
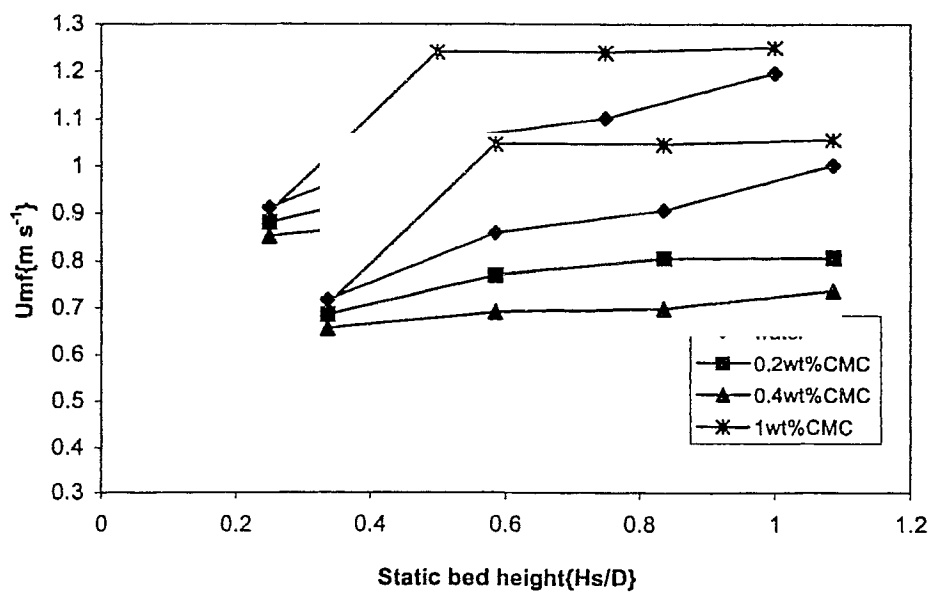


Figure A-50 Effect of static bed height on minimum fluidization
velocity at dp=38mm, L=2gpm

118
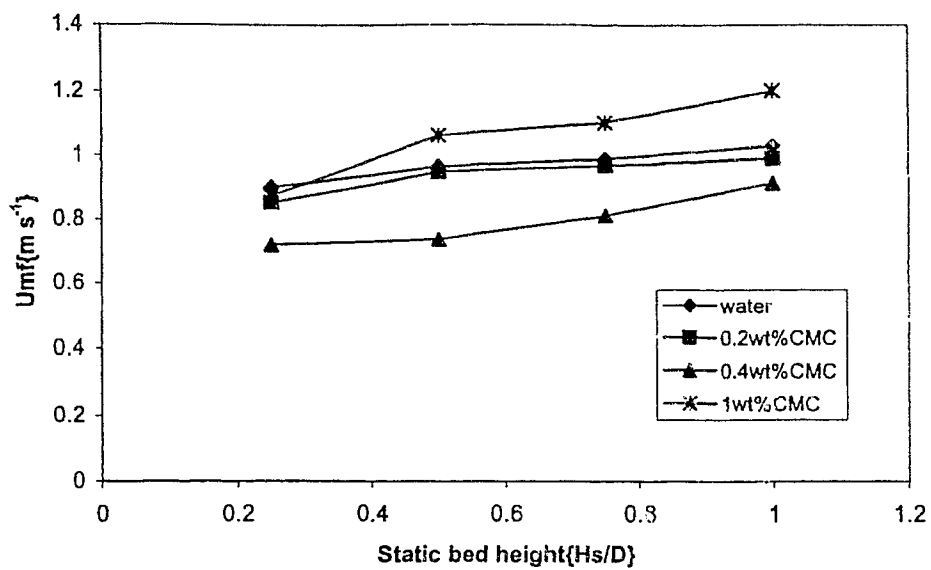
Figure A-51  Effect of static bed height on minimum
fluidization velocity at dp=38mm, L=4gpm
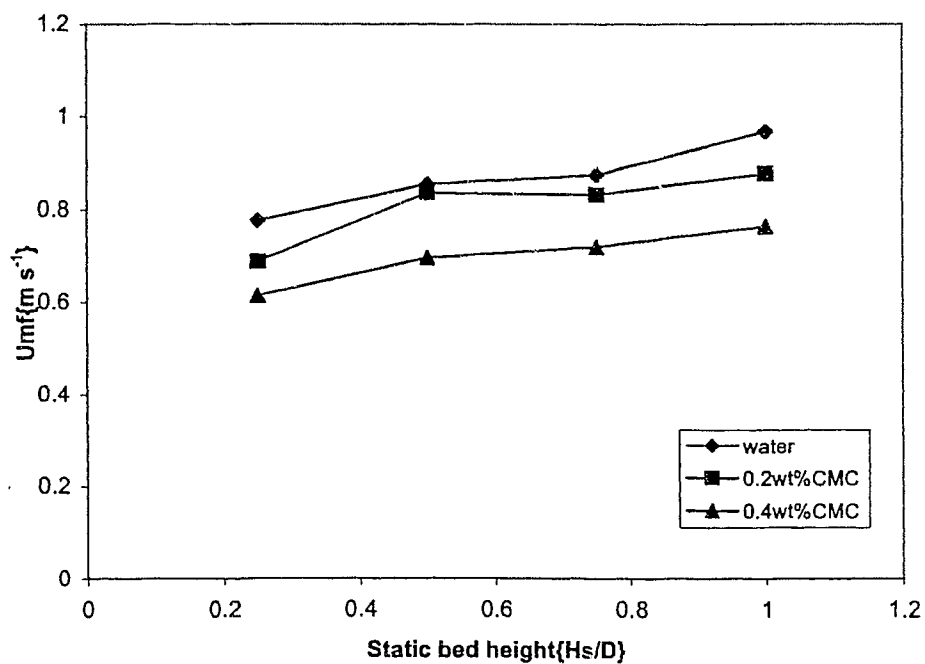


Figure A-52  Effect of static bed height on minimum
fluidization velocity at dp=38mm,L=8gpm

119
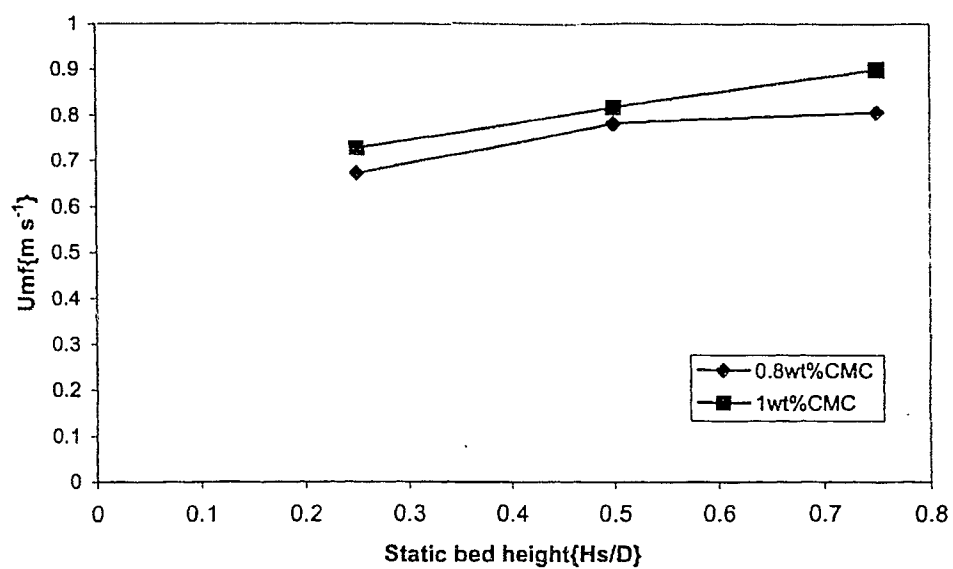
Figure A-53  Effect of static bed height on minimum fluidization velocity at dp=38mm,L=8gpm
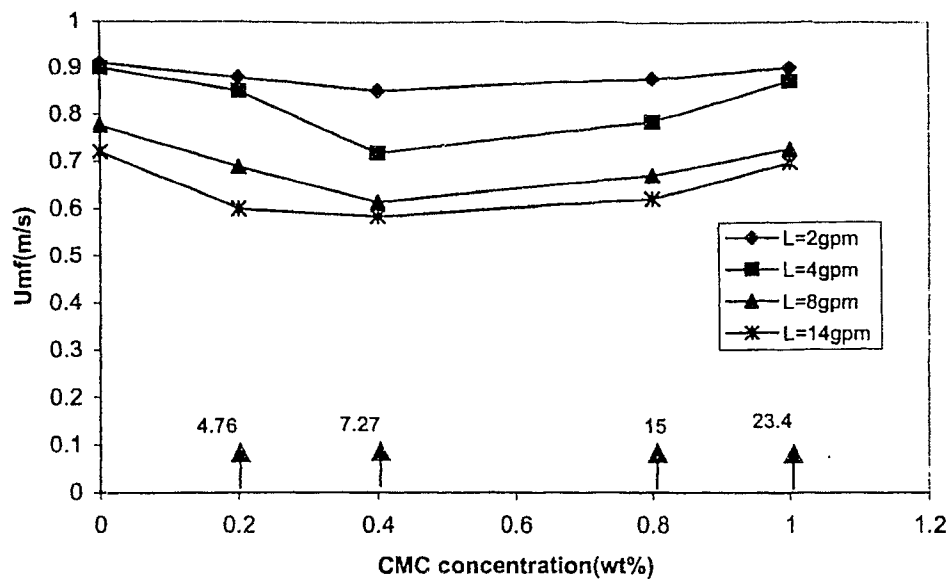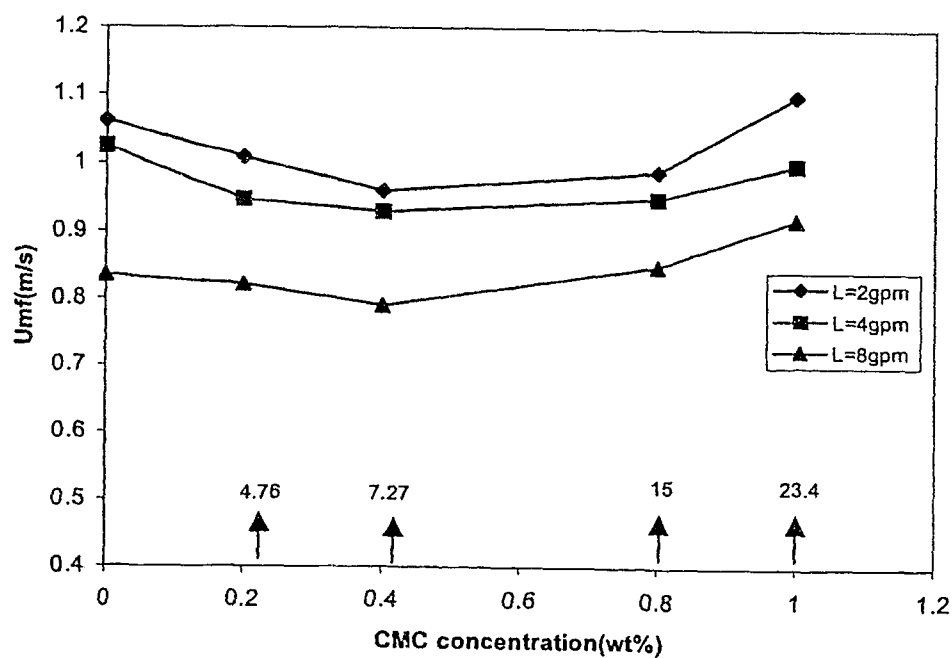
Figure A- 54  Effect of CMC concentration on minimum
fluidization velocity at Hs/D=0.25,dp=38mm,
( ↑ viscosity,cP,10 s$^{-1}$)
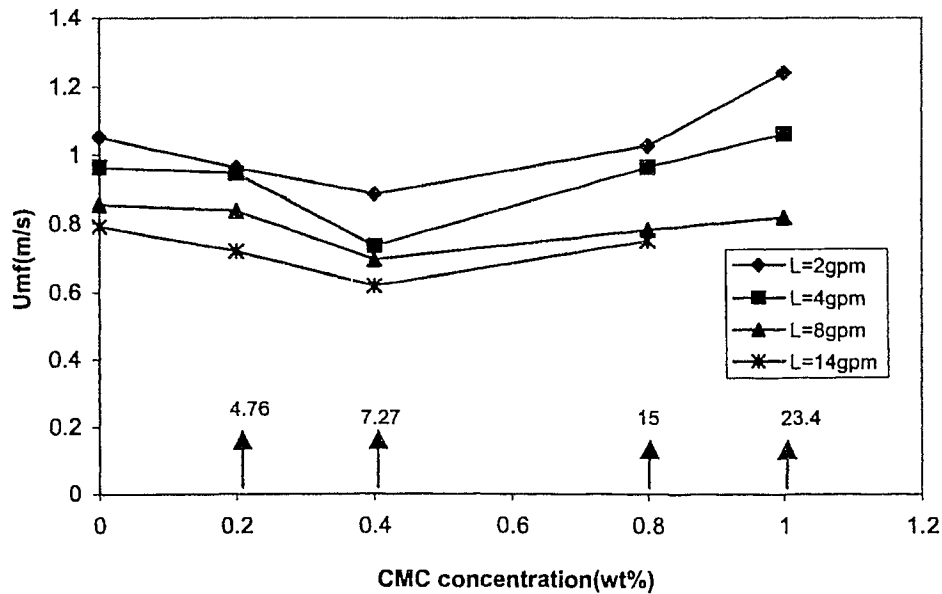


Figure A-55  Effect of CMC concentration on minimum
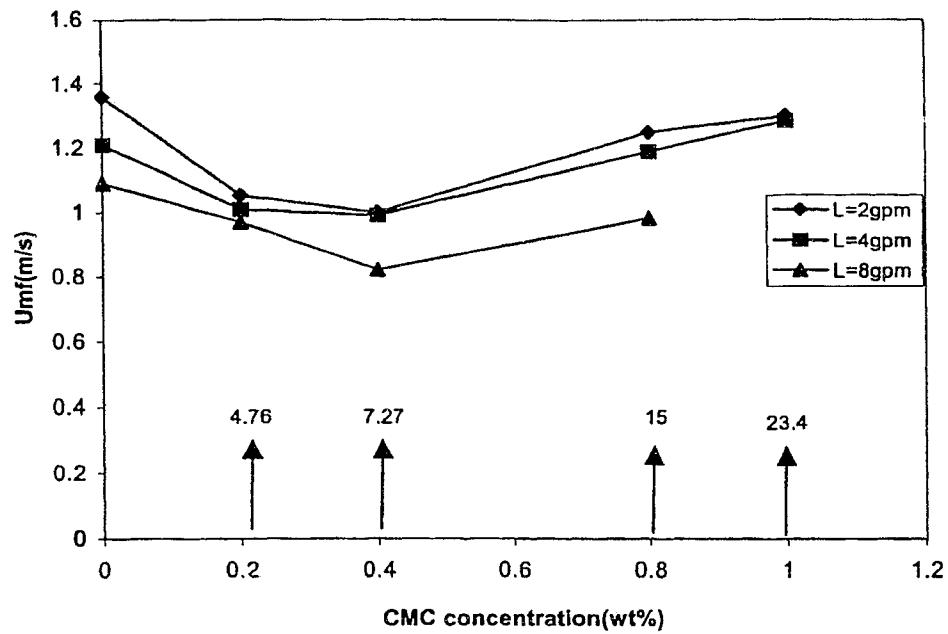fluidization velocity at Hs/D=0.5 ,dp=38mm
( ↑ viscosity,cP,at 10 s$^{-1}$)

121
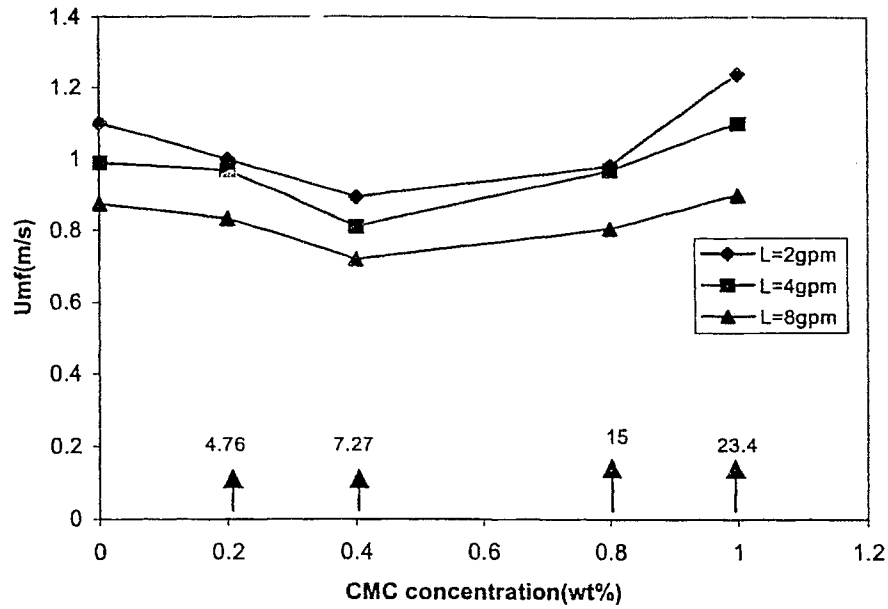
Figure A-56 Effect of CMC concentration on minimum
fluidization velocity at Hs/D=0.75,dp=38mm
($\uparrow$ viscosity,cP,at 10 s$^{-1}$)
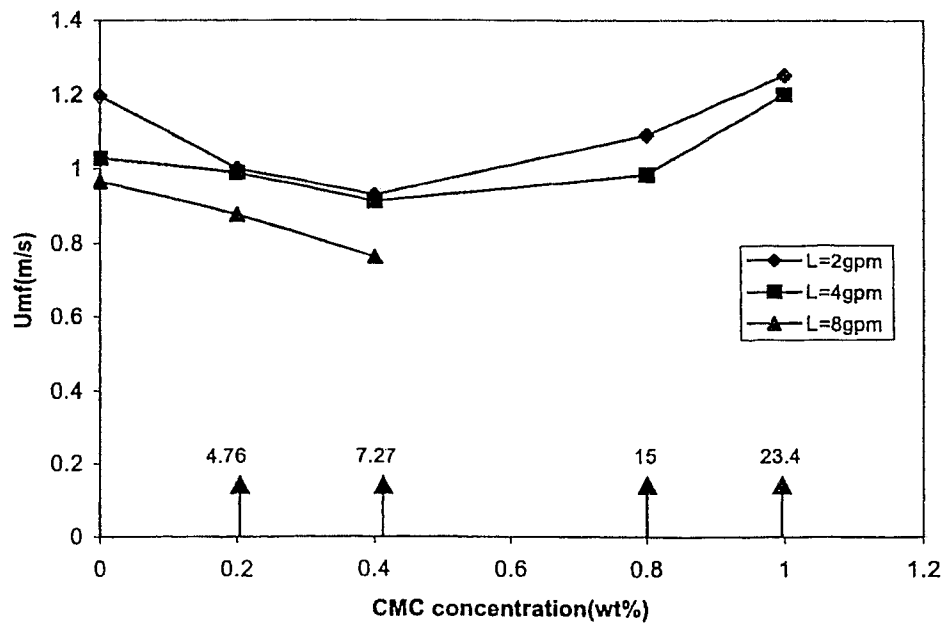

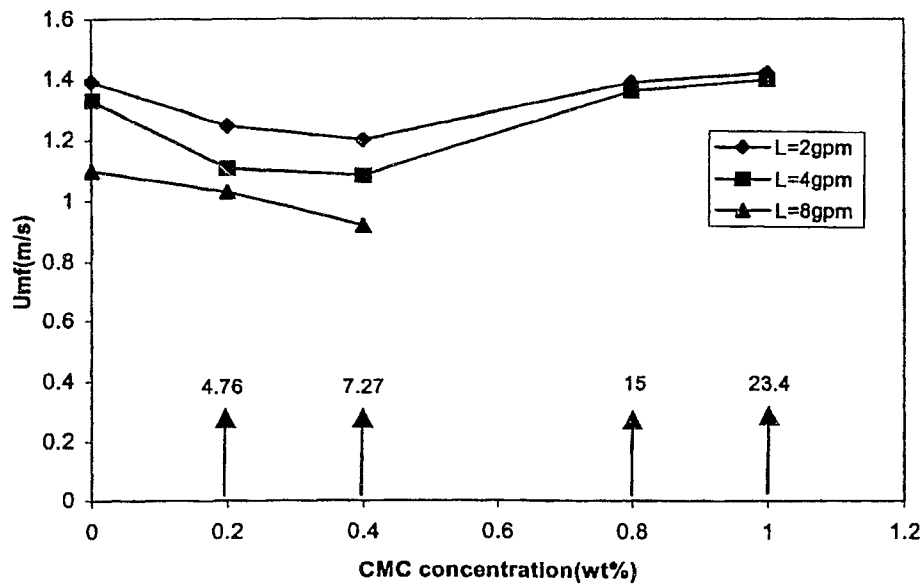
Figure A-57 Effect of CMC concentration on minimum
fluidization velocity at Hs/D=1,dp=38mm
($\uparrow$ viscosity,cP,at 10 s$^{-1}$)

122
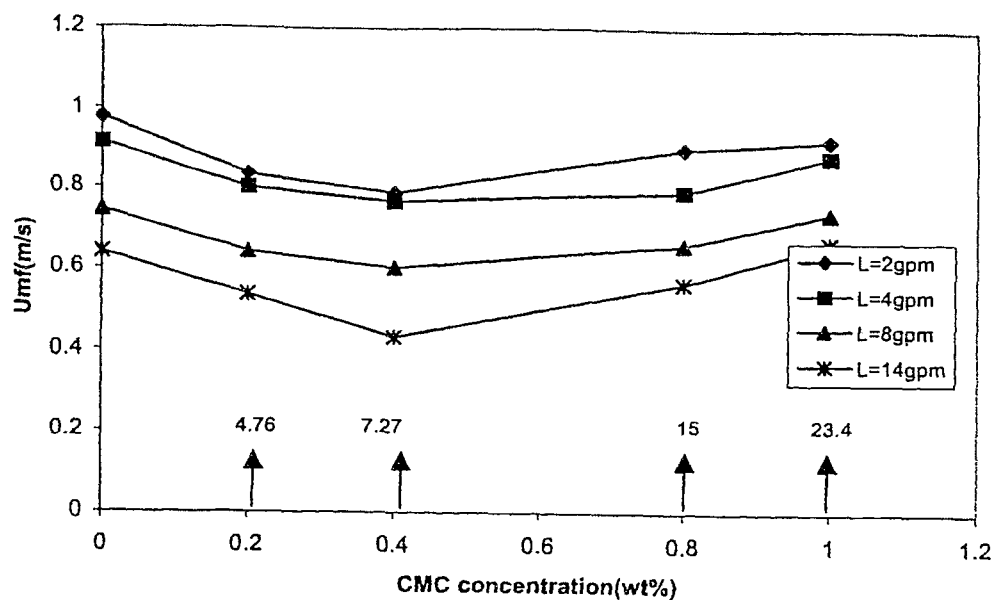
Figure A-58  Effect of CMC concentration on minimum
fluidization velocity at dp=20mm,Hs/D=0.25

($\uparrow$ viscosity,cP, at 10 s$^{-1}$)



Figure A-59  Effect of CMC concentration on minimum
fluidization velocity at Hs/D=0.5,dp=20mm,
($\uparrow$ viscosity,cP, at 10 s$^{-1}$)

123

Figure A-60 Effect of CMC concentration on minimum
fluidization velocity at Hs/D=0.75,dp=20mm,
($\uparrow$ viscosity,cP,at 10 s$^{-1}$)



Figure A-61 Effect of CMC concentration on minimum
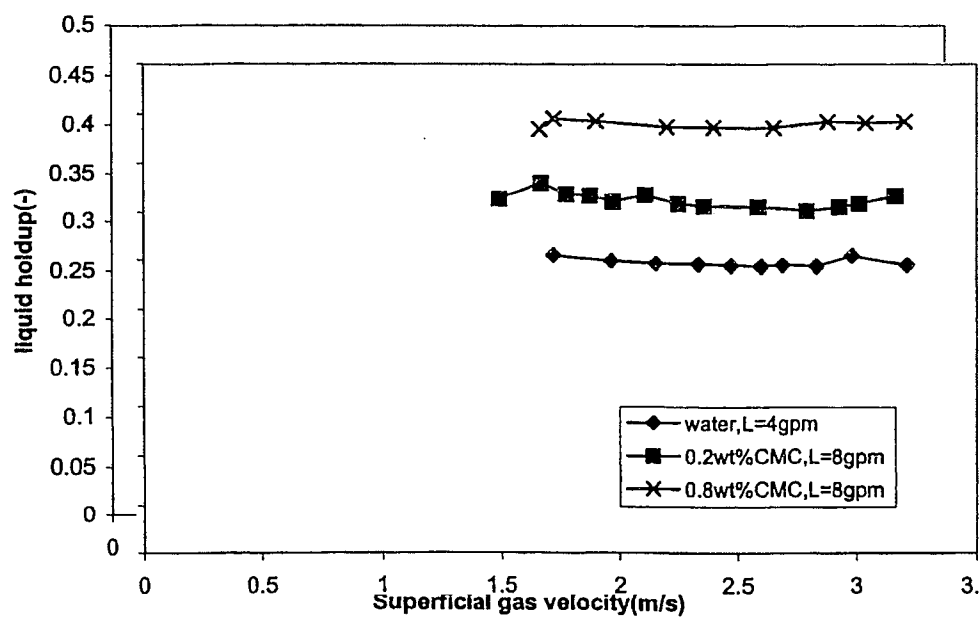fluidization velocity at Hs/D=1,dp=20mm,
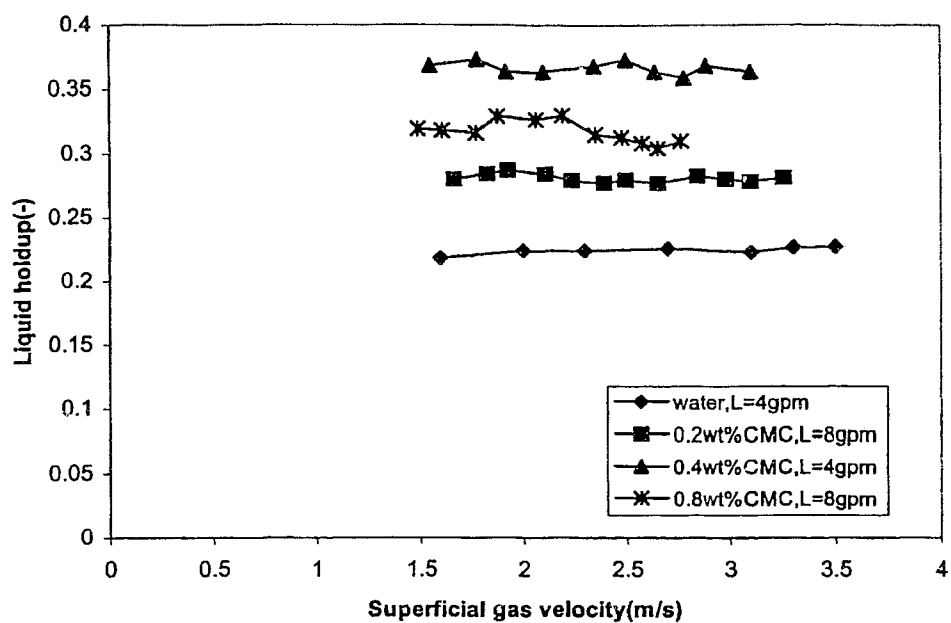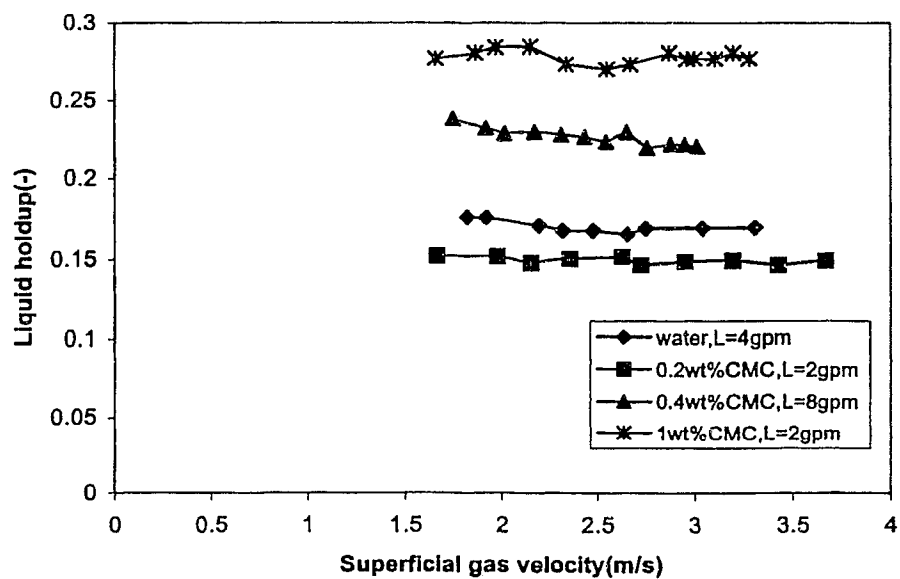($\uparrow$ viscosity, cP, 10 s$^{-1}$)

124
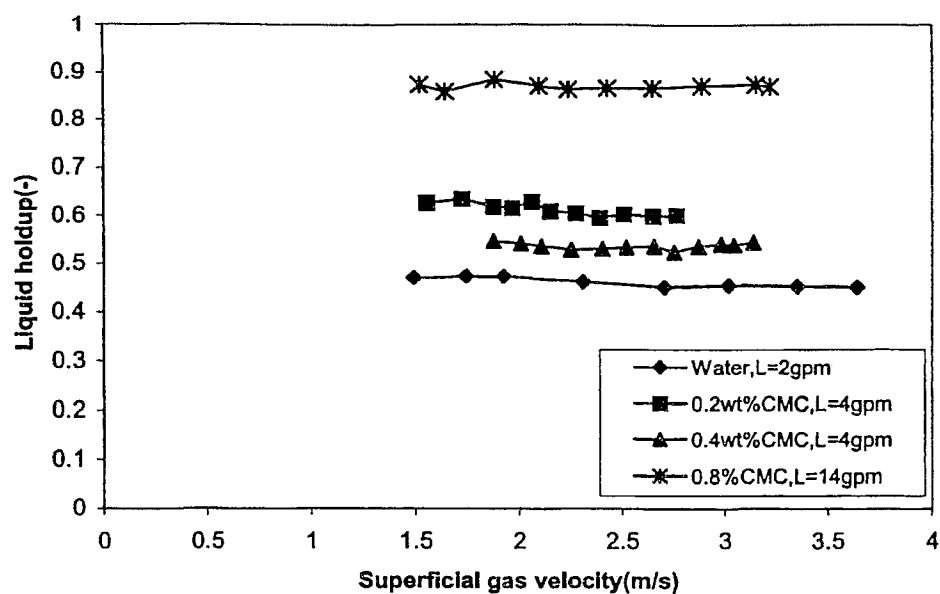
Figure A-62 Effect of superficial gas velocity on liquid holdup at
Hs/D=0.25, dp=38mm



Figure A-63 Effect of superficial gas velocity on liquid holdup at
Hs/D=0.5, dp=38mm

125

Figure A-64  Effect of superficial gas velocity on liquid holdup at
Hs/D=0.75,dp=38mm



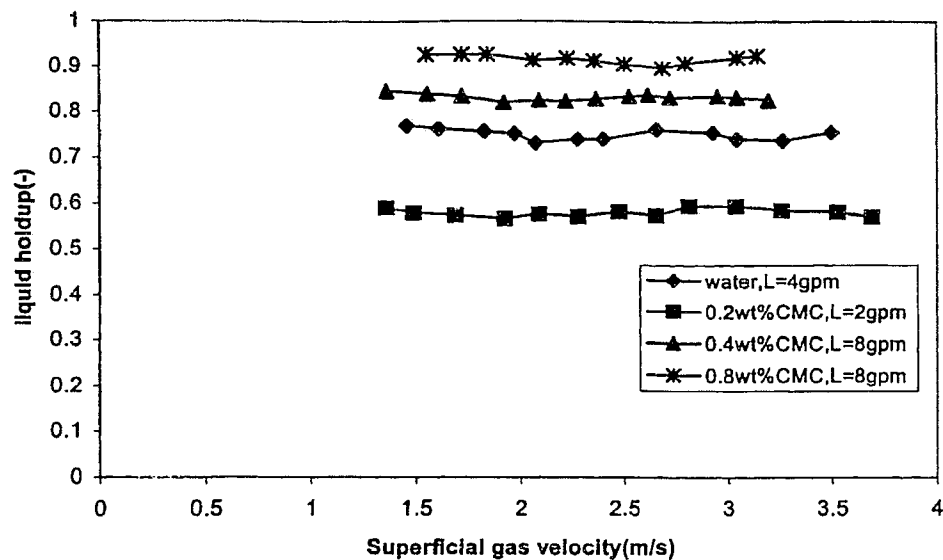Figure A-65  Effect of superficial gas velocity on liquid holdup at
Hs/D=1,dp=38mm

126

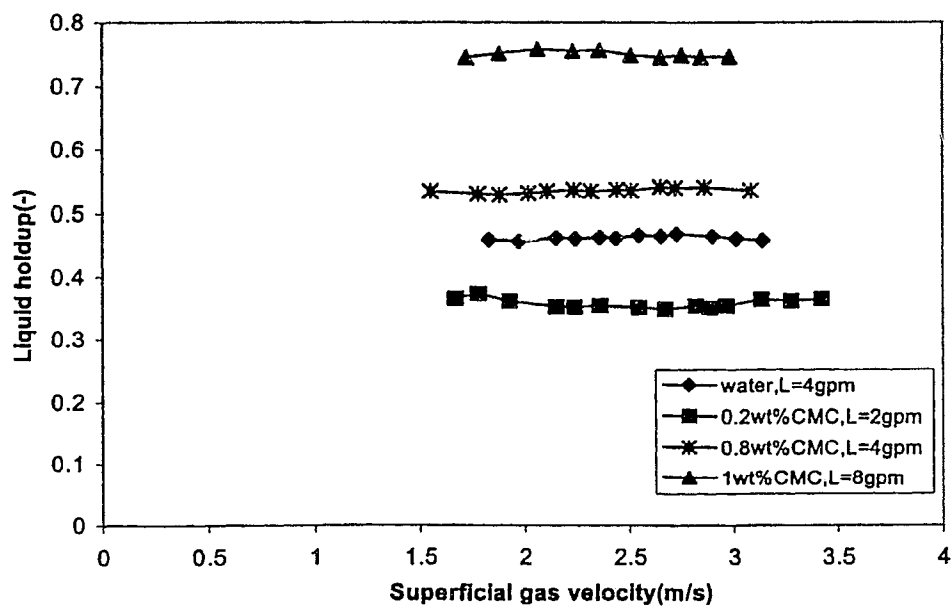Figure A-66  Effecr of superficial gas velocity on liquid holdup at
dp=20mm,Hs/D=0.25



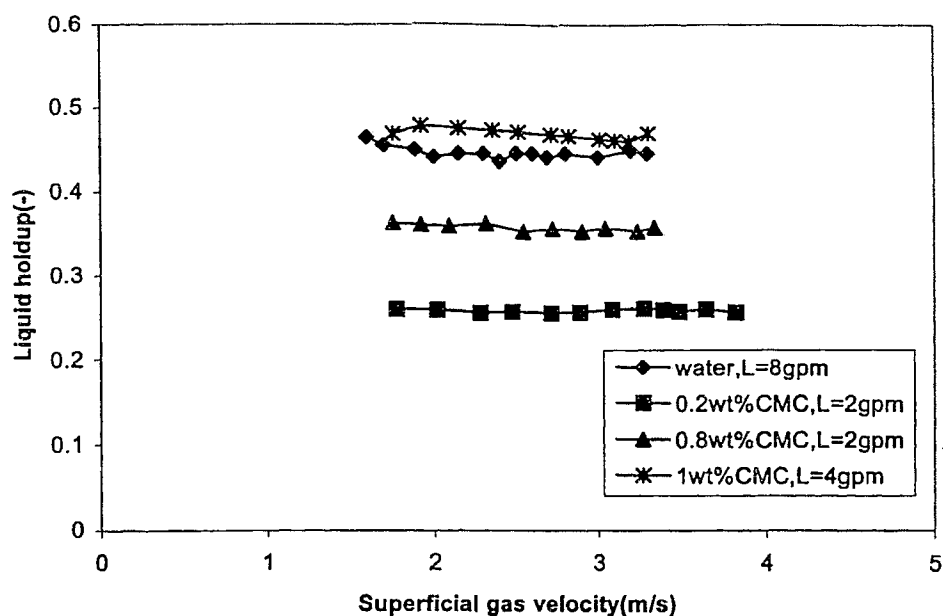Figure A-67  Effect of superficial gas velocity on liquid holdup at
Hs/D=0.5,dp=20mm

127

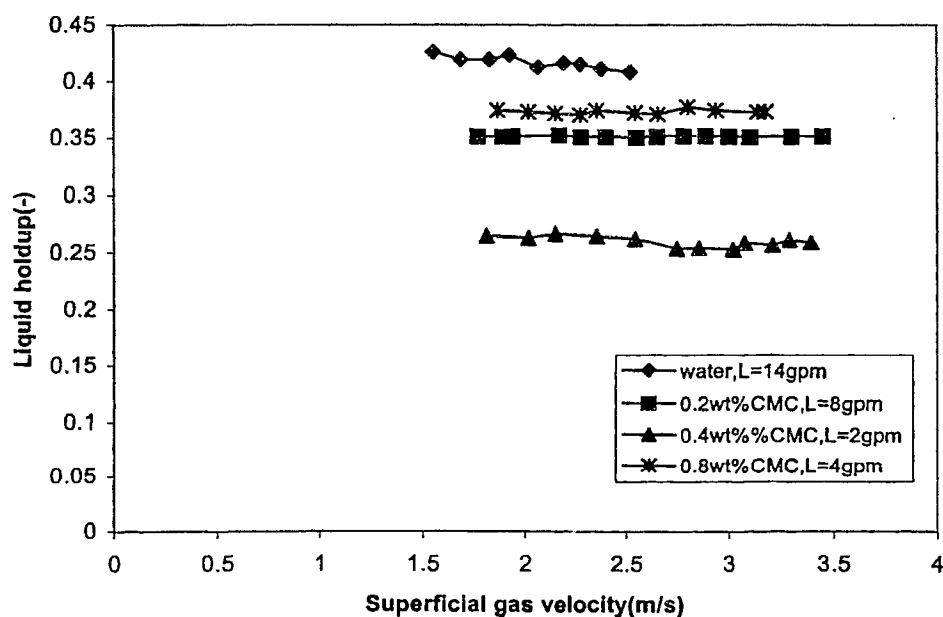Figure A-68  Effect off superficial gas vellocity on liquid holdup at
Hs/D=0.75,dp=20mm



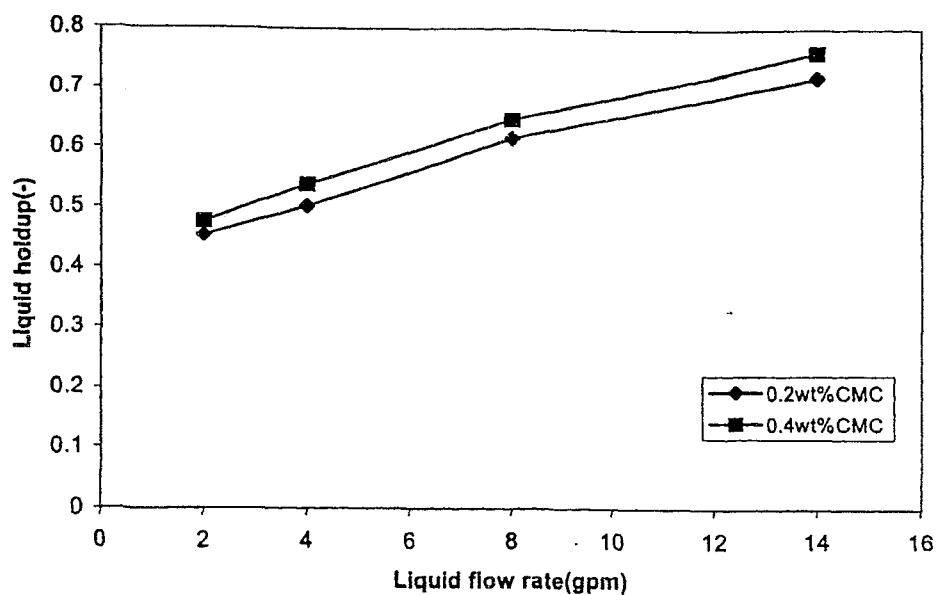Figure A-69  Effect of superficial gas velocity on liquid holdup at
Hs/D=1,dp=20mm

128

Figure A-70 Effect of liquid flow rate on liquid holdup at Hs/D=0.25
dp=38mm


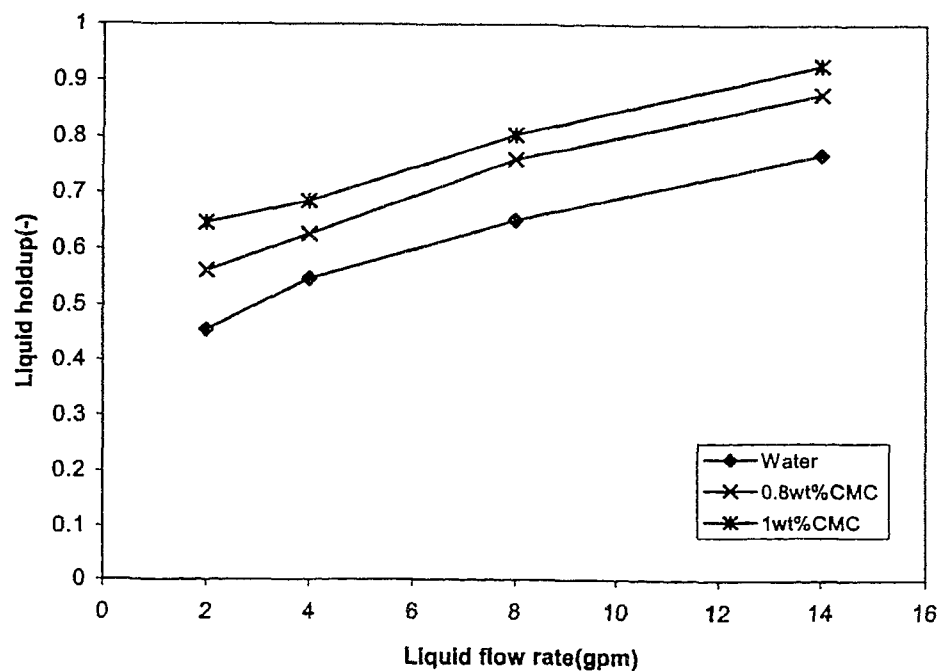
Figure A-71 Effect of liquid flow rate on liquid holdup
at Hs/D=0.25 dp=38mm

129

Figure A-72  Effect of liquid flow rate on liquid holdup
at Hs/D=0.5, dp=38mm



Figure A-73  Effect of liquid flow rate on liquid holdup at
Hs/D=0.75,dp=38mm

130

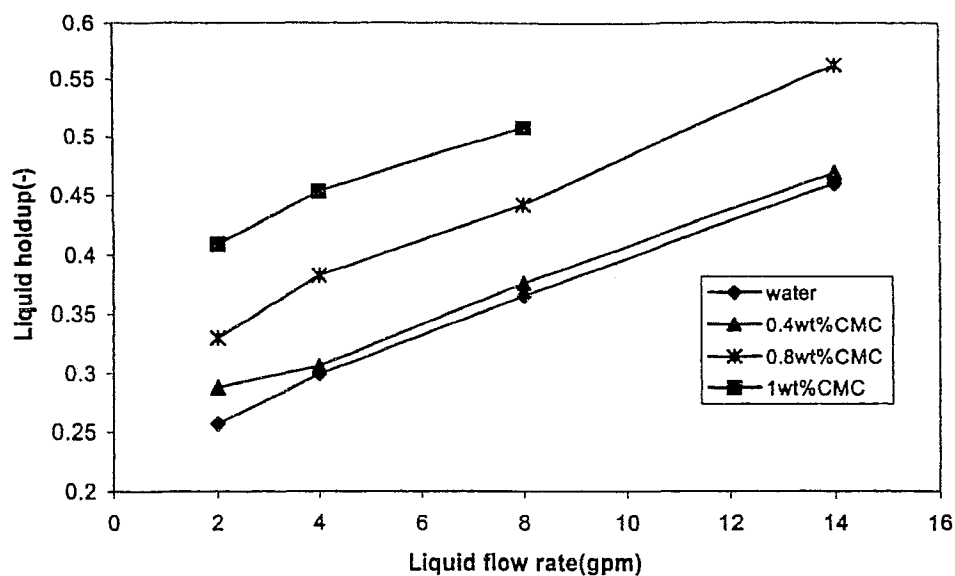Figure A-74 Effect of liquid flow rate on liquid holdup at
Hs/D=1,dp=38mm



Figure A-75 Effect of liquid flow rate on liquid holdup at
dp=20mm,Hs/D=0.25

131
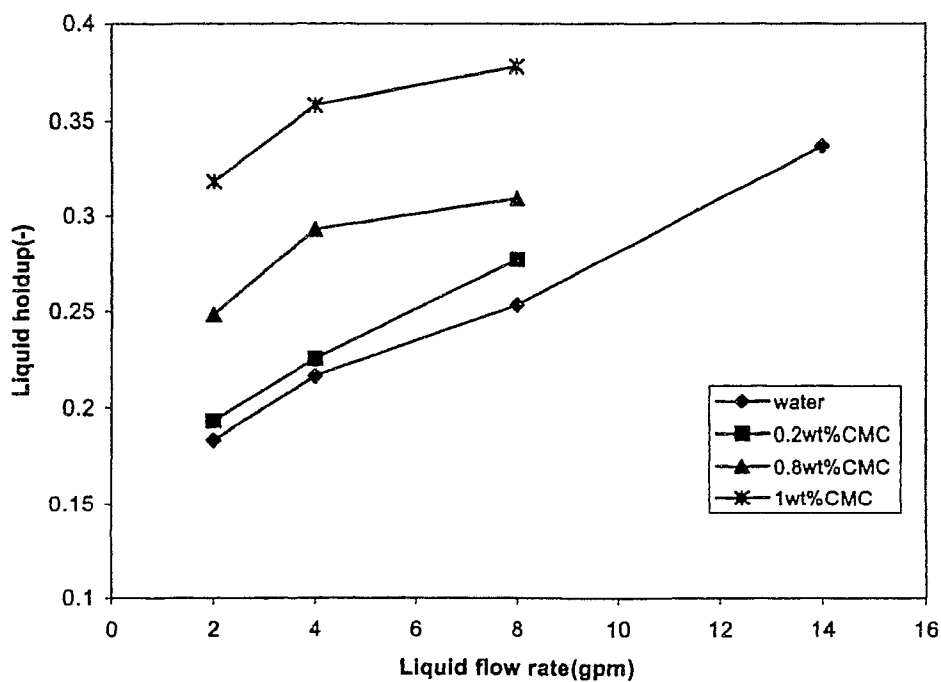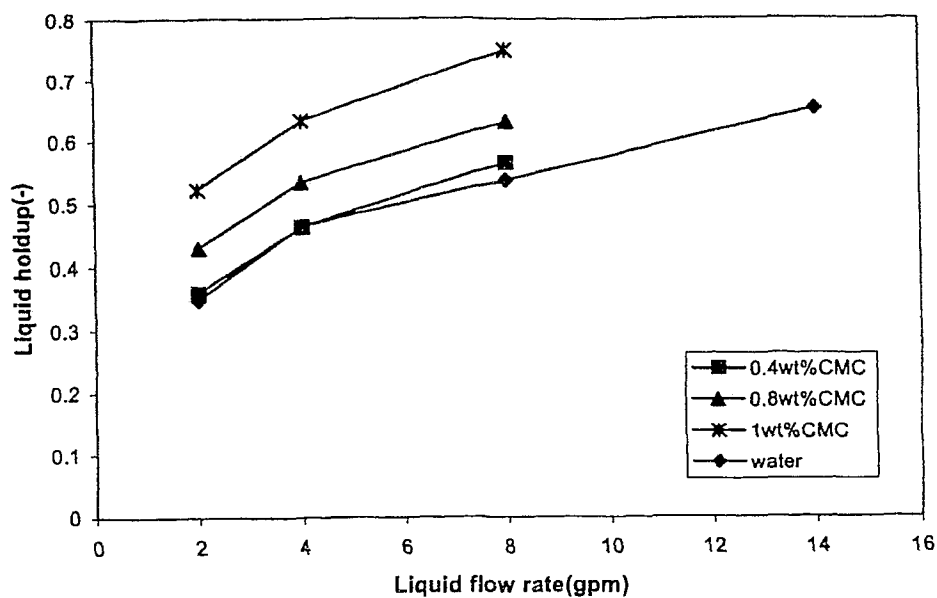
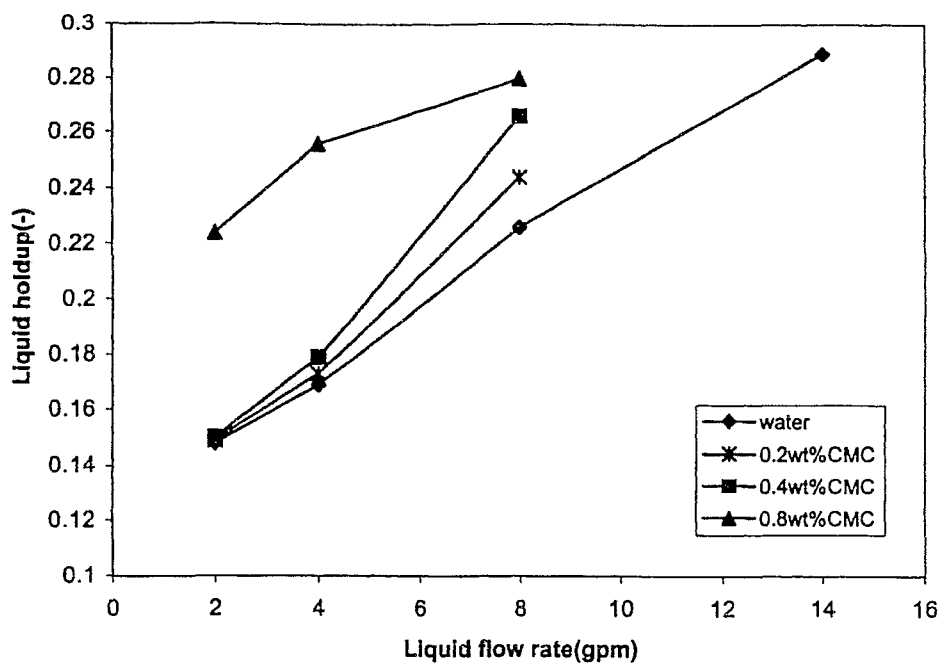Figure A-76  Effect of liquid flow rate on liquid holdup at
Hs/D=0.5,dp=20mm
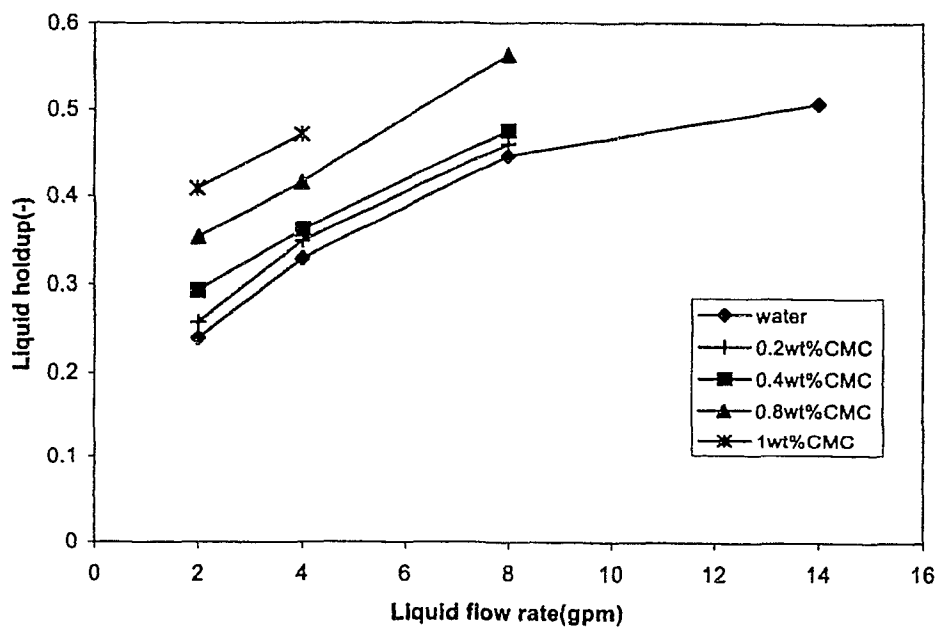


Figure A-77  Effect of liquid flow rate on liquid holdup at
Hs/D=0.75,dp=20mm

132

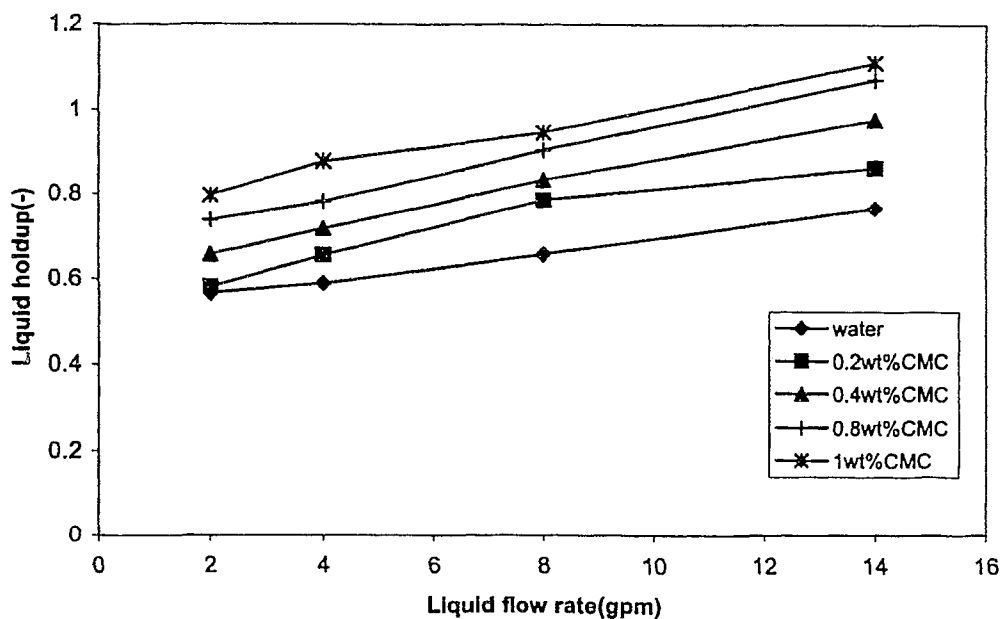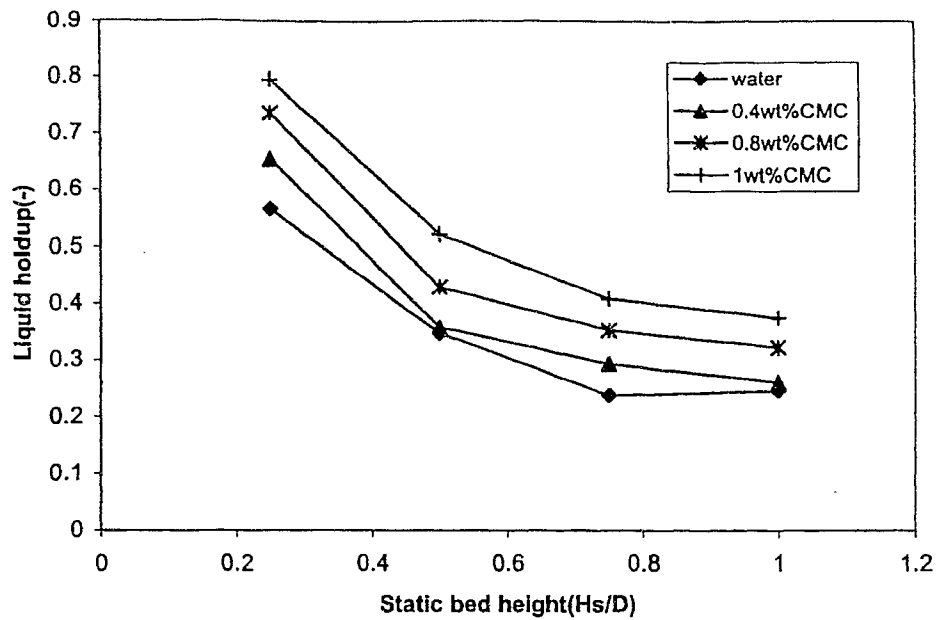Figure A-78  Effect of static bed height on liquid holdup
at dp=20mm, L=2gpm
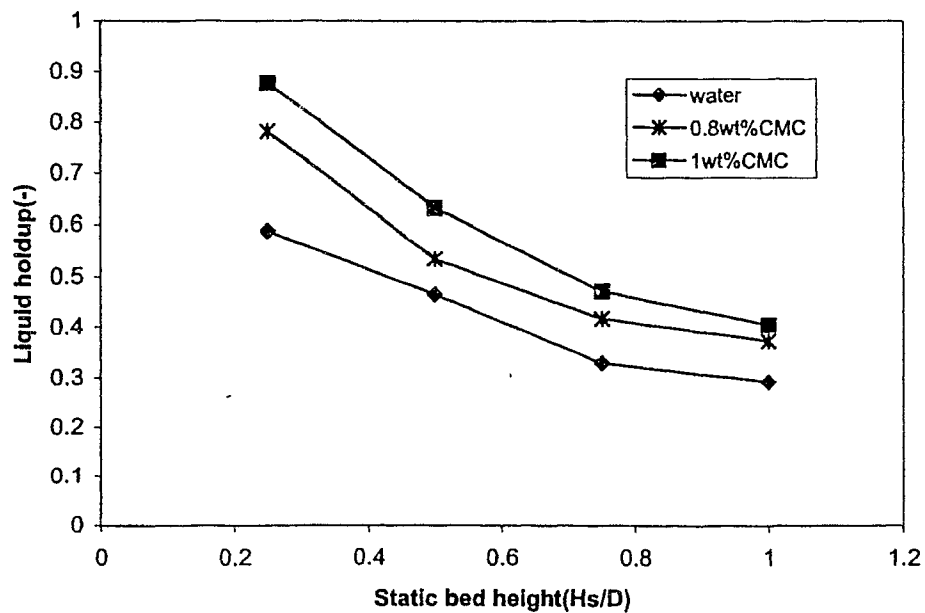


Figure A-79  Effect of static bed height on liquid holdup at
dp=20mm, L=4gpm

133
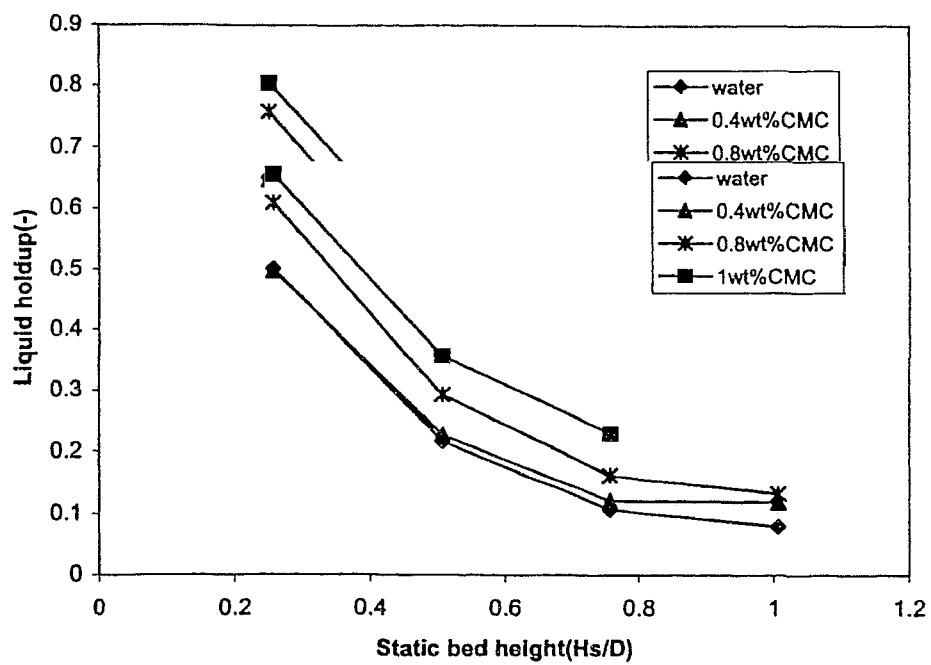
Figure A-82  Effect of static bed height on liquid holdup at
dp=38mm, L=8gpm

135
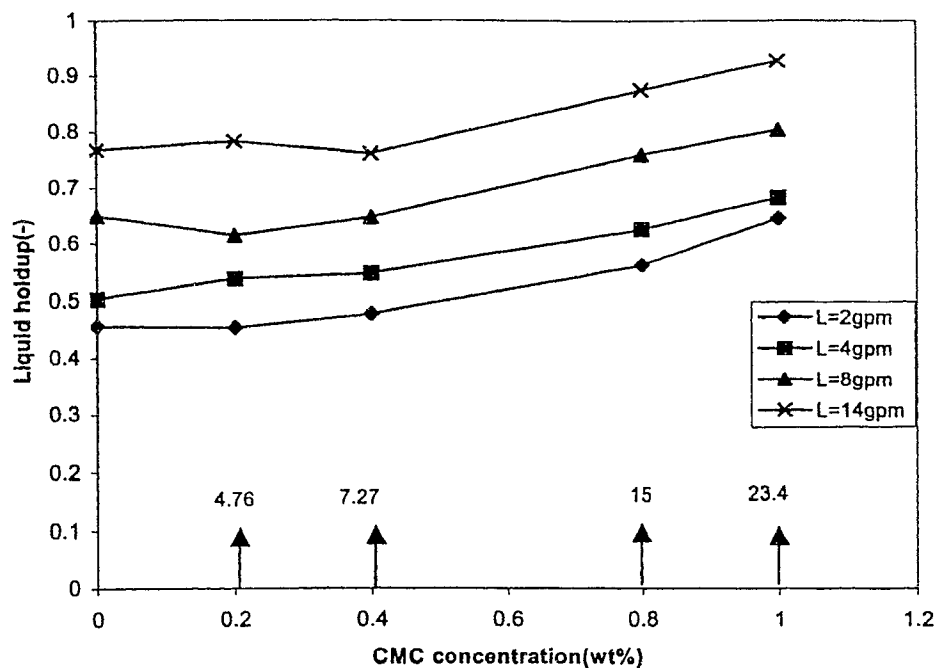
Figure A-83  Effect of CMC concentration on liquid holdup at Hs/D=0.25, dp=38mm, (▲ viscosity,cP,10 s$^{-1}$)
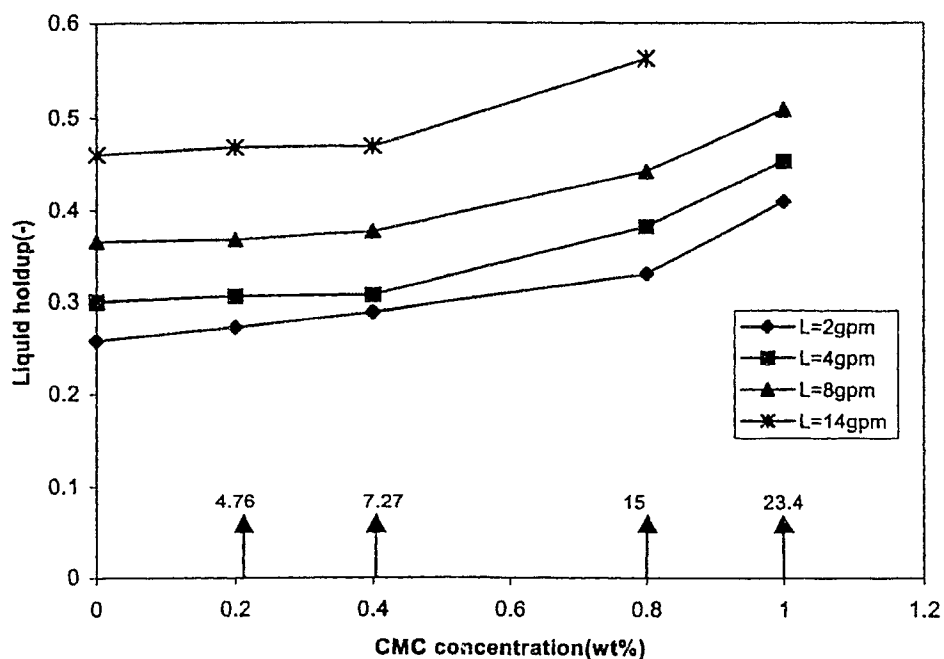


Figure A-84  Effect of CMC concentration on liquid holdup at Hs/D=0.5,dp=38mm, (▲ viscosity,cP,at 10 s$^{-1}$)

136
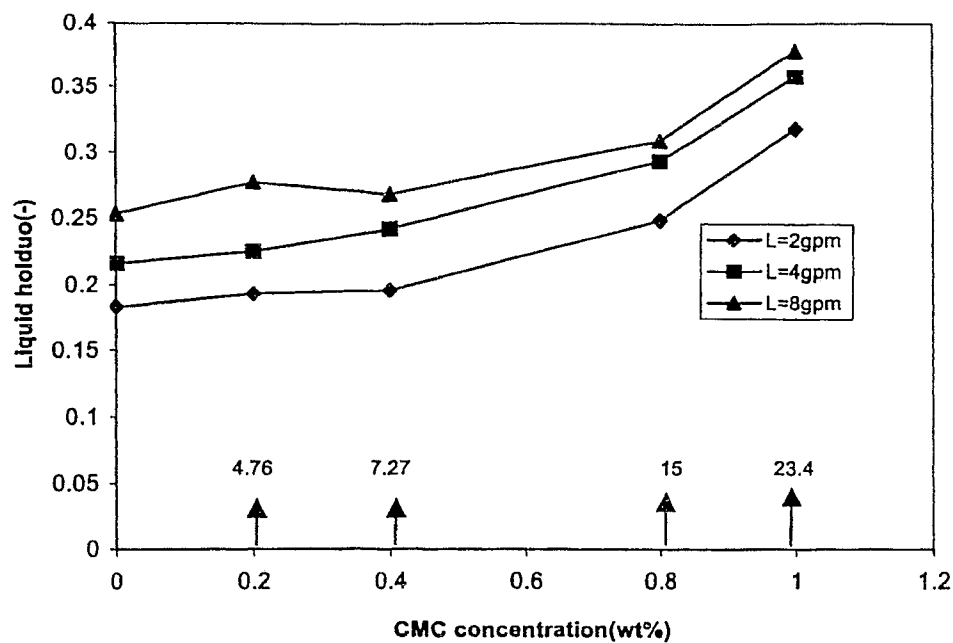
Figure A-85 Effect of CMC concentration on liquid holdup at
Hs/D=0.75 dp=38mm,( ↑ viscosity,cP,at 10 s$^{-1}$)
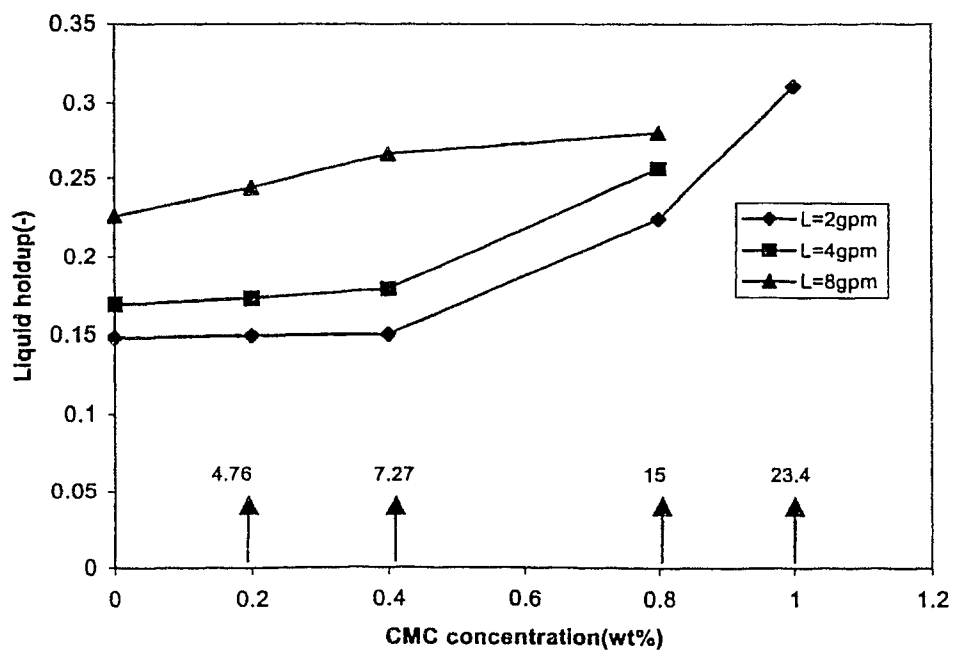


Figure A-86 Effect of CMC concentration on liquid holdup at
Hs/D=1,dp=38mm,( ↑ viscosity,cP,at 10 s$^{-1}$)

137
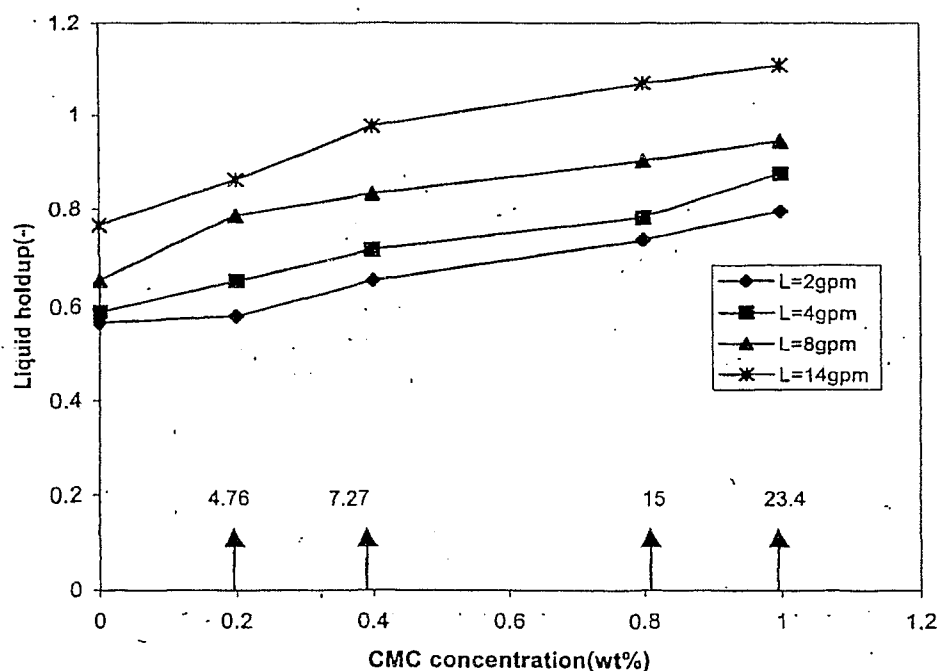
Figure A-87  Effect of CMC concentration on liquid holdup at dp=20mm; Hs/D=0.25,( ↑ viscosity,cP, at $10,s^{-1}$)
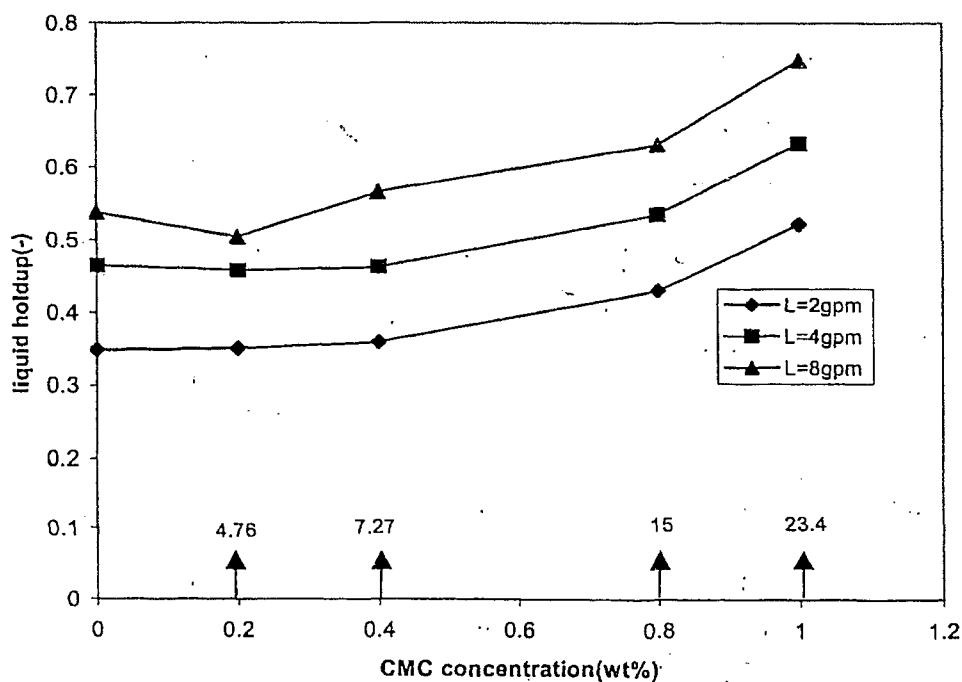


Figure A-88  Effect of CMC concentration on liquid holdup at Hs/D=0.5,dp=20mm,( ↑ viscosity,cP,at $10 s^{-1}$)

138
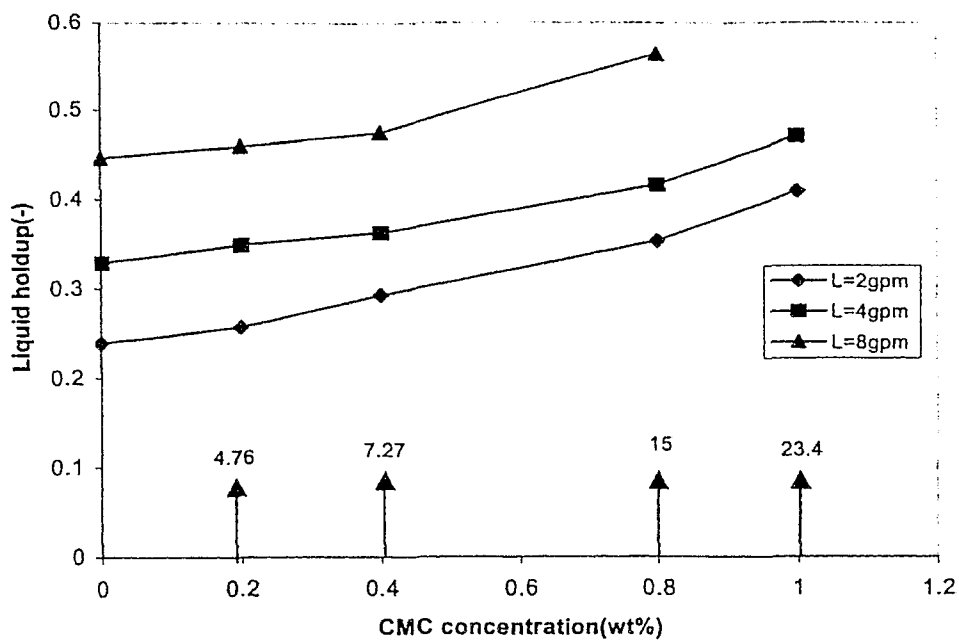
Figure A-89  Effect of CMC concentration on liquid holdup at
Hs/D=0.75,dp=20mm,(▲ viscosity,cP,at 10 s⁻¹)
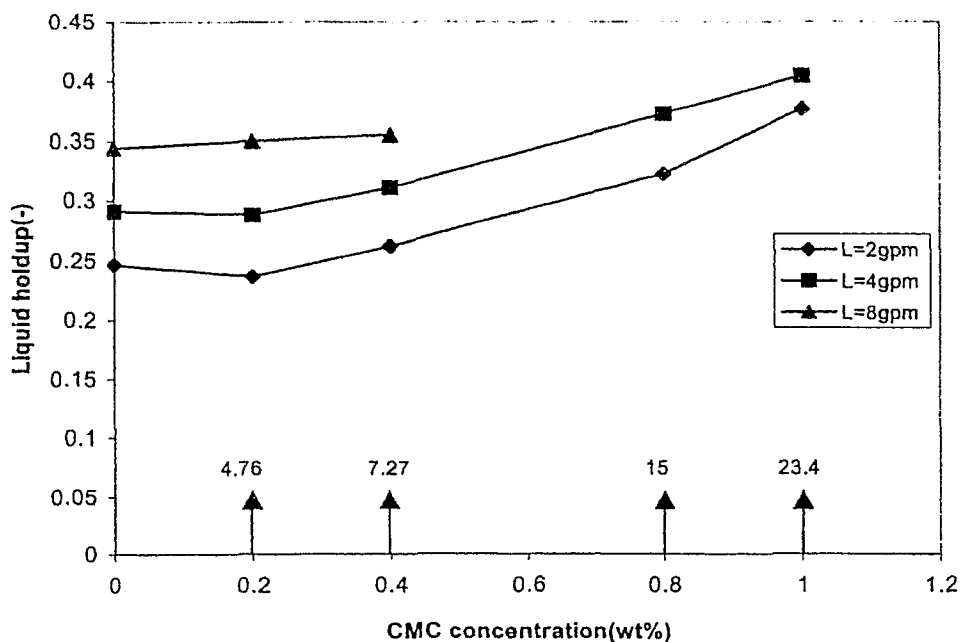


Figure A-90  Effect of CMC concentration on liquid holdup at
Hs/D=1,dp=20mm, (▲ viscosity,cP,at 10 s⁻¹)

139
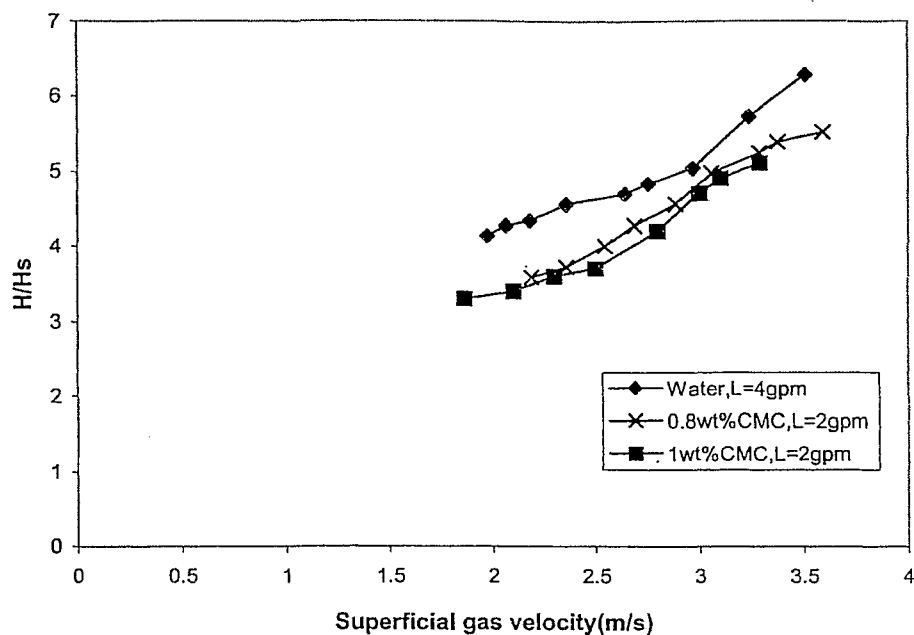
Figure A-91  Effect of superficial gas velocity on relative expanded bed
height at Hs/D=0.25 dp=38mm
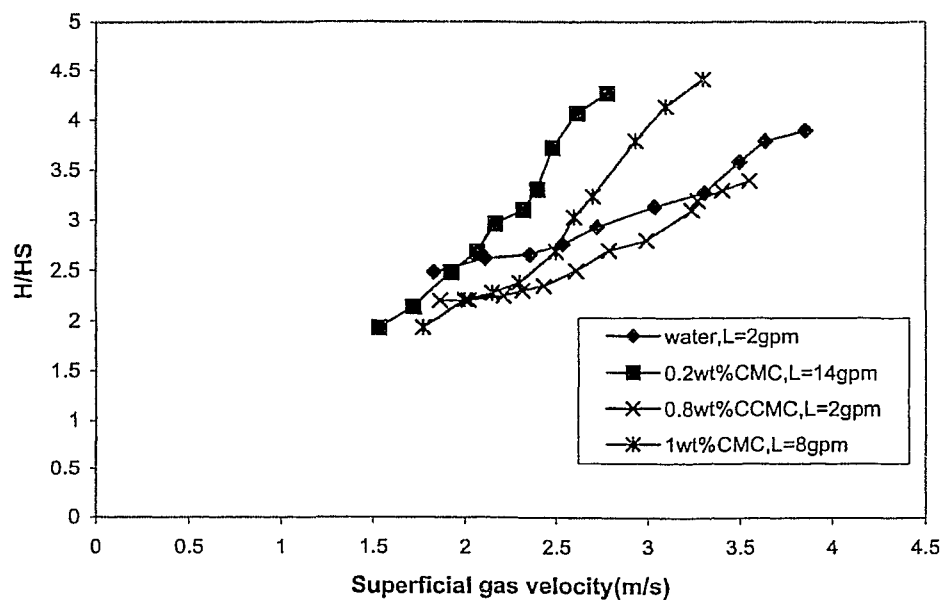


Figure A-92  Effect of superficial gas velocity on relative expanded  bed
height at Hs/D=0.5, dp=38mm

140
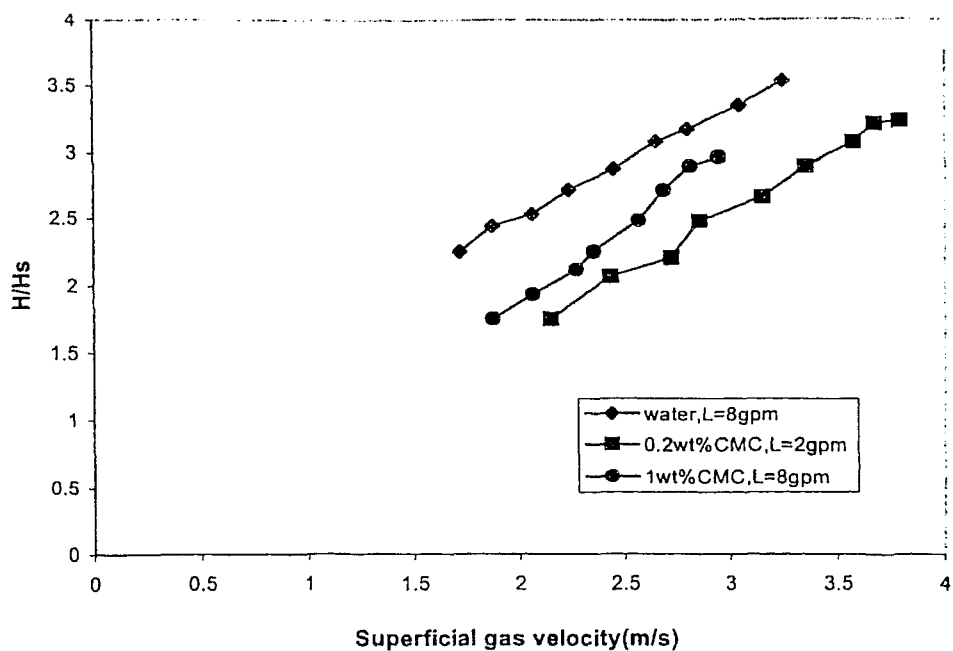
Figure A-93  Effect of superficial gas velocity on relative expanded bed
height at Hs/D=0.75,dp=38mm
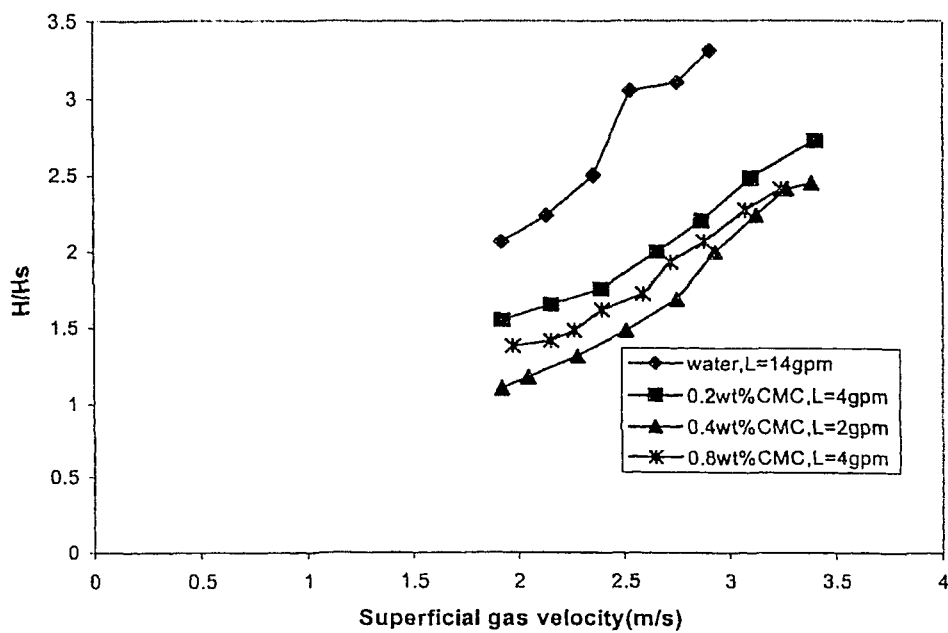


Figure A-94  Effect of superficial gas velocity on relative expanded bed
height at Hs/D=1,dp=38mm

141
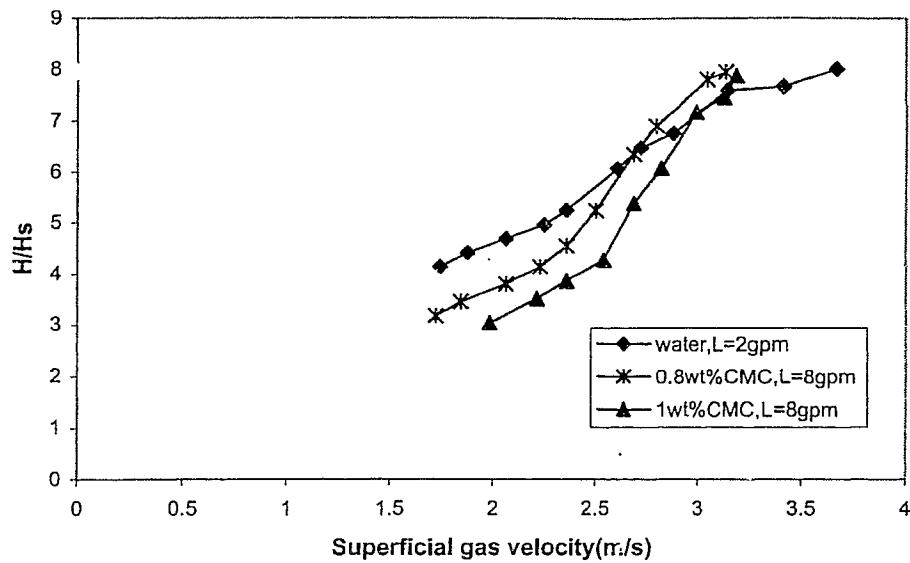
Figure A-95  Effect of superficial gas velocity on relative expanded bed
height at dp=20mm,Hs/D=0.25
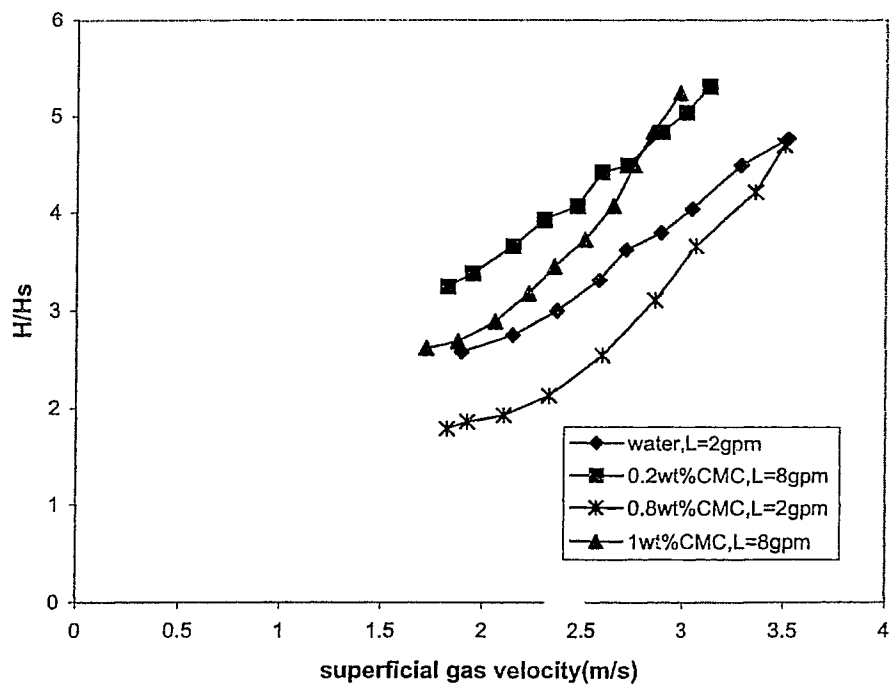


Figure A-96  ffect of superficial gas velocity on relative expanded bed
height at Hs/D=0.5,dp=20mm

142
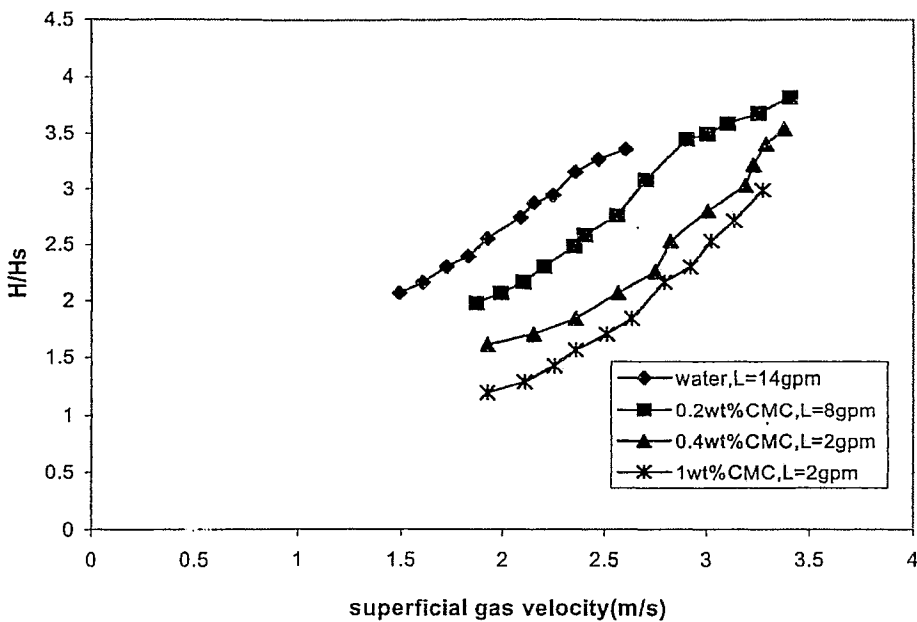
Figure A-97  Effect of superficial gas velocity on relative expanded bed
height at Hs/D=0.75,dp=20mm
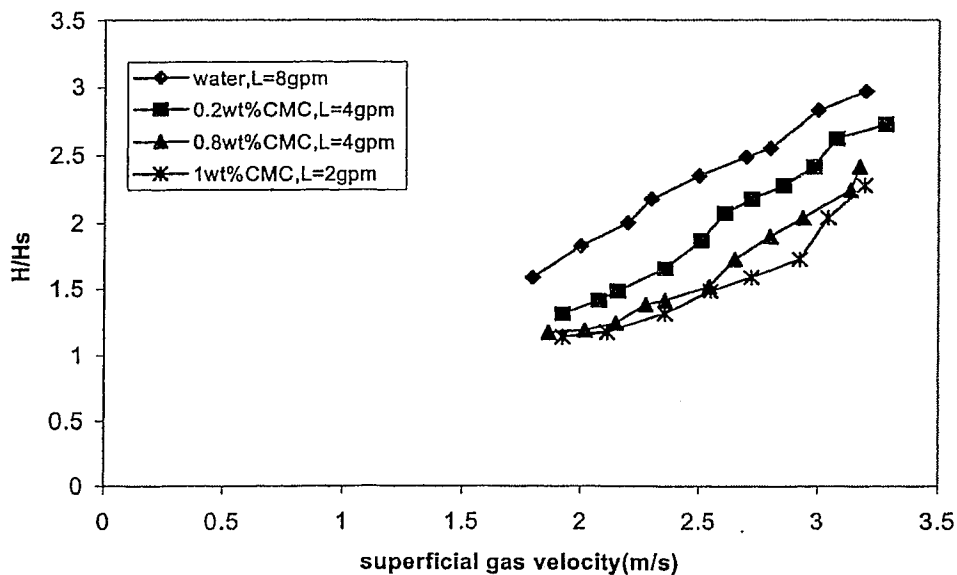


Figure A-98  Effect of superficial gas velocity on relative expanded bed
height at Hs/D=1,dp=20mm

143
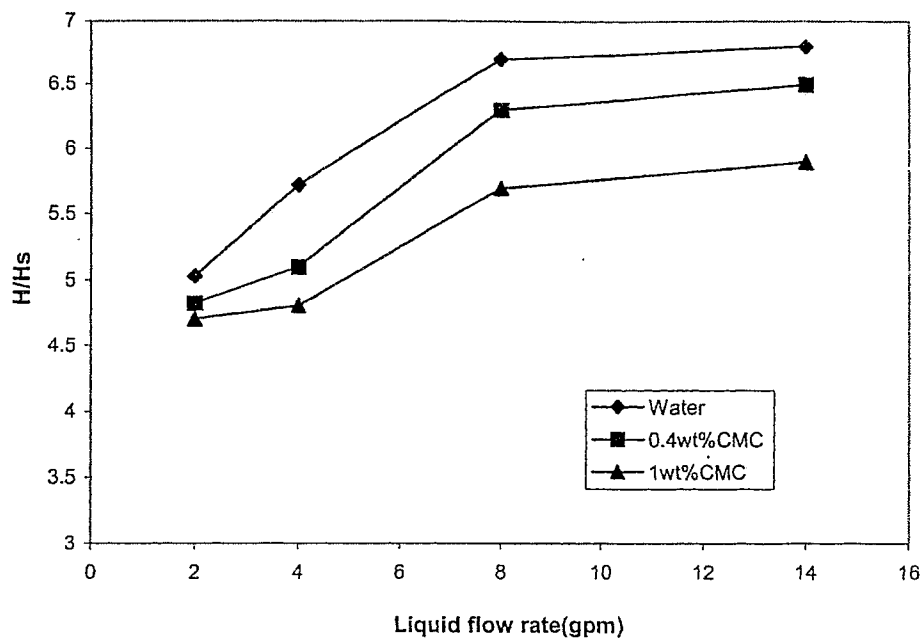
Figure A-99  Effect of liquid flow rate on relative expanded bed
height at Hs/D=0.25 dp=38mm
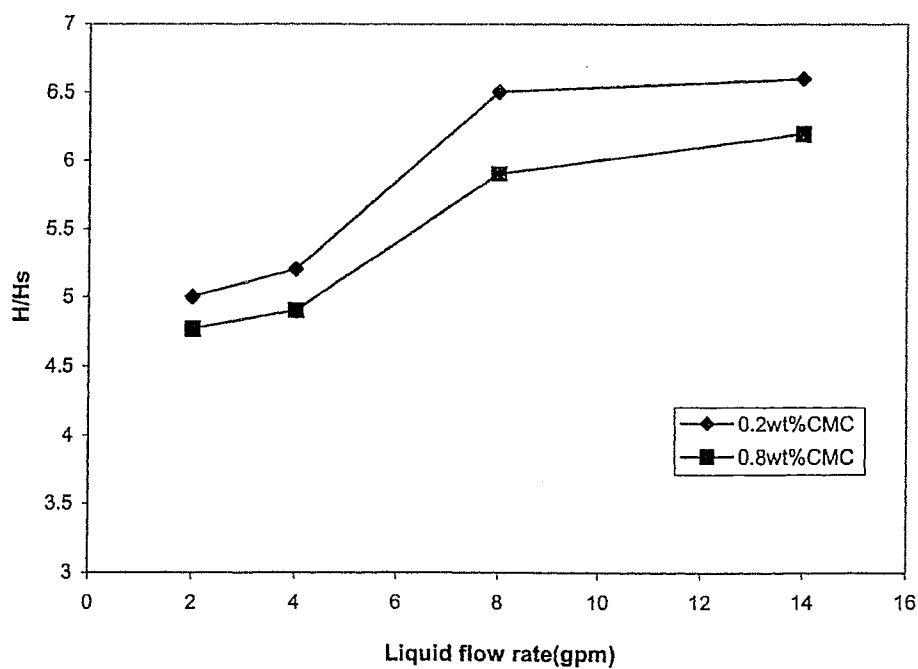


Figure A-100  Effect of liquid flow rate on relative expanded bed
height at Hs/D=0.25 dp=38mm

144
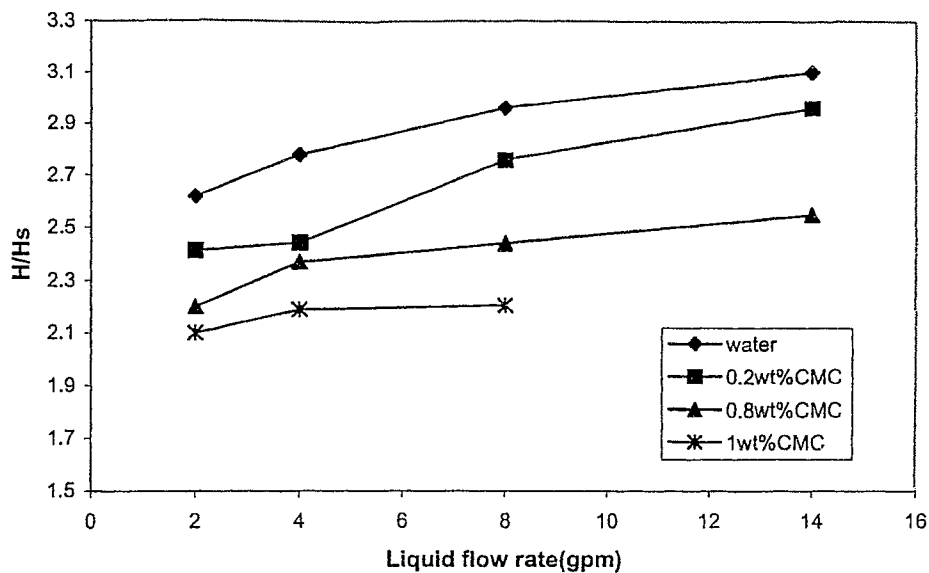
Figure A-101  Effect of liquid flow rate on relative expanded
bed height at Hs/D=0.5, dp=38mm
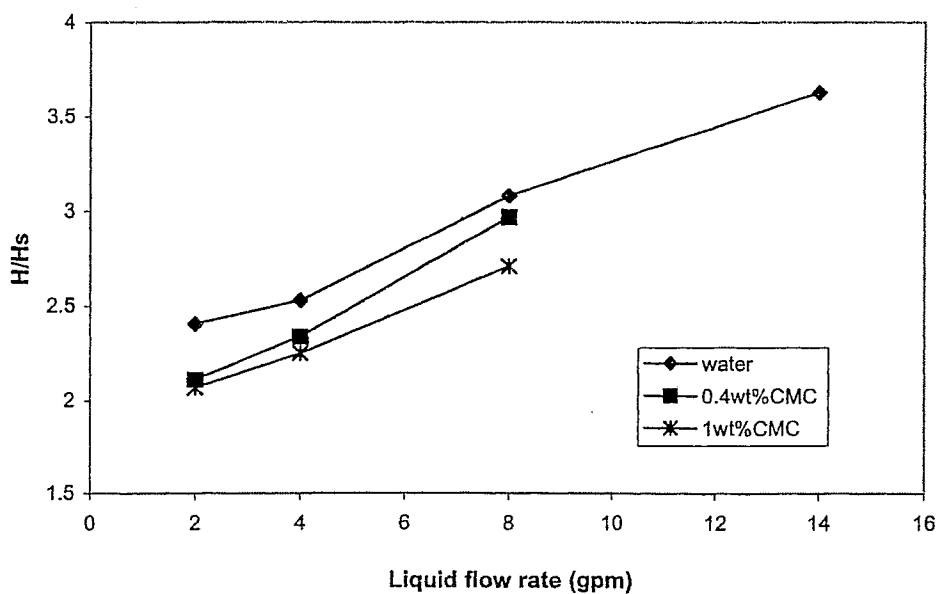


Figure A-102  Effect of liquid flow rate on relative expanded
bed height at Hs/D=0.75,dp=38mm

145
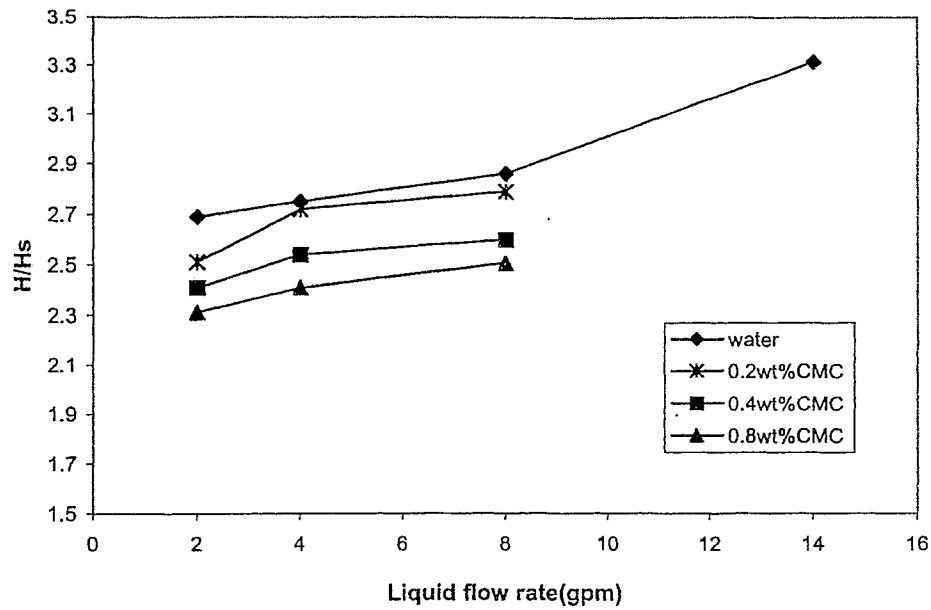
Figure A-103  Effect of liquid flow rate on relative expanded bed
height  at Hs/D=1,dp=38mm
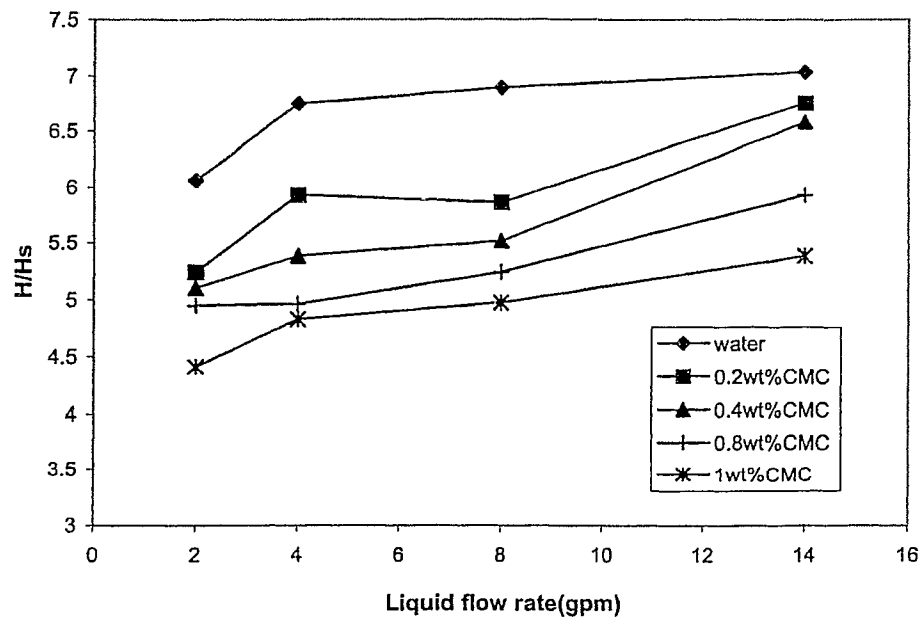


Figure A-104  Effect of liquid flow rate on relative expanded
bed height at dp=20mm,Hs/D=0.25

146
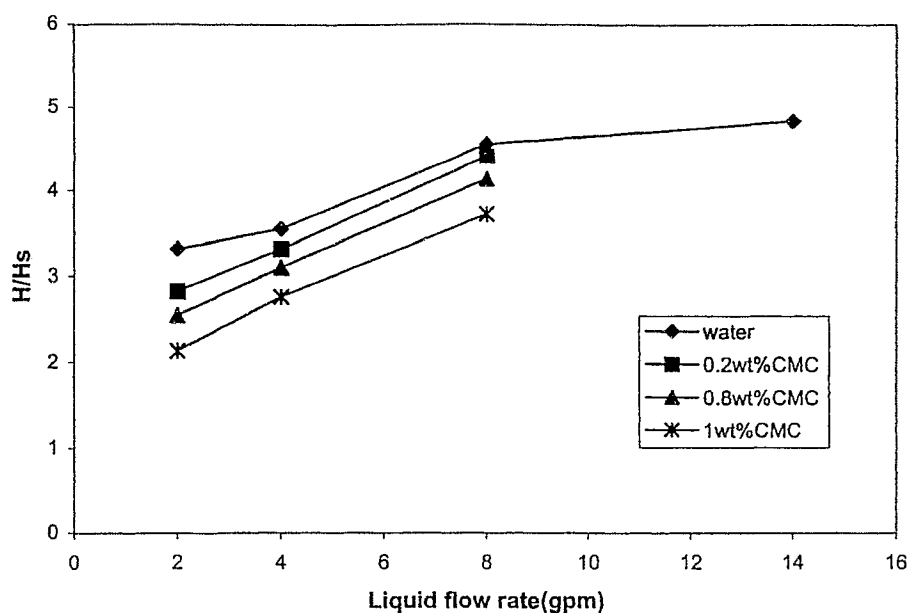
Figure A-105  Effect of liquid flow rate on relative expanded
bed height at Hs/D=0.5,dp=20mm
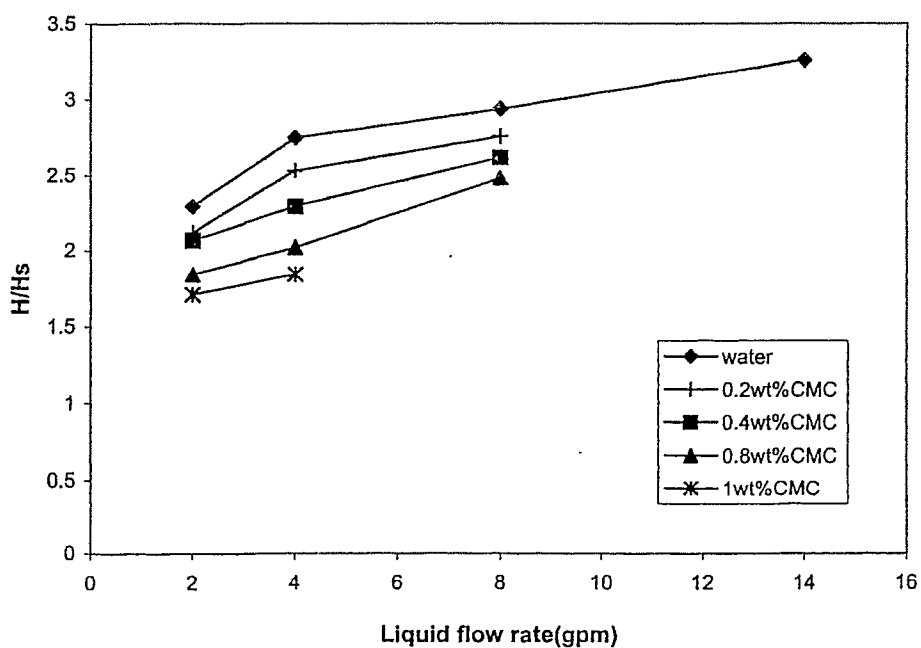


Figure A-106  Effect of liquid flow rate on relative expanded
bed height at Hs/D=0.75,dp=20mm

147
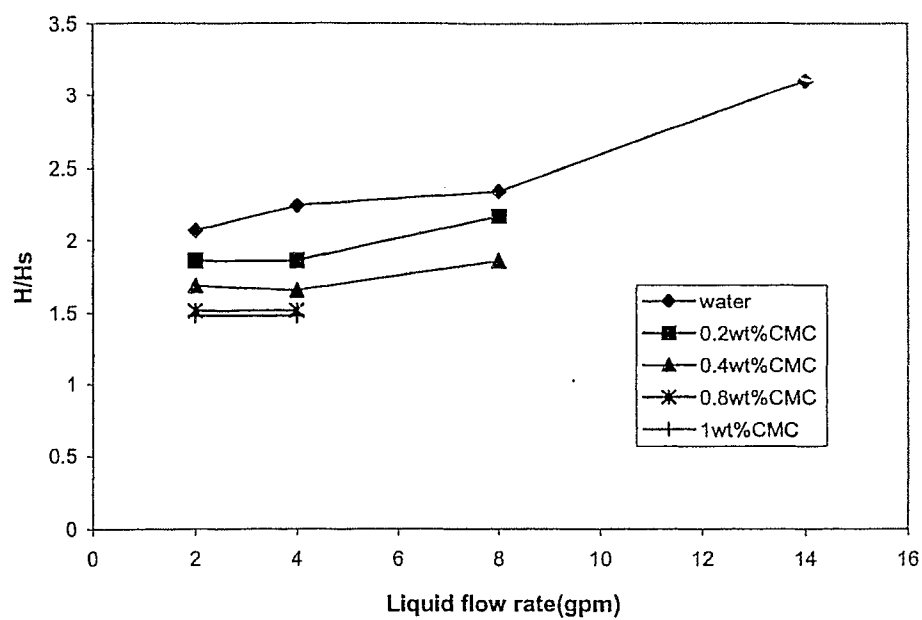
Figure A-107  Effect of liquid flow rate on relative expanded
bed height at Hs/D=1,dp=20mm

148
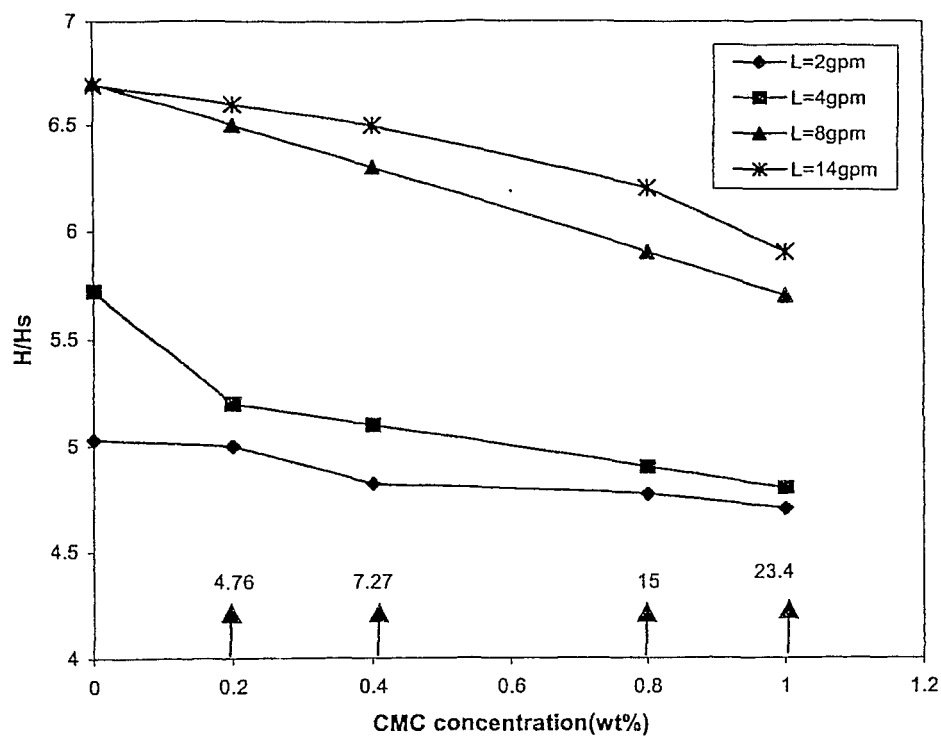
Figure A-108  Effect of CMC concentration on H/Hs at
Hs/D=0.25, dp=38mm, ( ↑ viscosity,cP,10 s⁻¹)
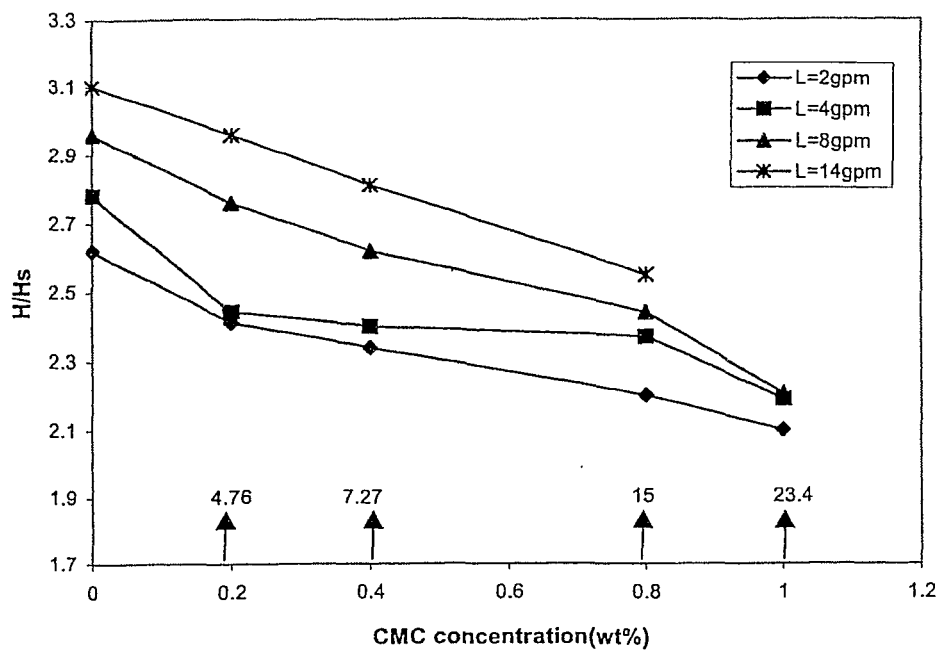


Figure A-109  Effect of CMC concentration on H/Hs at
Hs/D=0.5,dp=38mm, ( ↑ viscosity,cP,at 10 s⁻¹)

149
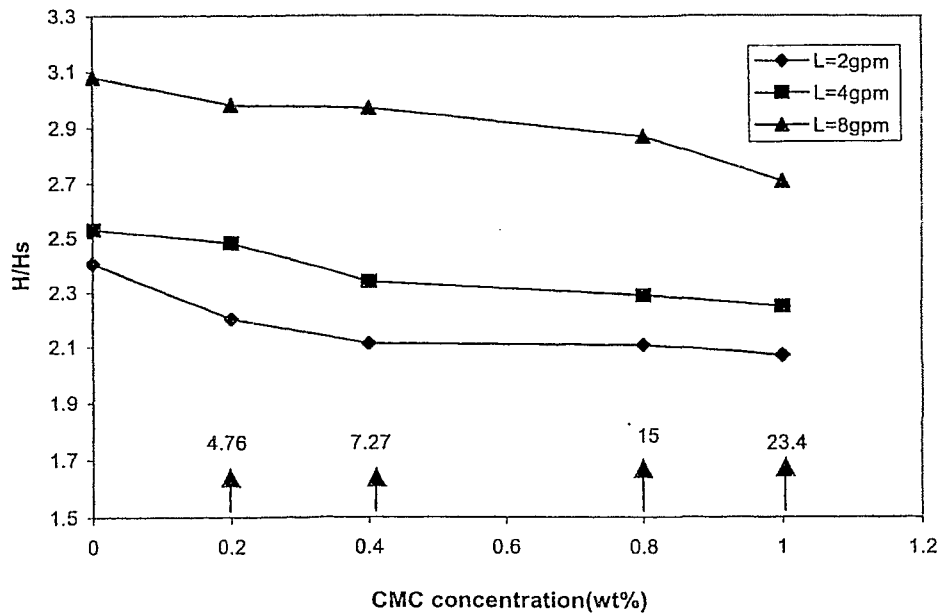
Figure A-110  Effect of CMC concentration on H/Hs at
Hs/D=0.75 dp=38mm, (↑ viscosity,cP,at 10 s$^{-1}$)
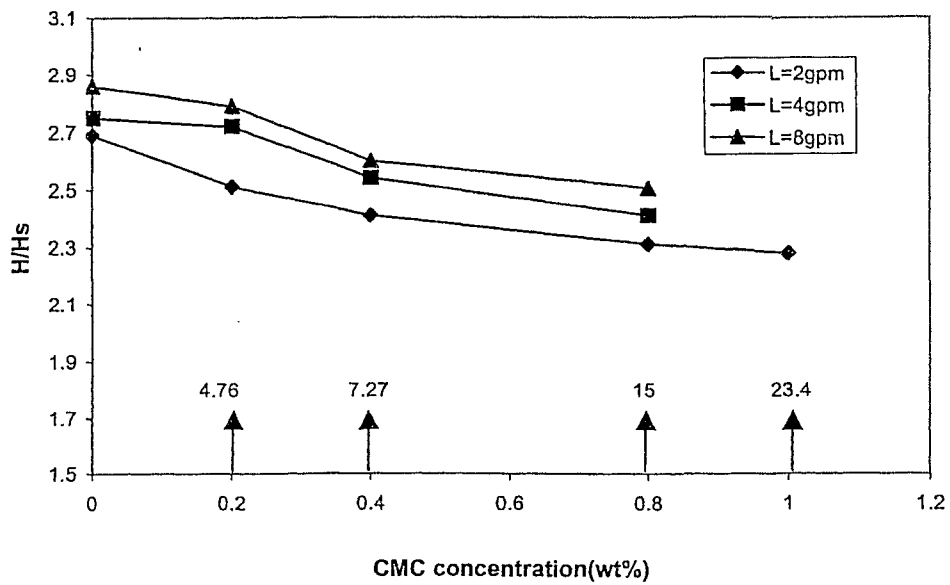


Figure A-111  Effect of CMC concentration on H/Hs at
Hs/D=1,dp=38mm,(↑ viscosity,cP,at 10 s$^{-1}$)

150
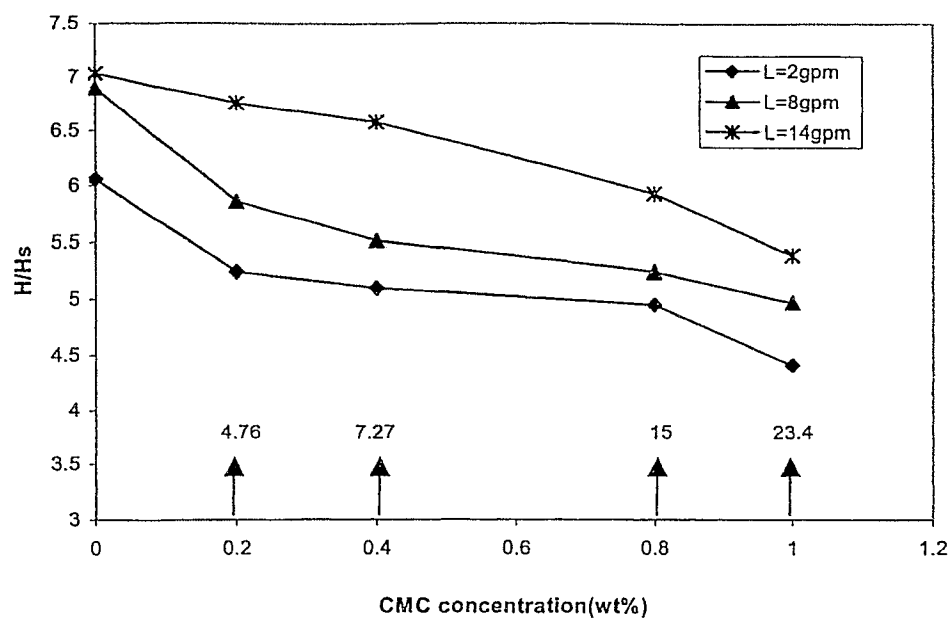
Figure A-112  Effect of CMC concentration on H/Hs at Hs/D=0.25
,dp=20mm (  viscosity,cP, at 10 s$^{-1}$)
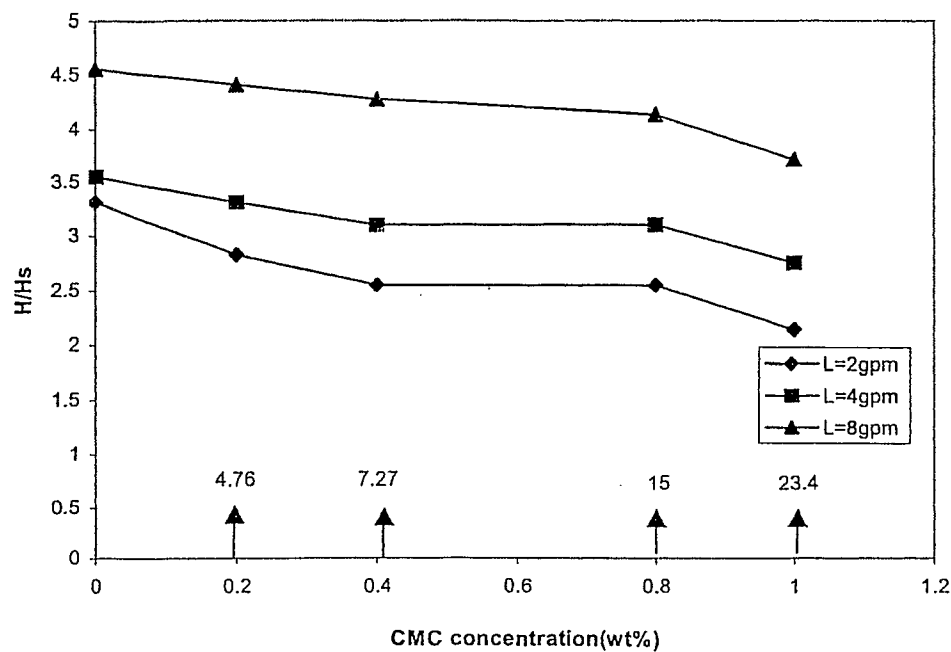


Figure A-113  Effect of CMC concentration on H/Hs at
Hs/D=0.5,dp=20mm,( viscosity,cP,at 10 s$^{-1}$)

151
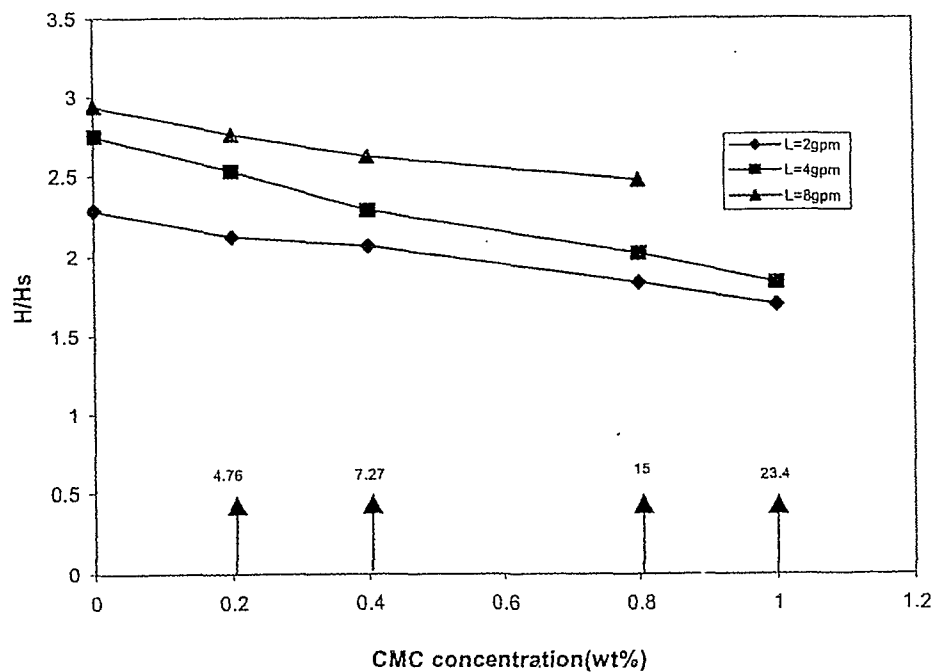
Figure A-114  Effect of CMC concentration on H/Hs at
Hs/D=0.75,dp=20mm,(↑ viscosity,cP,at 10 s$^{-1}$)
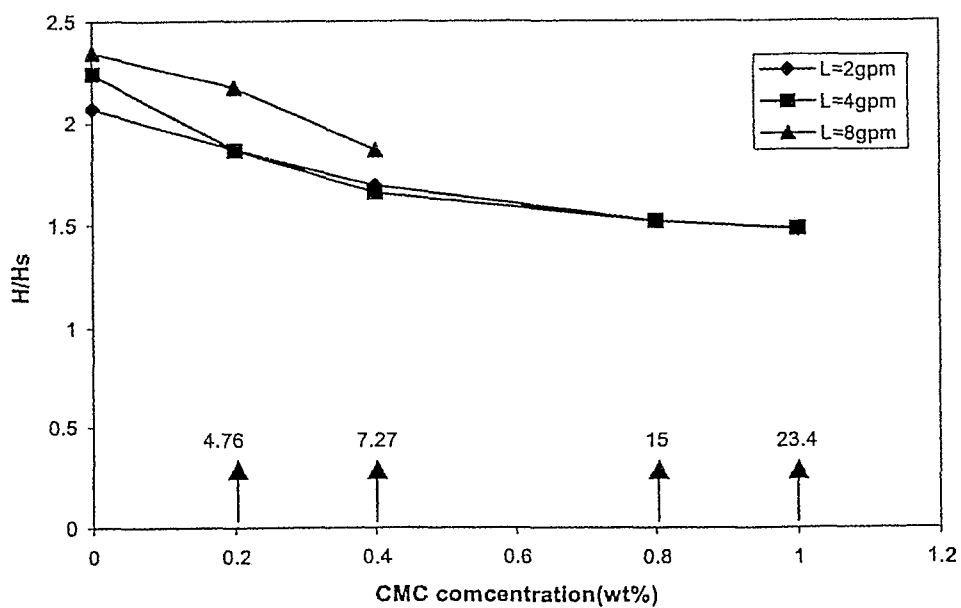


Figure A-115  Effect of CMC concentration on H/Hs at
Hs/D=1,dp=20mm, (↑ viscosity, cP, at 10 s$^{-1}$)

152
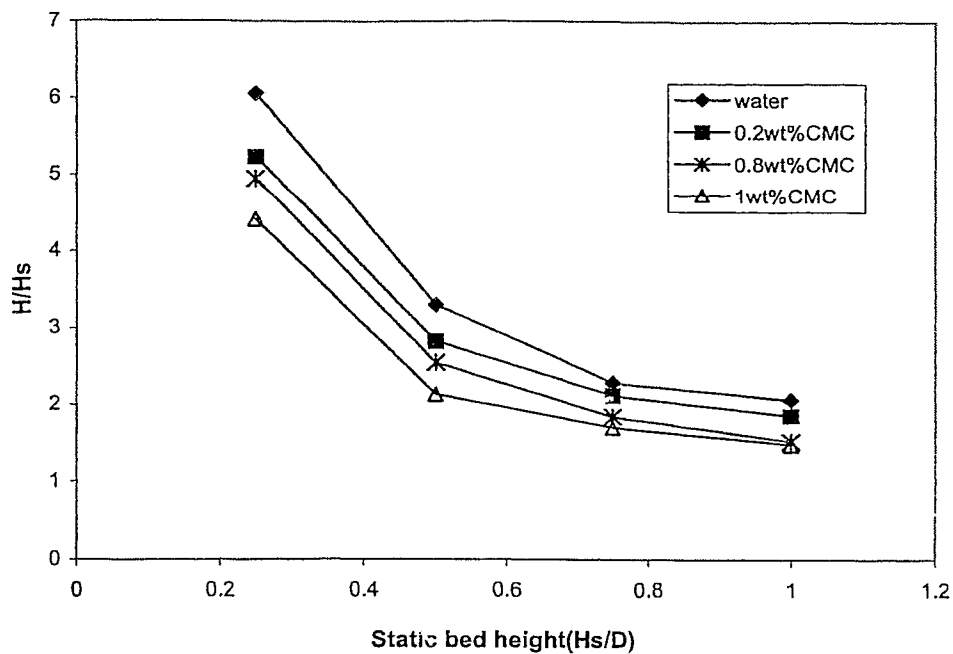
Figure A-116  Effect of static bed height on relative expanded
bed height at dp=20mm, L=2gpm
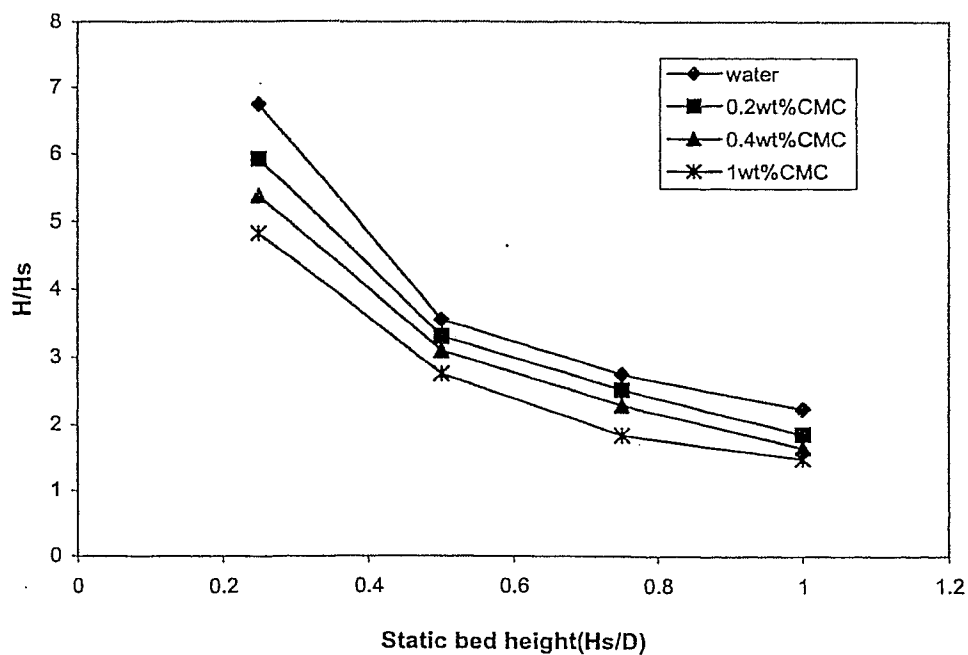


Figure A-117  Effect of static bed height on relative expanded
bed height at dp=20mm, L=4gpm

153
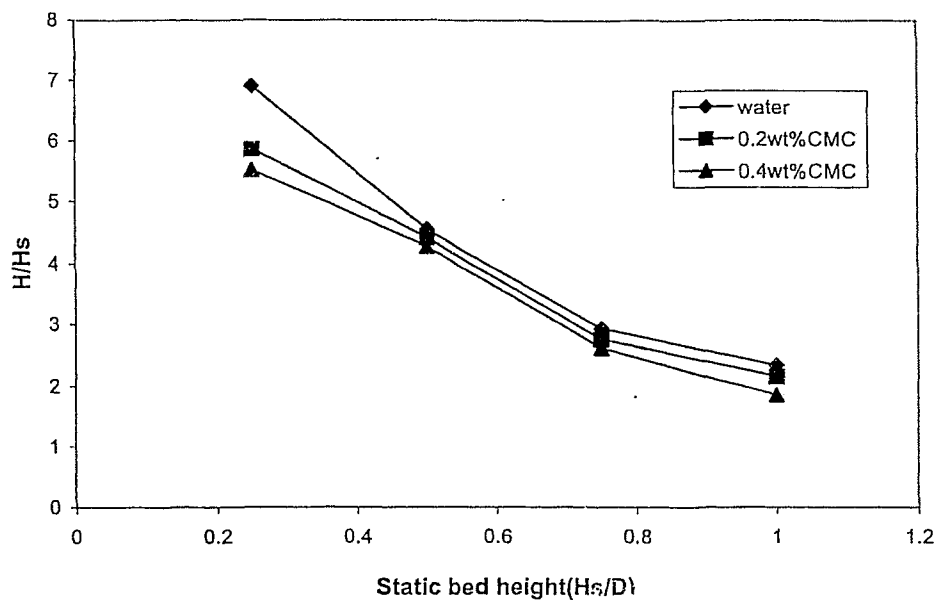
Figure A-118  Effect of static bed height on relative expanded
bed height  at dp=20mm, L=8gpm
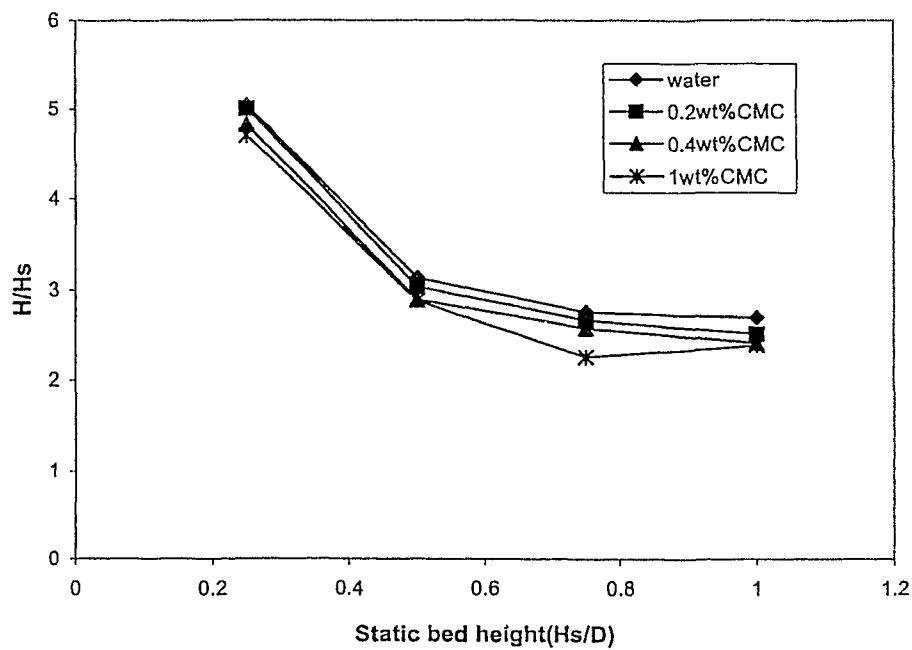


Figure A-119  Effect of static bed height on relative expanded
bed height at dp=38mm,L=2gpm

154
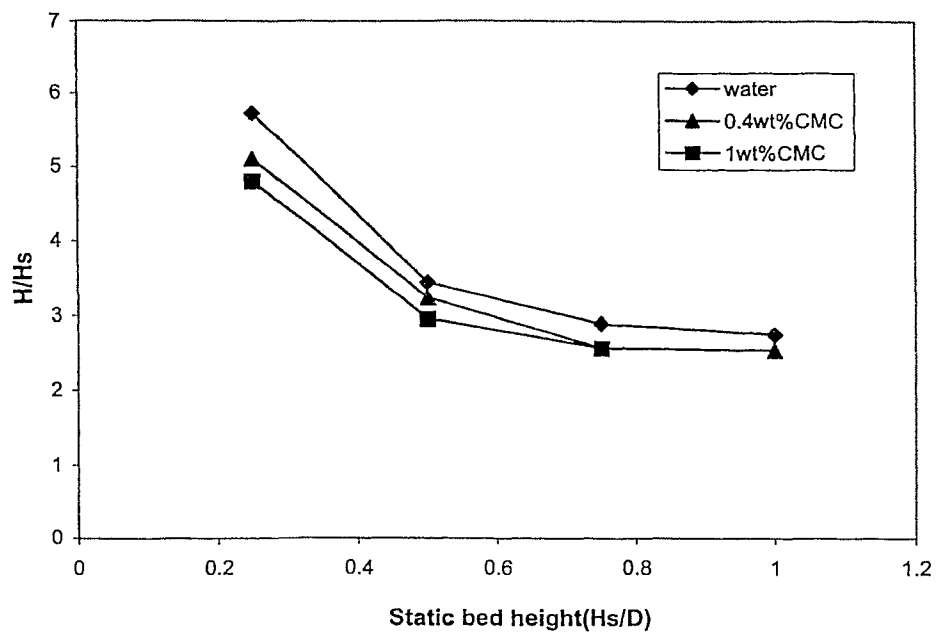
Figure A-120  Effect of static bed height on relative expanded bed height at dp=38mm,L=4gpm
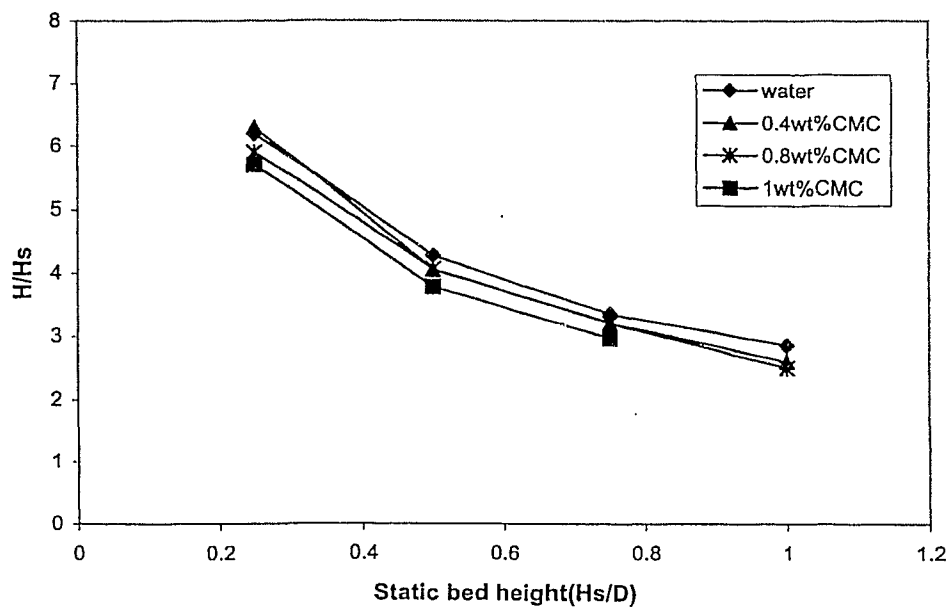


Figure A-121  Effect of static bed heoght on relative expanded bed height at dp=38mm,L=8gpm

155
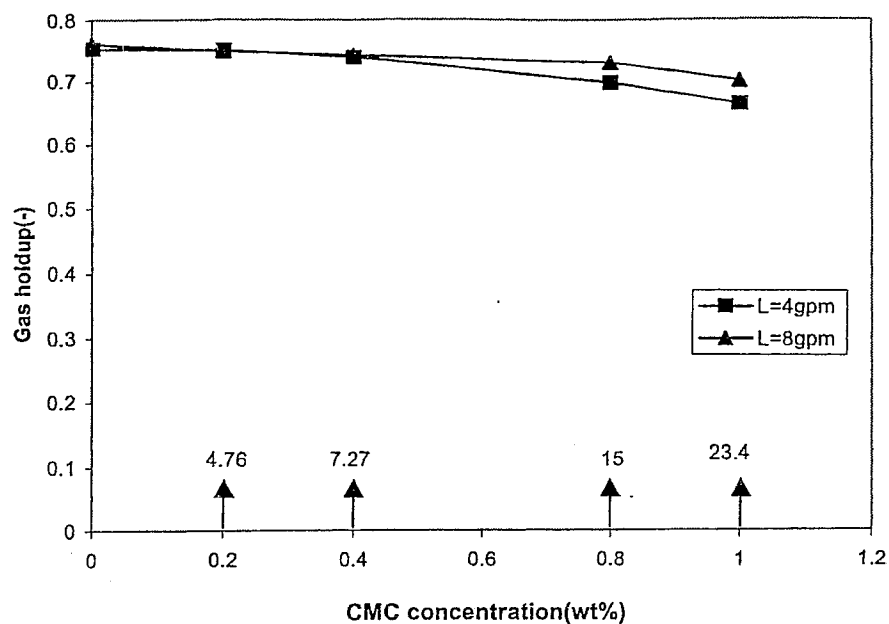
Figure A-122 Effect of CMC concentration on gas holdup at
Hs/D=0.25, dp=38mm, (↑ viscosity,cP,10 s$^{-1}$)
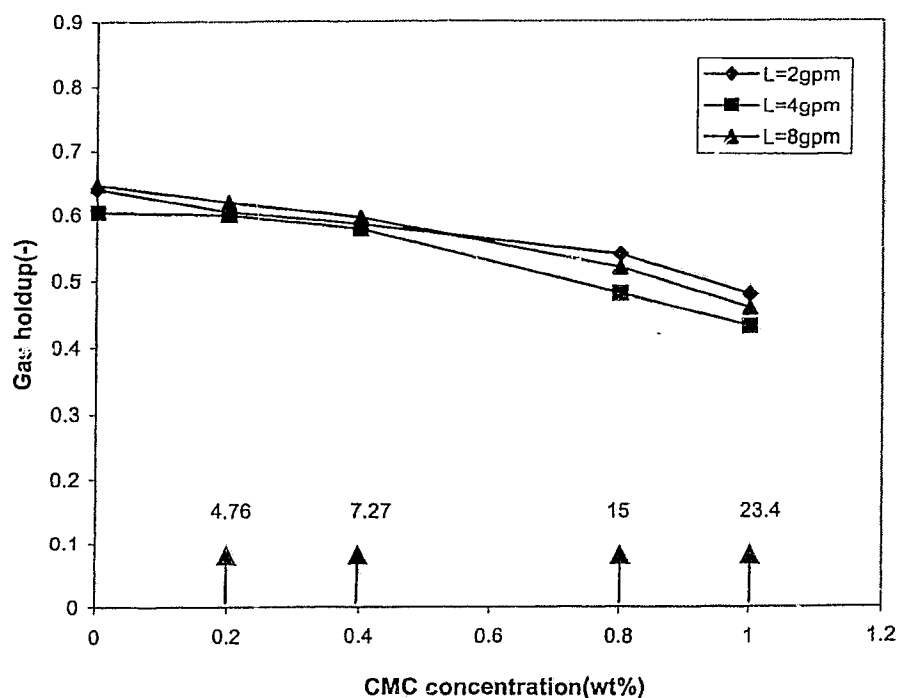


Figure A-123 Effect of CMC concentration on gas holdup at
Hs/D=0.5,dp=38mm, (↑ viscosity,cP,at 10 s$^{-1}$)

156
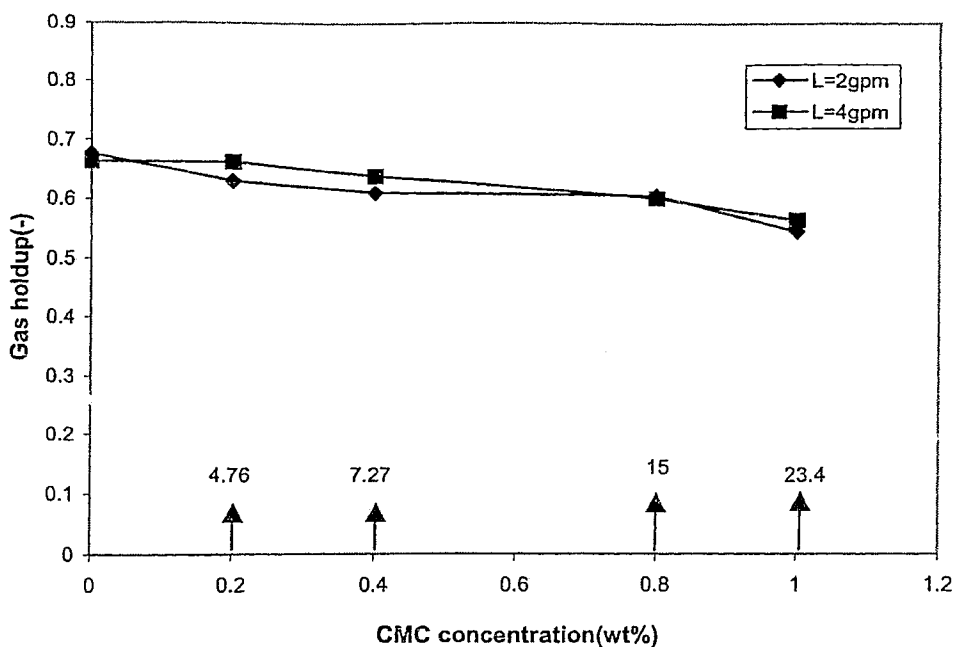
Figure A-124  Effect of CMC concentration on gas holdup at
Hs/D=0.75,dp=38mm,(▲ viscosity,cP,at 10 s$^{-1}$)
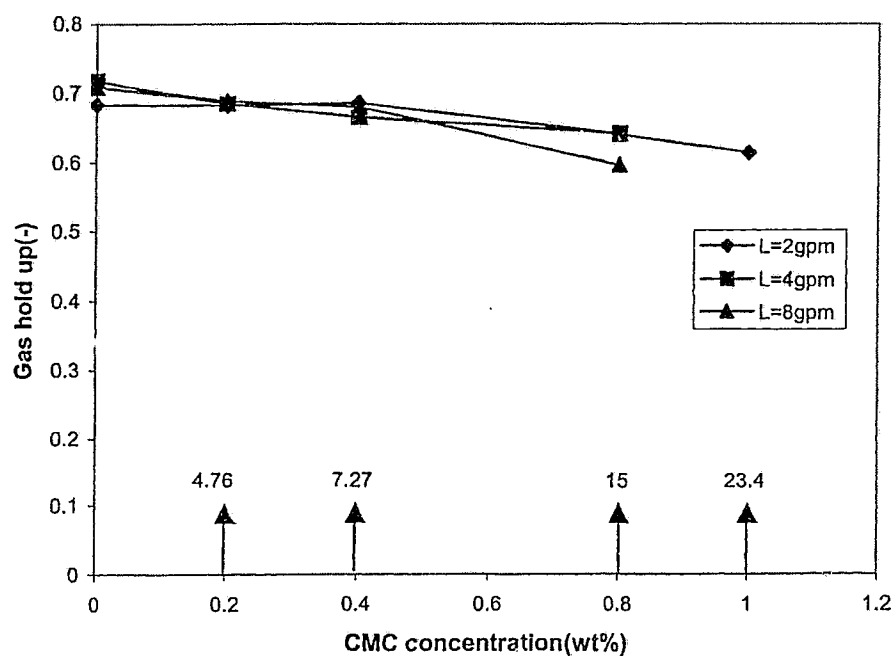


Figure A-125  Effect of CMC concentration on gas hold up at
Hs/D=1,dp=38mm, (▲ viscosity,cP,at 10 s$^{-1}$)

157
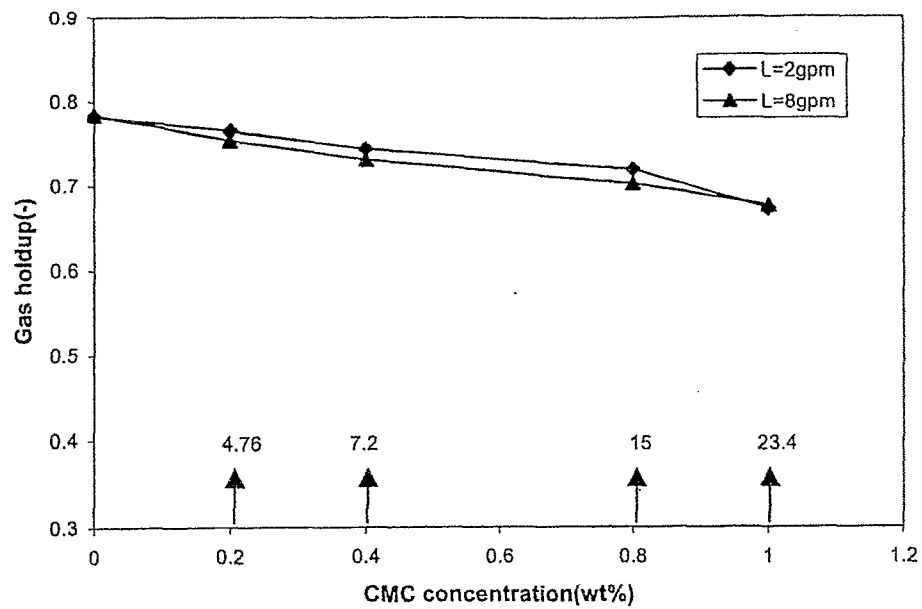
Figure A-126  Effect of CMC concentration on gas holdup at dp=20mm.Hs/D=0.25, (↑ viscosity,cP, at 10 s$^{-1}$)
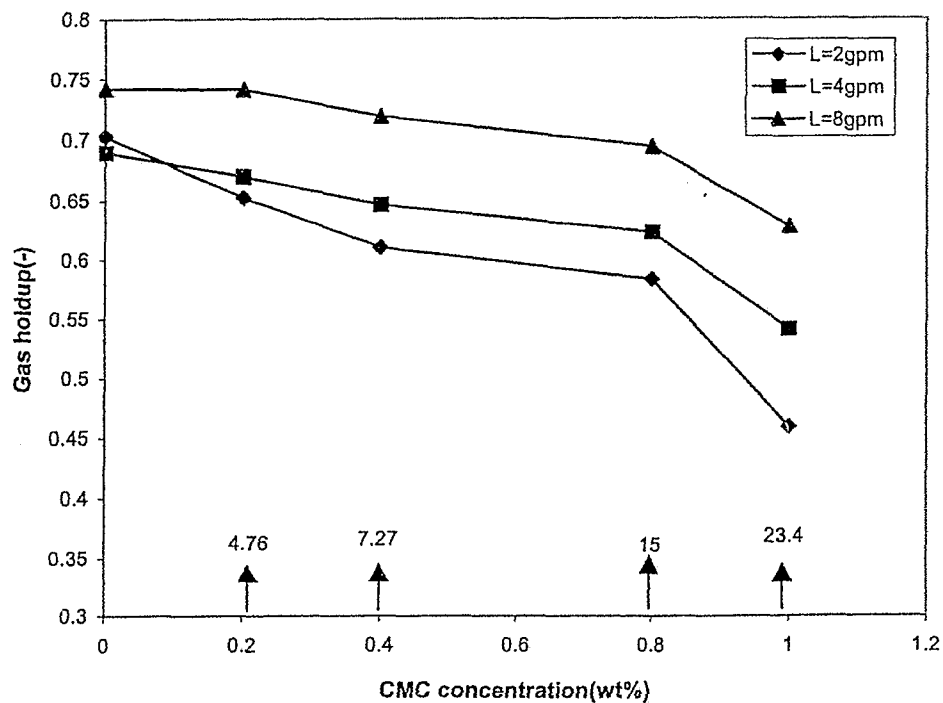


Figure A-127  Effect of CMC concentration on gas holdup at Hs/D=0.5,dp=20mm,(↑ viscosity,cP,at 10 s$^{-1}$)

158
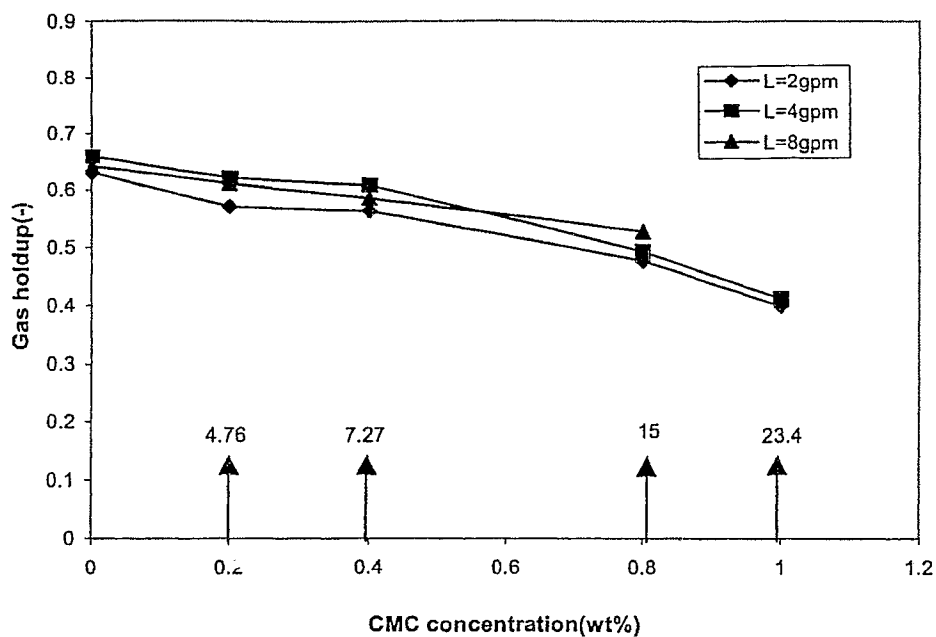
Figure A-128  Effect of CMC concentration on gas holdup at
Hs/D=0.75,dp=20mm,(↑ viscosity,cP,at 10 s⁻¹)
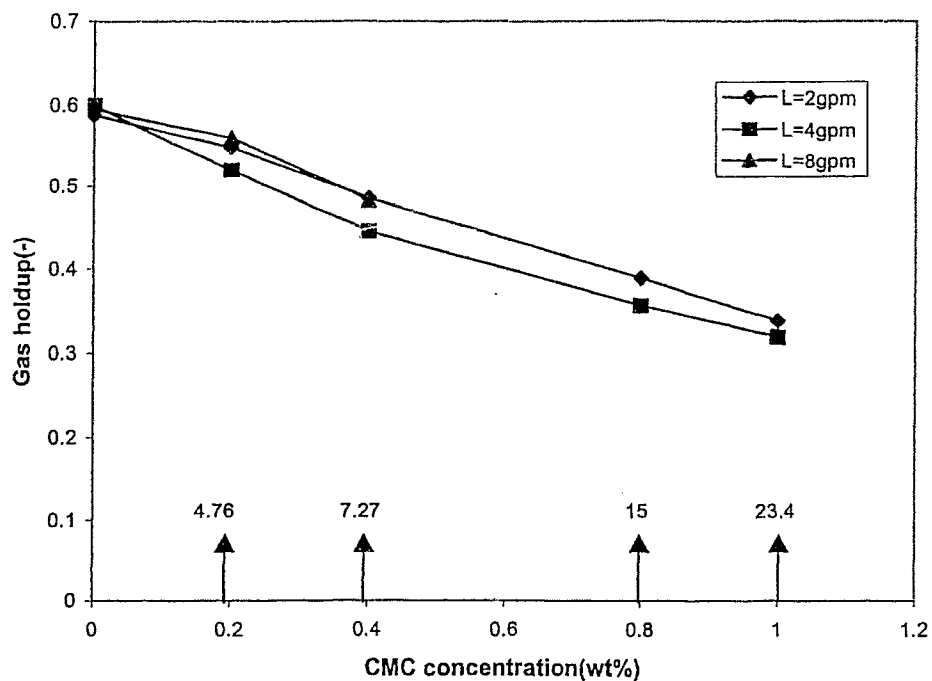


Figure A-129  Effect of CMC concentration on gas holdup at
Hs/D=1,dp=20mm,(↑ viscosity,cP,at 10 s⁻¹)

159
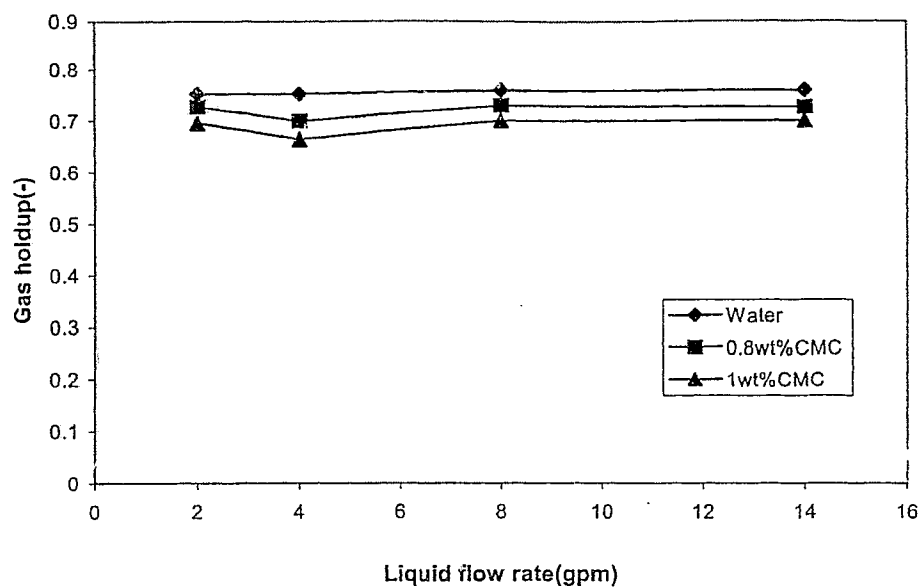
Figure A-130  Effect of liquid flow rate on gas holdup at
Hs/D=0.25 dp=38mm
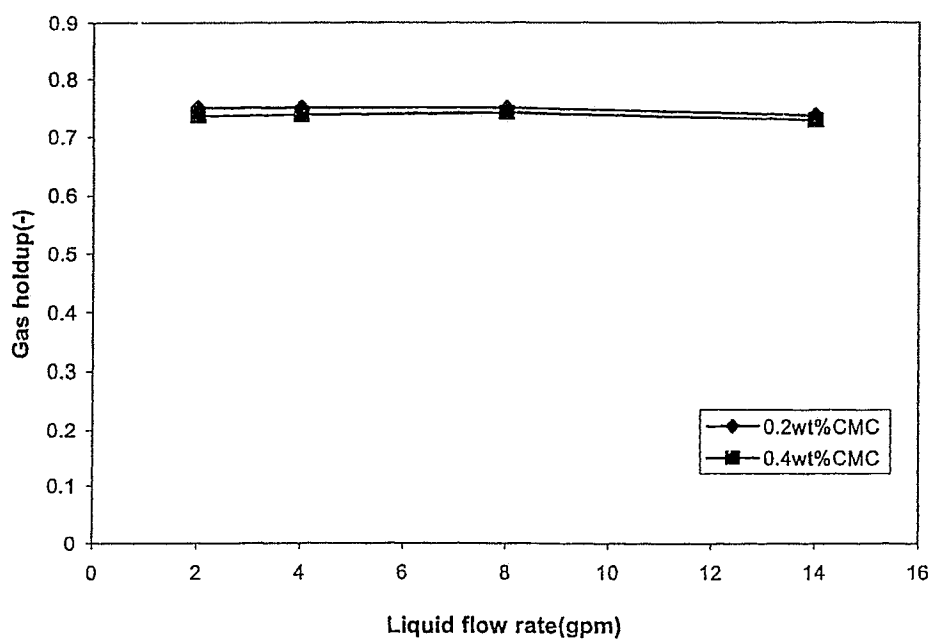


Figure A-131  Effect of liquid flow rate on gas holdup at
Hs/D=0.25 dp=38mm

160
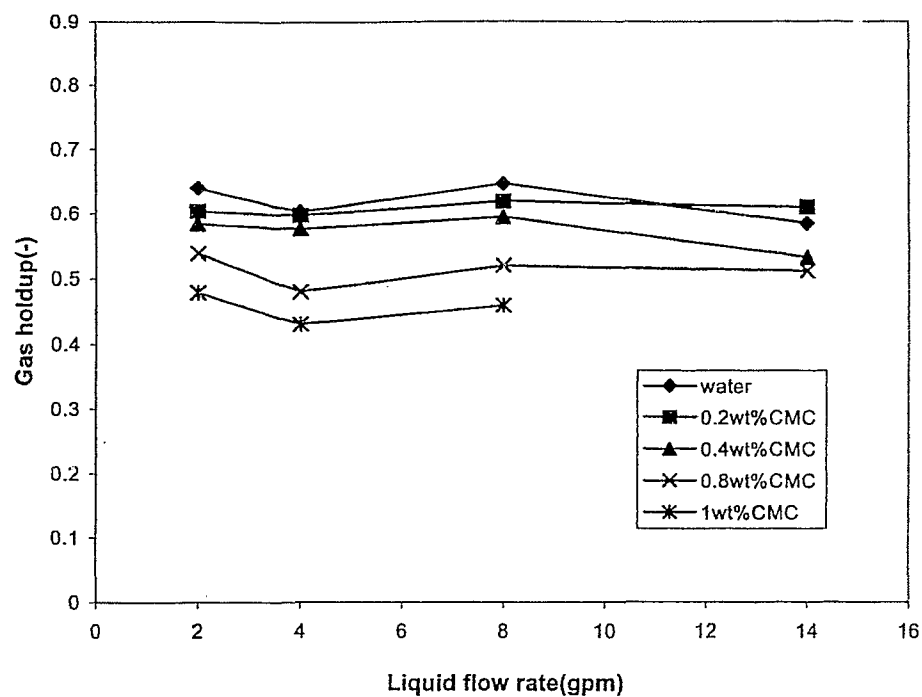
Figure A-132  Effect of liquid flow rate on gas holdup at
Hs/D=0.5 ,dp=38mm
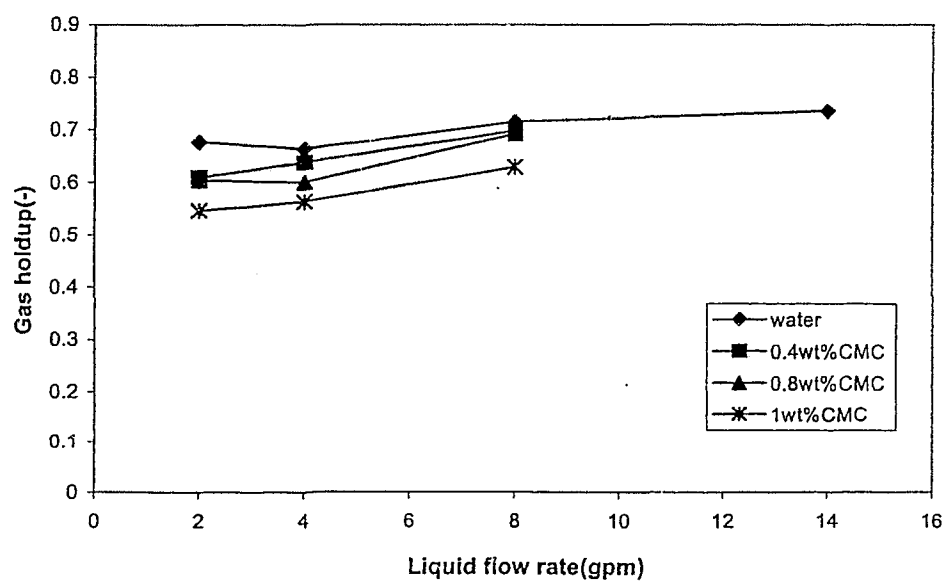


Figure A-133  Effect of liquid flow rate on gas holdup at
Hs/D=0.75, dp=38mm

161
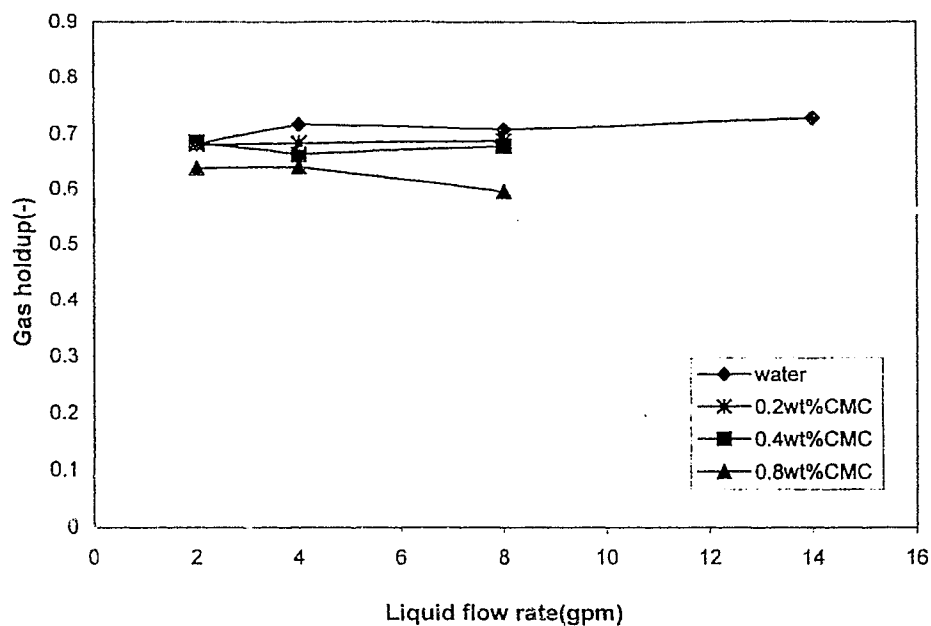
Figure A-134  Effect of liquid flow rate on gas holdup at
Hs/D=1,dp=38mm
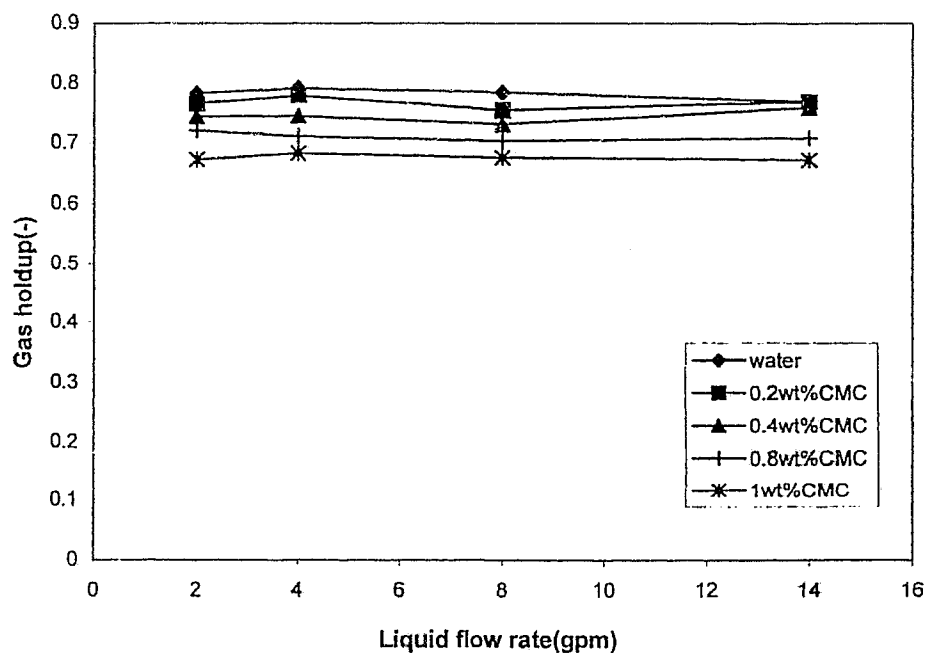


Figure A-135  Effect of liquid flow rate on gas holdup at
dp=20mm,Hs/D=0.25

162
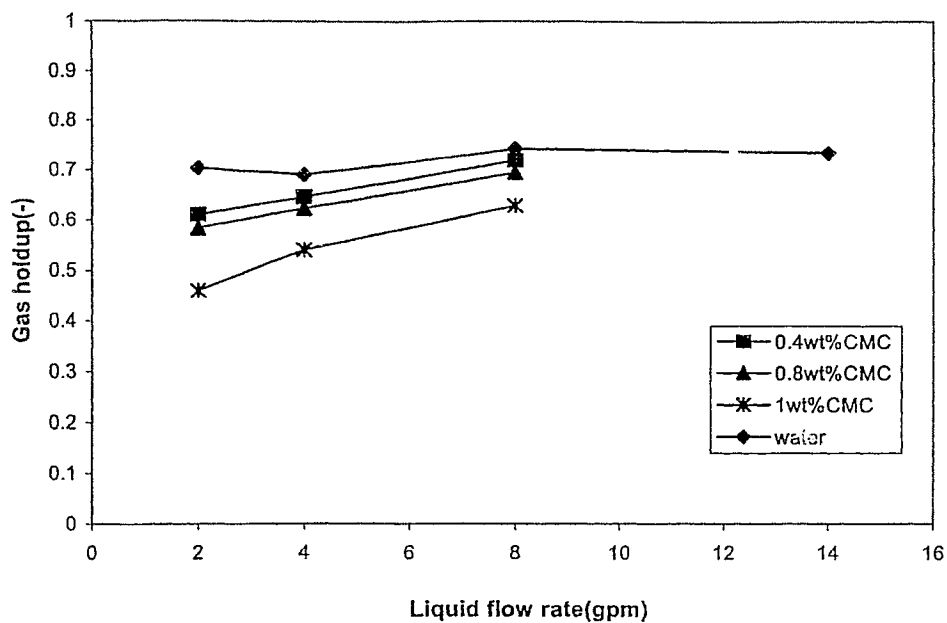
Figure A-136  Effect of liquid flow rate on gas holdup at
Hs/D=0.5,dp=20mm
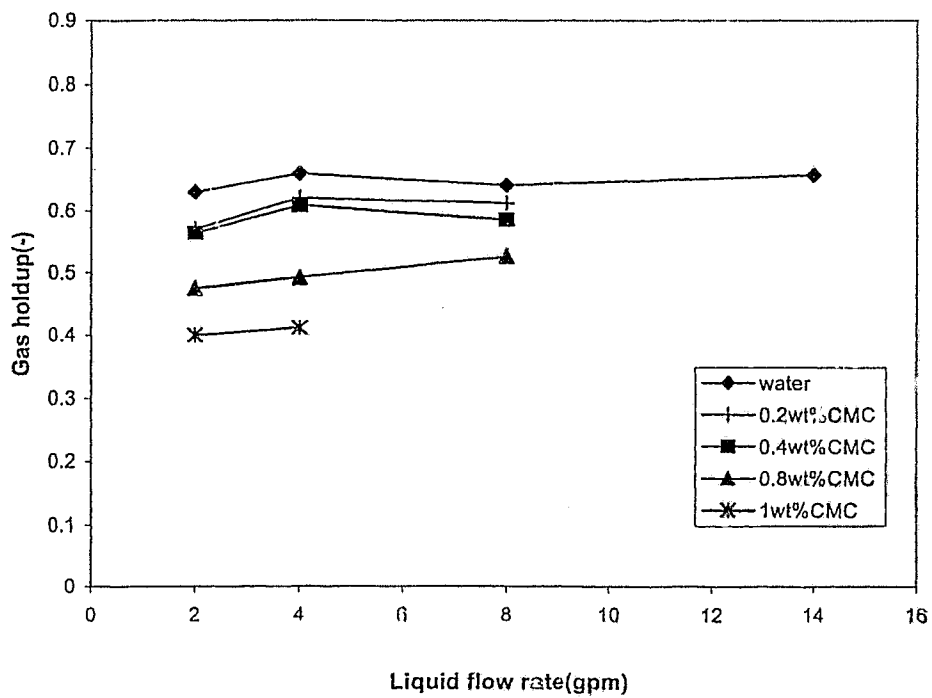


Figure A-137  Effect of liquid flow rate on gas holdup at
Hs/D=0.75,dp=20mm

163
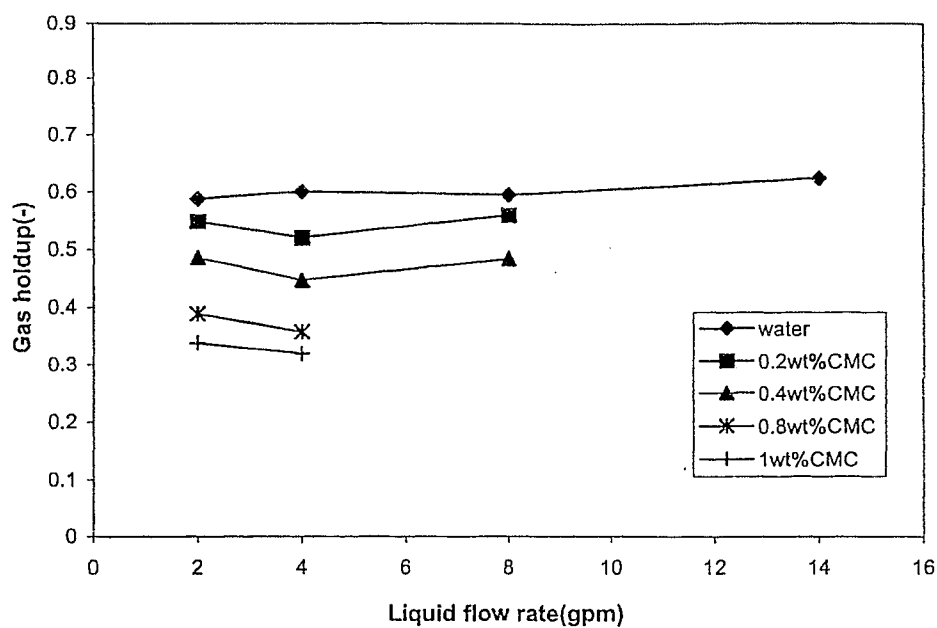
Figure A-138  Effect of liquid flow rate on gas holdup at
Hs/D=1,dp=20mm

164
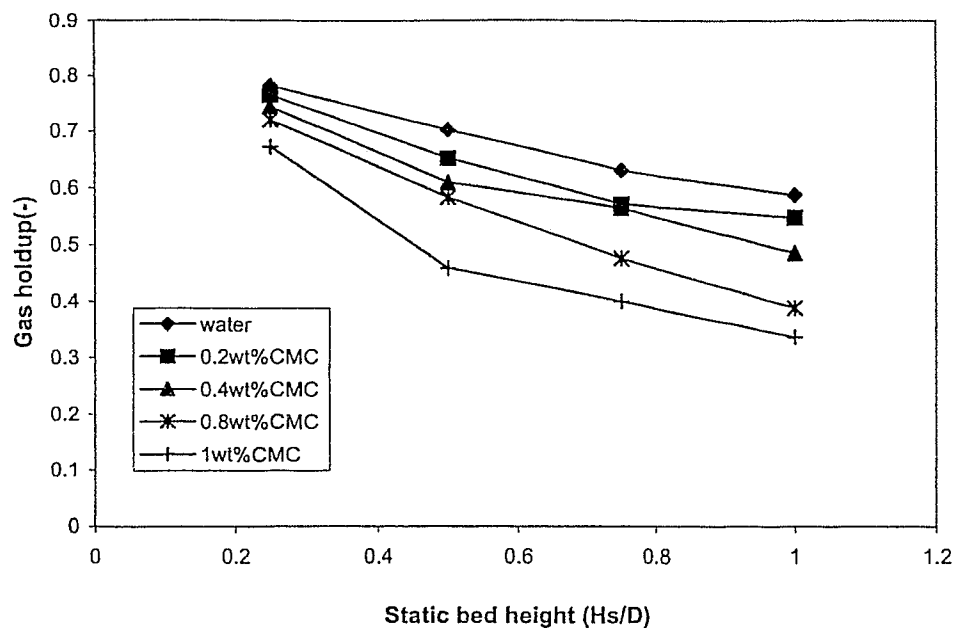
Figure A-139   Effect of static bed height on gas holdup at
dp=20mm,L=2gpm
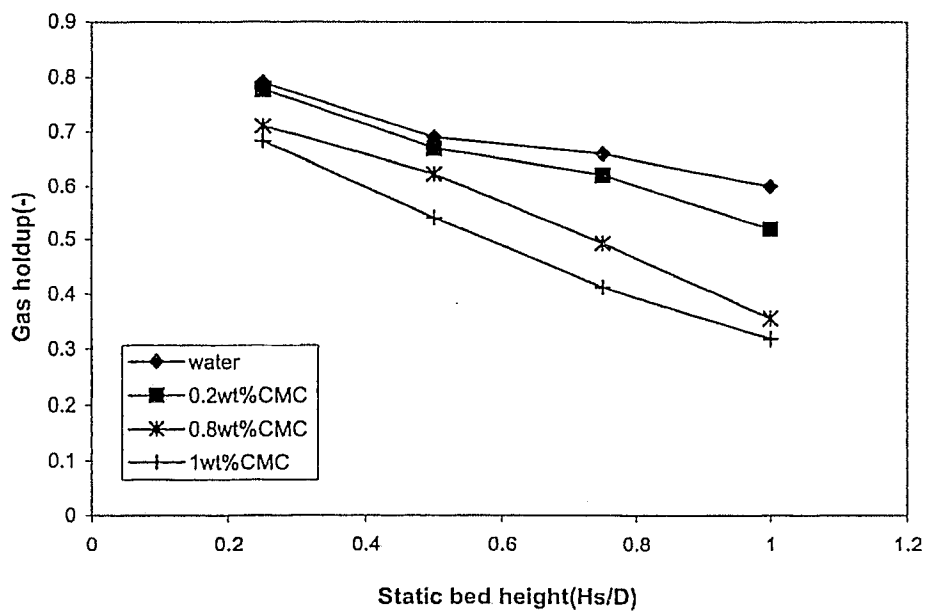


Figure A-140   Effect of static bed height on gas holdup at
dp=20mm,L=4gpm
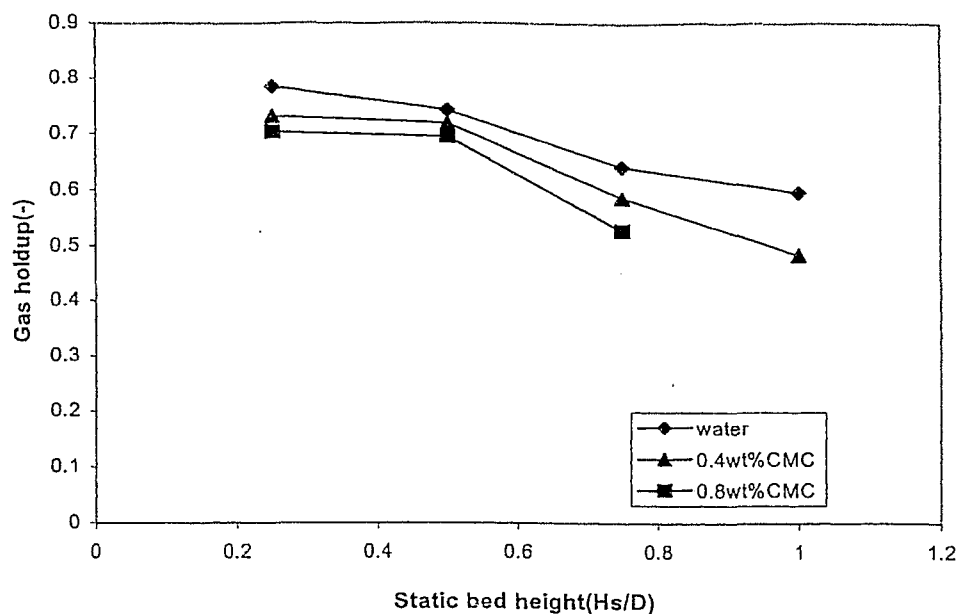
Figure A-141  Effect of static bed height on gas holdup at
dp=20mm,L=8gpm
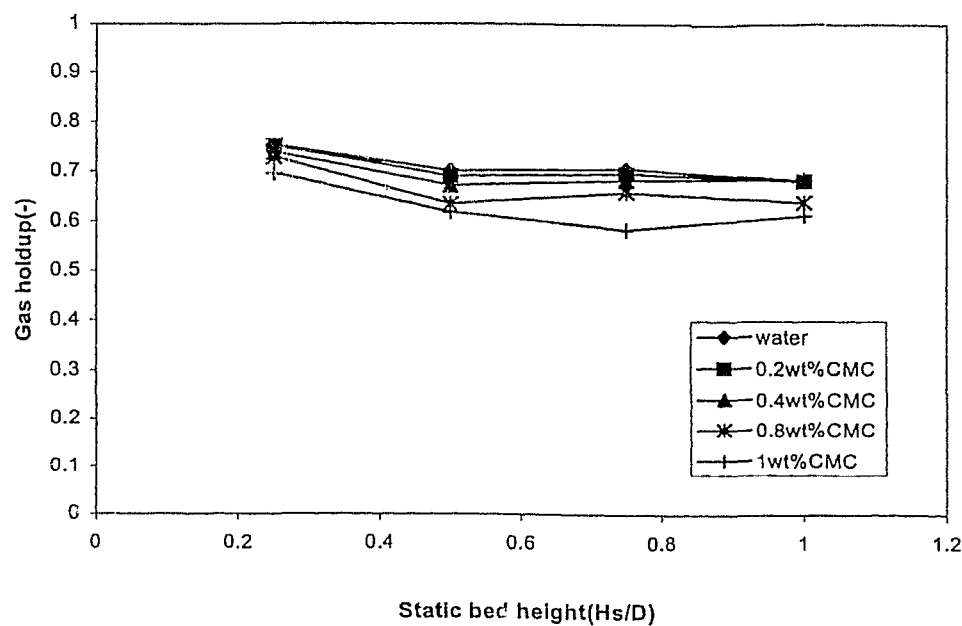


Figure A-142  Effect of static bed height on gas holdup at
dp=38mm,L=2gpm

166
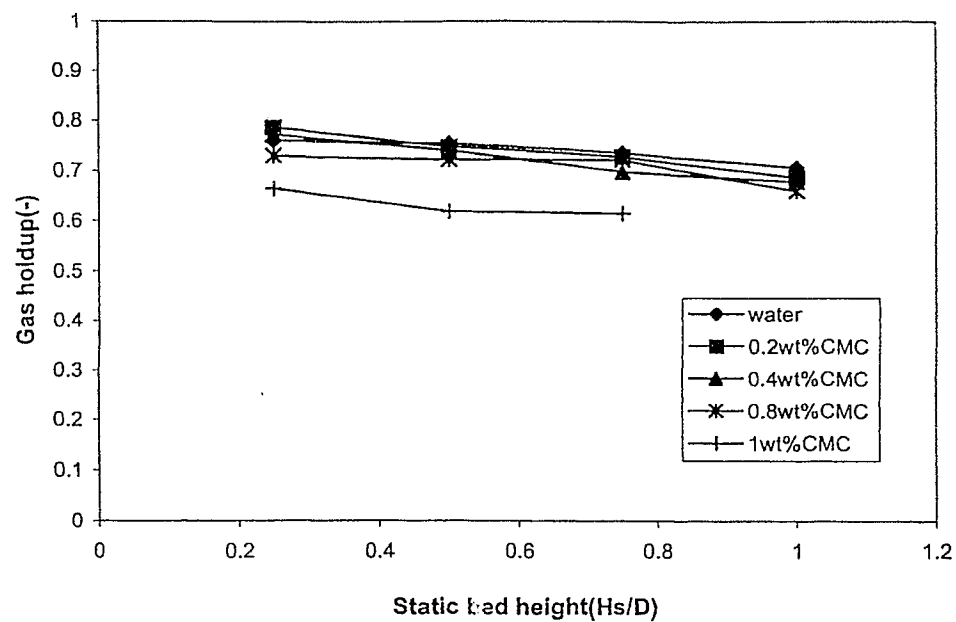
Figure A-143  Effect of static bed height on gas holdup at
dp=38mm,L=4gpm
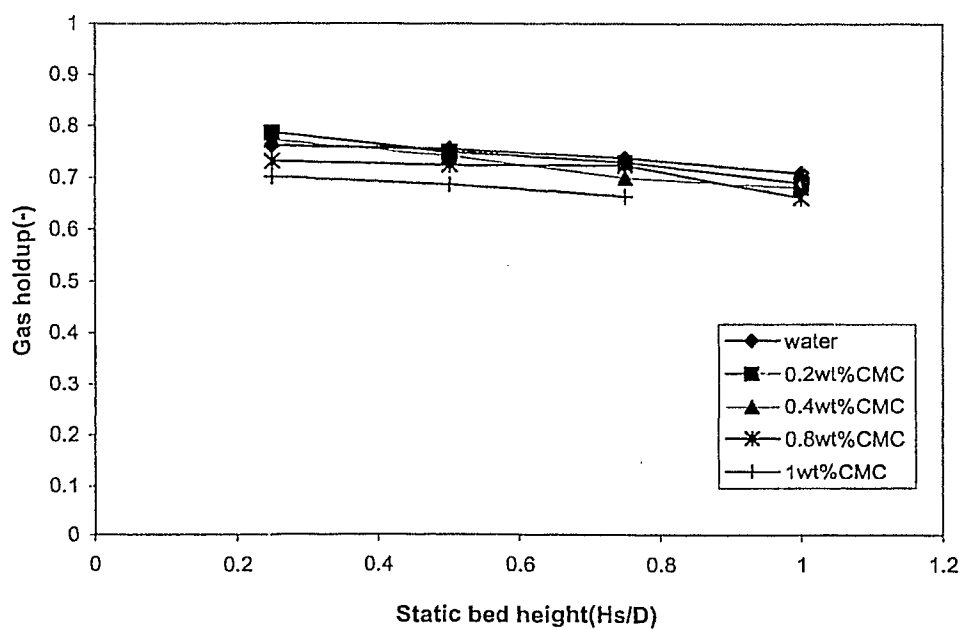


Figure A-144  Effect of static bed height on gas holdup at
dp=38mm,L=8gpm
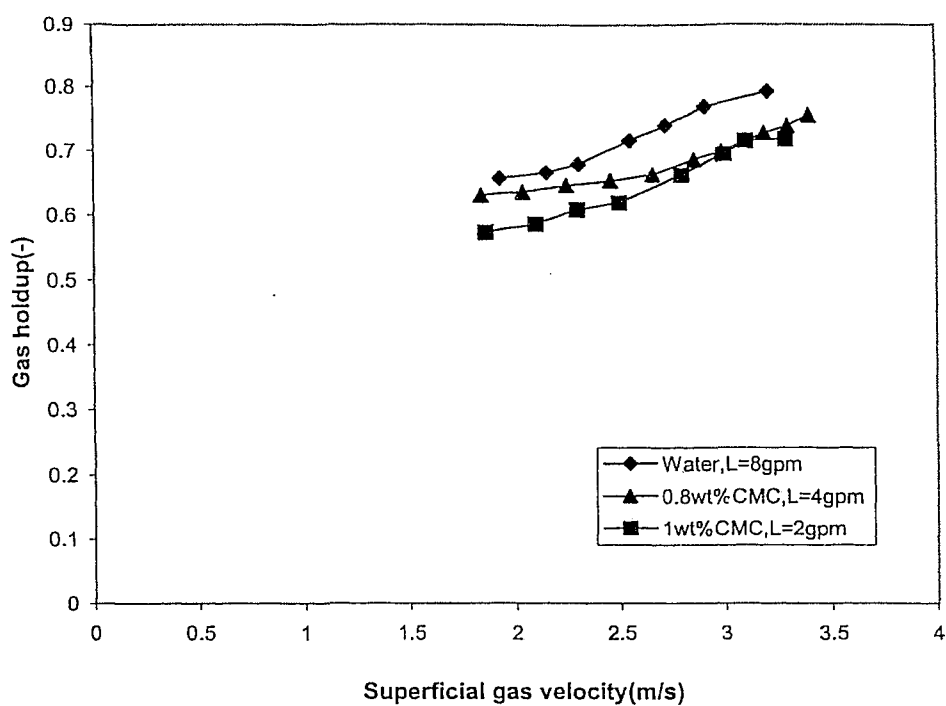
Figure A-145  Effect of superficial gas velocity on gas holdup at
Hs/D=0.25 dp=38mm
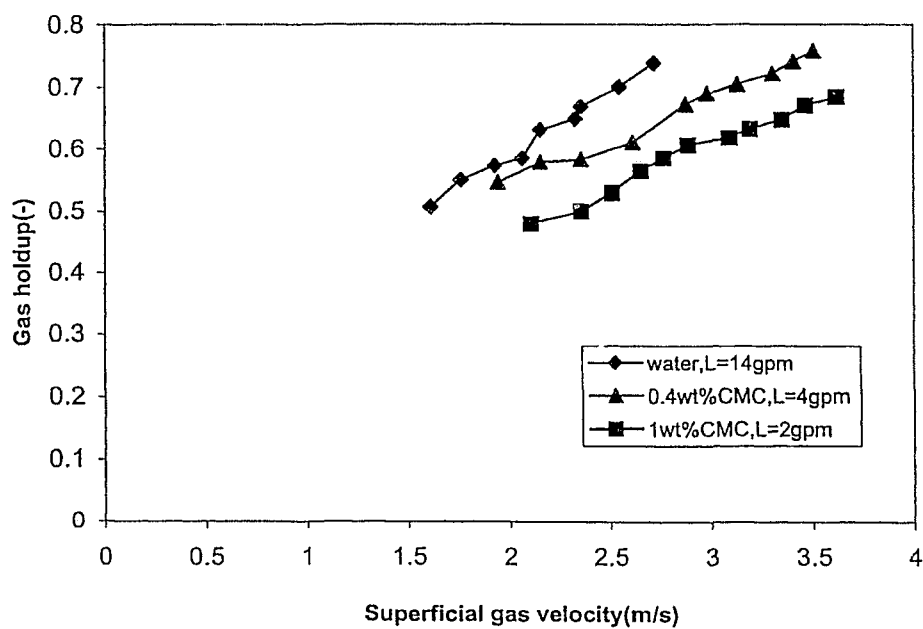


Figure A-146  Effect of superficial gas velocity on gas holdup at
Hs/D=0.5, dp=38mm

168
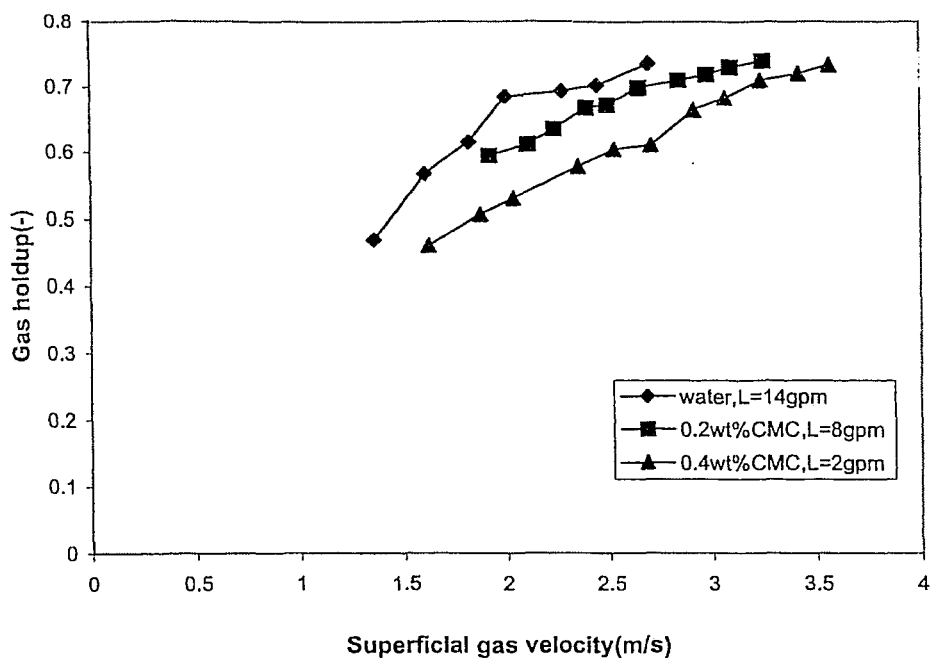
Figure A-147  Effect of superficial gas velocity on gas holdup
at Hs/D=0.75 ,dp=38mm
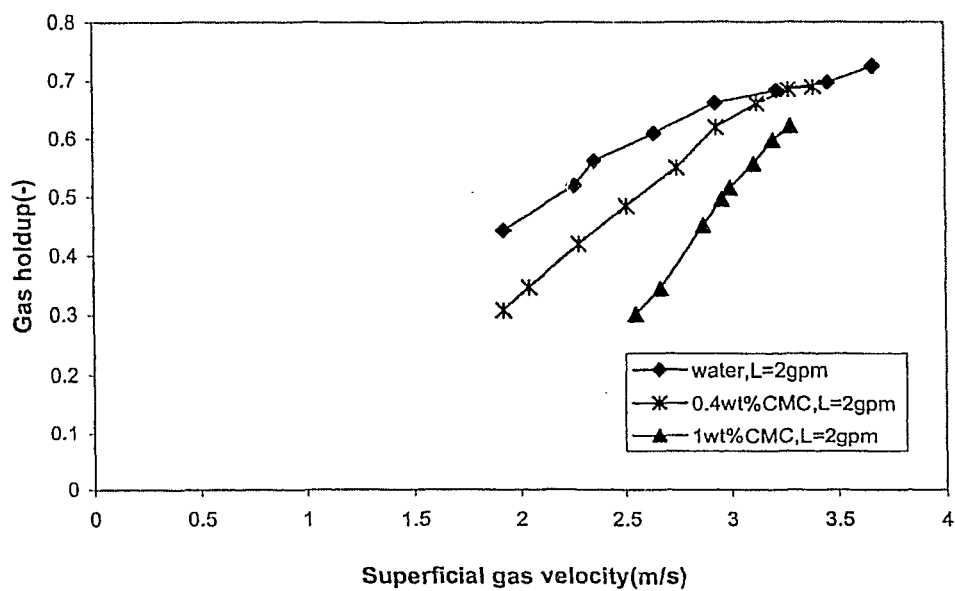


Figure A-148  Effect of superficial gas velocity on gas holdup at
Hs/D=1,dp=38mm

169
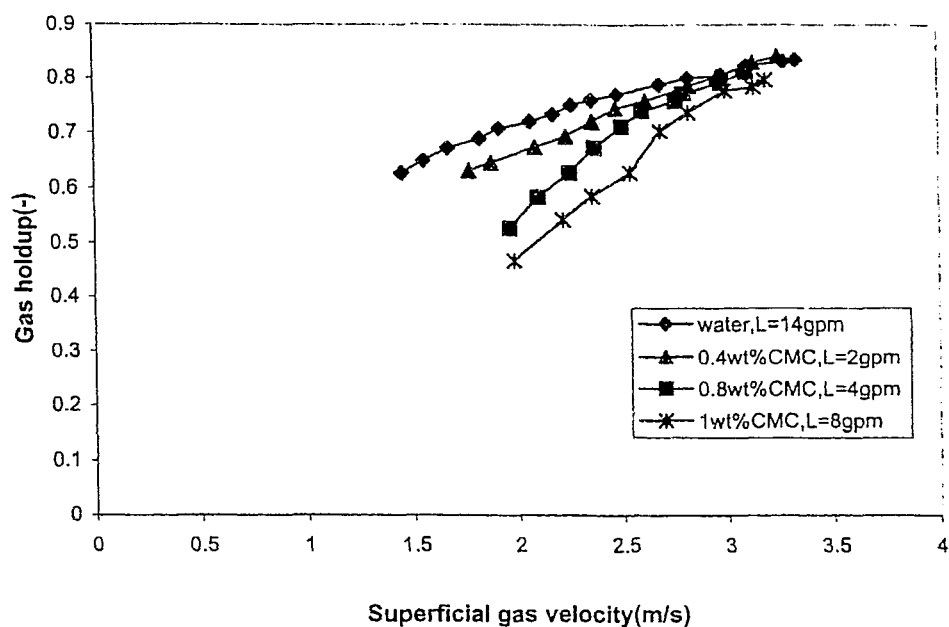
Figure A-149  Effect of superficial gas velocity on gas holdup
at dp=20mm,Hs/D=0.25
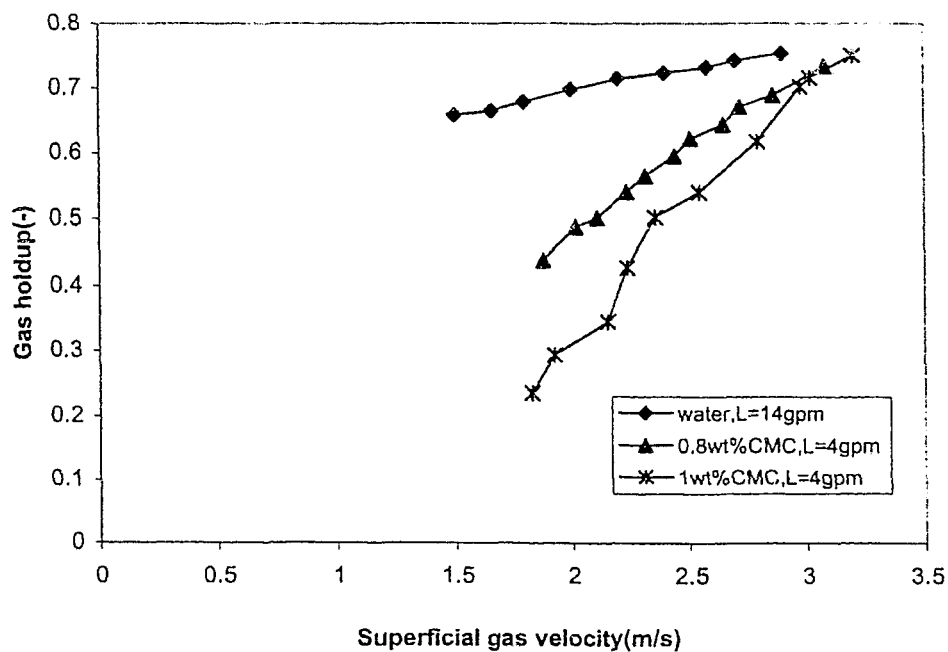


Figure A-150  Effect of superficial gas velocity on gas holdup
at Hs/D=0.5,dp=20mm

170
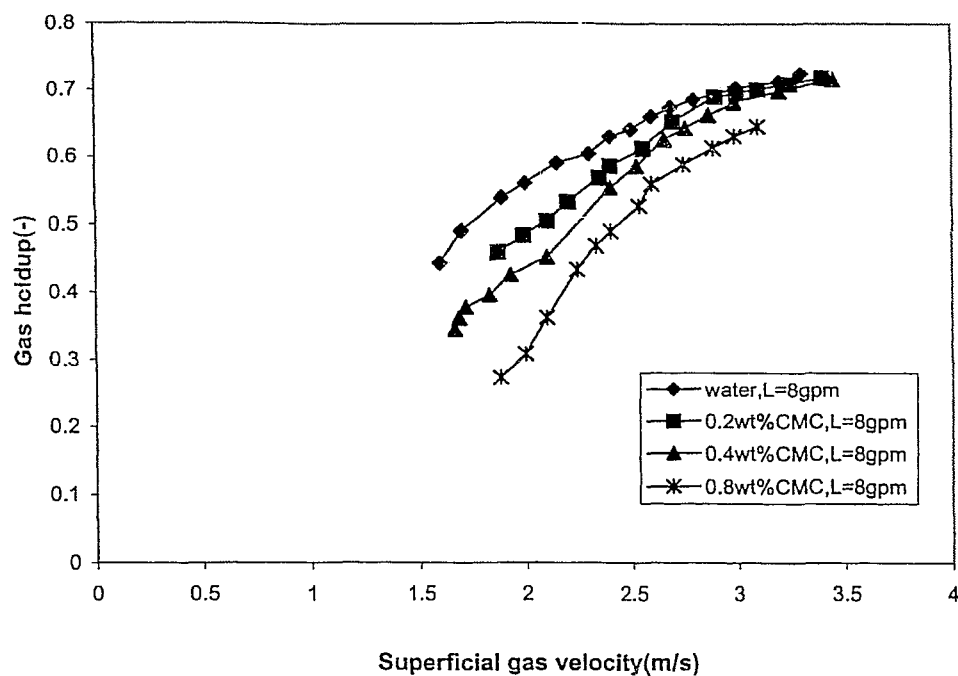
Figure A-151  Effect of superficial gas velocity on gas holdup
at Hs/D=0.75,dp=20mm
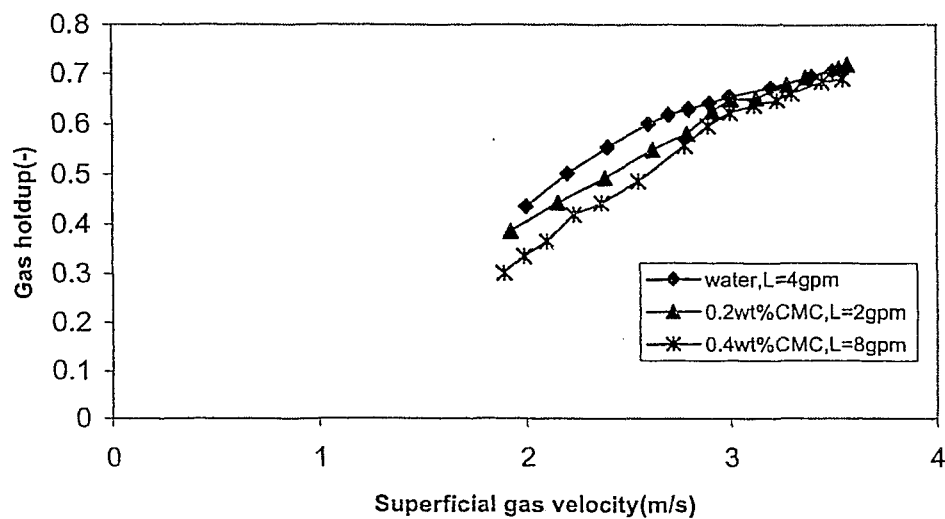


Figure A-152  Effect of superficial gas velocity on gas holdup at
Hs/D=1,dp=20mm

171

# APPENDIX B

# TABLES OF EXPERIMENTAL RESULTS

| normal stress | shear rate | shear stress | strain | % strain | temperature | time | torque | velocity | viscosity |
|---|---|---|---|---|---|---|---|---|---|
| Pa | 1/s | Pa | | | °C | s | micro N.m | rad/s | Pa.s |
| -135.4 | 1 | 0.01659 | 59.723 | 5972.3 | 20 | 60.14 | 0.94 | 8.59E-03 | 0.01659 |
| -148.4 | 1.585 | 0.03143 | 94.465 | 9446.5 | 20 | 124.1 | 1.78 | 1.36E-02 | 0.01983 |
| -165.3 | 2.512 | 0.0356 | 149.84 | 14984 | 20 | 188.1 | 2.01 | 2.16E-02 | 0.01417 |
| -192.4 | 3.981 | 9.37E-03 | 237.31 | 23731 | 20 | 252.2 | 0.53 | 3.42E-02 | 2.35E-03 |
| -228.4 | 6.31 | 0.03276 | 375.3 | 37530 | 20 | 316.1 | 1.85 | 5.42E-02 | 5.19E-03 |
| -283.3 | 10 | 0.01286 | 595.95 | 59595 | 20 | 380.2 | 0.73 | 0.08591 | 1.29E-03 |
| -336.2 | 15.85 | 0.07666 | 944.57 | 94457 | 20 | 444.2 | 4.34 | 0.1362 | 4.84E-03 |
| -397.8 | 25.12 | 0.05678 | 1497.4 | 1.50E+05 | 20 | 508.2 | 3.21 | 0.2158 | 2.26E-03 |
| -478.4 | 39.81 | 0.09825 | 2372.1 | 2.37E+05 | 20 | 572.3 | 5.56 | 0.342 | 2.47E-03 |
| -561.9 | 63.1 | 0.07462 | 3755.5 | 3.76E+05 | 20 | 636.2 | 4.22 | 0.5421 | 1.18E-03 |
| -643.2 | 100 | 0.09925 | 5966.7 | 5.97E+05 | 20 | 700.1 | 5.61 | 0.8591 | 9.93E-04 |
| -702.9 | 158.5 | 0.1547 | 7862.1 | 7.86E+05 | 20 | 754.2 | 8.75 | 1.362 | 9.76E-04 |
| -761.7 | 251.2 | 0.2516 | 12467 | 1.25E+06 | 20 | 808.2 | 14.23 | 2.158 | 1.00E-03 |
| -800.8 | 398.1 | 0.3865 | 19692 | 1.97E+06 | 20 | 862.1 | 21.85 | 3.42 | 9.71E-04 |
| -825.5 | 631 | 0.6085 | 31232 | 3.12E+06 | 20 | 916.2 | 34.41 | 5.421 | 9.64E-04 |
| -842.7 | 1000 | 0.9631 | 49697 | 4.97E+06 | 20 | 970.2 | 54.46 | 8.591 | 9.63E-04 |
| -847.5 | 1100 | 1.055 | 43400 | 4.34E+06 | 20 | 1014 | 59.67 | 9.45 | 9.59E-04 |

Table B-1 Rheological results for water

172

| normal stress | shear rate | shear stress | strain | % strain | temperature | time | torque | velocity | viscosity |
|---|---|---|---|---|---|---|---|---|---|
| Pa | 1/s | Pa | | | °C | s | micro N.m | rad/s | Pa.s |
| -80.01 | 10 | 0.2339 | 392.62 | 39262 | 20 | 39.64 | 13.23 | 8.59E-02 | 0.02339 |
| -81.58 | 12.59 | 0.2797 | 499.79 | 49979 | 20 | 83.7 | 15.82 | 1.08E-01 | 0.02222 |
| -83.37 | 15.85 | 0.3372 | 630.9 | 63090 | 20 | 127.8 | 19.07 | 1.36E-01 | 0.02128 |
| -86.35 | 19.95 | 0.4161 | 786.23 | 78623 | 20 | 171.7 | 23.53 | 1.71E-01 | 0.02086 |
| -89.19 | 25.12 | 0.5097 | 996.2 | 99620 | 20 | 215.6 | 28.82 | 2.16E-01 | 0.02029 |
| -94.65 | 31.62 | 0.6383 | 1253.2 | 1.25E+05 | 20 | 259.7 | 36.09 | 0.2717 | 0.02018 |
| -96.98 | 39.81 | 0.7905 | 1582.5 | 1.58E+05 | 20 | 303.7 | 44.7 | 0.342 | 0.01986 |
| -104.6 | 50.12 | 0.9914 | 1984.9 | 1.98E+05 | 20 | 347.8 | 56.06 | 0.4306 | 0.01978 |
| -110.7 | 63.1 | 1.243 | 2495 | 2.50E+05 | 20 | 391.6 | 70.3 | 0.5421 | 0.0197 |
| -118.4 | 79.43 | 1.563 | 3141.3 | 3.14E+05 | 20 | 435.7 | 88.36 | 0.6824 | 0.01967 |
| -125 | 100 | 1.966 | 3962.7 | 3.96E+05 | 20 | 479.7 | 111.2 | 0.8591 | 0.01966 |
| -137.3 | 125.9 | 2.475 | 4965.9 | 4.97E+05 | 20 | 523.6 | 139.96 | 1.082 | 0.01966 |
| -147.1 | 158.5 | 3.103 | 6285.6 | 6.29E+05 | 20 | 567.7 | 175.49 | 1.362 | 0.01958 |
| -160.7 | 199.5 | 3.898 | 7900.4 | 7.90E+05 | 20 | 611.7 | 220.42 | 1.714 | 0.01954 |
| -180.8 | 251.2 | 4.903 | 9947 | 9.95E+05 | 20 | 655.7 | 277.26 | 2.158 | 0.01952 |
| -206 | 316.2 | 6.137 | 12501 | 1.25E+06 | 20 | 699.6 | 347.02 | 2.717 | 0.01941 |
| -229.4 | 398.1 | 7.674 | 15751 | 1.58E+06 | 20 | 743.7 | 433.95 | 3.42 | 0.01928 |
| -274.3 | 501.2 | 9.572 | 19807 | 1.98E+06 | 20 | 787.6 | 541.31 | 4.306 | 0.0191 |
| -306.3 | 631 | 11.91 | 24947 | 2.49E+06 | 20 | 831.7 | 6.74E+02 | 5.421 | 0.01888 |
| -367 | 794.3 | 14.78 | 31473 | 3.15E+06 | 20 | 875.7 | 8.36E+02 | 6.824 | 0.01861 |
| -411.7 | 1000 | 18.27 | 39512 | 3.95E+06 | 20 | 919.6 | 1.03E+03 | 8.591 | 0.01827 |
| -469 | 1100 | 20.02 | 43797 | 4.38E+06 | 20 | 963.8 | 1.13E+03 | 9.45 | 0.0182 |

Table B-2 Rheological results for 1 wt% CMC solution

| normal stress | shear rate | shear stress | strain | % strain | temperature | time | torque | velocity | viscosity |
|---|---|---|---|---|---|---|---|---|---|
| Pa | 1/s | Pa | | | °C | s | micro N.m | rad/s | Pa.s |
| -160.9 | 10 | 0.15 | 398.18 | 39818 | 20 | 40.08 | 8.48 | 8.59E-02 | 0.015 |
| -167 | 12.59 | 0.1812 | 497.42 | 49742 | 20 | 84.09 | 10.25 | 1.08E-01 | 0.01439 |
| -173 | 15.85 | 0.2131 | 624.6 | 62460 | 20 | 128 | 12.05 | 1.36E-01 | 0.01345 |
| -180.2 | 19.95 | 0.2615 | 792.03 | 79203 | 20 | 172 | 14.79 | 1.71E-01 | 0.01311 |
| -187.5 | 25.12 | 0.3129 | 994.59 | 99459 | 20 | 216.1 | 17.69 | 2.16E-01 | 0.01245 |
| -197.1 | 31.62 | 0.3907 | 1246.2 | 1.25E+05 | 20 | 260.1 | 22.09 | 0.2717 | 0.01236 |
| -209.8 | 39.81 | 0.4826 | 1578.4 | 1.58E+05 | 20 | 304.1 | 27.29 | 0.342 | 0.01212 |
| -223.4 | 50.12 | 0.6015 | 1984.5 | 1.98E+05 | 20 | 348 | 34.02 | 0.4306 | 0.012 |
| -239.2 | 63.1 | 0.753 | 2512.4 | 2.51E+05 | 20 | 392.2 | 42.58 | 0.5421 | 0.01193 |
| -261.6 | 79.43 | 0.9387 | 3139.7 | 3.14E+05 | 20 | 436.2 | 53.08 | 0.6824 | 0.01182 |
| -292 | 100 | 1.172 | 3949.9 | 3.95E+05 | 20 | 480.2 | 66.29 | 0.8591 | 0.01172 |
| -327.1 | 125.9 | 1.467 | 4970.1 | 4.97E+05 | 20 | 524.1 | 82.98 | 1.082 | 0.01166 |
| -372.3 | 158.5 | 1.835 | 6266.5 | 6.27E+05 | 20 | 568 | 103.75 | 1.362 | 0.01158 |
| -422.1 | 199.5 | 2.295 | 7871.6 | 7.87E+05 | 20 | 612 | 129.79 | 1.714 | 0.0115 |
| -487.4 | 251.2 | 2.873 | 9949.8 | 9.95E+05 | 20 | 656 | 162.47 | 2.158 | 0.01144 |
| -554.1 | 316.2 | 3.592 | 12588 | 1.26E+06 | 20 | 700.2 | 203.11 | 2.717 | 0.01136 |
| -626 | 398.1 | 4.476 | 15741 | 1.57E+06 | 20 | 744.1 | 253.12 | 3.42 | 0.01124 |
| -694.5 | 501.2 | 5.573 | 19831 | 1.98E+06 | 20 | 788.1 | 315.17 | 4.306 | 0.01112 |
| -730 | 631 | 6.929 | 25026 | 2.50E+06 | 20 | 832.1 | 3.92E+02 | 5.421 | 0.01098 |
| -744.3 | 794.3 | 8.599 | 31468 | 3.15E+06 | 20 | 876.2 | 4.86E+02 | 6.824 | 0.01083 |
| -766.8 | 1000 | 10.63 | 39651 | 3.97E+06 | 20 | 920.2 | 6.01E+02 | 8.591 | 0.01063 |
| -794.4 | 1100 | 11.61 | 43493 | 4.35E+06 | 20 | 964.1 | 6.56E+02 | 9.45 | 0.01055 |

Table B-3 Rheological results for 0.8wt % CMC

174

| normal stress | shear rate | shear stress | strain | % strain | temperature | time | torque | velocity | viscosity |
|---|---|---|---|---|---|---|---|---|---|
| Pa | 1/s | Pa | | | °C | s | micro N.m | rad/s | Pa.s |
| -112.6 | 10 | 0.07268 | 500.76 | 50076 | 20 | 50.45 | 4.11 | 8.59E-02 | 7.27E-03 |
| -113.7 | 12.59 | 0.08701 | 499.72 | 49972 | 20 | 94.67 | 4.92 | 1.08E-01 | 6.91E-03 |
| -117 | 15.85 | 0.1036 | 627.47 | 62747 | 20 | 138.6 | 5.86 | 1.36E-01 | 6.54E-03 |
| -120.7 | 19.95 | 0.1272 | 787.95 | 78795 | 20 | 182.6 | 7.19 | 1.71E-01 | 6.37E-03 |
| -124.9 | 25.12 | 0.1525 | 990 | 99000 | 20 | 226.5 | 8.63 | 2.16E-01 | 6.07E-03 |
| -129.4 | 31.62 | 0.1907 | 1248.4 | 1.25E+05 | 20 | 270.5 | 10.78 | 0.2717 | 6.03E-03 |
| -133.1 | 39.81 | 0.2343 | 1578.1 | 1.58E+05 | 20 | 314.6 | 13.25 | 0.342 | 5.89E-03 |
| -138.1 | 50.12 | 0.2927 | 1973.2 | 1.97E+05 | 20 | 358.5 | 16.55 | 0.4306 | 5.84E-03 |
| -142.9 | 63.1 | 0.3671 | 2500.2 | 2.50E+05 | 20 | 402.6 | 20.76 | 0.5421 | 5.82E-03 |
| -149.2 | 79.43 | 0.4594 | 3151.7 | 3.15E+05 | 20 | 446.7 | 25.98 | 0.6824 | 5.78E-03 |
| -155.9 | 100 | 0.5761 | 3934.3 | 3.93E+05 | 20 | 490.5 | 32.58 | 0.8591 | 5.76E-03 |
| -163 | 125.9 | 0.7208 | 4987.2 | 4.99E+05 | 20 | 534.4 | 40.76 | 1.082 | 5.73E-03 |
| -171.7 | 158.5 | 0.9034 | 6264.5 | 6.26E+05 | 20 | 578.5 | 51.09 | 1.362 | 5.70E-03 |
| -181.7 | 199.5 | 1.138 | 7908.2 | 7.91E+05 | 20 | 622.6 | 64.36 | 1.714 | 5.70E-03 |
| -193.5 | 251.2 | 1.427 | 9955.4 | 9.96E+05 | 20 | 666.6 | 80.72 | 2.158 | 5.68E-03 |
| -206.9 | 316.2 | 1.798 | 12517 | 1.25E+06 | 20 | 710.6 | 101.67 | 2.717 | 5.69E-03 |
| -224.7 | 398.1 | 2.256 | 15699 | 1.57E+06 | 20 | 754.5 | 127.55 | 3.42 | 5.67E-03 |
| -245.5 | 501.2 | 2.829 | 19854 | 1.99E+06 | 20 | 798.6 | 159.99 | 4.306 | 5.65E-03 |
| -276.8 | 631 | 3.542 | 24875 | 2.49E+06 | 20 | 842.6 | 2.00E+02 | 5.421 | 5.61E-03 |
| -317.7 | 794.3 | 4.433 | 31287 | 3.13E+06 | 20 | 886.4 | 2.51E+02 | 6.824 | 5.58E-03 |
| -372.6 | 1000 | 5.531 | 39635 | 3.96E+06 | 20 | 930.6 | 3.13E+02 | 8.591 | 5.53E-03 |
| -425.1 | 1100 | 6.06 | 43591 | 4.36E+06 | 20 | 974.6 | 3.43E+02 | 9.45 | 5.51E-03 |

Table B-4 Rheological results for 0.4wt % CMC

| normal stress | shear rate | shear stress | strain | % strain | temperature | time | torque | velocity | viscosity |
|---|---|---|---|---|---|---|---|---|---|
| Pa | 1/s | Pa | | | °C | s | micro N.m | rad/s | Pa.s |
| -133.8 | 10 | 0.04761 | 501.22 | 50122 | 20 | 50.38 | 2.69 | 8.59E-02 | 4.76E-03 |
| -137.2 | 12.59 | 0.05722 | 750.11 | 75011 | 20 | 114.5 | 3.24 | 1.08E-01 | 4.55E-03 |
| -140.1 | 15.85 | 0.06771 | 625.82 | 62582 | 20 | 158.5 | 3.83 | 1.36E-01 | 4.27E-03 |
| -146.9 | 19.95 | 0.08199 | 1187.6 | 1.19E+05 | 20 | 222.5 | 4.64 | 1.71E-01 | 4.11E-03 |
| -150.5 | 25.12 | 0.09897 | 990.24 | 99024 | 20 | 266.4 | 5.6 | 2.16E-01 | 3.94E-03 |
| -155.6 | 31.62 | 0.1251 | 1254 | 1.25E+05 | 20 | 310.5 | 7.08 | 0.2717 | 3.96E-03 |
| -161.9 | 39.81 | 0.1517 | 1567.7 | 1.57E+05 | 20 | 354.4 | 8.58 | 0.342 | 3.81E-03 |
| -168 | 50.12 | 0.1904 | 1984.4 | 1.98E+05 | 20 | 398.4 | 10.76 | 0.4306 | 3.80E-03 |
| -176.9 | 63.1 | 0.2384 | 2493 | 2.49E+05 | 20 | 442.4 | 13.48 | 0.5421 | 3.78E-03 |
| -185.5 | 79.43 | 0.2966 | 3153.4 | 3.15E+05 | 20 | 486.5 | 16.77 | 0.6824 | 3.73E-03 |
| -197.3 | 100 | 0.3701 | 3938.7 | 3.94E+05 | 20 | 530.4 | 20.93 | 0.8591 | 3.70E-03 |
| -209.5 | 125.9 | 0.4633 | 4968.6 | 4.97E+05 | 20 | 574.4 | 26.2 | 1.082 | 3.68E-03 |
| -224.2 | 158.5 | 0.5786 | 6231 | 6.23E+05 | 20 | 618.5 | 32.72 | 1.362 | 3.65E-03 |
| -242.6 | 199.5 | 0.7245 | 7876.6 | 7.88E+05 | 20 | 662.4 | 40.97 | 1.714 | 3.63E-03 |
| -266.7 | 251.2 | 0.9044 | 9916.1 | 9.92E+05 | 20 | 706.3 | 51.14 | 2.158 | 3.60E-03 |
| -296.8 | 316.2 | 1.13 | 12556 | 1.26E+06 | 20 | 750.4 | 63.91 | 2.717 | 3.57E-03 |
| -337.9 | 398.1 | 1.419 | 15755 | 1.58E+06 | 20 | 794.4 | 80.25 | 3.42 | 3.57E-03 |
| -391 | 501.2 | 1.783 | 19784 | 1.98E+06 | 20 | 838.4 | 100.8 | 4.306 | 3.56E-03 |
| -449.8 | 631 | 2.232 | 24967 | 2.50E+06 | 20 | 882.3 | 1.26E+02 | 5.421 | 3.54E-03 |
| -514.6 | 794.3 | 2.793 | 31462 | 3.15E+06 | 20 | 926.4 | 1.58E+02 | 6.824 | 3.52E-03 |
| -590.3 | 1000 | 3.49 | 39787 | 3.98E+06 | 20 | 970.5 | 1.97E+02 | 8.591 | 3.49E-03 |
| -664.7 | 1100 | 3.822 | 43286 | 4.33E+06 | 20 | 1014 | 2.16E+02 | 9.45 | 3.47E-03 |

Table B-5 Rheological results for 0.2wt % CMC

176

| 12-Jan | 0.2%CMC, Hs/D=0.5, L=4gpm dp=26mm | | | | | |
|---|---|---|---|---|---|---|
| Delay between measurements: | 1 | | | | | |
| Delay to reach steady state: | 1 | | | | | |
| No. Batches: | 20 | | | | | |
| | | | | | | |
| Batch | Temp. liquid In(°C) | Temp. liquid. Out(°C) | Temp air in(°C) | Temp air out(°C) | Pitot tube reading(torr) | Pressure drop reading(torr) |
| 1 | 20.001 | 20.5298 | 20.02367 | 20.98555 | 0.008215001 | 2.151458 |
| 2 | 20.0615 | 20.33838 | 20.05392 | 20.91013 | 0.02042 | 4.096277 |
| 3 | 20.03 | 20.48668 | 20.3291 | 20.96214 | 0.02746 | 5.049968 |
| 4 | 20.105 | 20.27698 | 20.48663 | 20.89808 | 0.0353075 | 6.06596 |
| 5 | 20.0724 | 20.2341 | 20.64455 | 20.8873 | 0.037365 | 6.539485 |
| 6 | 20.0741 | 20.2212 | 20.81825 | 20.89245 | 0.0378325 | 6.940057 |
| 7 | 20.0407 | 20.22867 | 20.7547 | 20.879 | 0.0358425 | 7.358052 |
| 8 | 20.01592 | 20.17735 | 20.7779 | 20.83065 | 0.0395325 | 7.761964 |
| 9 | 20.03673 | 20.16605 | 21.3277 | 20.82647 | 0.124255 | 7.080958 |
| 10 | 20.05697 | 19.48877 | 22.0837 | 20.73783 | 0.23442 | 6.93345 |
| 11 | 20.08867 | 19.76165 | 21.8315 | 20.539 | 0.33845 | 6.952676 |
| 12 | 20.11815 | 20.0628 | 21.47945 | 20.4144 | 0.41113 | 6.9047 |
| 13 | 20.14363 | 20.62275 | 21.17318 | 20.36467 | 0.4786724 | 6.831895 |
| 14 | 20.16483 | 19.9178 | 20.88977 | 19.9784 | 0.57503 | 6.914113 |
| | | | | | | |

Table B-6   Sample for Tabulated results for a run

| Pitot tube reading (torr) | Gas velocity (m/s) | Pressure drop reading (torr) | Pressure drop for for empty column (kPa) | Total pressure drop (kPa) | Net pressure drop (kPa) |
|---|---|---|---|---|---|
| 0.00945 | 0.4184258 | 0.840405 | 0.001479588 | 1.12E-01 | 1.10E-01 |
| 1.27E-02 | 0.486023538 | 1.301805 | 0.0019256 | 1.73E-01 | 1.71E-01 |
| 0.01764 | 0.571678476 | 2.191665 | 0.002573453 | 2.91E-01 | 2.89E-01 |
| 0.0213075 | 0.628302517 | 2.90795 | 0.003052486 | 3.87E-01 | 3.84E-01 |
| 0.02883 | 0.730844313 | 3.885195 | 0.0040228 | 5.17E-01 | 5.13E-01 |
| 0.032275 | 0.773278039 | 4.575807 | 0.004463091 | 6.09E-01 | 6.04E-01 |
| 0.03205 | 0.770577932 | 4.926098 | 0.004434399 | 6.55E-01 | 6.51E-01 |
| 0.0359 | 0.815548466 | 5.253815 | 0.004924245 | 6.99E-01 | 6.94E-01 |
| 0.0391 | 0.851120262 | 6.035098 | 0.005329764 | 8.03E-01 | 7.97E-01 |
| 3.86E-02 | 0.845688301 | 6.4197 | 0.005266808 | 8.54E-01 | 8.49E-01 |
| 0.042955 | 0.892091523 | 6.883365 | 0.005816594 | 9.15E-01 | 9.10E-01 |
| 0.12 | 1.491053319 | 5 | 0.01534836 | 6.65E-01 | 6.50E-01 |
| 0.15 | 1.66704829 | 5.1 | 0.019008358 | 6.78E-01 | 6.59E-01 |
| 0.1858825 | 1.855759973 | 5.1 | 0.023366408 | 6.78E-01 | 6.55E-01 |
| 0.2131575 | 1.98725162 | 5.14319 | 0.026668291 | 6.84E-01 | 6.57E-01 |
| 0.25 | 2.152150088 | 5.2 | 0.03111696 | 6.92E-01 | 6.60E-01 |
| 0.287905 | 2.30954886 | 5.193673 | 0.035682894 | 6.91E-01 | 6.55E-01 |
| 0.3433076 | 2.521995223 | 5.24172 | 0.042340693 | 6.97E-01 | 6.55E-01 |
| 0.38105 | 2.657012109 | 5.262401 | 0.046867505 | 7.00E-01 | 6.53E-01 |
| 0.4196225 | 2.788251434 | 5.300295 | 0.051487806 | 7.05E-01 | 6.53E-01 |
| 0.4603024 | 2.920277823 | 5.306603 | 0.056354792 | 7.06E-01 | 6.49E-01 |
| 0.51058 | 3.075632563 | 5.473523 | 0.062363018 | 7.28E-01 | 6.66E-01 |

Table B-7   Sample of calculated results for 0.4wt% CMC, Hs/D=0.25, L=4gpm, dp=20mm

178

| Gas velocity (m/s) | liquid holdup | Bed expansion (H) cm | Gas holdup |
|---|---|---|---|
| 1.855759973 | 0.717123774 | 24 | 0.5867085 |
| 1.98725162 | 0.72056392 | 28 | 0.6448594 |
| 2.152150088 | 0.724940271 | 33 | 0.6977071 |
| 2.30954886 | 0.717323816 | 35 | 0.7165587 |
| 2.521995223 | 0.71694697 | 39 | 0.7456996 |
| 2.657012109 | 0.714445106 | 44 | 0.7750096 |
| 2.788251434 | 0.715036121 | 48 | 0.7936696 |
| 2.920277823 | 0.70936258 | 53 | 0.8139108 |
| 3.075632563 | 0.732169491 | 58 | 0.8271021 |

-Continue Table B-7-

| Gas velocity m/s | K eq (4-17) | ε eq (4-18) | Shear Rate (1/s) eq (4-5) | Apparent viscosity (Pa.s) eq (1-3) | Net pressure drop (kPa)(Kito) | Net pressure drop (kPa)(Vunjak) |
|---|---|---|---|---|---|---|
| 1.66 | 0.5114094 | 0.5926005 | 148.111666 | 0.012371982 | 0.952155125 | 0.401098605 |
| 1.72 | 0.5387893 | 0.5995313 | 151.6667247 | 0.012348382 | 0.951910428 | 0.40107365 |
| 1.9 | 0.6244164 | 0.6191944 | 162.1504261 | 0.01228212 | 0.951221288 | 0.401003345 |
| 2.2 | 0.7785841 | 0.6486749 | 179.1222344 | 0.012184093 | 0.950196043 | 0.400898679 |
| 2.4 | 0.8891878 | 0.666377 | 190.1602619 | 0.012125582 | 0.949580782 | 0.400835828 |
| 2.65 | 1.0361069 | 0.6866327 | 203.713454 | 0.012058565 | 0.94887301 | 0.400763488 |
| 2.88 | 1.1796678 | 0.7036588 | 215.9876129 | 0.012001906 | 0.948272035 | 0.400702032 |
| 3.04 | 1.2842305 | 0.7146944 | 224.4352719 | 0.011964895 | 0.947878185 | 0.400661741 |
| 3.2 | 1.3926125 | 0.7251271 | 232.8194528 | 0.011929622 | 0.947501871 | 0.400623232 |

Table B-8 Estimated values of shear rates and net pressure drop at Hs/D=0.5, dp=38mm, L=8gpm, 0.8 wt% CMC

```
DIM File$(30): File$ = A$ + F$ + n$ + E$
DIM Average$(30): Average$ = A$ + G$ + n$ + E$

PRINT ""
PRINT "Enter the desired delay time in seconds (d) between averages of 20 scans."
INPUT d
PRINT ""
PRINT "Enter the desired delay time in minutes (t) to reach steady state."
INPUT t
PRINT ""
PRINT "Enter the desired number of batches (m) of 20 averages"
INPUT m
PRINT ""
PRINT "Do you want the program to pause after each batch?  Enter 'y or n'."
PRINT "   (You will hit Enter to resume after each batch)"
INPUT S$
PRINT ""

OPEN File$ FOR APPEND AS #2
        WRITE #2, dat$, d$
        WRITE #2, "Delay between measurements:", d
        WRITE #2, "Delay to reach steady state:", t
        WRITE #2, "No. Batches:", m
        WRITE #2, "Batch", "Time", "Ch3", "Ch4", "Ch5", "Ch6", "Ch7", "Ch8", "Ch9",
"Ch10", "Ch11", "Ch12", "Ch13", "Ch14", "Ch15", "Ch16", "Ch17", "Ch18"
CLOSE #2

OPEN Average$ FOR APPEND AS #3
        WRITE #3, dat$, d$
        WRITE #3, "Delay between measurements:", d
        WRITE #3, "Delay to reach steady state:", t
        WRITE #3, "No. Batches:", m
        WRITE #3, "Batch", "Ch3", "Ch4", "Ch5", "Ch6", "Ch7", "Ch8", "Ch9", "Ch10",
"Ch11", "Ch12", "Ch13", "Ch14", "Ch15", "Ch16", "Ch17", "Ch18"
CLOSE #3

PRINT "Hit Enter to begin scans"
INPUT dummy$

DIM A(20, 17)
OPEN "COM2:9600,N,7,1" FOR RANDOM AS #1
ST = 0: FT = 0: LT = 0: SST = 0: SDT = 0: FDT = 0
ST = TIMER
SST = 60 * t
  FOR l = 1 TO m

PRINT l
    FOR i = 1 TO 20
    M1A = 0: M2A = 0: M3A = 0: M4A = 0: M5A = 0: M6A = 0: M7A = 0: M8A = 0: M9A = 0:
M10A = 0: M11A = 0: M12A = 0: M13A = 0: M14A = 0: M15A = 0: M16A = 0
        FOR j = 1 TO 20
        LT = TIMER
        PRINT #1, "SNP 3 TO 18"
        INPUT #1, M1, M2, M3, M4, M5, M6, M7, M8, M9, M10, M11, M12, M13, M14, M15,
M16
        M1A = M1A + M1
        M2A = M2A + M2
        M3A = M3A + M3
        M4A = M4A + M4
        M5A = M5A + M5
        M6A = M6A + M6
```

# APPENDIX C

# DATA ACQUISITION COMPUTER PROGRAMME

```
CLS

PRINT "                          _ PROGRAM FUNCTION"
PRINT " "
PRINT "This program scans channels 3 to 18 inclusive."
PRINT "20 rapid scans take place every (d) seconds, and are averaged."
PRINT "Operator can choose the delay time (d) between averages of 20 scans."
PRINT "The averages of certain channels are displayed every (d) seconds."
PRINT "Storage of all channels takes place in batches of 20 averages."
PRINT "The last average of each batch is printed for hard copy reference."
PRINT "The number of batches (m) of 20 averages can be chosen by the operator."
PRINT "Operator can choose a delay (t) after each batch, to reach steady state."
PRINT "Operator can choose to pause after each batch (continuous otherwise)."

PRINT "The data files are stored in directory C:\QB45\MELDATA."
PRINT "The files DATA###.PRN contain 20 averages for each batch."
PRINT "The files AVG###.PRN contain 1 overall average of the 20 averages for"
PRINT "in each batch."
PRINT " "




PRINT "Enter the date (ex. '11 Jun 02')"
DIM dat$(9): INPUT dat$
PRINT "Enter the name of the experiment (up to 40 characters)"
DIM d$(40): INPUT d$
PRINT " "
PRINT "Enter the number of this experimental run, in the form '001'."
DIM n$(4): INPUT n$
DIM dummy$(1)
PRINT " "

REM File path for data files
A$ = "C:\QB45\MELDATA\"

F$ = "DATA": E$ = ".PRN": G$ = "AVG"
```

180

```
                M7A = M7A + M7
                M8A = M8A + M8
                M9A = M9A + M9
                M10A = M10A + M10
                M11A = M11A + M11
                M12A = M12A + M12
                M13A = M13A + M13
                M14A = M14A + M14
                M15A = M15A + M15
                M16A = M16A + M16
            NEXT j

            FT = TIMER
            M1A = M1A / 20
            M2A = M2A / 20
            M3A = M3A / 20
            M4A = M4A / 20
            M5A = M5A / 20
            M6A = M6A / 20
            M7A = M7A / 20
            M8A = M8A / 20
            M9A = M9A / 20
            M10A = M10A / 20
            M11A = M11A / 20
            M12A = M12A / 20
            M13A = M13A / 20
            M14A = M14A / 20
            M15A = M15A / 20
            M16A = M16A / 20

            TM = (FT - ST)
            PRINT TM; M2A; M3A; M4A; M5A; M11A; M13A; M9A; M16A
            A(i, 1) = TM
            A(i, 2) = M1A
            A(i, 3) = M2A
            A(i, 4) = M3A
            A(i, 5) = M4A
            A(i, 6) = M5A
            A(i, 7) = M6A
            A(i, 8) = M7A
            A(i, 9) = M8A
            A(i, 10) = M9A
            A(i, 11) = M10A
            A(i, 12) = M11A
            A(i, 13) = M12A
            A(i, 14) = M13A
            A(i, 15) = M14A
            A(i, 16) = M15A
            A(i, 17) = M16A

                DO
                FT = TIMER
                LOOP UNTIL FT - LT > d

        NEXT i

        PRINT ""

    M1B = 0: M2B = 0: M3B = 0: M4B = 0: M5B = 0: M6B = 0: M7B = 0: M8B = 0: M9B = 0:
    M10B = 0: M11B = 0: M12B = 0: M13B = 0: M14B = 0: M15B = 0: M16B = 0
    FOR i = 1 TO 20
```

```
        M1B = M1B + A(i, 2)
        M2B = M2B + A(i, 3)
        M3B = M3B + A(i, 4)
        M4B = M4B + A(i, 5)
        M5B = M5B + A(i, 6)
        M6B = M6B + A(i, 7)
        M7B = M7B + A(i, 8)
        M8B = M8B + A(i, 9)
        M9B = M9B + A(i, 10)
        M10B = M10B + A(i, 11)
        M11B = M11B + A(i, 12)
        M12B = M12B + A(i, 13)
        M13B = M13B + A(i, 14)
        M14B = M14B + A(i, 15)
        M15B = M15B + A(i, 16)
        M16B = M16B + A(i, 17)
NEXT i

M1B = M1B / 20
M2B = M2B / 20
M3B = M3B / 20
M4B = M4B / 20
M5B = M5B / 20
M6B = M6B / 20
M7B = M7B / 20
M8B = M8B / 20
M9B = M9B / 20
M10B = M10B / 20
M11B = M11B / 20
M12B = M12B / 20
M13B = M13B / 20
M14B = M14B / 20
M15B = M15B / 20
M16B = M16B / 20




OPEN File$ FOR APPEND AS #2
   FOR k = 1 TO 20
      WRITE #2, 1, A(k, 1), A(k, 2), A(k, 3), A(k, 4), A(k, 5), A(k, 6), A(k, 7),
A(k, 8), A(k, 9), A(k, 10), A(k, 11), A(k, 12), A(k, 13), A(k, 14), A(k, 15), A(k,
16), A(k, 17)
   NEXT k
CLOSE #2

OPEN Average$ FOR APPEND AS #3
   WRITE #3, 1, M1B, M2B, M3B, M4B, M5B, M6B, M7B, M8B, M9B, M10B, M11B, M12B, M13B,
M14B, M15B, M16B
CLOSE #3

6 IF S$ = "y" AND 1 < m THEN INPUT dummy$
   IF 1 = m GOTO 100
        SDT = TIMER
        DO
        FDT = TIMER
        LOOP UNTIL FDT - SDT > SST

   NEXT 1
100 CLOSE #1
PRINT "Enter any additional information relevant to this run. (Max 100 characters)."
DIM AI$(100): INPUT AI$
```

```
OPEN File$ FOR APPEND AS #2
        WRITE #2, "Notes: ", AI$
CLOSE #2

OPEN Average$ FOR APPEND AS #3
        WRITE #3, "Notes: ", AI$
CLOSE #3

END
```